



University
of Glasgow

Myles, Rachel Claire (2009) *The relationship between repolarisation alternans and the production of ventricular arrhythmia in heart failure*. PhD thesis.

<http://theses.gla.ac.uk/714/>

Copyright and moral rights for this thesis are retained by the author

A copy can be downloaded for personal non-commercial research or study, without prior permission or charge

This thesis cannot be reproduced or quoted extensively from without first obtaining permission in writing from the Author

The content must not be changed in any way or sold commercially in any format or medium without the formal permission of the Author

When referring to this work, full bibliographic details including the author, title, awarding institution and date of the thesis must be given

**The relationship between repolarisation alternans and the production of
ventricular arrhythmia in heart failure**

by

Rachel Claire Myles MA (Oxon) MBBS MRCP (UK)

Submitted for the degree of Doctor of Philosophy

To

The University of Glasgow

From

The British Heart Foundation Cardiovascular Research Centre

University of Glasgow

Abstract

Microvolt T-wave alternans is thought to predict the risk of ventricular arrhythmias in patients with heart disease, although recent clinical studies have conflicting results. Understanding the cellular basis for alternans may not only inform more effective utilisation of the clinical test, but also provide new insights into the causes of lethal arrhythmias in man. Cellular repolarisation alternans is thought to underlie T-wave alternans and in recent years, the concept of discordant repolarisation alternans has emerged as a new paradigm for the induction of re-entrant ventricular arrhythmia. This experimental observation has not been examined in clinically relevant models of pathology and so the aim of this study was to investigate whether increased transmural heterogeneity of repolarisation as a result of heart failure following myocardial infarction in the rabbit would predispose to the development of arrhythmogenic discordant alternans. A rabbit ventricular wedge preparation was developed and the transmural electrophysiology of intact rabbit ventricle was characterised using optical imaging techniques. This revealed transmural gradients of repolarisation in intact rabbit myocardium, which appeared to be influenced by electrotonic load, rather than purely being a reflection of intrinsic cellular differences. Interestingly, repolarisation alternans also appeared in transmural patterns, which were also modified by activation sequence, underlining the role of conduction and electrotonic influences in dictating the spatial patterns of alternans, which may be crucial in determining spatially discordant alternans. In this study, similar baseline electrophysiological characteristics were apparent in the remodelled myocardium of failing hearts compared with normal hearts, underlining the possible importance of dynamic factors in producing the increased vulnerability to re-entrant arrhythmias observed in failing hearts. Repolarisation alternans, elicited by low temperature and rapid pacing, occurred at lower heart rates in failing hearts. At physiological temperature, repolarisation alternans was also more common in failing hearts. Spatially discordant alternans was not consistently observed on the transmural surface and did not appear to be directly related to the development of arrhythmia. Failing hearts displayed an increased vulnerability to ventricular arrhythmia. Although heart failure was associated with both alternans and ventricular arrhythmia, there was no demonstrable mechanistic link between alternans and ventricular arrhythmias in failing hearts. These data establish the occurrence of repolarisation alternans in a clinically relevant pathology, and so constitute an important step forward in our understanding of the experimental paradigm. However, a definitive mechanistic link between alternans and arrhythmia in heart failure is yet to be shown.

Table of Contents

Declaration.....	16
Chapter 1: Introduction.....	21
Sudden cardiac death in heart failure	22
The prevalence of SCD in heart failure.....	22
Defining and classifying SCD.....	22
Aetiology of SCD in heart failure	22
Prevention of SCD in heart failure.....	23
Pharmacological therapy.....	23
Implantable cardioverter-defibrillator.....	23
Risk stratification for SCD in heart failure	24
Microvolt T-wave alternans	24
Background	24
Methodology	25
Spectral MTWA testing	25
Time-domain analytic methods.....	28
Predictive value of MTWA.....	28
Following myocardial infarction.....	28
MADIT-II eligible patients	29
Ischaemic left ventricular systolic dysfunction.....	29
Left ventricular systolic dysfunction, irrespective of aetiology.....	30
Non-ischaemic left ventricular systolic dysfunction.....	30
Specificity of MTWA for arrhythmias.....	32
Repolarisation alternans	35
Cellular mechanisms of repolarisation alternans	35
Determinants of cellular repolarisation.....	36
AP restitution	38
Ca ²⁺ cycling.....	40
Interactions of restitution and Ca ²⁺ cycling	40
Discordant alternans.....	40
Mechanisms of discordant alternans	41
Is there a mechanistic link between alternans and arrhythmia?.....	45
The experimental paradigm.....	45
Temperature	45
Amplitude alternans	46

Translation to the clinical setting	47
Interspecies correlation	48
Temporality	48
Alternans and heart rate	48
Repolarisation alternans as a mechanism for arrhythmia in heart failure	49
Electrophysiological heterogeneity	49
Electrophysiological remodelling in heart failure.....	49
Heterogeneity of repolarisation in the rabbit coronary ligation model	50
Discordant repolarisation alternans as a mechanism of re-entry in heart failure.....	50
Aims and hypotheses	52
Aims	52
Hypotheses	52
Chapter 2: Methods.....	53
The rabbit coronary artery ligation model	54
Methods.....	54
Characteristics of the rabbit coronary ligation model	55
The arterially perfused rabbit left ventricular wedge preparation.....	56
Development of the preparation.....	57
Method	58
Viability of the preparation	60
Perfusion system	63
Physiological solution	64
Stimulation	64
Optical mapping	65
Introduction	65
Voltage sensitive dyes.....	65
Optics	66
CCD-based optical mapping system	66
System parameters	67
Motion artefact	69
2,3-butanedione monoxime.....	69
Optical action potentials.....	69
Experimental protocols	70
Epicardial imaging	70
Stimulation site protocol	70
Dynamic restitution protocol.....	70

Alternans protocol.....	71
Drug effects	71
Data analysis	72
Optical data analysis	72
Action potential characteristic analysis.....	72
Alternans analysis	75
Viability assessment.....	78
Statistical analyses	79
Chapter 3: Transmural electrophysiology in rabbit left ventricular myocardium	80
Introduction	81
Transmural electrophysiological heterogeneity	81
The midmyocardial ‘M’ cell	82
Transmural heterogeneity in intact ventricular myocardium	82
The role of intercellular coupling.....	83
Transmural electrophysiology at low temperature.....	83
Transmural heterogeneity of repolarisation and alternans	83
Aims	84
Methods.....	85
Experimental protocols	85
Data analysis	85
Statistical analyses	85
Results.....	86
Baseline characteristics	86
Transmural APD ₉₀ in the intact heart: comparison with isolated cell data.....	87
APD ₉₀ restitution	89
Transmural gradients of APD ₉₀ during rapid stimulation.....	90
Transmural APD ₉₀ restitution	92
The effect of low temperature on transmural electrophysiology	94
Transmural gradients of APD ₉₀ during rapid stimulation at low temperature	95
APD ₉₀ restitution at low temperature	97
A comparison of transmural and epicardial electrophysiology.....	101
Epicardial and transmural restitution	101
Transmural and epicardial electrophysiology at low temperature	103
Epicardial and transmural restitution at low temperature	103
Discussion	105
Comparison of optical action potentials with microelectrode recordings.....	105

APD differences between isolated cells and intact myocardium	105
Patterns of activation and conduction velocity	106
Transmural gradients of APD ₉₀ in intact rabbit myocardium.....	106
Rate dependence of APD ₉₀ and APD ₉₀ restitution.....	107
The effect of low temperature	107
Limitations	108
Conclusions	109
Chapter 4: The effect of transmural activation sequence on action potential duration	110
Introduction	111
Transmural gradients of APD in intact myocardium	111
Electrotonic modulation of APD.....	111
The effect of activation sequence on APD.....	111
Gap junctions	112
Aims	113
Methods.....	114
Experimental protocols	114
Paired stimulation	114
Gap junction modifiers.....	114
Carbenoxolone	114
Rotigaptide	115
Data analysis	115
Statistical analyses	115
Results	116
The effect of transmural activation sequence.....	116
Transmural activation wavefronts and conduction velocity	116
The effect of transmural activation sequence on transmural dispersion	117
The effect of transmural activation sequence on transmural APD ₉₀	117
The relationship between activation time and transmural APD ₉₀	120
The effect of transmural activation sequence on epicardial APD ₉₀	123
The effect of paired stimulation on transmural APD ₉₀	126
The effect pharmacological modification of gap junction conductance on the transmural modulation of APD ₉₀	128
Carbenoxolone	128
Rotigaptide	128
The effect of activation sequence on transmural electrophysiology at low temperature	131

Transmural conduction velocity at low temperature.....	131
Modulation of transmural APD ₉₀ by activation sequence at low temperature.....	131
Discussion	133
The effects of transmural activation sequence on activation wavefronts and transmural conduction velocity	133
Transmural dispersion of repolarisation.....	133
Modulation of APD ₉₀ by activation sequence.....	134
The relationship between activation time and APD ₉₀	134
Modulation of epicardial APD ₉₀ by transmural activation sequence.....	136
Pharmacological gap junction modification.....	136
Carbenoxolone	136
Rotigaptide	137
Conclusions	138
Chapter 5: Transmural electrophysiology in heart failure	139
Introduction	140
Electrophysiological changes in heart failure	140
Action potential characteristics	140
Calcium cycling in heart failure	142
Intracellular sodium in heart failure	143
Changes in electrical coupling in heart failure.....	143
Structural changes in failing hearts	143
Transmural electrophysiology in heart failure	144
Heterogeneity of repolarisation in the rabbit coronary ligation model	144
Repolarisation alternans in heart failure	145
Aims	146
Methods.....	147
Heart failure model	147
Experimental protocols	147
Data analysis	147
Analysis of optical action potentials	147
Statistical analyses	148
Results	149
Left ventricular remodelling in heart failure.....	149
Transmural electrophysiology in remodelled myocardium	150
APD ₉₀ restitution in heart failure	152
Transmural electrophysiology in heart failure at low temperature	157

APD ₉₀ restitution at low temperature.....	158
Discussion	162
Characterisation of a heart failure syndrome following coronary ligation in the rabbit	162
The LV wedge preparation in ligated hearts	162
Viability	162
Tissue dimensions	163
Transmural electrophysiological heterogeneity in heart failure.....	163
Conduction velocity	163
Transmural APD ₉₀ in heart failure	164
Transmural dispersion of repolarisation and APD ₉₀ in heart failure.....	164
APD ₉₀ restitution in failing hearts.....	165
Transmural electrophysiology in heart failure at low temperature	166
Conduction into the infarct zone	166
Limitations	168
Conclusions	169
Chapter 6: Transmural repolarisation alternans in rabbit ventricular myocardium.....	170
Introduction	171
The role of gradients of repolarisation in spatially discordant alternans	171
Aims	173
Methods.....	174
Experimental protocols	174
Data analysis	174
AP characteristics.....	174
Statistical analysis	174
Results.....	175
Definition of significant alternans.....	175
Repolarisation alternans	177
Alternans of AP amplitude.....	177
Spectral analysis of alternans magnitude and phase	179
Heart rate dependence of repolarisation alternans	181
Spatially discordant alternans	183
Alternans magnitude and ventricular arrhythmia.....	185
Transmural patterns of repolarisation alternans	187
Temperature dependence of alternans in normal hearts.....	189
Repolarisation alternans on the epicardial surface.....	191

Discussion	192
Induction and detection of repolarisation alternans	192
Alternans induction protocols	192
Alternans analysis	192
Electrophysiological behaviour during alternans.....	194
Alternans of AP amplitude.....	195
Heart rate dependence of alternans	195
Spatially discordant alternans	196
Spatially discordant alternans and ventricular arrhythmia.....	197
Alternans magnitude and ventricular arrhythmia.....	197
Transmural electrophysiological heterogeneity	197
Spatially discordant alternans in the transmural axis.....	198
Temperature dependence of repolarisation alternans.....	199
Alternans occurring on the epicardial surface.....	200
Limitations	200
Conclusions	201
Chapter 7: Repolarisation alternans and arrhythmogenesis in heart failure	202
Introduction	203
Alternans in heart failure.....	203
Aims	204
Methods.....	205
Experimental protocols	205
Data analysis	205
Statistical analyses	205
Results.....	206
The occurrence of repolarisation alternans in heart failure.....	206
Spatially discordant alternans in heart failure	206
Extent and magnitude of repolarisation alternans in normal and failing hearts....	208
Transmural gradients of repolarisation alternans in heart failure	209
Alternans and APD ₉₀ restitution in heart failure	210
Transmural dispersion during alternans	210
Transmural dispersion of activation time.....	211
Transmural dispersion of repolarisation time	212
Transmural dispersion of APD ₉₀	213
Ventricular arrhythmias in heart failure.....	214
The relationship between alternans and ventricular arrhythmia	216

Concordant alternans and ventricular arrhythmias during rapid pacing	216
Discordant alternans and ventricular arrhythmias during rapid pacing	216
Alternans magnitude and ventricular arrhythmias	216
Discussion	218
The occurrence of repolarisation alternans in heart failure.....	218
Spatially discordant alternans in heart failure.....	218
Magnitude and extent of alternans in heart failure.....	219
Transmural gradients of alternans in heart failure	219
APD ₉₀ restitution and alternans in heart failure	219
Vulnerability to ventricular arrhythmia in heart failure	220
Spatially discordant alternans and re-entrant ventricular arrhythmia	220
Limitations	220
Conclusions	221
Chapter 8: Summary and conclusions	222
Rationale for the current study.....	223
Aims and hypotheses	223
Baseline electrophysiology in normal rabbit ventricular myocardium.....	224
Electrophysiology in intact ventricular tissue	224
Transmural heterogeneity of repolarisation	224
Modulation of APD ₉₀ by activation sequence.....	225
Electrophysiological changes as a consequence of heart failure	225
The occurrence of repolarisation alternans	226
Spatially discordant repolarisation alternans	226
Repolarisation alternans as a mechanism of ventricular arrhythmia in heart failure....	227
Future directions.....	228
Conclusions	229
References	230
Appendix	253

List of Tables

Table 1.1 Published prospective observational studies of the predictive value of MTWA testing	31
Table 1.2 Distribution of all-cause mortality by MTWA test result	33
Table 1.3 Cause specific mortality by MTWA in Chow <i>et al</i> ⁵⁴	33
Table 3.1 Baseline transmural electrophysiology	86
Table 3.2 Transmural APD ₉₀ restitution curve characteristics.....	93
Table 3.3 Transmural electrophysiology at low temperature.....	95
Table 3.4 Transmural APD ₉₀ restitution curve characteristics at 30°C	99
Table 3.5 A comparison of transmural and epicardial dispersion.....	101
Table 3.6 A comparison of transmural and epicardial dispersion at low temperature.....	103
Table 4.1 Effect of activation sequence on transmural dispersion of activation, repolarisation and APD ₉₀	117
Table 5.1 Animal weights and LV wedge dimensions	149
Table 5.2 Left ventricular remodelling in heart failure.....	149
Table 5.3 Transmural electrophysiology in normal and failing hearts	150
Table 5.4 Transmural APD ₉₀ restitution curve characteristics in normal and heart failure	156
Table 5.5 The effect of temperature on transmural electrophysiology in heart failure.....	157
Table 5.6 Transmural electrophysiology at low temperature in normal and failing hearts	158
Table 5.7 Action potential characteristics in the border zone and infarct zone	160
Table 6.1 Contingency table for alternans magnitude and mean change in APD ₉₀	175
Table 6.2 A comparison of the magnitude and extent of alternans during concordant and discordant alternans.....	183
Table 6.3 Transmural patterns of alternans.....	188
Table 6.4 A comparison of the magnitude and extent of alternans across the transmural and epicardial surfaces	191
Table 7.1 APD ₉₀ restitution curve characteristics in alternans prone and resistant sites in normal and failing hearts.....	210
Table 7.2 Magnitude and extent of alternans according to the subsequent occurrence of ventricular arrhythmia.....	217

List of Figures

Figure 1.1 The spectral analytic method for the detection of alternans	26
Figure 1.2 Microvolt T-wave alternans.....	27
Figure 1.3 The determinants of cellular repolarisation	37
Figure 1.4 Theory of the production of APD alternans by AP restitution (Adapted from Nolasco and Dahlen ⁷⁸)	39
Figure 1.5 Potential mechanisms of discordant repolarisation alternans.....	44
Figure 2.1 Survival following surgical coronary arterial ligation in rabbits.....	56
Figure 2.2 The method for producing the left ventricular wedge preparation	59
Figure 2.3 The LV wedge preparation mounted for optical imaging	60
Figure 2.4 Perfusion of the LV wedge preparation assessed by TTC staining	61
Figure 2.5 Stability of transmural optical APs over time.....	62
Figure 2.6 The gradient of epicardial APD ₉₀ relative to the cut surface.....	63
Figure 2.7 Optical mapping system	68
Figure 2.8 Analysis of AP characteristics	74
Figure 2.9 Spectral analysis to quantify repolarisation alternans	77
Figure 3.1 Transmural optical action potentials.....	86
Figure 3.2 Transmural APD ₉₀ in isolated cells and intact myocardium	88
Figure 3.3 Mean APD restitution	89
Figure 3.4 Regional APD ₉₀ at rapid stimulation rates.....	91
Figure 3.5 Magnitude of the transmural APD ₉₀ gradient during rapid stimulation	92
Figure 3.6 Transmural APD ₉₀ restitution	93
Figure 3.7 Transmural APD ₉₀ restitution	94
Figure 3.8 Regional APD ₉₀ at rapid stimulation rates at low temperature.....	96
Figure 3.9 Magnitude of the transmural APD ₉₀ gradient during rapid stimulation at low temperature.....	97
Figure 3.10 The temperature dependence of APD ₉₀ restitution.....	98
Figure 3.11 Transmural APD ₉₀ restitution at low temperature	100
Figure 3.12 A comparison of transmural and epicardial APD ₉₀ restitution.....	102
Figure 3.13 A comparison of transmural and epicardial APD ₉₀ restitution at low temperature.....	104
Figure 4.1 Transmural activation wavefronts during endocardial and epicardial stimulation	116
Figure 4.2 Modulation of transmural APD ₉₀ by activation sequence	118
Figure 4.3 The effect of activation sequence on transmural APD ₉₀	119

Figure 4.4 Transmural APD ₉₀ as a function of mean activation time	120
Figure 4.5 Linear regression of the relationship between APD ₉₀ and activation time.....	121
Figure 4.6 Partitioning of APD ₉₀ data by activation time.....	122
Figure 4.7 Mean transmural APD ₉₀ by activation time.....	123
Figure 4.8 Activation sequence and epicardial APD ₉₀	124
Figure 4.9 The effect of activation sequence on subepicardial and epicardial APD ₉₀	125
Figure 4.10 The effect of activation sequence on epicardial APD ₉₀	125
Figure 4.11 The effect of paired stimulation on transmural APD ₉₀	127
Figure 4.12 The effects of gap junction uncoupling with carbenoxolone.....	129
Figure 4.13 The effect of rotigaptide on transmural conduction velocity and APD ₉₀	130
Figure 4.14 The temperature dependence of transmural conduction velocity	131
Figure 4.15 The temperature dependence of APD ₉₀	132
Figure 5.1 Measurement of conduction velocity into the infarct	148
Figure 5.2 The transmural pattern of APD ₉₀ in normal and failing hearts.....	151
Figure 5.3 Transmural APD ₉₀ gradient during rapid stimulation in normal and failing hearts	151
Figure 5.4 Mean APD ₉₀ restitution in normal and failing hearts	153
Figure 5.5 Transmural APD ₉₀ restitution in failing hearts	154
Figure 5.6 Transmural APD ₉₀ restitution curves in normal and failing hearts	155
Figure 5.7 The temperature dependence of APD ₉₀ restitution in heart failure	159
Figure 5.8 Transmural conduction into the infarct.....	161
Figure 5.9 Rationale for the border zone delay during epicardial stimulation.....	168
Figure 6.1 Correlation of spectral alternans magnitude with change in APD ₉₀ during alternans	176
Figure 6.2 Mean change in APD ₉₀ in the absence of alternans.....	176
Figure 6.3 Transmural repolarisation alternans	178
Figure 6.4 Alternans magnitude and phase	180
Figure 6.5 Heart rate dependence of repolarisation alternans.....	182
Figure 6.6 An example of ventricular arrhythmia induced during alternans	185
Figure 6.7 Episodes of spatially discordant alternans.....	186
Figure 6.8 Transmural repolarisation alternans	189
Figure 6.9 The effect of activation sequence on transmural patterns of alternans.....	190
Figure 7.1 The occurrence of repolarisation alternans in normal and failing hearts.....	207
Figure 7.2 The magnitude and extent of transmural repolarisation alternans in normal and failing hearts.....	208
Figure 7.3 Transmural alternans magnitude in normal and failing hearts	209

Figure 7.4 The relationship between transmural dispersion of activation time and cycle length.....	211
Figure 7.5 The relationship between transmural dispersion of repolarisation time and cycle length.....	212
Figure 7.6 The relationship between transmural dispersion of APD ₉₀ time and cycle length	213
Figure 7.7 Inducibility of ventricular arrhythmias in failing and normal hearts.....	215

Acknowledgements

This research has been one of the most challenging and enjoyable times of my professional life, and I am extremely grateful to all those who have been a part of it. The study was funded by the British Heart Foundation, and I am thankful for their generosity.

I am indebted to Professor Stuart Cobbe, not only for the opportunity to undertake this research, but also for his insightful supervision and unfailing professional support. An aspiring clinician scientist could not have asked for a better role model. The contribution made by Professor Godfrey Smith is impossible to overstate. His intellect and enthusiasm have challenged and sustained me on a daily basis, and the scientific integrity of this work is in large part down to his tireless availability. Most importantly, Godfrey has taught me about the type of academic I aspire to be. This research would not have been possible without Dr Francis Burton. His technical skill and brilliant programming have been the cornerstones of the work. More than this, Francis has made me laugh during the darkest of experiments. Dr Ole Johan Kemi has been calm and patient at times when I am neither. Mrs Aileen Rankin has looked after my lab and looked out for me.

In related projects, I have been fortunate enough to work with Professor John McMurray, who is an inspiration. Dr Mark Petrie has given me much-valued support and encouragement. I am grateful to Dr Colette Jackson, who has shared my enthusiasm for alternans as well as a few late nights in the office.

My friends have heard more about this thesis than they ever wanted to, and have listened nonetheless. Karen is always right about life, and she and Alan have provided refuge on countless occasions. I would have struggled (much more) without Gillian's sense of humour and common sense. I have relied on Bean for more than his reassuring brand of realism, and he has put up with me regardless.

I am truly lucky to find four of my best friends in my brother David, his fiancé, Kirsty and my parents, Grant and Marian. Any achievement of mine is built upon the foundation my parents have provided, and I cannot thank them enough.

Declaration

The work presented in this thesis is original and my own except where otherwise acknowledged. None of the work presented has been submitted for the fulfilment of any other degree. Coronary ligation procedures and echocardiography were carried out by Mr Michael Dunne and the late Dr Martin Hicks. Dr Francis Burton assisted in all the CCD-based optical imaging experiments and wrote the analysis software used. The single cell data shown in Chapter 3 were provided by Dr Marie MacIntosh. The rotigaptide used in the experiments discussed in Chapter 4 was provided by Professor David Newby and Dr Ninian Lang. The two-photon experiments described in the appendix were developed and performed with Professor Godfrey Smith and Dr Ole Johan Kemi.

Publications arising from this work:

Is Microvolt T-wave alternans the answer to risk stratification in heart failure?

RC Myles, CE Jackson, I Tsorlalis, MC Petrie, J JV McMurray and SM Cobbe.

Circulation. 2007;116:2984-91.

The link between repolarisation alternans and ventricular arrhythmia: does the cellular phenomenon extend to the clinical problem?

RC Myles, FL Burton, SM Cobbe and GL Smith. *J. Mol. Cell. Cardiol.* 2008;41:1-10.

Repolarization alternans in ventricular arrhythmia in a rabbit model of heart failure.

RC Myles, FL Burton, SM Cobbe and GL Smith. *Heart Rhythm* 2008; 5 Supplement (May 2008): S113.

CCD-based and 2P confocal measurements of electrical alternans on the epicardial surface of isolated perfused rabbit left ventricle using voltage sensitive dyes.

RC Myles, OJ Kemi, FL Burton, SM Cobbe and GL Smith. *Biophysical Journal* 2008 Supplement, 600a, Abstract, 2995-Pos.

The vascular effects of rotigaptide in vivo in man.

NN Lang, **RC Myles**, FL Burton, DP Hall, YZ Chin, NA Boon, DE Newby.

Biochem Pharmacol. 2008; 76(10):1194-200.

Presentations of this work:

Vulnerability to repolarisation alternans in failing rabbit hearts.

RC Myles, FL Burton, GL Smith and SM Cobbe. *Medical Research Society* 2008.

Transmural patterns of action potential duration are altered by activation sequence.

RC Myles, FL Burton, SM Cobbe and GL Smith. *Proc LifeSciences* 2007, PC 357.

Transmural discordant repolarisation alternans in rabbit ventricular myocardium.

RC Myles, FL Burton, SM Cobbe and GL Smith. *Scottish Society for Experimental Medicine* 2007.

Microvolt T-wave alternans: a mechanism for arrhythmogenesis?

RC Myles, Invited Lecture, Norwegian Cardiac Society Winter Meeting 2007.

Abbreviations

ABCD	Alternans before cardioverter defibrillator
ACEi	Angiotensin converting enzyme inhibitors
ACM	All-cause mortality
AF	Atrial fibrillation
ALPHA	Microvolt T-wave Alternans in Patients with Heart Failure
ANOVA	Analysis of variance
AP	Action potential
APA	Action potential amplitude
APD	Action potential duration
APD ₉₀	Action potential duration at 90% repolarisation
ARI	Activation recovery interval
AT	Activation time
ATP	Adenosine triphosphate
BDM	2,3 butanendione monoxime
BNP	Brain natriuretic peptide
Ca ²⁺	Calcium
[Ca ²⁺] _i	Intracellular calcium concentration
Ca ²⁺ _T	Calcium transient
CCD	Charge coupled device
CHD	Coronary heart disease
CHF	Chronic heart failure
CICR	Calcium induced calcium release
Cl ⁻	Chloride
CL	Cycle length
CO ₂	Carbon dioxide
CV	Conduction velocity

Cx	Connexin
DC	Direct current
DI	Diastolic interval
DOR	Dispersion of repolarisation
EC	Excitation contraction
ECG	Electrocardiogram
EPS	Electrophysiological study
HR	Heart rate
Hz	Hertz
I_{CaL}	L-type calcium current
I_{NaCa}	Sodium calcium exchange current
ICD	Implantable cardioverter defibrillator
IVS	Interventricular septum
K^+	Potassium
KCl	Potassium chloride
kHz	kilohertz
LA	Left atrium
LAD	Left atrial diameter
LMCA	Left main coronary artery
LQTS	Long QT syndrome
LTCC	L-type calcium channel
LV	Left ventricle
LVEDD	Left ventricular end diastolic diameter
LVEF	Left ventricular ejection fraction
LVH	Left ventricular hypertrophy
LVSD	Left ventricular systolic dysfunction
MADIT	Multicenter Automatic Defibrillator Implantation Trial

MAP	Monophasic action potential
MASTER	Microvolt T-Wave Alternans Testing for Risk Stratification of Post MI Patients
MI	Myocardial infarction
MMA	Modified moving average
mmol/L	Millimoles per litre
ms	Milliseconds
MTWA	Microvolt T-wave alternans
Na ⁺	Sodium
[Na ⁺] _i	Intracellular sodium concentration
NCX	Sodium calcium exchange
NHE	Sodium hydrogen exchange
NPV	Negative predictive value
NS	Non-significant
NYHA	New York Heart Association
O ₂	Oxygen
PDA	Photodiode array
PMT	Photomultiplier tube
PPV	Positive predictive value
RT	Repolarisation time
RV	Right ventricle
RVOT	Right ventricular outflow tract
RyR	Ryanodine receptor
SCD	Sudden cardiac death
SCD-HeFT	Sudden Cardiac Death in Heart Failure Trial
SEM	Standard error of the mean
SERCA	Sarcoplasmic reticulum ATPase
S/N	Signal to noise

SR	Sarcoplasmic reticulum
TNF α	Tumour necrosis factor alpha
TTC	Triphenyl tetrazolium chloride
TWA	T-wave alternans
V _m	Membrane potential
VA	Ventricular arrhythmia
VER	Ventricular electrical remodelling
VF	Ventricular fibrillation
VGNa	Voltage-gated sodium channel
VT	Ventricular tachycardia
VTE	Ventricular tachyarrhythmic events

Chapter 1: Introduction

Sudden cardiac death in heart failure

Heart failure is a common condition which is associated with an extremely high mortality¹. It is a diverse, complex clinical syndrome in which patients are exposed to competing risks, of sudden arrhythmic death or death from progressive pump failure². Prevention of arrhythmic sudden cardiac death (SCD) constitutes a particular challenge because accurate risk prediction is difficult in such a large and heterogeneous population³. Achieving effective prevention of SCD in heart failure is one of the principal challenges facing contemporary cardiovascular medicine.

The prevalence of SCD in heart failure

Defining and classifying SCD

Sudden cardiac deaths are, by definition, unexpected and so are often unwitnessed, making the classification of the exact cause of death difficult in many cases. Estimates of the prevalence of SCD in heart failure come mainly from observational studies or from clinical trials, in which the definition of SCD is necessarily both arbitrary and pragmatic⁴. The accepted definition is death from a cardiac cause which is sudden and unexpected, in the absence of progressive cardiac deterioration, either within one hour of cardiac symptoms, in bed during sleep or within 24 hours of last being seen alive⁵. Where these tight definitions in endpoint classification are used, as much as 50% of total mortality in heart failure is due to SCD⁶.

Aetiology of SCD in heart failure

Sudden cardiac death may be caused by a number of different underlying pathologies, including ventricular arrhythmia, acute cardiogenic shock, tamponade, acute pulmonary embolism. The relative importance of arrhythmic or vascular events as causes of SCD in heart failure is debated⁷. Data regarding the specific aetiology of SCD are difficult to gather, but where they are available, recordings from monitored episodes of SCD show that the cause is ventricular arrhythmia in around 85% of cases⁸. It is therefore reasonable to conclude that the majority of SCD in heart failure is arrhythmic in nature.

The main substrate for ventricular arrhythmia in heart failure is left ventricular (LV) remodelling, which includes varying degrees of scar formation, chamber dilatation and hypertrophy, depending on the aetiology of heart failure⁹. Electrophysiological changes

have been shown to accompany LV remodelling in both human hearts and animal models¹⁰. In man, pharmacological attenuation of LV remodelling is associated with a reduction in mortality¹¹. Coronary heart disease (CHD) is among the most common causes of heart failure¹² and patients with heart failure and CHD remain at risk of acute myocardial ischaemia and myocardial infarction (MI), either of which may trigger ventricular arrhythmia. Autopsy studies suggest that acute coronary events are implicated in around 50% of sudden deaths in heart failure patients¹³. Optimal pharmacological therapy for low ejection fraction heart failure now includes renin-angiotensin-aldosterone system blockade¹⁴, often with multiple agents and in addition to diuretic therapy, in patients who commonly have impaired renal function¹⁵. These combinations may precipitate electrolyte abnormalities, particularly abnormalities of serum potassium, which can predispose to ventricular arrhythmia.

Prevention of SCD in heart failure

Pharmacological therapy

Until recently, attempts to prevent SCD have relied upon pharmacological therapy to reverse LV remodelling. Disease modifying therapy with β-blockers^{16;17}, angiotensin-converting enzyme inhibitors (ACEi)¹¹, angiotensin receptor blockers¹⁸ and aldosterone antagonists¹⁹ modestly reduces the risk of SCD in patients with heart failure and after MI. However, even patients on optimal medical therapy remain at high risk of SCD^{6;18} and more specific anti-arrhythmic therapy has failed to improve survival²⁰⁻²².

Implantable cardioverter-defibrillator

The treatment of ventricular arrhythmia has been revolutionised by the implantable cardioverter-defibrillator (ICD)²³ which is extremely effective in treating the majority of ventricular arrhythmias²⁴. However, ICD implantation has numerous potential complications and it is estimated that as many as one-quarter of those who receive an ICD will experience a complication over a 5-year period²⁵. ICD therapy is also associated with significant financial costs²⁶.

Secondary prevention

The indication for ICD implantation in survivors of a life-threatening ventricular tachyarrhythmia (secondary prevention) is clear cut²⁷. These patients are at high risk and a favourable risk: benefit ratio has been well demonstrated^{28;29}. Also, the secondary

prevention population is relatively small and readily identified, thus the financial costs are not insurmountable³⁰.

Primary prevention

The majority of victims of SCD do not experience a prior arrhythmic event to identify them as high risk³¹, and because of this, a primary prevention ICD strategy is also required. A significant mortality benefit has been demonstrated in large randomised controlled trials of prophylactic ICD therapy in patients with a low left ventricular ejection fraction (LVEF) and a history of either chronic heart failure ²²or MI³². Analyses based on these results have suggested an acceptable cost-effectiveness profile for primary prevention ICD therapy³³. However, the available evidence suggests that selection for ICD therapy on the basis of LVEF alone is inefficient. For example, in the largest published trial, the Sudden Cardiac Death in Heart Failure Trial (SCD-HeFT), 79% of patients in the ICD arm did not use their device over the first five years²². Moreover, the absolute risk reduction in the group randomised to ICD implantation was modest (7.2% over 5 years). This suggests that there is scope for better definition of the target population and underscores the need for improved risk stratification to achieve substantial mortality benefit without prohibitive cost or the morbidity related to unnecessary device implantation³.

Risk stratification for SCD in heart failure

Although ICDs have reduced the risk of SCD, they are expensive and can be associated with significant morbidity, hence precisely targeting their use is crucial. None of the many available non-invasive risk stratification tools have the required sensitivity or specificity for predicting SCD^{31;34}. The challenge of delivering effective population-wide prevention of SCD through ICD therapy is dependent upon the development of improved risk stratification techniques. The use of microvolt T-wave alternans (MTWA) testing provides a potential solution to this complex problem.

Microvolt T-wave alternans

Background

T-wave alternans (TWA) describes regular fluctuations in the amplitude, morphology or polarity of the ECG T-wave which occur on an every-other-beat basis. Macroscopic TWA is relatively rare in clinical practice, but nonetheless has been anecdotally noted to occur immediately prior to the onset of ventricular arrhythmia³⁵. Building on this association,

Cohen and colleagues have developed ECG signal-processing techniques which are able to resolve TWA at the microvolt-level^{36;37}. In initial clinical studies, MTWA during atrial pacing was measured during cardiac electrophysiological studies (EPS) in selected patients being evaluated for risk of SCD. The occurrence of MTWA below a threshold heart rate was associated with an increased risk of spontaneous ventricular arrhythmia during follow-up³⁸. Since, there has been an interest in developing MTWA testing for widespread clinical use and in determining whether it may be useful as a non-invasive risk stratification tool for patients at risk of SCD.

Methodology

Spectral MTWA testing

MTWA testing is now usually performed during a heart rate limited exercise, using a commercially available system (CH2000TM or HearTWaveTM, Cambridge Heart), which employs an automated spectral analysis algorithm to detect alternans. Similar algorithms can be used to detect action potential (AP) alternans in experimental recordings, or alternans in intracardiac electrogram recordings from ICD traces or during EPS. The spectral analytic method for alternans detection is illustrated in Figure 1.1. Firstly, a series of ECG complexes are recorded at a stable heart rate. They are then aligned by the QRS complex and the amplitude of each T-wave at the same time with respect to the QRS complex is plotted. These data are then transformed to the frequency domain, using a Fast Fourier Transform, which determines the magnitude of T-wave fluctuation occurring on alternate beats (i.e. a frequency of 0.5 cycles/beat)³⁹. This process is then repeated for each point along the ECG T-wave and spectral power at the alternans frequency for the whole T-wave is then noise-corrected and averaged for each ECG lead. If sufficient alternans is sustained at heart rates <110bpm, the test is deemed positive.

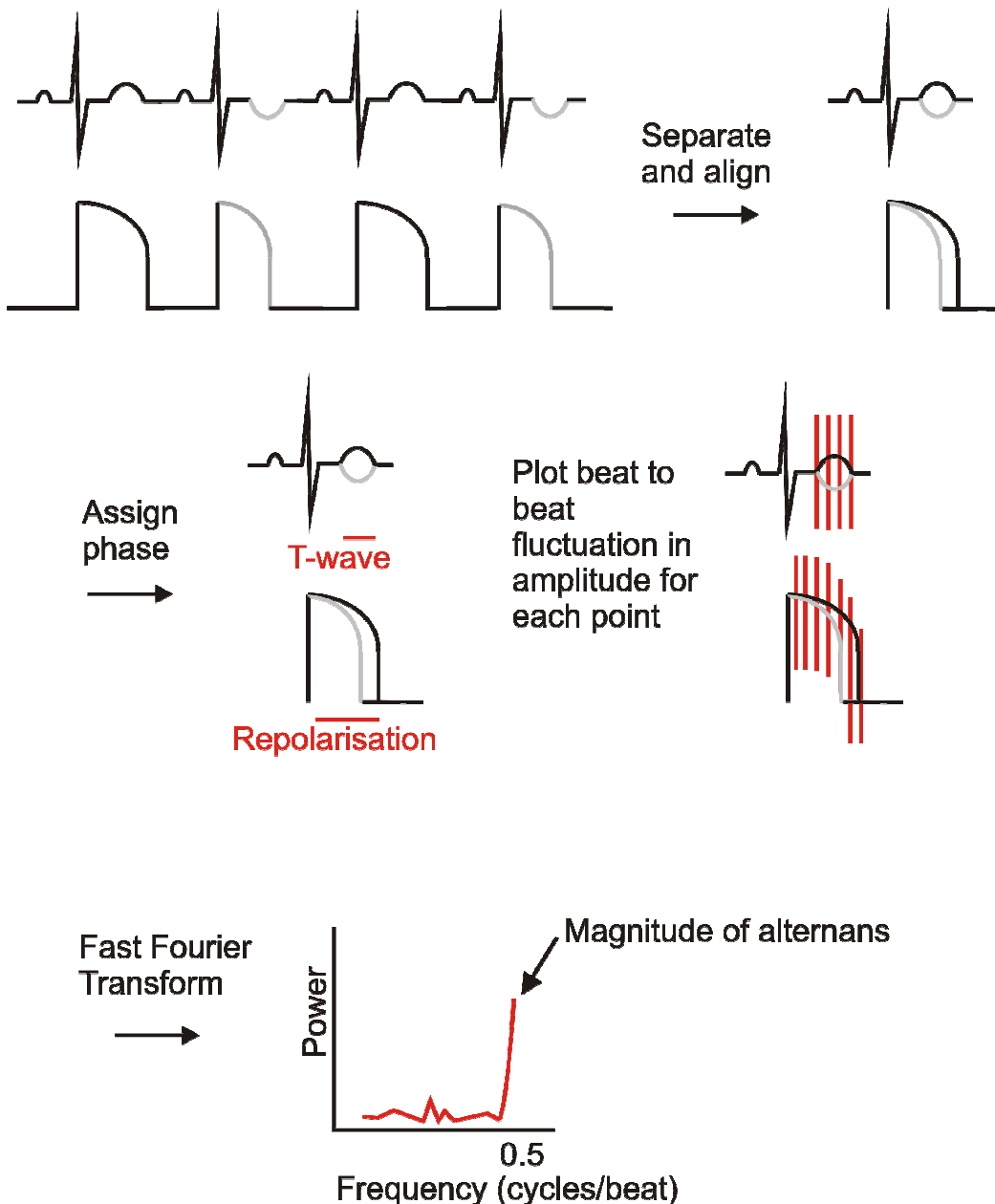


Figure 1.1 The spectral analytic method for the detection of alternans

An illustration of the determination of alternans by the spectral method for the ECG T-wave and the cardiac action potential. ECG or action potential traces for each beat are separated and consecutive traces are aligned, by stimulus artefact for APs and by QRS complex for ECG traces. The section of the trace to be analysed is then determined. For ECG traces the section from the end of the QRS complex to the end of the T-wave is interrogated. For AP traces arbitrary definitions of depolarisation and repolarisation are required. In published algorithms depolarisation is defined by a 8ms window centred on the maximum upstroke, and the remaining part of the trace is designated as repolarisation⁴⁰. The designated sections of the superimposed traces are then sampled at different points in time and the amplitude of each trace at that point is plotted. This results in a plot of trace amplitude fluctuation over time for each point along the trace. These data are then transformed to the frequency domain, usually using a Fast Fourier Transform. The power of the frequency spectrum at 0.5 cycles per beat indicates the magnitude of trace fluctuation occurring on an every-other-beat basis, and therefore indicates the magnitude of T-wave, or repolarisation alternans.

Absence of MTWA at a heart rate of 110bpm constitutes a negative test. A test satisfying neither set of criteria is classified as “indeterminate”. The system presents the data, along with an automated classification, as shown in Figure 1.2. Indeterminate test results occur relatively frequently (20-50%) and are commonly caused by ectopy, excessive motion artefact or inability to reach target HR. MTWA testing by this method is not applicable to patients in atrial fibrillation (AF) as the irregularity of the R-R intervals confounds the frequency analysis. Small studies have shown high short term reproducibility⁴¹, but little is known about the reproducibility of MTWA testing outside a timescale of a few hours⁴².

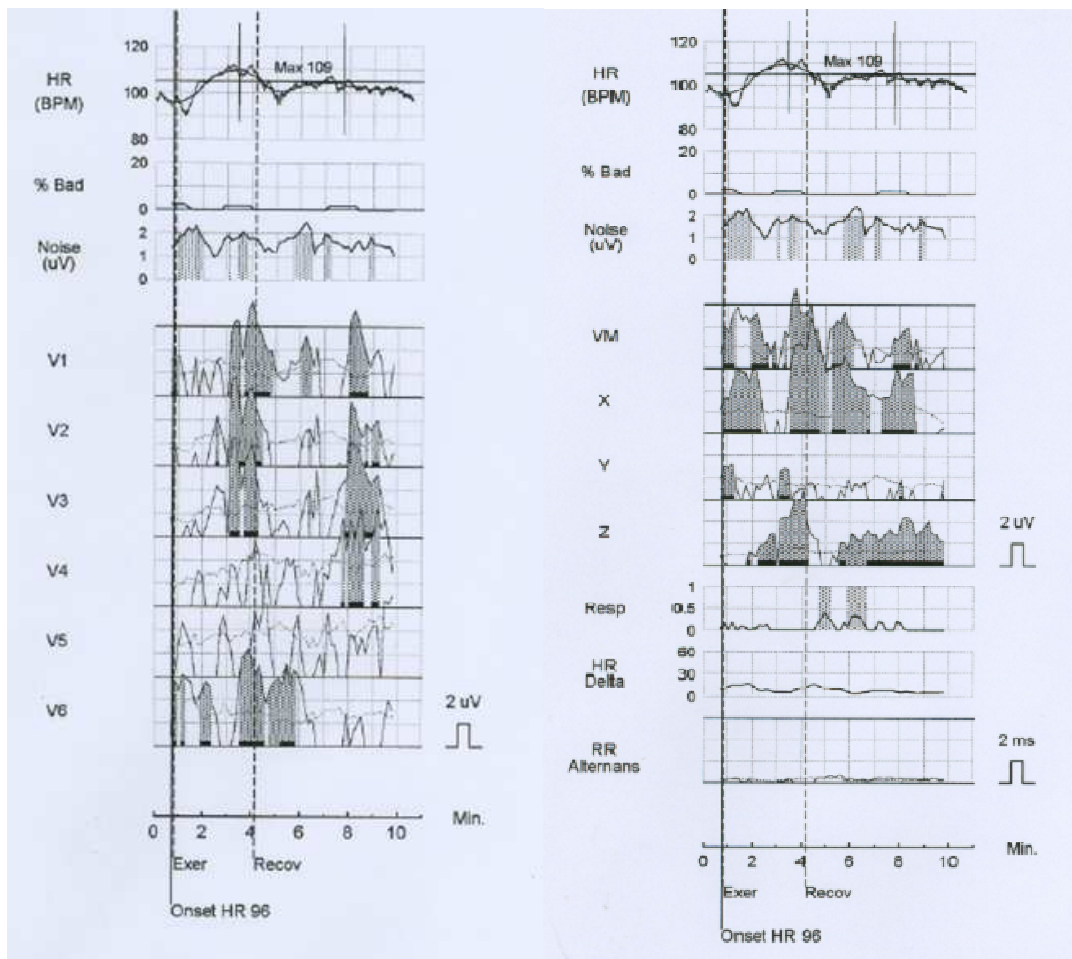


Figure 1.2 Microvolt T-wave alternans

An example of an Alternans Report Classification, showing a positive MTWA result, courtesy of Dr Colette Jackson. Left panel shows from top: smoothed heart rate (HR) profile, percentage irregular (“bad”) beats and noise levels over the duration of the test. Alternans magnitude recorded from the six chest leads is then shown, with significant alternans shaded in grey. The right panel shows HR, bad beats and noise as before, then alternans magnitude from the orthogonal leads. The last three panels show potential sources of false alternans- respiratory variations, changes in HR and any R-R interval alternans.

Time-domain analytic methods

Microvolt T-wave alternans can also be measured by methods which employ averaging in the time-domain rather than the frequency-domain. One such system is the modified moving average (MMA) method⁴³. In MMA analysis a 15 second stream of ECG complexes is sampled and divided into odd and even beats. An averaged morphology is then calculated for odd and even beats. The difference in amplitude between the averaged odd and even beat is then used to calculate the magnitude of alternans. This method has some practical advantages over the spectral method, in that it is applicable to patients with AF, and that it can be analysed from ambulatory ECG records. This makes MMA testing potentially more widely applicable, simpler to implement and would theoretically allow simultaneous assessment of autonomic function and ambient arrhythmias in a single test. MTWA testing by this method has been validated in atrial pacing studies⁴⁴ and Holter-based testing has been correlated with arrhythmic risk in retrospective cohorts⁴⁵. However, there are no prospective data regarding the prognostic utility of MTWA testing by this method.

Predictive value of MTWA

The studies which have assessed the predictive value of MTWA testing during exercise in patients with sinus rhythm are summarised in Table 1.1. Predictive value is presented both in terms of the risk of events (relative risk or hazard ratio) and in terms of the positive and negative predictive value. The positive predictive value (PPV) describes the proportion of patients who experience an event who are correctly identified as at risk by the test. The negative predictive value (NPV) describes the proportion of those who do not experience an event who were correctly identified as being at low risk by the test. A value as close as possible to 100% is desirable for each. It should be noted that in an early study, indeterminate MTWA test results were common and those patients were found to have similar event rates to the group with positive tests, so these groups were pooled and designated as abnormal (or non-negative)⁴⁶. In the majority of studies discussed here, the comparison is made between negative and non-negative (positive or indeterminate) tests.

Following myocardial infarction

Three studies have investigated the prognostic utility of MTWA in patients following MI, regardless of LVEF. The largest enrolled 850 consecutive patients and found that MTWA predicted SCD or resuscitated VF, although the event rate in this population was low at 3%⁴⁷. Another large study confirmed this result in patients with preserved LVEF following

MI⁴⁸. Two smaller studies have suggested that MTWA is not prognostically useful after MI. In one, 140 consecutive patients were investigated in the first 30 days following MI, and MTWA result did not predict events (death or ventricular tachyarrhythmic events [VTE])⁴⁹. The second examined the predictive value of MTWA for all-cause mortality (ACM), 17% were MTWA positive and none of the 26 deaths occurred in this group⁵⁰.

MADIT-II eligible patients

Three studies specifically selected patients meeting MADIT-II entry criteria (previous MI, LVEF ≤ 30% without prior VF/VT). In 129 such patients, none of the twelve who experienced SCD or resuscitated VF were in the MTWA negative group⁵¹. In a subgroup analysis of a larger study, 177 patients meeting MADIT-II criteria had MTWA tests classified as abnormal (positive/indeterminate, 68%), or normal (negative, 32%), and again the event rate in the MTWA negative group was low⁴⁶. However, results from the Microvolt T-Wave AlternanS Testing for Risk Stratification of Post MI Patients (MASTER)-I study, suggest the NPV in MADIT-II eligible patients may not be so high. MASTER-1 performed MTWA testing on 654 MADIT-II eligible patients, all of whom then underwent ICD implantation. MTWA test result (negative vs. non-negative) did not predict the primary endpoint of arrhythmic death or appropriate ICD discharge⁵².

Ischaemic left ventricular systolic dysfunction

Three studies have specifically examined the prognostic value of MTWA in patients with ischaemic LVSD. The first performed MTWA testing in 144 non-consecutive patients referred for cardiac EPS⁵³. A positive MTWA test did not predict the primary endpoint (death/VTE) in the primary prevention subgroup. The second study examined 768 consecutive patients with CHD and LVSD⁵⁴. The authors analysed positive and indeterminate tests together and separately, addressed cause-specific mortality as a secondary endpoint and performed a more extensive multivariable analysis than has been seen in other studies. A non-negative MTWA test independently predicted all-cause mortality (HR 2.24 [95% CI:1.34-3.75]) and arrhythmic mortality (HR 2.29 [95% CI:1.0-5.24]) in the whole population. The Alternans Before Cardioverter Defibrillator (ABCD) study recruited 566 patients with ischaemic LVSD and NSVT, and compared the ability of MTWA and EPS to predict VTE. Preliminary results show that the 1-year event rate was lowest when both tests were negative (2.3%), highest when both were abnormal (12.6%) and intermediate when only one test was abnormal (MTWA non-negative 5%; EPS abnormal 7.5%). Appropriate ICD therapies (shock or anti-tachycardia pacing) accounted

for the majority (55/65) of endpoints. However, ICD implantation was not mandated if both tests were normal, and so patients in this group ($n = 99$) may have been less likely to reach an endpoint. Furthermore, as appropriate ICD therapies occur more frequently in patients with ICDs than do sudden deaths in patients without ICDs, a significant proportion of the endpoints in this study may have been attributable to subclinical arrhythmias⁵⁵.

Left ventricular systolic dysfunction, irrespective of aetiology

One study recruited 549 patients with LVSD, including patients with ischaemic ($n = 267$) and non-ischaemic ($n = 282$) cardiomyopathy⁵⁶. The primary endpoint was a composite of death and VTE. Over 20 months, there were 2 deaths and 2 ICD discharges in the normal MTWA group ($n = 189$) compared with 38 deaths and 9 ICD discharges in the abnormal group ($n = 360$) (the proportion with an ICD in each group was the same).

Non-ischaemic left ventricular systolic dysfunction

Three studies have examined the prognostic utility of MTWA in non-ischaemic cardiomyopathy. The first performed MTWA testing in 104 patients and concluded that a positive MTWA test was associated with VTE⁵⁷. However, the number of endpoints was very small ($n = 12$), as was the sample size, limiting the multivariable analysis. The second study recruited 137 patients and compared MTWA with other arrhythmic markers⁵⁸. MTWA was the only independent predictor of VTE after a mean of 14 months follow-up. However, the multivariable model did not include age or LVEF. The cohort included patients with an ICD (27%), mostly for prior ventricular arrhythmia, limiting extrapolation of these results to a primary prevention population. The largest study ($n = 263$) excluded secondary prevention patients and conducted longer follow-up⁵⁹. A positive MTWA test was not associated with the occurrence of VTE.

Population /Study	n	Mean Age (years)	Mean LVEF (%)	Prior VA (%)	Pre-test βblocker stopped?	MTWA result (%)			Event	Mean FU (months)	n=	Predictive Value		
						Positive	Indeterminate	Negative				RR/HR [§] (95%CI)	PPV	NPV
Prior myocardial infarction														
Ikeda ⁴⁷	850	63	NA	0	NA	36	13 [†]	51	SCD/ VF	25	25	RR 5.9 [§] (1.6-21)	7%	99%
Schwab ⁴⁹	140	60	56	0	One dose	20	27 [†]	53	Death/ VTE	15	3	NS	4%	97%
Tapanainen ⁵⁰	323	62	45	0	No	17	38	45	ACM	14	26	NS	0%	99%
Ikeda ⁴⁸	1041	64	55	0	No	17	9	74	VTE	32	18	19.7 [§]	9%	99%
Low LVEF with prior myocardial infarction														
Hohnloser ⁵¹	129	63	26	0	NA	60	13	27	SCD/ VF	17	12	RR 5.5	13%	99%
Bloomfield ⁴⁶	177	61	23	0	No	27	41	32	ACM	20	20	HR 4.8 (1.1-20)	NA	NA
Low LVEF with coronary heart disease														
Rashba ⁵³	144	64	28	39	>24hrs	49	25	26	ACM/ VTE [‡]	17	50	HR 2.2 [§] (1.1-4.7)	40%	84%
Chow ⁵²	768	~67	~27	0	>24hrs	46	21	33	ACM	18	99	HR 2.2 [§] (1.3-3.8)	15%	92%
Low LVEF														
Bloomfield ⁵⁶	549	56	25	0	No	29	35	36	ACM/ VTE [‡]	20	51	HR 6.5 [§] (2.4-18)	13%	98%
Low LVEF without coronary heart disease														
Kitamura ⁵⁷	104	52	41	0	NA	44	20 [†]	36	VTE	21	12	RR 8.9 [§] (2-34)	38%	95%
Hohnloser ⁵⁸	137	55	29	20	NA	48	27 [†]	25	VTE [‡]	14	18	RR 3.4 [§]	22%	94%
Grimm ⁵⁹	263	~49	~30	0	>24hrs	52	21	27	VTE	52	38	NS	13%	90%
Heart failure with low LVEF														
Baravelli ⁶⁰	73	64	36	10	>48hrs	41	23 [†]	36	VTE [‡]	17	8	∞	24%	100%
Sarzi ⁶¹	46	59	29	0	NA	52	20 [†]	28	Cardiac death	19	7	NA	30%	100%
Klingenheben ⁶²	107	56	28	0	NA	49	20	31	VTE	14	13	∞	21%	100%

ACM, all-cause mortality; CI, confidence interval; FU, follow-up; HR, hazard ratio; LVEF, left ventricular ejection fraction; NA, not available; NPV, negative predictive value; NS, not significant; PPV, positive predictive value; RR, relative risk; SCD, sudden cardiac death; VTE, ventricular tachyarrhythmic events. [†]excluded, [‡]including ICD therapies, [§]multivariable.

Table 1.1 Published prospective observational studies of the predictive value of MTWA testing

Symptomatic heart failure with low LVEF

A number of small studies have suggested that MTWA testing is useful in patients with low ejection fraction heart failure⁶⁰⁻⁶². However, these studies are small, appear to be highly selected, and lack proper multivariable adjustment. Two larger studies have now reported preliminary results. The Microvolt T-wave Alternans in Patients with Heart Failure (ALPHA) study recruited 446 patients with non-ischaemic cardiomyopathy (LVEF $\leq 40\%$) and stable NYHA II/III CHF on optimal medical therapy⁶⁰. A non-negative MTWA test was associated with an increased risk of cardiac death or VTE over 18-24 months. However, patients in this group were also older, more symptomatic and had a lower mean LVEF, imbalances which highlight the need for careful multivariable adjustment in such studies. In the SCD-HeFT T-wave alternans sub-study, MTWA testing was performed in 490 patients with LVEF $\leq 35\%$ and NYHA II/III CHF⁶³. 41% of tests were indeterminate and over 35 months there was no difference in the rate of VTE between MTWA groups for patients receiving either ICD or placebo.

Specificity of MTWA for arrhythmias

The contradictory results in these large studies mean that some doubt remains regarding the value of MTWA for predicting arrhythmic risk following MI and in CHF. In MASTER-1, MTWA result could not predict verified arrhythmic events, although a negative test was associated with a lower risk of ACM, the secondary endpoint. These data tend to question the specificity of MTWA for arrhythmias, and should be interpreted in the broader context of all the large MTWA studies. As shown in Table 1.1, the endpoints used have varied, making direct comparisons between studies problematic. However, if we examine outcomes in MTWA positive and indeterminate groups from studies which have examined ACM, in each case, mortality was higher in the indeterminate group (Table 1.2). Clearly, an indeterminate test indicates an unfavourable prognosis, but the nature of this risk is unclear. Only one study enrolled a sufficiently large cohort to examine cause-specific mortality (Table 1.3)⁵⁴. Indeterminate tests accounted for 159 of 514 abnormal MTWA tests and predicted both arrhythmic and non-arrhythmic death, whereas a positive test only predicted all-cause mortality. Therefore, indeterminate, rather than positive tests accounted for the predictive value for arrhythmia, questioning the proposition that MTWA identifies a specific pro-arrhythmic substrate. This raises the possibility that an indeterminate test may actually predict both non-arrhythmic and arrhythmic risk. Patients with extensive comorbidity may be more likely to fail the HR requirements for completion of the MTWA test, and so to have an indeterminate result.

Table 1.2 Distribution of all-cause mortality by MTWA test result

Study	n =	Population	Mean follow-up (months)	All-cause mortality (%)		
				Positive	Indeterminate	Negative
Chow ⁵⁴	768	Ischemic LVSD	18	12	21	8
Bloomfield ⁴⁶	177	Ischemic LVSD	2-year mortality rate	14.5	20.1	3.8
Bloomfield ⁵⁶	549	LVSD	2-year event rate*	12.3 (5 ICD discharges)	17.8 (4 ICD discharges)	2.4 (2 ICD discharges)
Tapanainen ⁵⁰	323	Post MI	14	0	15	<1

*all-cause mortality and ICD discharges.

Table 1.3 Cause specific mortality by MTWA in Chow *et al*⁵⁴

HR (95%CI)	MTWA result		
	Non-negative (n = 514)	Positive (n = 355)	Indeterminate (n = 159)
All deaths	2.24 (1.34-3.75)	2.08 (1.18-3.66)	2.78 (1.55-4.99)
Arrhythmic deaths	2.29 (1.00-5.24)	NS	3.62 (1.44-9.13)
Non-arrhythmic deaths	NS	NS	2.47 (1.17-5.22)

CI, confidence interval; HR, hazard ratio; NS, non-significant.

They are also likely to be at higher risk of non-arrhythmic mortality due to their comorbidity. It is also possible that patients with unsustained alternans or ectopy on exercise may be prone to ventricular arrhythmia. Recent analyses of indeterminate tests concluded that such patients were at high risk^{64;65}, as distinct from those patients with indeterminate tests due to noise, artefact or a sharp rise in HR. This suggests that the prognostic value of MTWA may be improved by reclassification of indeterminate tests⁶⁴.

The key to reconciling the divergent results of these clinical studies lies in understanding the relationship between alternans and arrhythmia. Experimental evidence to date suggests that there may be a mechanistic link between alternans and arrhythmia, although the relevance of this paradigm to heart failure has not been tested. If alternans and arrhythmia merely coincide in patients with heart disease, then the rationale for widespread use of MTWA testing for the prediction of arrhythmias may be weak. However, if a specific relationship exists between alternans and arrhythmia, then MTWA testing could be refined and developed in order to exploit that association for clinical benefit.

Repolarisation alternans

Understanding of the cellular basis for MTWA is important, not only as it may inform better clinical use of MTWA testing, but also as it may well provide new insight into the causes of the lethal arrhythmias associated with MTWA in man. Repolarisation alternans is believed to be the cellular basis for TWA, and describes a regular variation between two patterns of repolarisation on an every-other-beat basis, at a constant cycle length. The evidence linking alternate changes of the repolarisation phase of the ventricular AP to ECG T-wave alternans comes from two experimental models. Firstly, in a canine wedge preparation, pharmacological prolongation of the QT interval in conjunction with rapid pacing produced TWA on a pseudo-ECG⁶⁶. These measurements were graphically correlated with alternation of the action potential duration (APD) recorded from an intracellular microelectrode in the midmyocardial M-cell layer. Secondly, in the isolated guinea-pig heart after endocardial cryoablation, alternating AP morphology has been recorded from the epicardial surface during rapid pacing at low temperature⁴⁰. Alternans occurring during the repolarisation phase of the AP was co-incident with TWA on a pseudo-ECG. In this model, at high stimulation rates, repolarisation alternans became spatially discordant, a state which was associated with significant gradients of repolarisation and the induction of re-entry. This has lead to the emergence of the concept of repolarisation alternans as a new paradigm for the induction of re-entrant ventricular arrhythmia³⁸, and also raises the possibility that repolarisation alternans may cause the ventricular arrhythmias for which MTWA is a marker. For this reason, repolarisation alternans has become the focus of much experimental study.

Cellular mechanisms of repolarisation alternans

A striking feature of both cellular and clinical alternans is that they arise under a wide range of conditions. In the laboratory, repolarisation alternans has been induced by hypothermia⁴⁰, rapid pacing^{40;67;68}, pharmacological APD prolongation^{66;69}, acute ischaemia⁷⁰ and acidosis⁷¹. Clinically, macroscopic TWA has been associated with electrolyte disturbance⁷², tachycardia⁷³, the long QT syndrome (LQTS)⁷⁴ and coronary arterial spasm⁷⁵. MTWA is induced by elevation in heart rate, but the heart rate threshold is lower in patients with CHF⁶², coronary disease^{46;54}, LVSD⁵⁶, left ventricular hypertrophy (LVH) and hypertrophic cardiomyopathy⁷⁶. A major challenge in understanding repolarisation alternans is to reconcile whether there can be a single mechanism for a phenomenon that occurs under a diverse range of experimental circumstances.

Determinants of cellular repolarisation

At a cellular level, repolarisation is governed by both sarcolemmal ion currents and intracellular calcium ($[Ca^{2+}]_i$), as illustrated in Figure 1.3. Voltage-gated sodium channels (VGNa) open in response to a depolarising stimulus, and I_{Na} causes rapid depolarisation before inactivating. The L-type calcium channel (LTCC) is also activated, producing I_{CaL} , which maintains depolarisation during the plateau phase. Given the stoichiometry of NCX, which exchanges one Ca^{2+} ion for every three Na^+ ions, reverse I_{NaCa} favours repolarisation. NCX then switches to forward mode, removing Ca^{2+} from the cytosol. The remaining Ca^{2+} is taken up into the SR by the sarcoplasmic reticulum ATPase (SERCA2a). Inactivation of I_{CaL} , along with increased magnitude of I_{to} and activation of I_K and I_{K1} reset V_m . Intracellular Ca^{2+} cycling is responsible for linking the AP to myocyte shortening (excitation-contraction coupling). During the AP upstroke, the increase in local $[Ca^{2+}]_i$ produced by I_{CaL} triggers Ca^{2+} release from the sarcoplasmic reticulum (SR) release channels (RyR) by a process called Ca^{2+} -induced Ca^{2+} release (CICR). Cytosolic Ca^{2+} ions bind to the myofilament protein troponin C, activating contraction. During the diastolic interval (DI) of the cardiac cycle $[Ca^{2+}]_i$ falls, allowing relaxation. This is achieved by pumping of Ca^{2+} back into the SR via SERCA and extrusion of Ca^{2+} from the cell via NCX, with minor contribution from sarcolemmal ATPases.

V_m and $[Ca^{2+}]_i$ are bidirectionally coupled, such that the AP affects the concurrent Ca^{2+} transient (Ca^{2+}_T) and vice versa. Ca^{2+}_T is dictated by both the AP trigger and by the SR Ca^{2+} load. As Ca^{2+} reuptake to the SR occurs during the diastolic interval (DI), the SR Ca^{2+} load also indirectly depends upon the APD of the previous beat. V_m is affected by $[Ca^{2+}]_i$ in opposing ways: SR Ca^{2+} release inactivates the L-type calcium current (I_{CaL}) favouring repolarisation, but the increase in $[Ca^{2+}]_i$ also drives calcium extrusion from the cell by NCX, which carries an inward current tending to maintain depolarisation. In some species, including rabbit, a Ca^{2+} activated chloride current also exists and will affect the AP. A larger Ca^{2+}_T can either lengthen or abbreviate APD, depending on which of these predominates. In order to maintain a long-term stability of the intracellular Ca^{2+} levels within a cardiac cell, the Ca^{2+} entering the cytosol via the L-type Ca^{2+} current and the SR Ca^{2+} release must be removed before the next beat. This occurs by Ca^{2+} extrusion from the cell mainly via NCX and Ca^{2+} reuptake to the SR via SERCA. APD and the systolic Ca^{2+}_T have been shown to display alternans at a cellular level, and occur linked in space and time, independent of activation site⁷⁷. Both have therefore been implicated as the primary cause of repolarisation alternans.

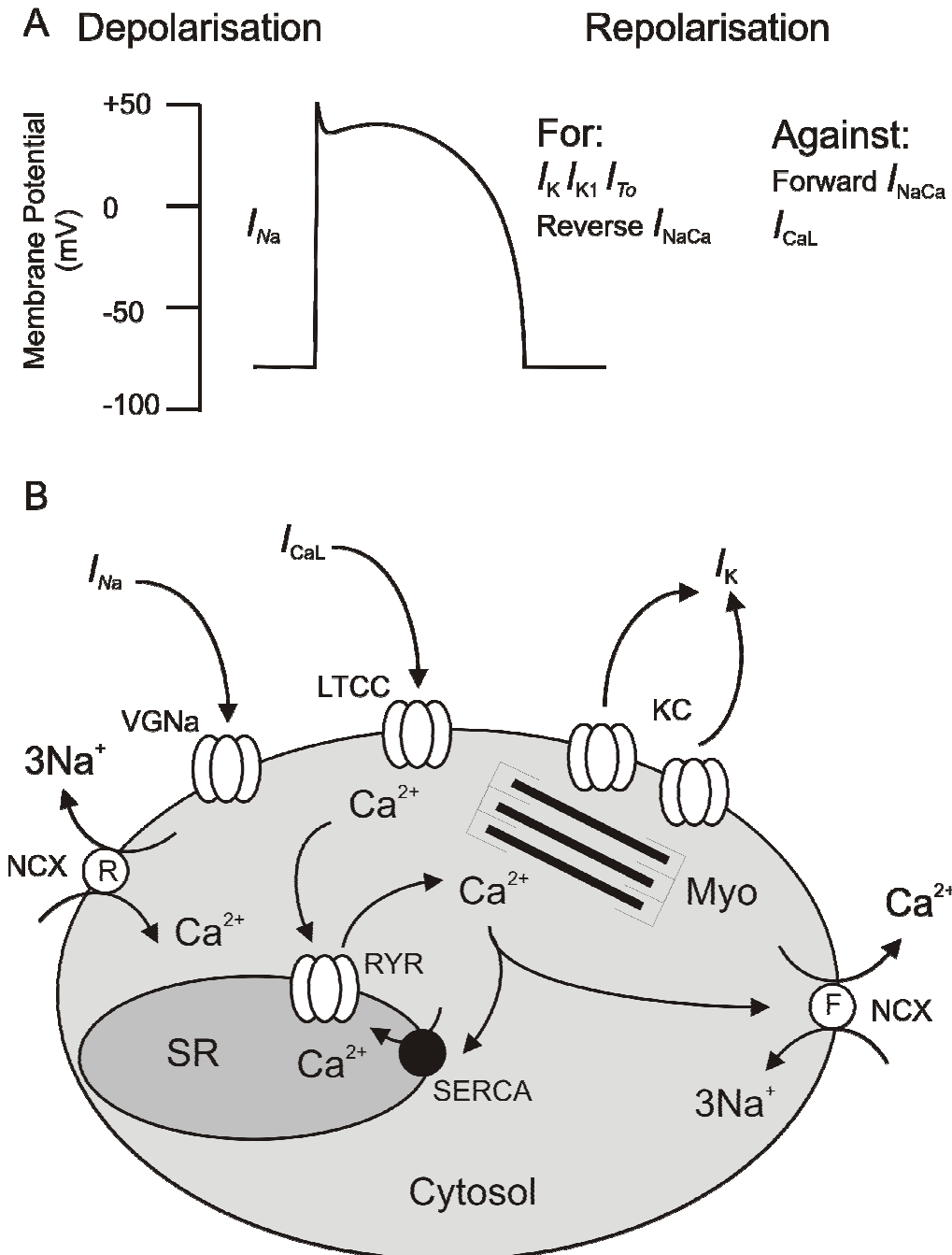


Figure 1.3 The determinants of cellular repolarisation

A. The changes in membrane potential which produce the cardiac action potential, along with the currents responsible. B. A cardiac cell with the sarcolemmal ion currents and intracellular calcium fluxes which influence repolarisation. LTCC, L-type Ca channel; Myo, myofilaments; RYR, ryanodine receptor; SR, sarcoplasmic reticulum; SERCA, sarcoplasmic reticulum ATPase; NCX, sodium calcium exchange; VGNa, voltage gated sodium channel; KC, potassium channel. F indicates forward mode NCX and R indicates reverse mode.

AP restitution

The main hypothesis for the generation of repolarisation alternans is based on the AP restitution relationship. AP restitution describes the change in APD which occurs when DI is altered (usually by a change in stimulation rate) and is attributable to the time-dependence of recovery from inactivation of the ionic currents responsible for the AP. The relationship is quantified by the APD restitution curve, which is plotted using experimental measurements of APD and DI, typically during the application of extrastimuli at progressively shorter coupling intervals. A steep restitution curve describes the situation where a change in DI has a larger effect on the subsequent APD. The generation of repolarisation alternans by steep APD restitution was first described in 1968 by Nolasco and Dahlen⁷⁸. The authors constructed a cobweb diagram to illustrate the way in which the slope of the APD restitution curve dictated the presence or absence of APD alternans following a shortening in cycle length (CL) (see Figure 1.4) In the case of a steep restitution curve, shortening of DI produces a short APD in the next cycle and, given that cycle length is constant, a long DI. This in turn gives rise to a long APD with an associated short DI, and so to alternans. In contrast, a shallow APD restitution curve means that variation in APD would be progressively diminished. There is both experimental^{79;80} and simulation-based^{81;82} evidence that an APD restitution slope > 1 promotes repolarisation alternans. Although the cobweb diagram illustrates the generation of alternans on a single restitution curve, in reality the situation is more complex. In isolated myocytes, restitution curves differ depending on whether the extrastimulus follows the beat with the long or short action potential⁸³. Temporal heterogeneity of restitution has also been demonstrated in multicellular preparations^{40;67;68}.

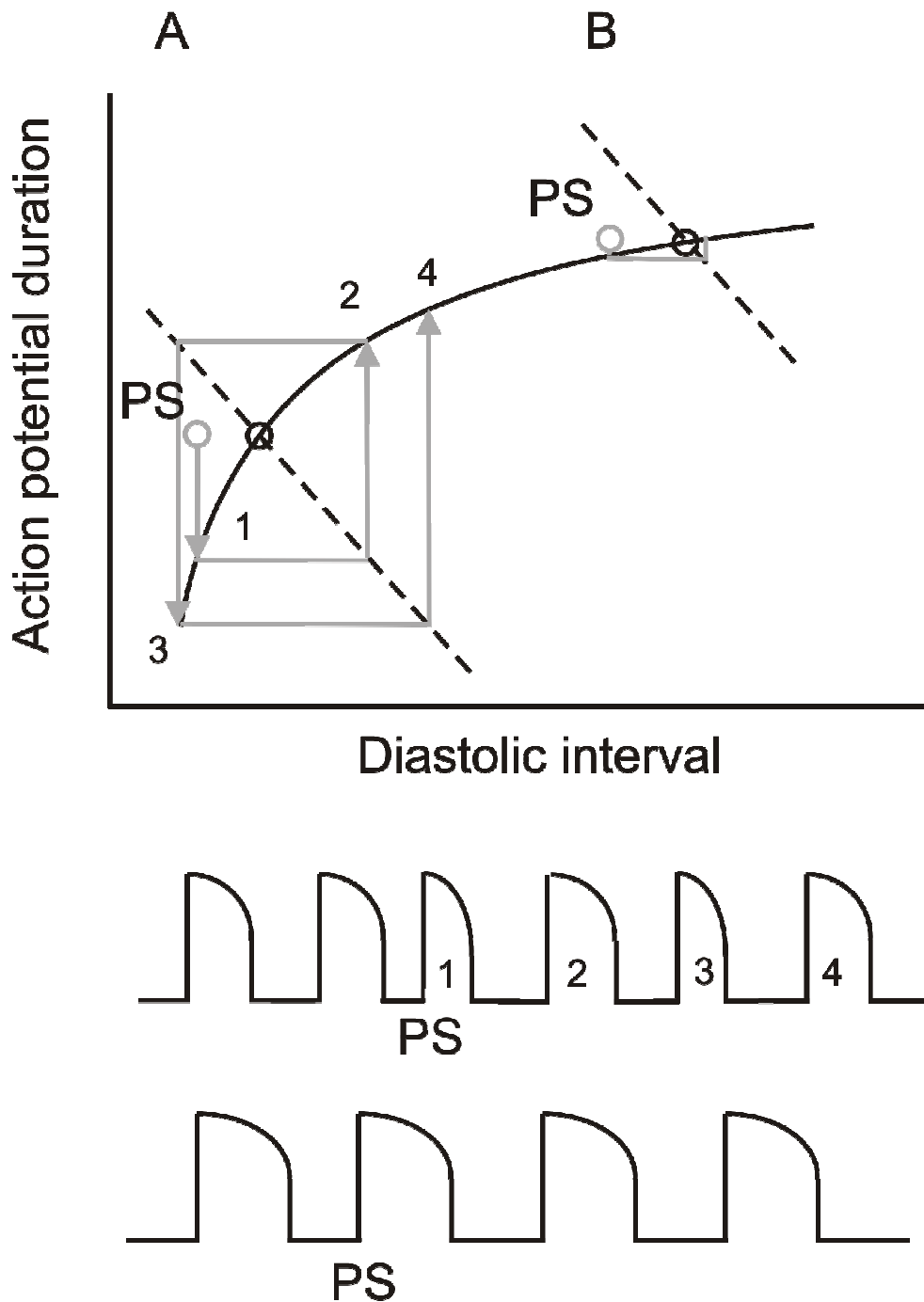


Figure 1.4 Theory of the production of APD alternans by AP restitution (Adapted from Nolasco and Dahlen⁷⁸)

Illustration of the production of APD alternans as a result of APD restitution, adapted from Nolasco and Dahlen⁷⁸. The dashed line satisfies the condition: $APD + DI = CL$ and is illustrated to describe behaviour with respect to the curve, assuming that CL is constant. Example action potentials are illustrated for each step. A: indicates a system operating on a steep part of the AP restitution curve and PS indicates the application of a premature stimulus to that system. Because the curve is steep, the short DI produced by the extrastimulus (1) means that the associated APD is long (2), which in turn leads to a short DI (3), which dictates a longer APD (4), meaning that the subsequent DI will be short, and producing self-sustaining alternans. B: indicates a system operating on a shallow part of the AP restitution curve and PS indicates the application of the same premature stimulus to that system. Where the APD restitution curve is shallow, a perturbation in DI has a negligible effect on APD and no alternans is generated.

Ca²⁺ cycling

Simultaneous measurements of [Ca²⁺]_i and V_m have shown that APD alternans is accompanied by alternating changes in Ca²⁺_T^{77;84}. In isolated ventricular cells and whole hearts a reduced Ca²⁺_T amplitude generally accompanies a shorter APD (electromechanically in-phase alternans)^{77;83;84}. There have been fewer reports of the opposite phenomenon: a larger Ca²⁺_T associated with a shorter APD (electromechanically out-of-phase alternans)^{85;86}. Ca²⁺_T alternans does not appear to require APD alternans since the former has been observed in isolated voltage-clamped cardiomyocytes^{87;88}. Recent work suggests that at particularly high SR Ca²⁺ loads, small variations in the SR Ca²⁺ content can give rise to large variations in SR Ca²⁺ release and therefore amplitude of the Ca²⁺ transient⁸⁹. If this behaviour is coupled to a very steep relationship between cytoplasmic Ca²⁺ and the Ca²⁺ efflux from the cell, then prominent alternans in the SR Ca²⁺ release will be generated⁹⁰. An additional factor is the steepness of the relationship between cytoplasmic Ca and SERCA activity, as demonstrated by theoretical studies^{91;92}. Other mechanisms for Ca²⁺ transient alternans involve alternation in the metabolic regulation of SR function⁸⁶ or alternating properties of the SR Ca²⁺ release channel that are independent of the SR Ca²⁺ content⁹³.

Interactions of restitution and Ca²⁺ cycling

Intracellular Ca²⁺ modulates the magnitude of ionic currents active during the repolarisation phase of the action potential. Therefore it is conceivable that instabilities in the SR Ca²⁺ release mechanism and the subsequent Ca²⁺ transient may affect APD alternans. In support of this theory, APD alternans in isolated cardiomyocytes can be abolished using interventions which affect Ca²⁺ cycling, including blockade of SR Ca²⁺ release⁹⁴, application of I_{CaL} antagonists⁹⁵, depletion of SR Ca²⁺⁹⁶ and chelation of intracellular Ca²⁺⁹⁶. These findings are borne out in multicellular preparations under long-QT conditions⁶⁶ and with acute myocardial ischaemia, where Ca²⁺ channel blockade reduced both the occurrence of TWA and susceptibility to VF⁹⁷. A study on single rabbit cardiomyocytes provides a potential explanation of these results⁹⁶. It showed that the presence of an intracellular Ca²⁺ transient, rather than a steep restitution curve was a pre-requisite for repolarisation alternans.

Discordant alternans

Repolarisation alternans has been mechanistically linked to the production of re-entrant ventricular arrhythmia in experimental models. With the combination of low temperature

and high stimulation rates in the cryoablated guinea pig heart, optically recorded action potentials alternated with opposite phase in adjacent regions of epicardium⁴⁰. During this discordant alternans, spatial gradients of repolarisation were significantly increased and these gradients appeared to be responsible for unidirectional conduction block, which was consistently seen when pacing cycle length was shortened during discordant alternans. Re-entrant VF in this context was therefore not simply a consequence of elevated heart rate but was due to a specific interaction between a premature impulse and the extreme gradients of repolarisation produced by discordant alternans. Interestingly, during rapid pacing in a canine model of LQTS, in which dispersion was extreme, a premature stimulus was not required for the induction of ventricular arrhythmia from discordant alternans^{69;98}. On the basis of these observations, spatially discordant alternans has emerged as a possible mechanism of re-entrant arrhythmia and much experimental study has focused on understanding the conditions creating discordant, as distinct from concordant alternans.

Mechanisms of discordant alternans

The paradigm of discordant alternans identifies spatial heterogeneity of alternans as the link to ventricular arrhythmia, and there are a number of theories as to how such heterogeneity of alternans arises. These are illustrated in Figure 1.5, and can be broadly classified as underlying tissue heterogeneity or dynamic modulation of repolarisation. Normal cardiomyocytes exhibit heterogeneities in both APD restitution behaviour and Ca²⁺ handling, giving rise to physiological spatial heterogeneity of repolarisation. Furthermore, in intact ventricular tissue, electrotonic coupling between cells, cardiac memory, conduction velocity restitution and ectopic beats can lead to dynamic spatial and temporal modulation of repolarisation.

Heterogeneity of repolarisation

In the guinea-pig model, spatial patterns of alternans in the surviving subepicardium are consistently orientated along an apex-base axis, independent of activation site⁴⁰, as are epicardial gradients of repolarisation and restitution in this species⁹⁹. This suggests that the development of discordant alternans may be related to intrinsic spatial differences in cellular repolarisation. If baseline APD or restitution characteristics differ between cells, then these cells will be expected to respond differently (in terms of APD) to a uniform DI. This is a relatively straightforward concept in the guinea-pig model, in which the only viable myocytes are a thin layer of epicardial cells. In the intact left ventricle, however, spatial gradients of repolarisation also exist in the transmural plane¹⁰⁰. In the canine wedge,

under long QT conditions, transmural heterogeneity of alternans was attributed to the differing repolarisation properties of cells across the ventricular wall^{66;101}. These differences in repolarisation have been shown to lead to discordant alternans in this model⁹⁸. The relative contributions of apex-base and transmural gradients of repolarisation to the development of discordant alternans have yet to be established. Moreover, although the apex-base gradient of repolarisation is known to exist on the epicardial surface, whether this gradient is maintained through the depth of the ventricular wall is not known. Indeed, optical mapping studies of repolarisation in perfused ventricular sheets suggest that no such gradient exists at the endocardium¹⁰².

Heterogeneity of calcium cycling

Under normal conditions, Ca^{2+} handling in ventricle exhibits both apex-base¹⁰³ and transmural¹⁰⁴ heterogeneity, and these patterns have been linked to heterogeneity of Ca^{2+} alternans^{40;104}. As has already been discussed, Ca^{2+} cycling is important in the generation of repolarisation alternans, and it is therefore reasonable to propose that spatially discordant alternans may also be mediated through heterogeneity of Ca^{2+} cycling. In tissue with heterogeneous Ca^{2+} cycling it is certainly conceivable that spatially concordant alternans could be converted to discordant alternans, by differential coupling between $[\text{Ca}^{2+}]_i$ and V_m or by spatial heterogeneities in phase of Ca^{2+} alternans (Figure 1.5B). Intercellular Ca^{2+} diffusion is limited¹⁰⁵, so the phase of Ca^{2+} alternans between cells can desynchronise more easily than V_m . Indeed, both dyssynchronous Ca^{2+} alternans between cells and subcellular Ca^{2+} alternans have been demonstrated in intact atrial and ventricular myocardium^{106;107}. Thus spatial heterogeneities in Ca^{2+} handling may be crucially important in desynchronising APD alternans and producing discordant alternans.

Disruption of electrotonic coupling

Under normal circumstances, gradients of repolarisation are minimised by intercellular gap junctions, which mediate electrotonic coupling between cells. Therefore, gap junction uncoupling, which increases spatial gradients of repolarisation, would be expected to increase vulnerability to discordant alternans. Reduced intercellular gap junction coupling occurs during LV remodelling following myocardial infarction¹⁰⁸, which is associated both clinically and experimentally with an increased risk of ventricular arrhythmia. So, this ‘unmasking’ of repolarisation heterogeneity is a possible mechanism by which alternans-induced arrhythmia may be more likely to occur in pathology, although, this has yet to be demonstrated experimentally. In the guinea-pig model of alternans, an epicardial laser burn

has been shown to promote the production of discordant, as distinct from concordant alternans⁶⁷, presumably by electrically isolating different regions and promoting any differences in phase which might arise from different baseline cellular properties. However the relevance of this type of structural barrier to cardiac pathology is limited. Traditionally, full-thickness myocardial infarction is thought to produce an electrically inert scar. However, there are viable myocytes within infarcted myocardium and recent evidence shows that electrical impulses propagate into the infarct¹⁰⁹. Moreover, following myocardial infarction the border zone and remodelled ventricular myocardium both have altered electrophysiological properties. The ways in which these changes might influence the development of discordant alternans are unknown at present.

Dynamic mechanisms

The role of conduction velocity restitution in spatially discordant alternans

Conduction velocity (CV) displays restitution behaviour at short cycle lengths and theoretical work has suggested that engagement of CV restitution could mediate a localised change in alternans phase, resulting in spatially discordant alternans (Figure 1.5C). If CV is slowed when DI is short, then as the impulse travels from the stimulus site, DI will prolong, producing inhomogeneity of DI in space. This will result in inhomogeneity of the subsequent APD which, during alternans, could lead to spatial discordance. This mechanism has been illustrated both experimentally⁹⁸ and in simulations⁸¹.

Ectopic stimulation can induce discordant alternans

In simulated sheets of cardiac cells derived from computational models, an ectopic premature stimulus can induce discordant alternans at pacing rates which, in the absence of ectopic stimulation, would be expected to produce concordant alternans⁸². Indeed, an ectopic may induce discordant alternans even if no alternans is present at baseline. The premature ectopic produces an altered gradient of DI in space, which in a way analogous to that described for CV restitution, produces inhomogeneity of APD in space and allows APD alternans to become discordant (Figure 1.5D). The spatially discordant alternans observed following ectopic stimulation is typically transient, reverting back to concordant alternans, or to baseline behaviour over a period of time.

Dynamic instability arising from Ca^{2+} cycling

In a model of a paced one-dimensional cable of cardiac cells, in which alternans was induced by rendering SR Ca^{2+} release steeply dependent on SR Ca^{2+} content, variation of the coupling between $[\text{Ca}^{2+}]_i$ and V_m from positive (generating electromechanically in-phase alternans) to negative (generating electromechanically out-of-phase alternans)

promoted the induction of discordant alternans¹¹⁰. The authors postulated that the negative bidirectional coupling between $[Ca^{2+}]_i$ and V_m amplified minor spatial differences between cells, eventually resulting in discordant alternans.

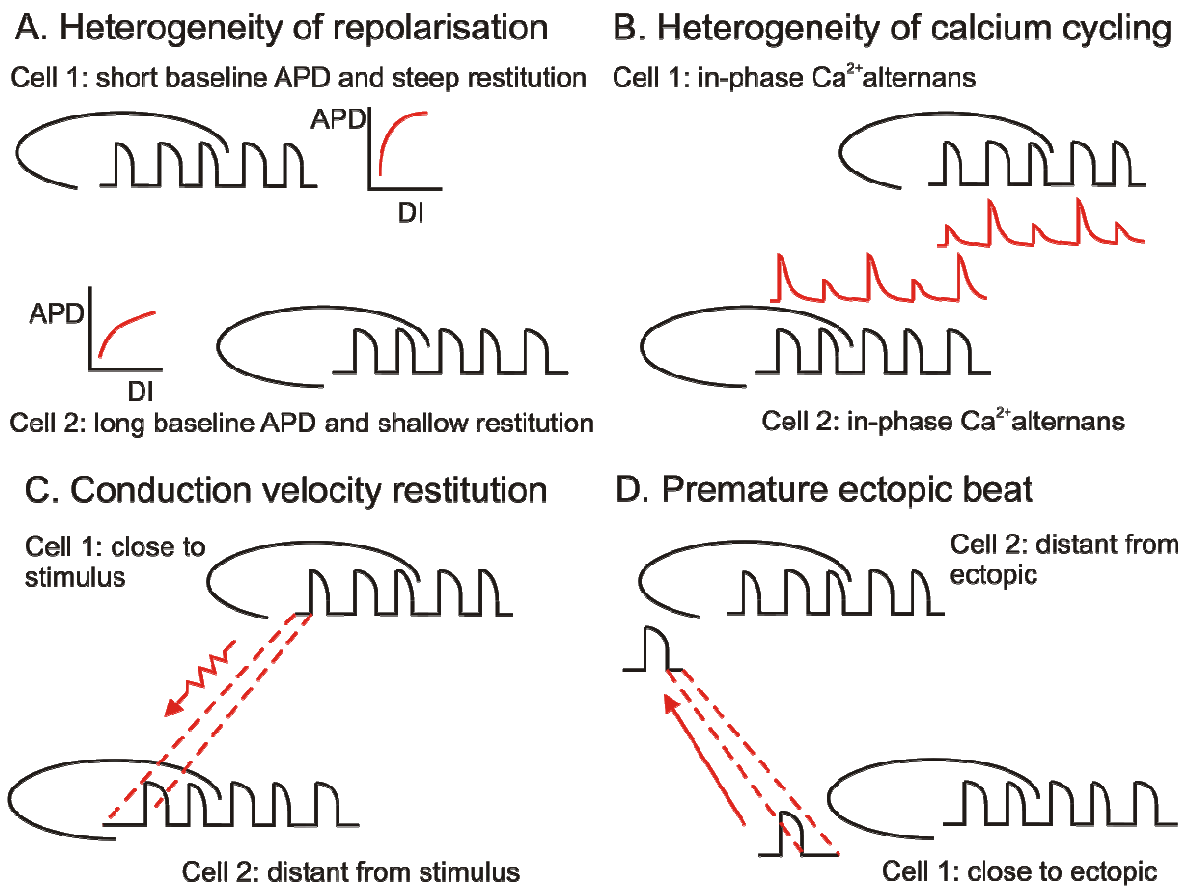


Figure 1.5 Potential mechanisms of discordant repolarisation alternans

A. The effect of spatial heterogeneities of restitution on concordant alternans. The same diastolic interval will elicit different responses in terms of APD from different areas of the tissue which have different restitution properties and leading to desynchronisation of alternans in space. B. Where heterogeneity of Ca^{2+} cycling exists, differential feedback effects of Ca^{2+} on V_m produce spatially discordant alternans of APD. C. When conduction velocity (CV) restitution is present (i.e. when increasing stimulus rates produce a slowing of conduction), DI will increase with increasing distance from the stimulus. Over that distance, the lengthening DI elicits different responses in terms of APD, setting up spatially discordant alternans. D. An ectopic premature stimulus during concordant alternans will result in shortening DI as it propagates through the tissue. This means that different areas of the tissue will receive a different DI, so resulting in different responses in terms of APD in space, which may produce spatially discordant alternans.

Is spatially discordant alternans alone sufficient to induce re-entry?

The theoretical link between spatially discordant alternans and re-entrant ventricular arrhythmia describes the production of such extreme gradients of repolarisation that re-entry can occur. Whether there is an absolute requirement for a premature stimulus prior to induction of re-entry is an important question. After pharmacological prolongation of the QT interval, a premature stimulus was not required for re-entry; however, this constitutes an extreme baseline abnormality of repolarisation and has limited relevance to the majority of clinical arrhythmias⁹⁸. In the guinea-pig model, extreme gradients of repolarisation during spatially discordant alternans lead to the induction of re-entry after a shortening of cycle length⁴⁰. This may indicate that in the absence of an increasing stimulation rate or a premature beat, spatially discordant alternans is in fact a stable situation. More research is required to determine whether spatially discordant repolarisation alternans is sufficient for re-entry in the absence of an ectopic trigger.

Is there a mechanistic link between alternans and arrhythmia?

The fact that MTWA is linked to the occurrence of ventricular arrhythmia, along with the experimental evidence that discordant repolarisation alternans may promote re-entry, raises the possibility of a mechanistic link between alternans and arrhythmia in man. However, there are a number of important questions which must be answered before such a link could be established. In particular, clarification of laboratory data is required before it can be translated to the clinical setting.

The experimental paradigm***Temperature***

Low temperature has been used to elicit alternans in a number of studies^{40;67;87;111}; however, the mechanisms underlying the temperature dependence of alternans have not been established. It is recognised that cooling over the range used in these experiments (27-34°C) has significant effects on the physiology of mammalian ventricle. Firstly, there is marked positive inotropy at low temperature¹¹², which has been linked to changes in the dynamics of Ca²⁺ cycling, principally a slowing of Ca²⁺ extrusion from the cytosol, leading to increased [Ca²⁺]_i^{113;114}. Cooling also results in a reduction in the activity of energy-dependent processes, such as the sarcolemmal sodium pump¹¹⁵. This raises intracellular sodium ([Na⁺]_i), thereby promoting Ca²⁺ entry into the cell via NCX and increasing [Ca²⁺]_i. Hypothermia, in the range commonly used to elicit alternans, may therefore be regarded as a Ca²⁺-overload state. APD is also modulated by temperature, such that APD is longer at

lower temperatures¹¹⁶. The exact mechanism for this is unknown, but temperature-dependence of ion channel gating kinetics is well recognised, and differing activation and inactivation of ionic currents will have potentially complex effects on the action potential¹¹⁷. It is also important to consider the effects of cooling at the organ level. In guinea pig papillary muscles, APD restitution is steeper at 27°C than 37°C degrees¹¹⁸. Spatial dispersion of repolarisation has also been shown to be increased during hypothermia¹⁰², and this may be expected to predispose to the development of discordant repolarisation alternans. Conduction velocity is also slowed at low temperature¹⁰² and this may increase the propensity of discordant alternans to proceed to unidirectional block.

Even from this brief exploration of the cellular effects of low temperature, it is clear that there are a number of ways in which cooling may modify cellular processes to promote alternating behaviour. Indeed, many of the cellular consequences of lowering temperature, raised $[Na^+]$ _i and $[Ca^{2+}]$ _i and prolonged APD, resonate with other experimental interventions that provoke alternans. It is interesting to note that investigators working with intact guinea pig hearts at physiological temperatures have failed to induce discordant repolarisation alternans with rapid pacing⁸⁴. Instead Choi *et al* observed transient alternating behaviour following an abrupt reduction in cycle length, and production of alternans relied upon the longer refractory period at the base of the ventricle producing slowing of conduction on alternate beats. These discrepancies only serve to emphasise that the mechanisms underlying the temperature dependence of repolarisation alternans must be investigated before extrapolating the paradigm to arrhythmogenesis *in vivo*.

Amplitude alternans

Alternating behaviour is not usually confined to the repolarisation phase of the AP. Indeed, a striking feature of many published records of alternans is that changes in action potential duration are frequently accompanied by changes in action potential amplitude^{40;67;77;87;111}. In many cases, the alternation of amplitude appears more marked, in percentage terms, than that of APD. It is not clear whether AP amplitude alternans occurs in single cells, and published records from microelectrode studies are conflicting^{66;87;111}. If the alternation in AP amplitude were primary, then this might be expected to have an effect on the APD (i.e. producing “secondary” repolarisation alternans). Amplitude alternans requires careful consideration, because it raises the possibility that other parameters, aside from cellular repolarisation, may display alternating behaviour and so may conceivably be responsible for both TWA and proarrhythmia.

Much of the experimental work examining repolarisation alternans at the whole-heart level has employed optical mapping^{40;67;68;77;84} which relies on the spectral properties of voltage-sensitive dyes. Although the time-course of optical APs has been shown to correlate well with those recorded using intracellular microelectrodes¹¹⁹, the amplitude of an optical AP is a function of the intensity of fluorescence produced by the dye in the cardiomyocyte plasma membrane. The absolute fluorescence level is dependent on a number of variables aside from V_m , including dye penetration into the tissue, membrane uptake of dye and excitation light levels at a given site. Moreover, depending on the particular conditions in each experiment, the signal recorded in a single pixel may represent the summation of electrical activity from a few hundred to a few thousand cardiomyocytes. Despite this, consecutive action potentials from a single pixel would be expected to have the same amplitude, given the same magnitude of change in V_m during depolarisation. As the depolarisation phase of the cardiac AP is thought to be an all or nothing phenomenon, it is unlikely that this represents alternating amplitudes of depolarisation at the level of a single cell. Alternating amplitude in consecutive action potentials from the same site may therefore indicate an alternating magnitude of the summed depolarisation from the cells contributing to the AP in a given pixel area. However, the possibility exists that some cells in the pixel area are failing to respond on an every other beat basis. For example, if some cells displayed rate-dependent 2:1 phase-locking while others responded 1:1 then an alternating amplitude might be observed in the optically recorded AP. The precise cellular basis for alternating changes in action potential amplitude has yet to be uncovered. If alternans of AP amplitude is seen in single cells, then the mechanisms, which remain uninvestigated, may be quite different from those described for repolarisation alternans. Similarly, if amplitude alternans is an artefact of optical records then the possible explanations for this extend beyond alternans of repolarisation. In either case, it is conceivable that changes in recorded AP amplitude may have implications for the development of unidirectional conduction block. Amplitude alternans therefore requires careful consideration, as it raises the possibility that other aspects of electrical activity, aside from repolarisation, may be responsible for both TWA and the accompanying proarrhythmic status.

Translation to the clinical setting

In the guinea-pig model, discordant alternans is well demonstrated as a potential mechanism for ventricular arrhythmia, as it was always present prior to unidirectional block and re-entry. However, in order to determine whether re-entry commonly occurs by this mechanism in man, a number of questions must be addressed.

Interspecies correlation

Although alternation of cellular repolarisation is correlated with ECG TWA in animal models, the link to MTWA in patients needs to be considered. There are three studies regarding the occurrence of repolarisation alternans in humans¹²⁰⁻¹²². In a small group of patients with coronary heart disease, rapid atrial pacing induced MTWA, and this was associated with alternation in the amplitude of the portion of the intracardiac electrogram corresponding to repolarisation¹²¹. Although alternans of the intracardiac electrogram commonly occurred without body surface MTWA, there did appear to be a correlation, in that patients with electrogram alternans at a greater number of intracardiac sites were more likely to display MTWA. Another study recorded alternans of endocardial monophasic action potentials and found that this correlated with body surface MTWA during atrial pacing, but not to endocardial monophasic AP (MAP) restitution slope¹²². The relationship between spatially discordant repolarisation alternans, MTWA and ventricular arrhythmia in humans remains to be explored, for instance how spatially discordant alternans would be manifest in an ECG signal is unclear.

Temporality

The link between cellular repolarisation alternans and MTWA in patients involves a further order of complexity. In the clinical context, MTWA is a marker of distant arrhythmic risk whereas the experimental paradigm suggests a causative role immediately prior to the onset of ventricular arrhythmia. There are a limited number of case reports from ambulatory ECG data and bipolar electrograms recorded by implantable defibrillators that suggest an increase in MTWA may occur immediately prior to some spontaneous ventricular arrhythmias in man^{123;124}, but this requires further substantiation.

Alternans and heart rate

It is clear that the relationship between alternans and heart rate is crucial. Experimentally, repolarisation alternans is almost universally a function of rapid stimulation rates and MTWA in patients occurs with an elevation of heart rate. Ventricular arrhythmia and sudden cardiac death, however, are not always preceded by an increase in heart rate, and this is difficult to reconcile with a causative role for repolarisation alternans in arrhythmia. If tachycardia is indeed a pre-requisite for alternans, as it appears to be in the laboratory, then repolarisation alternans may be a mechanism for the degeneration of VT to VF, rather than for initiation of tachycardia *per se*. In experimental studies metabolic derangement, pharmacological QT prolongation and adrenergic stimulation have been demonstrated to

produce alternans at normal heart rates, and it is possible that these may play an important role in the production of T-wave alternans at normal heart rates in man.

Repolarisation alternans as a mechanism for arrhythmia in heart failure

Electrophysiological heterogeneity

The theory of discordant alternans identifies spatial heterogeneity of alternans as the link to ventricular arrhythmia. Although in simulations homogenous cardiac tissue is capable of developing discordant alternans when conduction velocity restitution is steep⁸², it occurs more readily in the presence of tissue heterogeneity⁸¹. In the guinea pig model, spatial patterns of alternans were consistently orientated in an apex-base direction^{40;77}, independent of pacing site, as are gradients of repolarisation and restitution in this species⁹⁹. This suggests that the development of discordant alternans is related to intrinsic spatial differences in cellular repolarisation. In the left ventricle, gradients of repolarisation also exist transmurally¹⁰⁰. Transmural heterogeneity of alternans has been demonstrated in LQTS^{66;69}, and in isolated ventricular myocytes⁸⁷, as has increased magnitude of calcium transient alternans at the sub-endocardium in a canine wedge preparation¹⁰⁴. The relative contribution of transmural and apex-base heterogeneities to the development of discordant alternans has not been established.

Under normal circumstances, gradients of repolarisation are attenuated by intercellular gap junctions, which allow electrotonic coupling between cells. Therefore cellular uncoupling, as occurs as part of LV remodelling following MI¹²⁵, would also be expected to increase vulnerability to discordant alternans. In the guinea-pig preparation uncoupling was modelled by the introduction of an epicardial scar, which did indeed facilitate the development of discordant alternans⁶⁷. Pharmacological potentiation of gap junction conductance during ischaemia has been shown to suppress discordant alternans¹²⁶, but the effect of pharmacological gap junction uncoupling on alternans has not been investigated.

Electrophysiological remodelling in heart failure

Experimentally, ventricular arrhythmias are more readily generated in hearts that have undergone remodelling following myocardial infarction. In Langendorff perfused human hearts explanted at the time of transplantation for end-stage heart failure, re-entrant excitation has been demonstrated. In these studies, the structural arrangement of the scar, and particularly the surviving myocardial strands within the scar and in the border zone, appeared important for the initiation and maintenance of re-entry¹²⁷. The

electrophysiological changes manifest in the remote, non-infarcted myocardium are also important¹²⁸. APD prolongation is the most consistent change found in animals¹²⁹ and humans^{129;130} with heart failure. The increased heterogeneity of APD in the remodelled hypertrophied LV can result in dispersion of refractoriness, a critical substrate for the development of re-entrant tachyarrhythmias. Hypertrophy-induced increase in interstitial tissue with possible impairment of cellular coupling can also contribute to the occurrence of re-entry. Prolongation of APD is considered the priming step for the development of early afterdepolarisations (EADs). EADs are more easily induced in the hypertrophied rabbit wedge¹³¹. Triggered activity from DADs is yet another potential mechanism of arrhythmias in the post-MI heart. DADs have been shown to be more easily induced in hypertrophied myocytes under the influence of increased extracellular Ca²⁺¹³² or in the presence of β-adrenergic agonists¹³³

Heterogeneity of repolarisation in the rabbit coronary ligation model

Our group has developed and extensively characterised a model of heart failure produced by coronary arterial ligation in the rabbit¹³⁴⁻¹³⁷. Following ligation, rabbits develop a heart failure syndrome and have decreased survival compared with sham-operated controls. Ligated hearts have a lower VF threshold, suggesting that re-entry occurs more readily⁹. Furthermore, this model displays two major areas of electrophysiological heterogeneity as a consequence of heart failure following MI. In the non-infarcted hypertrophied myocardium, APD is prolonged, as has been demonstrated in humans with heart failure¹³⁰. However, this APD prolongation is not uniform across the wall¹³⁴ and transmural dispersion of repolarisation, as measured in isolated cells, is increased. Secondly, there is a defined infarct border zone where surviving myocytes interdigitate with scar tissue at the epicardium and form a thin layer in the subendocardium. Local dispersion of refractoriness, estimated by the VF interval technique, is increased in this border zone⁹.

Discordant repolarisation alternans as a mechanism of re-entry in heart failure

Heart failure gives rise to increased electrophysiological heterogeneity, which would be expected to increase propensity to discordant repolarisation alternans. However, this has yet to be shown definitively. Investigation of contractile dysfunction has demonstrated that mechanical alternans occurs more readily in failing hearts^{138;139}. Calcium transient alternans was observed with rapid pacing in mice over-expressing cardiac tumour necrosis factor (TNF)α¹⁴⁰, but this was not mechanistically linked to arrhythmia. Although the transgenic animals developed a heart failure syndrome, they displayed an overall reduction

in heart rate. There were no tachyarrhythmic deaths, indicating important differences from human heart failure.

In summary, our current knowledge offers some explanation for the use of alternans as a marker for arrhythmic risk, and raises the possibility that repolarisation alternans may be causative in the clinical arrhythmias predicted by MTWA. Although the cellular mechanisms of repolarisation alternans are becoming established and the theoretical conditions which may promote spatially discordant alternans are well understood, the link between repolarisation alternans and clinical MTWA is not yet made. Moreover, although the link between discordant repolarisation alternans and arrhythmias has been shown in animal models, its relevance to clinical arrhythmias in heart failure has yet to be demonstrated directly. An important step in extrapolating the experimental paradigm to the clinical situation is to examine it in a clinically relevant model of heart failure.

Aims and hypotheses

Aims

This study was designed to investigate whether increased regional heterogeneity of repolarisation as a result of heart failure will predispose to the development of arrhythmogenic spatially discordant alternans.

Hypotheses

In the presence of alternans, at a given cycle length, the transmural pattern of alternans is dependent on intrinsic cellular repolarisation properties, and hence is independent of stimulus site.

Heterogeneity of alternans is greater in the transmural plane than across the epicardial surface.

Heterogeneity of alternans increases with increasing stimulation rate until discordant alternans develops. Discordant alternans is a necessary pre-condition for unidirectional conduction block and re-entry.

In heart failure, there is increased transmural heterogeneity of repolarisation in the surviving hypertrophied myocardium. This predisposes to discordant alternans, such that it occurs at slower stimulation rates and with greater magnitude than in normal hearts.

In failing hearts, the onset of discordant alternans and the induction of re-entry occur at slower stimulation rates than in normal hearts.

Chapter 2: Methods

The rabbit coronary artery ligation model

This study used a model of left ventricular dysfunction following myocardial infarction in the rabbit.

Methods

Surgical procedures and *in vivo* echocardiography were carried out by Dr Martin Hicks and Mr Michael Dunne in accordance with the UK Animals (Scientific Procedures) Act 1986 under Project Licence (PPL60/3538) and conform to the Guide for the Care and Use of Laboratory Animals published by the US National Institutes of Health (NIH Publication No. 85-23, revised 1996). Adult male New Zealand White rabbits were given premedication with 0.4ml/kg intramuscular Hypnorm [fentanyl citrate (0.315mg/ml): fluanisone (10mg/ml), Janssen Pharmaceuticals]. Anaesthesia was induced with 0.25-0.5mg/kg midazolam (Hypnovel, Roche) given via a cannula in the marginal ear vein. The rabbit was intubated and ventilated using a Harvard small animal ventilator with a 1:1 mixture of nitrous oxide and oxygen containing 1% halothane at a tidal volume of 50ml and a frequency of 40 per minute. Preoperative antibiotic prophylaxis was given with 1ml intramuscular Amfipen (ampicillin 100 mg/ml, Mycofarm UK Ltd). A left thoracotomy was performed through the 4th intercostal space. Intravenous quinidine hydrochloride 10mg/kg (Sigma Pharmaceuticals) was administered prior to coronary artery ligation to reduce the incidence of ventricular fibrillation. The marginal branch of the left circumflex coronary artery was ligated halfway between the atrioventricular groove and the cardiac apex to produce an ischaemic area of 30-40% of the left ventricle. As there is relatively little collateral circulation in the rabbit, a homogenous apical infarct was produced occupying on average 14% of the total endocardial and epicardial surfaces towards the apex of the left ventricle⁹. If VF occurred, defibrillation was undertaken with a 5-10J epicardial DC shock. Once the animal was stable, the thoracotomy was closed. The animal was then given 20ml of isotonic saline intravenously to replace perioperative fluid losses and allowed to convalesce in a warm clean environment with adequate monitoring for any early signs of distress. Analgesia was given with 0.04mg/kg intramuscular Vetergesic (buprenorphine hydrochloride 0.3mg/ml, Reckitt & Colman Products Ltd) immediately after surgery and the next morning. Sham-operated animals underwent thoracotomy with the heart manipulated in a similar fashion except that the artery was not tied.

Characteristics of the rabbit coronary ligation model

Previous work has detailed the effects of coronary ligation in the mid-course of the marginal artery in the rabbit after 8 weeks^{9;135;137;141}. As shown in Figure 2.1, ligated animals have reduced survival compared with sham-operated controls. Echocardiography was performed 1 week prior to sacrifice to assess *in vivo* cardiac function, using a 5 MHz paediatric probe with a Toshiba sonograph (Sonolayer 100). The rabbit was sedated with 0.3 mg/kg Hypnorm and a small area of the anterior chest wall was shaved to allow a satisfactory echo window. Echocardiographic examination reveals that the ligated animals have LV hypertrophy, significantly increased left atrial diameter and LV end diastolic diameter; and reduced LV ejection fraction¹³⁵. Direct *in vivo* haemodynamic measurements demonstrate a reduction in cardiac output and an increase in LV end diastolic pressure¹³⁷. Post mortem measurements reveal that lung and liver wet weights are also increased as a consequence of LV dysfunction. Heart failure is a heterogeneous clinical syndrome, and therefore difficult to reproduce in animal models, and because of this an objective Heart Failure Index has been proposed to determine the presence of heart failure produced by experimental manipulations in animals¹²⁹. The criteria for heart failure by this measure are met in the rabbit coronary ligation model. Ligated hearts display an increased dispersion of refractoriness along with an increased susceptibility to ventricular arrhythmias and a lowered VF threshold *in vitro*^{9;136}. Optical mapping studies have demonstrated slowed conduction in the infarct border zone¹⁰⁹, along with prolongation and heterogeneity of calcium transients (Ca_T) in the intact heart¹³⁵. Detailed studies in isolated cardiomyocytes have characterised the changes manifest at a cellular level as a result of remodelling following MI. These include increased cell size, and changes in APD_{90} and Ca_T . Importantly the magnitude and of the changes in APD_{90} and Ca_T depended on which transmural layer of myocardium the cells were isolated from, resulting in significantly increased transmural electrophysiological heterogeneity in heart failure¹³⁴.

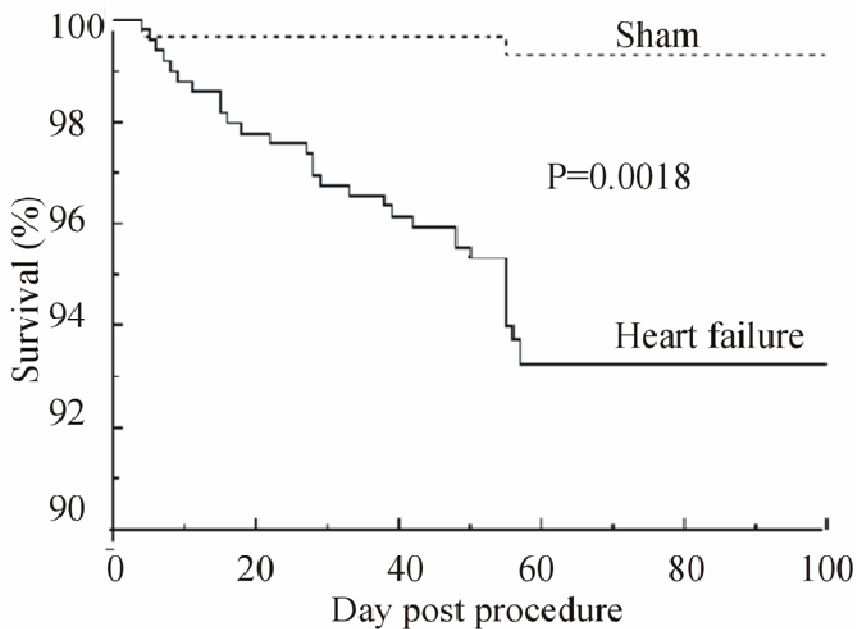


Figure 2.1 Survival following surgical coronary arterial ligation in rabbits
Kaplan-Meier curves showing survival in rabbits following coronary artery ligation compared with that in sham-operated controls.

The arterially perfused rabbit left ventricular wedge preparation

The study of ventricular electrophysiology at the tissue level has relied on a number of different experimental techniques, each of which has been designed to closely reproduce different aspects of normal physiology. Open-chest experiments have the advantage that they employ blood perfusion and preserve cardiac autonomic innervation. However, the imaging techniques and experimental protocols are limited by the practicalities of working with anaesthetised animals. Isolated Langendorff-perfused hearts are commonly used in cardiac electrophysiology, as the technique is relatively straightforward and hearts remain stable over a period of many hours. Depending on the particular set of experimental conditions being studied, modified blood perfusion may be more appropriate. In working heart experiments, preload and afterload are reproduced, such that electrophysiology can be studied under different mechanical conditions. Each of these has their own advantages, but they share a common drawback, namely that recordings of electrical activity are confined to the immediate subepicardial layer of cardiomyocytes. Significant heterogeneity exists in the electrophysiological properties of cardiomyocytes isolated from different layers of the ventricular wall. Therefore, given that regional heterogeneities of membrane repolarisation properties can influence the electrophysiological substrate for re-entry, the transmural axis may be extremely important in the study of arrhythmogenesis. The study of repolarisation in isolated cardiomyocytes is limited because electrotonic coupling between

cells is an important determinant of repolarisation in intact ventricle¹⁴². For these reasons, arterially perfused LV wedge preparations, which allow access to the transmural surface in intact ventricle, have been developed in canine. These are now well established for the study of transmural ventricular electrophysiology using both microelectrodes¹⁴³⁻¹⁴⁵ and optical imaging with voltage-sensitive dyes¹⁴⁶. However, canine ventricle has a prominent M-cell layer, which is not thought to be found in humans¹⁴⁷. Moreover, circulatory differences mean that the pattern of myocardial infarction in canine is quite different to that seen in humans. For these two reasons, a rabbit left ventricular wedge preparation was developed for this study.

Development of the preparation

An arterially perfused rabbit LV wedge preparation has been developed by one group of investigators¹³¹. Published accounts of the methodology of preparing a rabbit LV wedge preparation describe a similar approach to that used in larger canine hearts. Blocks of tissue are dissected from the left ventricular free wall around a major coronary branch, which is then cannulated and through which the preparation is then perfused. Although these preparations have been used for the study of transmural electrophysiology, because of the difficulties associated with impaling single cells on the cut surface, this has only been possible by inserting shank intracellular electrodes more than 2mm into the tissue. These manipulations are technically challenging, meaning that electrode recordings can only be taken from three discrete sites at any one time¹³¹. These issues have limited the use of the rabbit wedge preparation in the study of transmural ventricular electrophysiology, and to date there have been no reports of optical imaging of voltage across the entire transmural surface of the rabbit LV wedge.

A series of different techniques were explored during the development of the arterially perfused rabbit LV wedge preparation used in this study. Trials of initial techniques were undertaken in hearts already used in Langendorff mode for other experiments. Various different cannula types and cannulation approaches were tried and the area of perfusion achieved with each was assessed by perfusing the preparation with methylene blue dye. The largest area of reliable perfusion was achieved with direct cannulation of the left main coronary artery from its aortic ostium, and this was found to be superior to arterial cut-down approaches. Various adaptations to allow fixation of the cannula in the artery were tested. These included purse-string sutures around the cannula in the aortic wall and addition of struts to the cannula to facilitate suturing. The most reliable method was found to be oversewing of the cannula proximal to a bleb. Different flow settings were trialled to

achieve a perfusion pressure of 50-60mmHg. A series of chambers was designed, custom built (by the IBLS workshop, University of Glasgow) and tested before the final design was chosen.

Method

Rabbits were killed with an intravenous injection of sodium pentobarbitone (100mg/kg). Hearts were excised and immersed in ice cold Tyrode's solution, and transferred to a custom-built Perspex chamber for dissection and imaging. The method for preparing the perfused LV wedge from an isolated whole heart is shown in Figure 2.2. The aorta was opened, and the left main coronary arterial ostium identified. The modified cannula was passed into the artery with perfusate running to avoid air embolism. As soon as the cannula was in position the flow rate was immediately increased to 30ml/min. The correct cannula position was verified by visual inspection, by identifying washout of blood from the perfused area of myocardium, and by observing an appropriate pressure rise in the perfusion system (~50-60mmHg). The time from excision to cannulation and perfusion was < 4 minutes. The right ventricular outflow tract (RVOT) was then removed to allow identification of the cannula marker for suturing, and the cannula was secured by oversewing. The left and right atria and the right ventricular (RV) free wall were then removed. In most preparations this could be done without compromising perfusion; in some suturing of atrial and RV vessels was required to maintain perfusion pressure. At this stage, the preparation was loaded with voltage-sensitive dye by a slow bolus injection through an injection port in line with the cannula. An incision was then made through the interventricular septum (IVS) at the base of the aorta and any unperfused tissue at the base of the aorta was then removed. Any cut vessels causing a reduction in perfusion pressure were sutured closed. Once the perfusion was stabilised, the septum was removed with a microtome blade, leaving a cut surface of perfused LV free wall for optical imaging.

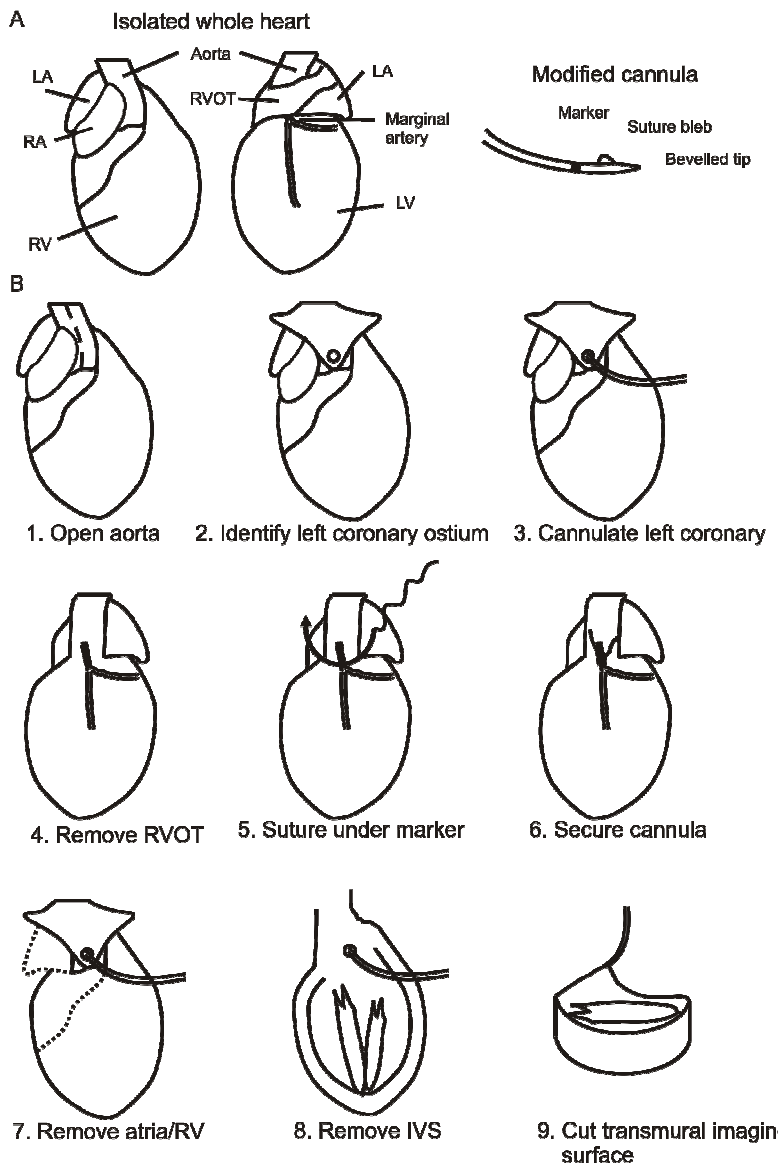


Figure 2.2 The method for producing the left ventricular wedge preparation.

An illustration of the isolated whole heart from both sides, along with the modifications to the cannula, which include placement of a marker to guide suturing, a bleb which sits distal to the suture and a bevelled tip to facilitate cannulation with minimal risk of arterial trauma. B. An illustration of the method of cannulation employed for the perfused LV wedge preparation. The ascending aorta is opened with a longitudinal incision (1) and the left main coronary ostium is identified (2) and cannulated (3). From the other side of the heart, the RVOT is then removed (4), the cannula position is ascertained using the suture maker and the bleb and a suture is placed between the two (5) and the cannula is then secured (6). Next the atria and RV are removed (7), followed by the IVS (8), before the transmural imaging surface is cut with a dissecting blade (9).

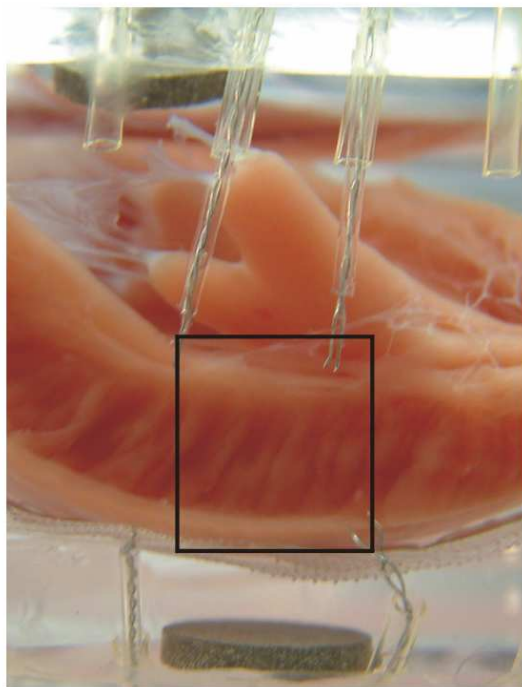


Figure 2.3 The LV wedge preparation mounted for optical imaging

A photograph of the LV wedge preparation mounted for transmural imaging. The optical imaging window is indicated by the black square. The extracellular disc electrodes for recording the pseudoECG can be seen above and below the preparation, as can pairs of epicardial and endocardial stimulating electrodes.

The perfused LV wedge preparation was then moved to the imaging part of the chamber and secured with dissecting pins to Sylgard mounts designed to optimally orientate the preparation for imaging, as shown in Figure 2.3.

Viability of the preparation

Ensuring the viability of the preparation was paramount throughout these studies. Viability parameters were noted during each dissection, throughout each experiment as well as during the analysis of each dataset. Only preparations which satisfied all of these checks were included in the final dataset.

During the procedure, it was usual for healthy preparations to develop spontaneous activity following cannulation and perfusion with warm solution (usually in under 1 minute). Spontaneous activity tended to persist following removal of the atria and the RV free wall and following the first cut into the IVS, and was then usually lost around the time of the second cut to completely remove the IVS. As any reduction in perfusion pressure was quickly reversed by ligating cut vessels, this loss of spontaneous activity is likely to be due to a loss of LV muscle mass and His-Purkinje tissue. Any deviations from this normal

pattern were recorded and considered in the viability assessment. Ventricular arrhythmias during dissection were unusual, but where they occurred were recorded and considered in the viability assessment. In all experiments, at the end of the protocol the perfusion was changed to oxygenated Tyrode's solution without motion uncouplers at 37°C and stimulation was continued for 15-20 minutes to assess the contractile state of the preparation. Only wedge preparations which contracted well at the end of the experiment were included in the final dataset.

In all experiments, the perfusion pressure was monitored throughout and recorded at regular intervals during each experiment, such that any major changes indicating either a change in cannula position or an insult to the preparation could be addressed. Any slow increment in pressure was taken into account during the viability assessment. In a subset of initial experiments ($n = 3$), viability was also assessed using 2,3,5 triphenyltetrazolium chloride (TTC, Sigma-Aldrich, Steinheim, Germany) staining, which indicated good perfusion of the LV free wall including the transmural surface, as shown in Figure 2.4.



Figure 2.4 Perfusion of the LV wedge preparation assessed by TTC staining

An example of a wedge preparation after staining with TTC at the end of the experiment. The preparation has been sectioned, and both sides of each section are shown. TTC stains viable myocardium red and leaves unperfused tissue white.

In a subset of initial experiments ($n = 2$), the stability of transmural optical AP morphology during baseline pacing was assessed and indicated that AP parameters were stable over a timescale of 90-120 minutes, despite a progressive decrement in signal amplitude and S/N ratio, which was partially restored by further injections of voltage-sensitive dye (see Figure 2.5). As APD shortening is an early and sensitive sign of ischaemia, and no major APD shortening was seen in these experiments, subsequent protocols were designed such that all transmural recordings were performed within this timescale, and dye levels were supplemented at ~ 40 minute intervals.

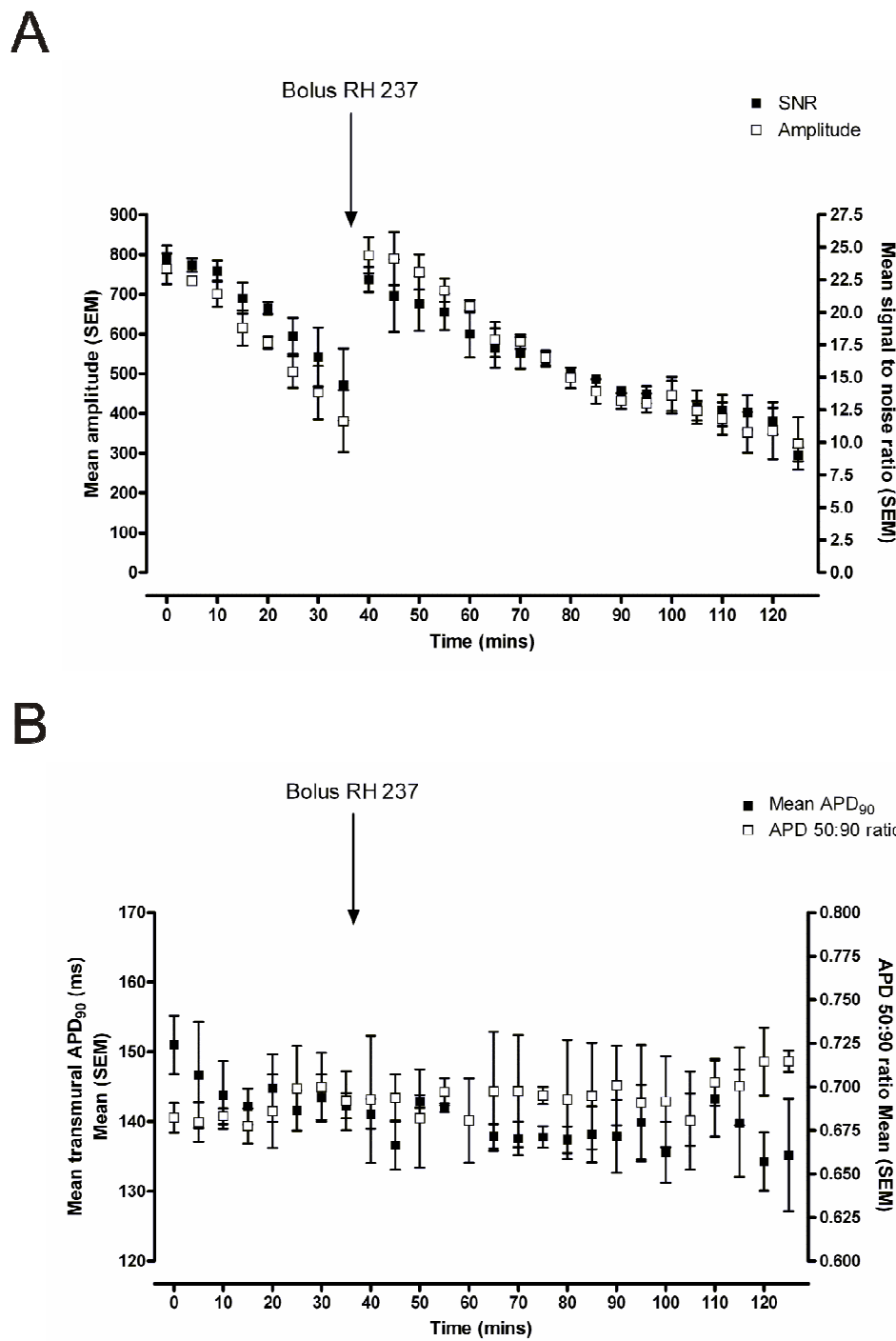


Figure 2.5 Stability of transmural optical APs over time

A. Signal parameters over time ($n = 2$) shows the gradual reduction in S/N ratio and amplitude, which responds to dye loading. B. Mean APD₉₀ and APD50:90 ratio over time.

In a further subset of experiments ($n = 3$), the transmural surface APs were compared to those recorded from the epicardial surface. The cut surface was positioned at the top border of the imaging window, and mean APD₉₀ was compared for each pixel row back from the cut surface, to quantify the gradient of damage in terms of APD₉₀. The results are shown in Figure 2.6, and indicate a 5% shortening of mean APD₉₀, relative to that which would be expected on the epicardial surface. Due to the orientation of the cut surface during

epicardial imaging, this should not be confounded by apex-base gradients of APD₉₀, which should be comparable in each pixel row.

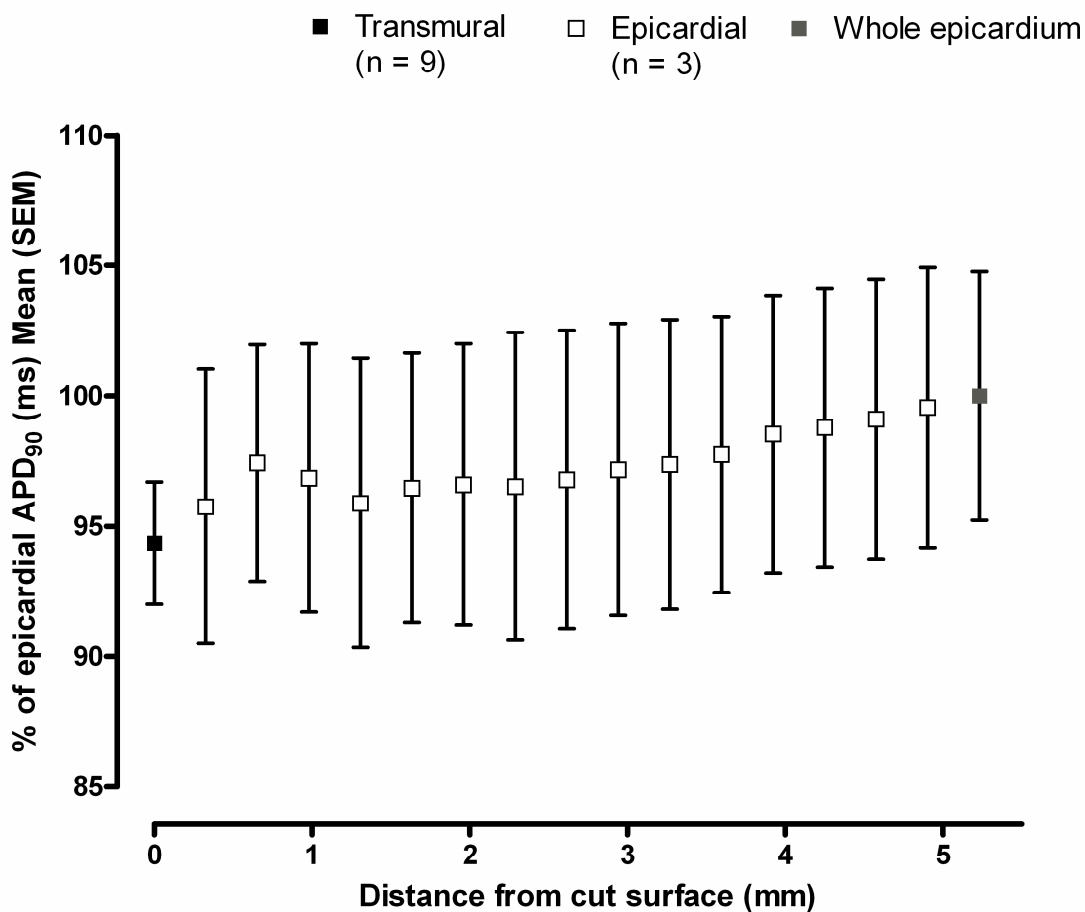


Figure 2.6 The gradient of epicardial APD₉₀ relative to the cut surface

Mean epicardial APD₉₀ for each row of pixels back from the cut surface (open squares), expressed as a percentage of mean APD₉₀ across the whole epicardial imaging window (grey square). The mean subepicardial value from transmural imaging is shown for comparison (black square). n = 3 at 37°C.

Perfusion system

A single pass perfusion system was built for the perfused LV wedge preparation. This comprised heating components and a pumping system to deliver warmed oxygenated physiological solution to the preparation. Pressure was monitored using an inline pressure monitor. Pressure, temperature and flow calibrations were performed regularly, and after any change in equipment to ensure a constant flow of 30ml/minute and a constant temperature of 30°C or 37°C, depending on the experimental protocol.

Physiological solution

The LV wedge preparation was perfused with Tyrode's solution at pH 7.4, containing, in mmol/L: Na⁺ 134.5, Mg²⁺ 1.0, K⁺ 5.0, Ca²⁺ 1.9, Cl⁻ 101.8, SO₄ 1.0, H₂PO₄ 0.7, HCO₃ 20, acetate 20 and glucose 10. The solution was filtered through a 5µm filter (Millipore) and continuously bubbled with gaseous mixture of 95% oxygen (O₂) and 5% carbon dioxide (CO₂) to maintain pH 7.4.

Stimulation

LV wedge preparations were paced using bipolar platinum stimulating electrodes, placed on the endocardial or epicardial surface, at the border with the transmural surface, in the mid portion of the LV free wall. Preparations were paced at twice diastolic threshold at a baseline pacing CL of 350ms. Electrodes were connected to a pulse generator (Digitimer DS7) which provided a constant voltage square pulse with a width of 2ms. Timing of the pulse was controlled using a computer program written by Dr Francis Burton. The preparation was stimulated at twice diastolic threshold. Pairs of silver chloride disc electrodes (Laboratory Instruments) were arranged in the tissue bath to record a pseudo ECG from the preparation. The pseudo ECG was continuously recorded onto a laptop computer using a USB compatible digitizer (DI-158U, Dataq Instruments Inc).

Numbers

A total of 56 animals were used for these experiments including 30 normal animals, 4 sham operated animals and 12 ligated animals. Sham-operated animals were included in the normal group, except for the comparison of echocardiographic data between sham and ligated animals in Chapter 5.

Optical mapping

In this study, an optical mapping system was used to record electrical activity from across the transmural and epicardial surfaces of the perfused LV wedge preparation.

Introduction

Optical mapping is a method which allows recording of electrical activity by staining a preparation with a voltage-sensitive dye and using a photodetector to measure the changes in fluorescence during depolarisation and repolarisation. Since the development of voltage sensitive dyes which are non-toxic and able to faithfully represent membrane potential measured with microelectrodes, optical mapping has become widely used in experimental cardiac electrophysiology. One of the major attractions of this technique is that instrumentation with electrodes is not required. Multiple electrode impalements or contact points are difficult to maintain and this significantly limits the number of simultaneous recordings which can be made from different areas using electrodes. Optical mapping allows simultaneous sampling from many hundreds of sites, and is therefore ideally suited to the study of electrophysiology in multicellular preparations. Moreover, unipolar electrode recordings do not allow accurate study of repolarisation. Equally, there are some drawbacks to optical mapping. The recordings are sensitive to movement artefact and preparations must be immobilized, either mechanically or with uncoupling agents, some of which may have effects on cellular electrophysiology. The spatial resolution, depending on the exact parameters used in each system, is such that each optical AP, derived from a single pixel, may represent the summation of the electrical activity from a number of cells, rather than a single cell AP, meaning that optical APs must be interpreted accordingly.

Voltage sensitive dyes

Voltage-sensitive dyes are compounds which display differing spectra of fluorescence depending on membrane potential. Once bound to the cardiomyocyte plasma membrane, dye molecules can be excited by incident photons of a given wavelength, and on returning to their basal state, they then emit photons of higher wavelength. The wavelength spectrum of this fluoresced light varies with V_m , such that the intensity of fluoresced light above a given wavelength is nearly proportional to V_m . Excitation and emission takes around 10^{-6} ms, meaning that even the rapid (~5ms) upstroke of the AP can be represented accurately by changes in dye fluorescence. Side effects of voltage-sensitive dyes on cardiac tissue can include phototoxicity and pressure changes, although these are reduced by careful dye loading. The voltage-sensitive dye used in this study was RH237 (Molecular Probes Inc,

Oregon), which has been widely used in the study of cardiac electrophysiology. The dye was made up into 1mg/ml stock solution in DMSO, of which aliquots were then protected from the light and stored at -20°C, to be thawed just prior to use. A 100µl bolus of RH237 (concentration 2mmol/L) was injected slowly into the port proximal to the modified cannula.

Optics

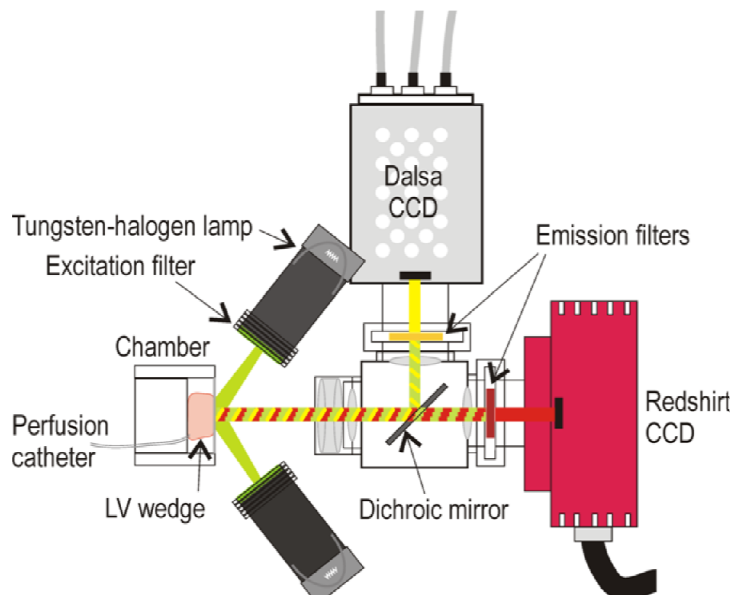
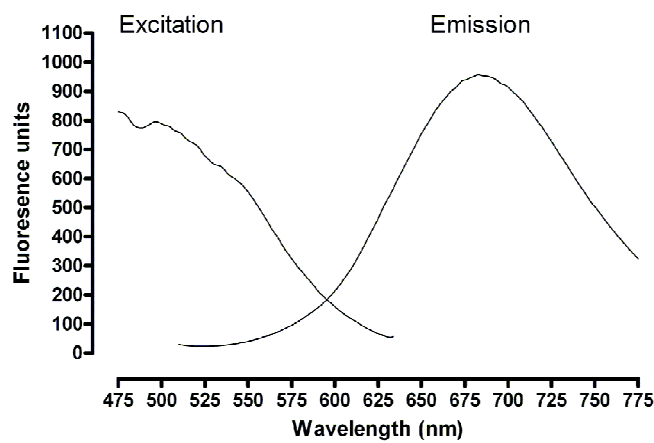
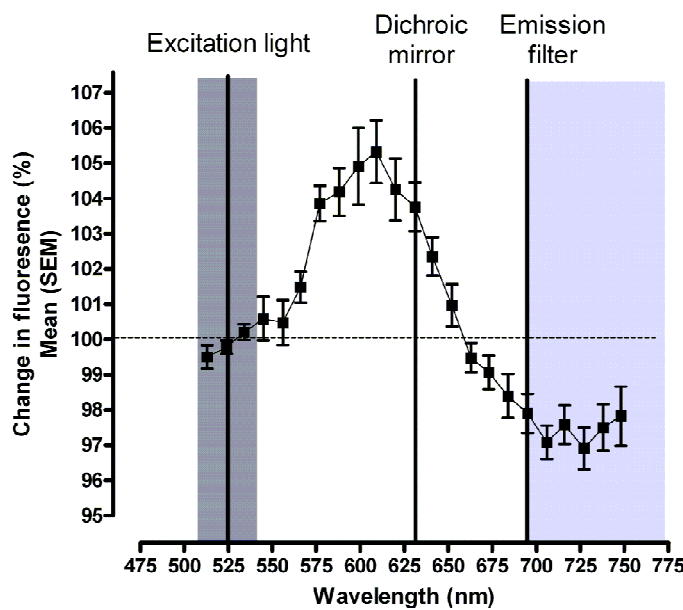
In order to follow V_m changes, a simple series of optics must be set up to collect the fluorescent light produced by the voltage-sensitive dye. Excitation light is passed through a filter to produce the optimal wavelength for excitation of the chosen voltage-sensitive dye. For light collection, long-pass (LP) or band-pass (BP) filters remove the shorter wavelength excitation light and so allow exclusive collection of the longer wavelength emitted light. When these filters are correctly placed with respect to the spectral shift of the dye fluorescence on depolarisation, they provide a cut point above which changes in the intensity of the emitted light will represent changes in V_m . Magnification reduces the amount of light collected, by reducing the area available as a source of fluorescence, and so a balance must be struck between light collection (and consequently, signal to noise ratio) and spatial resolution.

CCD-based optical mapping system

The CCD-based optical mapping system used in this study is illustrated in Figure 2.7A. Illumination was provided by four tungsten halogen lamps, directed towards the imaging surface. Excitation light from each lamp was passed through interference filters ($525 \pm 15\text{nm}$). Light was then collected through a photographic lens and split with a dichroic mirror at 630nm. The longer wavelength portion passed through a long pass emission filter ($> 695\text{nm}$) and was focused onto the CCD camera (RedShirt, Woods Hole, MA). The shorter wavelength portion was focused onto a second CCD camera (Dalsa), which was used to acquire plain images of the preparation at higher resolution. Voltage sensitive dyes may have different excitation peaks, emission peaks and spectral shifts under different experimental conditions. This means that each dye must be calibrated, in order that optimal filter settings can be chosen to optimise signal to noise (S/N) ratio. The voltage-dependence of RH237 fluorescence in rabbit cardiomyocytes was ascertained using spectrophotometry. The excitation and emission spectra for RH237 are shown in Figure 2.7B. The optics of the system relative to the measured fluorescence change on depolarisation of single cells are shown in Figure 2.7C.

System parameters

The CCD camera was set up to image an array of 26 x 26 (676) pixels with a sampling rate of 5kHz. A close up lens gave a field width of 8.5mm, resulting in a single pixel dimension of 327 x 327 μm . The volume of this tissue over which the signal is averaged is determined by the optical magnification used and the depth of penetration. The proportion of the fluorescent signal which originates from deeper layers of myocardium can be estimated by characterising the light transmission properties of cardiac tissue¹⁴⁸. In our system, we estimate that 80% of the signal originates from a depth of 700 μm , with the majority of the signal coming from the first 400 μm . Including an estimated depth penetration of 700 μm we estimate that our optical APs represent around 3000 cardiomyocytes per pixel in a layer ~100 cells thick.

A.**B.****C.****Figure 2.7 Optical mapping system**

- A. Illustration of the CCD-based optical mapping system, courtesy of Dr Francis Burton.
 B. Excitation and emission spectra for RH237 in isolated rabbit ventricular cardiomyocytes. C. Fractional change in RH237 fluorescence on administration of KCl, with the optics for the imaging system illustrated.

Motion artefact

Motion artefact is a major consideration during optical recording, and various methods have been proposed to ameliorate this. These include mechanical restraint, pharmacological excitation-contraction uncoupling and reducing intracellular $[Ca^{2+}]$. In this study, pharmacological approaches were chosen to minimise motion artefact for optical imaging. The rationale for this was twofold: firstly, it was crucial to maintain normal intracellular $[Ca^{2+}]$, because of its importance in the development of repolarisation alternans; and secondly mechanical restraint of a delicate cut surface was not desirable. As all pharmacological motion uncoupling agents have some reported electrophysiological effects, their use was minimised as far as possible.

2,3-butanedione monoxime

2,3-butanedione monoxime (BDM, Sigma-Aldrich, Steinheim, Germany) is an inhibitor of myofibrillar ATPase¹⁴⁹, and so prevents myocardial contraction in response to an increase in intracellular $[Ca^{2+}]$. BDM has been widely used to eliminate motion for optical mapping in cardiac preparations, but it does have effects on myocardial cell electrophysiology and calcium handling. In isolated rat myocytes 10mmol/L BDM reduced SR Ca^{2+} content¹⁵⁰. In rabbit ventricular myocardium 20mmol/L BDM virtually abolished LV developed pressure with a minor slowing of conduction velocity, but without any effect on monophasic APD_{90}^{151} . Concentrations of BDM above 20mmol/L reduced the slope of electrical restitution (measured by an S1S2 protocol). For this study a concentration of 15mmol/L was chosen, in an attempt to minimise any effects of BDM on restitution.

Optical action potentials

Optical APs have a number of unique characteristics, that are determined by the way in which they are collected, and which must be considered during their interpretation. Firstly, optical APs have been shown to represent accurately the morphology and time course of changes in membrane potentials recorded with intracellular microelectrode techniques¹⁵². However, because only changes in fluorescence are measured, optical APs contain no information regarding the absolute values of V_m . Secondly, optical APs represent a spatial average of changes in transmembrane potential from cells in a given volume of tissue. This spatial averaging produces an increase in the rise time of the optical AP, compared with that seen in an AP recorded by an intracellular microelectrode.

Experimental protocols

In each experiment, baseline pacing from the endocardial surface at a CL of 350ms was initiated after the preparation had been mounted in the imaging section of the chamber. Optical recordings were taken for 2 seconds during steady state pacing, and at least 30s after any change in pacing CL. Baseline recordings were repeated at the end of each protocol, to assess for any changes in the condition of the preparation caused by the protocol.

Epicardial imaging

In a subset of experiments, epicardial imaging was performed, in order to allow comparison of transmural and epicardial AP parameters and electrophysiology. Following transmural imaging, the preparation was repositioned, such that the epicardial surface was presented to the optical mapping system. The cut edge was consistently positioned at the upper border of the imaging window, and the same part of the LV free wall (in its apex-base axis) was imaged. The stimulating electrodes were positioned directly opposite one another, with the epicardial electrode visible in the mapping field. In these experiments the same temperature and stimulation protocols were used.

Stimulation site protocol

To investigate the effect of stimulation site on baseline AP characteristics, stimulating electrodes were positioned on the endocardial and epicardial border of the transmural surface, opposite one another and perpendicular to the transmural axis. The preparation was stimulated at 350ms from the endocardium for 30s prior to optical recordings. The stimulation was then changed to the epicardial electrode for 30s and optical recordings were repeated, before stimulation was returned to the endocardium.

Dynamic restitution protocol

Pacing CL was progressively shortened in 50ms decrements to 200ms and then in 10ms decrements, and recordings were taken after 30s of pacing at each CL. Pacing CL was progressively reduced until loss of 1:1 capture or a ventricular arrhythmia (VA) was induced. Where VA was sustained, overdrive pacing was attempted, and where this failed pacing was terminated and a rapid bolus of $25\mu\text{l } 1\text{mol/L KCl}$ was administered to induce asystole. At the end of the protocol pacing was returned to a CL of 350ms.

Alternans protocol

Alternans experiments were initially performed at 30°C, in keeping with other published accounts of this behaviour. Optical recordings were taken during baseline endocardial pacing at a CL of 350ms. Pacing CL was then progressively shortened in 50ms decrements to 200ms and then in 10ms decrements, and recordings were taken after 30s of pacing at each CL. Pacing CL was progressively reduced until loss of 1:1 capture or VA was induced. Where VA was sustained, overdrive pacing was attempted, and where this failed pacing was terminated and a rapid bolus of 25µl 1M KCl was administered to induce asystole. At the end of the protocol pacing was returned to a CL of 350ms. In a subset of experiments, the endocardial pacing protocol was completed and then repeated during epicardial stimulation. In a separate group of experiments the same protocol was performed at 37°C. In some hearts, both temperatures were tested, and in these experiments the initial temperature was 37°C, and was then reduced to 30°C, to avoid any rewarming effects.

Drug effects

The effects of carbenoxolone and rotigaptide on baseline behaviour were investigated. For each drug a time control recording during baseline pacing was established 15 minutes prior to the start of the drug administration. After 15 minutes another baseline recording was taken and then the drug infusion was started. Recordings were taken during baseline pacing and after 30s of epicardial pacing every 5 minutes during the protocol. 15 minute washouts were performed at the end of the protocol and repeat recordings taken.

Data analysis

Data analysis was performed using a number of custom analysis programs, written by Dr Francis Burton. All automated analysis was visually verified and regular checks were performed to ensure accuracy.

Optical data analysis

The data files were saved using the Redshirt camera software and were stored on two hard drives as well as on CD/DVD. Each data file contained 2s worth of APs for each of the 676 sites in the imaging window. These files were read into the analysis program and the AP traces were inspected for general condition and for any major artefacts. A Gaussian spatial filter (radius 2 pixels) was applied to the data prior to analysis. The picture of the imaging surface was then read in and an analysis ‘selection’ was constructed, which identified only those pixels which corresponded to the transmural surface (see Figure 2.8). These selections were saved and re-used for each type of analysis, to maintain consistency. It was also possible, after the analysis was done, to make more specific selections (e.g. subendocardial, midmyocardial and epicardial) and interrogate the saved data matrix with these selections, to avoid repeat analysis and to minimise error.

Action potential characteristic analysis

Automated algorithms were used to determine AP characteristics across all sites in the transmural selection. The section of the trace corresponding to each individual AP for analysis was marked using two cursors, in relation to the stimulus. The automated algorithm was then started, which calculated trace characteristics (e.g. baseline, amplitude and S/N ratio) and AP characteristics for each pixel within the selection. AP characteristics were analysed using two different approaches. The first employed a standard algorithm, which identified the peak, baseline, first and second derivative of the trace and from those was able to calculate the AP characteristics. The second used a template fitting algorithm designed by Dr Francis Burton, which uses a least squares method to fit smooth AP templates to the experimental data, and derives AP characteristics from the template. For each analysis type, settings were modifiable based on the data characteristics, and a number of settings were tested before the optimal settings were identified. For each analysis approach, the same definitions were used for AP characteristics. Activation time (AT) was defined as the time at the first derivative (i.e. the fastest rate of rise during the AP upstroke). As the shape of optical AP upstrokes can be variable, particularly at rapid stimulation rates, we also identified the midpoint of the upstroke (AT-mid). Repolarisation

time (RT) was defined as the time at return to baseline from the peak. As is standard in this type of analysis, due to the S/N ratio typical of optical APs, the time at 90% repolarisation was used to calculate the action potential duration at 90% repolarisation (APD₉₀). APD₉₀ was defined as RT₉₀ minus AT (or AT-mid). At the end of the analysis, the program had calculated a total of 78 parameters for each pixel in the analysis selection. The data for each parameter were displayed by colour scale in a pixel array, and the most commonly used parameters (AT, RT₉₀, APD) were visually checked for outliers and mistakes.

Outliers due to artefact in the recorded data could be removed at this point, and mistakes by the automated algorithm could be corrected by resetting the analysis session. This was usually done by setting more appropriate cursor positions, only occasionally were different filter settings or parameter definitions required. All of these data were saved along with pixel identifiers and cursor position as a data matrix, which could be read back into the same program for second order analysis when required. The process was then repeated for the next AP. For each experiment, 5-12 APs (depending on CL) were analysed at each CL and these were averaged to produce a mean value for each CL. This meant that where alternans occurred, differences were averaged over series of beats to produce representative value at each CL.

Second order analysis

Second order analysis included determining basic descriptive statistics (e.g. mean, SEM, range) for a particular parameter for all the data points in an analysed selection, and calculation of secondary parameters. Dispersion of activation time, repolarisation time or APD₉₀ was defined as the 5-95% range of the relevant parameter, and was expressed in ms/mm² in order to correct for differences in area (i.e. when comparing transmural and epicardial imaging). During this process, the saved data matrices were also interrogated using different selections. Transmural conduction velocity was calculated using speed = distance / time. Transmural conduction time was measured using 3 by 1 pixel selections perpendicular to the transmural surface, at the point of earliest activation on the endocardial border to earliest activation on the epicardial border. Transmural distance between the centre sampled pixels was calculated from the corresponding images using: distance = $\sqrt{((\text{start x} - \text{end x})^2 + (\text{start y} - \text{end y})^2 * \text{pixel width})}$. Batch files were written in MATLAB by Dr Francis Burton to facilitate rapid processing during this secondary analysis. Isochronal contour maps were plotted using MATLAB. For the more complex analytic manipulations, the data matrices were read into GraphPad Prism.

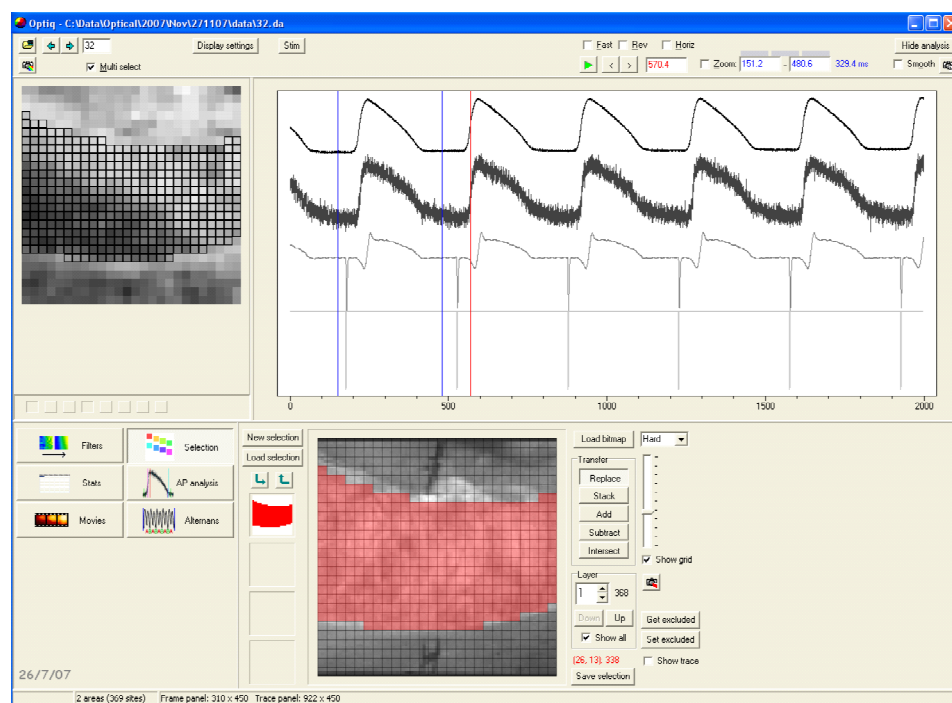
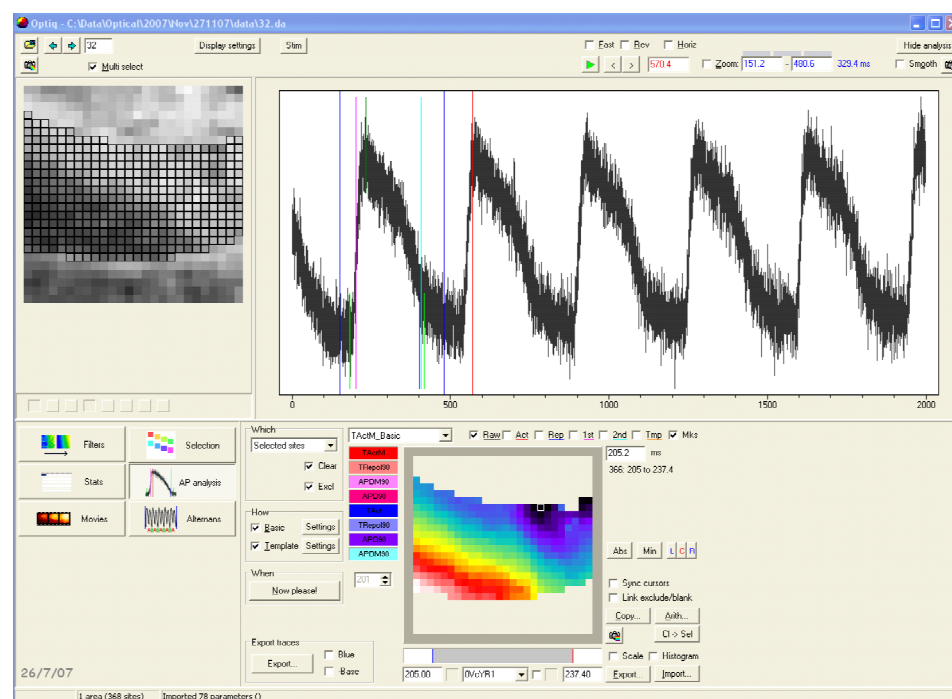
A.**B.**

Figure 2.8 Analysis of AP characteristics

The data analysis program. A. Top left pixel array shows the data and the selected pixels. The lower pixel array shows the pixel selection derived from the fluorescence image. The top right panel displays the averaged trace from all the selected pixels (top trace), a single pixel trace from the midmyocardium (second top trace), the pseudoECG (second lower trace) and the stimulus (lower trace). The blue cursors are positioned to analyse the first AP and the red cursor indicates the time point displayed in the top left pixel array. B. Following the completion of the automated analysis, the data are displayed in a colour pixel array, along with coloured lines to identify the main parameter positions on the trace.

Restitution curves

APD₉₀ restitution curves were generated using batch files written in MATLAB software by Dr Francis Burton. For each experiment, the mean APD₉₀ within a particular sampling area at each CL was calculated from the individual optical APs in each pixel. The sampling areas used were changed to allow measurement of both global (i.e. transmural or epicardial) and regional (i.e. subendocardium, midmyocardium and subeicardium) restitution behaviour. Mean APD₉₀ was then plotted against the corresponding DI (DI = pacing CL – APD₉₀) to yield a restitution curve. A subset of restitution curves were also calculated manually, in order to verify the automated processing. The mean datasets were then fitted with one-phase exponential curves using the equation $Y = Y_{\max}^*(1 - \exp(-K^*X))$, where the curve starts at zero and ascends to Y_{\max} with a rate constant, K. In order to determine and compare the slope of the restitution curves, each curve was then differentiated, allowing the slope of the curve to be plotted against DI. The relationship between DI and CL for each dataset was then used to transform DI to CL, allowing the slope of the restitution curve to be plotted against CL. The maximal restitution slope was also calculated by fitting a linear function to the five data points at the shortest CLs.

Alternans analysis

A separate algorithm employed a spectral analysis, based on the clinical MTWA algorithm, to identify and quantify repolarisation alternans. The program was custom written by Dr Francis Burton to determine the presence of alternans in optical AP traces. The same selection and filtering used in the AP analysis were applied to the raw data, and the cursors were placed to identify the start and end of the AP run to be analysed. The trace, along with the corresponding stimuli, were then inspected, and an repolarisation window was determined that particular trace. The repolarisation window defined a standardised part of each AP, along which each point would be compared with that from subsequent APs in a spectral analysis, to determine the magnitude of alternans. This time window could be set relative to either the stimulus or the activation time. Once the window was determined, the analysis was started and the program displayed ‘Alternans graphs’ for each pixel (see Figure 2.9). This included a display of the repolarisation window and the parameters from which it was derived over each AP, such that the appropriateness of the window could be visually checked, and adjusted if necessary. For each pixel, the program scaled the amplitude of each trace between 0 and 1. The program then superimposed each AP in the trace and subjected each point within the repolarisation window to a spectral analysis. The power at a frequency of 0.5 cycles/beat was then cumulated over all the data points lying within the repolarisation window and divided by the number of points in the segment, to

produce a value for alternans magnitude. Alternans phase was determined using the cumulative sum of the signed difference between the normalised trace segments from successive beats, divided by the number of data points, and by the number of beats. As a result of the amplitude scaling, the units of these two values were arbitrary but relative to the proportion of total trace amplitude. The data for each parameter were displayed by colour scale in a pixel array, and the key parameters were visually checked for outliers and mistakes. Outliers due to artefact in the recorded data could be removed at this point, and mistakes by the automated algorithm could be corrected by resetting the analysis parameters. All of these data were saved along with pixel identifiers and cursor position as a data matrix, which could be read back into the same program for second order analysis when required. The process was then repeated for the next cycle length.

In addition to quantifying alternans of repolarisation, it was equally important to determine AP characteristics (and any changes from one beat to the next) during alternans. In order to achieve this, while maintaining the spatial arrangement of each data point by pixel, a data manipulation program written in MATLAB software was used. This allowed extraction of a spatial matrix of data points for a single parameter from the saved analysis file, along with visual inspection at this stage to allow for identification of outliers. This matrix was then held and the matrices for each subsequent beat in the trace could each be extracted. The program calculated, for each pixel, the difference in the value of the selected parameter from one beat to the next, along the trace, producing a spatial array of the mean difference in the chosen parameter from one beat to the next. This allowed correlation of spectral alternans magnitude to measured differences in APD₉₀ in milliseconds.

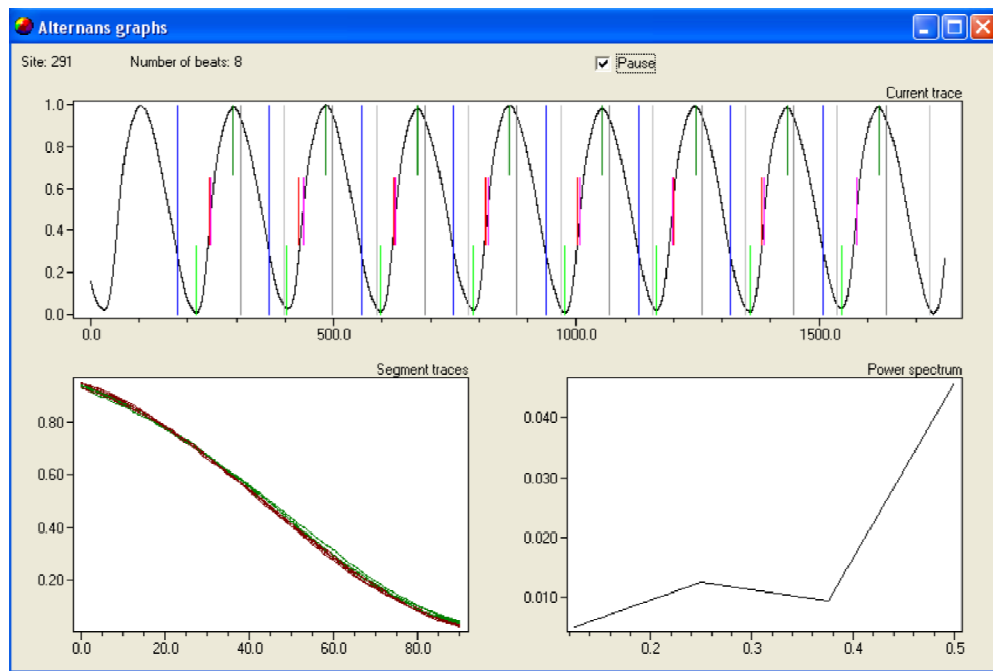
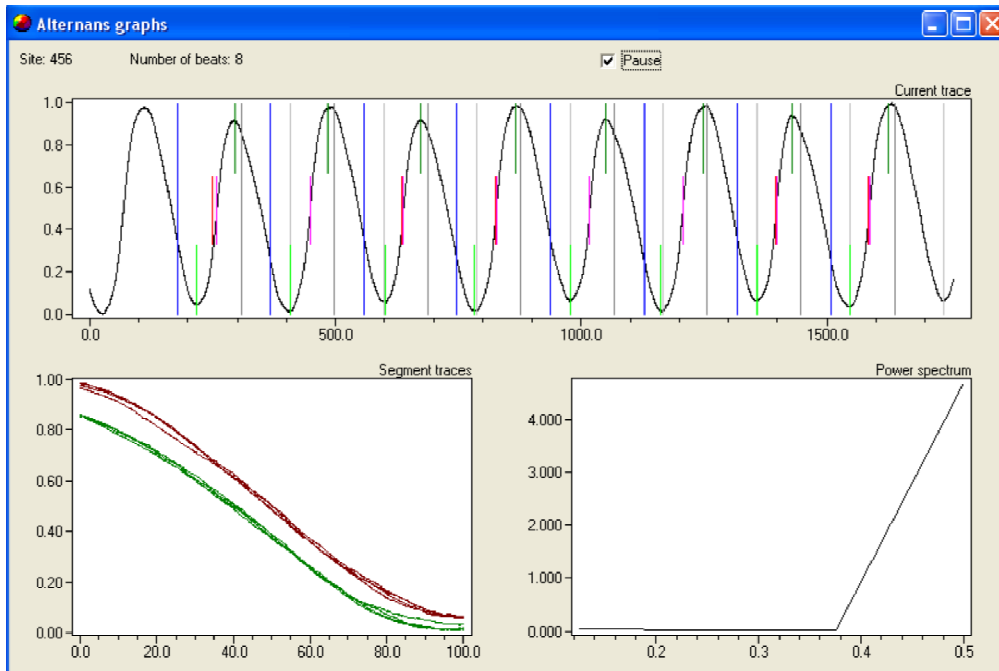
A.**B.**

Figure 2.9 Spectral analysis to quantify repolarisation alternans

The alternans analysis program. A. Spectral analysis for a representative pixel without alternans. The upper panel shows the trace with AT-mid (in pink), peak and baseline (in green), stimulus (in blue) and the repolarisation window (in grey) displayed over each AP. The lower left panel displays the section of each trace corresponding to the repolarisation window, with odd APs in green and even in red. The lower right panel displays the frequency spectrum for that pixel. B. The spectral analysis for a representative pixel displaying alternans.

Viability assessment

In the perfused LV wedge preparation, cellular ischaemia could be due to either trauma during the preparation of the cut surface, or to under-perfusion because of the presence of cut vessels within the myocardium. It was paramount to ensure, where possible, that only healthy transmural APs were included in the analysis. Nevertheless, it was accepted that perfusion of the cut surface would reduce over time and produce metabolic compromise, which may affect the results. Assessing viability is a complex problem, particularly in a novel preparation. A standardised assessment system was therefore developed. This took into account a number of parameters, from the original dissection to the data analysis stage, and only preparations which stayed within pre-defined ranges were included in the final datasets.

During the development of the preparation, a number of subjective parameters during the dissection were identified as discriminatory between healthy and unhealthy preparations. These included: an ideal step up in pressure of 50-60mmHg and not exceeding 100mmHg on cannulation of the left main coronary artery (LMCA); good washout of blood from the LV free wall; prompt spontaneous activity on perfusion of the LV free wall; persistence of spontaneous activity until the wedge was fully dissected; recovery of any drop in perfusion pressure by suturing after removal of the IVS and absence of VF. During the protocol it was noted whether there was a clear reduction in movement with addition of BDM to the perfusate and a low pacing threshold, both of which were thought to be associated with generally non-ischaemic tissue. As described earlier, the optimal timescale was thought to be 90-120 minutes, and so all protocols were performed within that time frame. At the end of each experiment, motion uncouplers were washed out during continued baseline pacing, to ensure that contractile function remained intact. These parameters provided a robust assessment of the viability of the preparation as a whole. However, the most direct and reliable test of the viability of the important transmural surface were the AP parameters recorded there. For this reason, further viability assessments were carried out at the data analysis stage.

Triangulation of the ventricular AP and associated shortening of the APD occur rapidly after the onset of ischaemia¹⁵³. Therefore, the demonstration of maintained APD over time would provide good evidence for a non-ischaemic tissue. Mean transmural APD₉₀, taken as a mean of the values measured in every pixel across the transmural surface at the start of each experiment, was determined for each experiment. Threshold values during baseline pacing were determined for each temperature, and where starting values fell below this, the

transmural recording for that preparation were not used. In addition to this, given that rapid pacing could produce functional ischaemia in cells with marginal perfusion, a second check of mean transmural APD₉₀ was performed at the end of each protocol on return to pacing at a CL of 350ms. Where this value fell by more than 10% from baseline to the end of the protocol, the values for that protocol were excluded.

Statistical analyses

All data are expressed as mean \pm standard error of the mean. Comparison between groups of data was made with Student's t-test (paired when appropriate). A two-tailed p-value of less than 0.05 was considered significant. Multiple comparisons were performed using a one-way ANOVA followed by post-testing to allow for multiple comparisons where appropriate. Adjustments for repeated measures were made where appropriate. Categorical comparisons were made using a Fisher's exact test. These statistical comparisons were performed in GraphPad Prism. Comparisons between two groups when two dependent variables were being examined was performed using a two-way ANOVA, which was carried out using R statistical software.

**Chapter 3: Transmural electrophysiology in rabbit left ventricular
myocardium**

Introduction

Significant electrophysiological heterogeneity is known to exist in mammalian ventricle. Gradients of action potential duration (APD) are present in normal myocardium in both the apex-base and the transmural axis. In isolated myocytes, transmural differences in the morphology of the action potential, APD, and the rate dependence and pharmacological responsiveness of APD have been observed in a wide variety of species, including humans¹⁰⁰. This transmural heterogeneity is potentially extremely important, as dispersion of repolarisation in ventricular myocardium is a powerful substrate for the generation of ventricular arrhythmia¹⁵⁴. Indeed, transmural heterogeneity of repolarisation has been implicated in arrhythmogenesis in a number of pathological conditions, principally ion channelopathies¹⁵⁵. Recently, the identification of spatially discordant alternans as a mechanism for re-entrant ventricular arrhythmia has led to increased interest in the potential pathophysiological role of such spatial heterogeneities. The development of spatially discordant alternans may depend upon baseline heterogeneities in repolarisation⁴⁰, including those spanning the ventricular wall^{66:101}. The experiments described in this Chapter were designed to characterise transmural electrophysiological heterogeneity in rabbit ventricular myocardium, and in particular to investigate those parameters which are relevant to the understanding of transmural repolarisation alternans.

Transmural electrophysiological heterogeneity

In canine ventricle, APDs recorded from cardiomyocytes isolated from the subendocardial layer are longer than those recorded from myocytes isolated from the subepicardial layer. Also, APs recorded from subepicardial myocytes are reported to have a more pronounced spike-and-dome morphology, which has been attributed to the presence of the transient outward current (I_{to}) in subepicardial cells¹⁵⁶.

The rate dependence of APD and APD restitution are interrelated phenomena which describe the shortening of APD in response to an increase in stimulation rate, and in response to the associated decrease in diastolic interval (DI) respectively. These changes are thought to be effected in the immediate phase by incomplete recovery from inactivation of ionic currents, and subsequently by a more gradual change in ionic current activity following a change in rate¹⁰⁰. Restitution curves generated from APDs

recorded from isolated subepicardial cells have been reported to be steeper than those from the subendocardial cells. As discussed in Chapter 1, steep restitution has been implicated in the production of repolarisation alternans, and steep restitution has also been associated with the production of ventricular arrhythmia⁹².

The midmyocardial 'M' cell

Unique electrophysiological behaviour has been recognised in some cells, which tend to be found in the deep subendocardium and midmyocardium and are referred to as 'M cells'. These cells show marked prolongation of APD at very low stimulation rates (CL > 2000ms), and in response to APD prolonging agents¹⁵⁷. M cells also display a faster rate of depolarisation (dV/dt_{max}) and relatively greater rate-dependent shortening of APD, such that APD values are comparable to subendocardial cells at faster stimulation rates¹⁵⁸. Pharmacological prolongation of the QT interval in intact ventricular preparations has been linked to preferential lengthening of APD in the M cell layer, which is thought to predispose the midmyocardium to developing afterdepolarisations and thus producing torsades de pointes arrhythmia¹⁵⁹. Transmural heterogeneity of repolarisation in canine has been widely characterised, as has the presence of M cells in this species. M cell type behaviour has also been reported in cells isolated from rabbit¹³⁴, guinea pig¹⁵⁸ and human ventricle¹⁶⁰.

Transmural heterogeneity in intact ventricular myocardium

There has been much debate as to the physiological relevance of these findings *in vivo* and conflicting reports as to the existence of APD gradients across the wall in intact ventricle have been published. There are two key issues. Firstly, the marked differences in M cell APD occur only at very slow stimulation rates^{159;161}. Secondly, in normal intact myocardium, strong electrotonic coupling exists between cells which would tend to mask any differences in APD between individual cells¹⁶². Therefore, in normal intact myocardium at physiological heart rates, transmural heterogeneity of repolarisation as seen in single cells may either be inapparent or functionally unimportant. Supporting this, *in vivo* studies using intramural plunge electrodes to record transmural activation recovery intervals (ARIs) have failed to show significant transmural gradients or M cell behaviour in canine¹⁶³ or human¹⁴⁷ ventricle. However, this may be due to insufficient resolution associated with these recording techniques¹⁶⁴ or to suppression of transmural heterogeneity with some anaesthetic compounds¹⁶⁵.

The role of intercellular coupling

In experiments using isolated myocytes, there are no external influences on the electrophysiological behaviour of the cell, aside from those imposed and controlled by the investigator. However, the situation in the intact heart is markedly different as each cell is coupled to neighbouring cells, allowing passive flow of charge between cells, which will tend to homogenise electrical behaviour in space.

Transmural electrophysiology at low temperature

As discussed in Chapter 1, there are a number of significant electrophysiological effects of lowering temperature in the mammalian heart. Hypothermia is commonly used in experiments to elicit alternans, as the heart rate threshold for alternans is lowered making it easier to study^{40;67}. However the basis for this temperature dependence is unclear and therefore it is important to establish the baseline effects of lowered temperature on ventricular electrophysiology, in particular on the parameters that may be crucial in the production of alternans and spatially discordant alternans, such as APD, dispersion of repolarisation and conduction velocity.

Transmural heterogeneity of repolarisation and alternans

As discussed in Chapter 1, during experimental studies with rapid pacing and low temperature, repolarisation alternans can become spatially discordant, setting up critical gradients of repolarisation which predispose to re-entrant arrhythmia. Repolarisation alternans may arise from alternans in intracellular Ca^{2+} cycling, or from primary alternans of APD, which can occur when the APD restitution slope is > 1 . There are a number of theoretical mechanisms by which spatially discordant alternans may occur, one of which is the presence of intrinsic gradients of APD and heterogeneity of APD restitution, which may give rise to regional differences in APD, particularly at high stimulation rates. Transmural heterogeneity of APD and APD restitution have been shown to be important for spatially discordant alternans and arrhythmia under long QT conditions^{66;69}. The extent to which transmural electrophysiological heterogeneity is important for alternans and arrhythmia is unknown. The experiments described in this Chapter were designed to characterise transmural electrophysiological heterogeneity in rabbit ventricular myocardium, to inform subsequent work examining repolarisation alternans.

Aims

The experiments described in this Chapter were designed to characterise transmural electrophysiological heterogeneity in rabbit ventricular myocardium, to inform subsequent work examining repolarisation alternans.

Specific aims were:

To record spatial patterns of depolarisation and repolarisation across the transmural surface of intact rabbit left ventricle at baseline and during rapid stimulation.

To quantify the transmural heterogeneity of repolarisation and restitution that exists in intact ventricular myocardium.

To compare transmural and epicardial heterogeneity of repolarisation and restitution.

To examine the effects of low temperature on transmural electrophysiology.

Methods

In order to investigate transmural electrophysiology in intact rabbit left ventricular myocardium, the CCD-based optical mapping system described in Chapter 2 was used to record optical action potentials from the transmural surface of perfused left ventricular wedge preparations. Hearts from 16 male New Zealand White rabbits were used in these experiments, which conform to standards set out in the UK Animals (Scientific Procedures) Act, 1986.

Experimental protocols

The left ventricular wedge preparations ($n = 16$) used in this set of experiments were prepared as described in Chapter 2. Perfusion was at 37°C ($n = 8$) except where low temperature was specifically investigated ($n = 9$). In two experiments, measurements were initially performed at 37°C before the preparation was cooled to 30°C and measurements were repeated. In a subset of experiments ($n = 4$) pacing protocols were repeated with the LV wedge preparation orientated for epicardial, rather than transmural imaging.

Data analysis

Data analysis was performed as detailed in Chapter 2. Regional behaviour was examined by using three 3×3 pixel selections, equally spaced across the transmural surface along a line perpendicular to the activation isochrones, as shown in Figure 3.1.

Statistical analyses

All data are expressed as mean \pm SEM. Groups of data were compared using a Student's t-test (paired where appropriate), or when more than two groups were compared, using a one-way ANOVA (repeated measures where appropriate) with a Tukey-Kramer multiple comparisons post-test. These statistical tests were performed using GraphPad software.

Results

Baseline characteristics

Transmural sampling sites and examples of raw AP traces are shown in Figure 3.1. Mean data for baseline transmural electrophysiological characteristics at 37°C during endocardial stimulation at a CL of 350ms are shown in Table 3.1 ($n = 8$). The mean distance across the transmural surface was $5.0 \pm 0.3\text{mm}$. Transmural conduction velocity (CV) during endocardial stimulation was of the order of 30cm/sec. A transmural gradient of APD_{90} was observed, with the longest APs at the subendocardium ($164.5 \pm 4.5\text{ms}$), intermediate values at the midmyocardium (155.6 ± 4.3 , $p < 0.01$ vs. subendocardium) and the shortest APs at the subepicardium ($147.1 \pm 3.7\text{ms}$, $p < 0.001$ and 0.01 vs. subendocardium and midmyocardium respectively). Mean transmural dispersion of activation time at baseline was 0.47ms/mm^2 , with larger mean dispersion values for repolarisation time and APD_{90} (1.77 and 1.10 ms/mm^2 respectively).

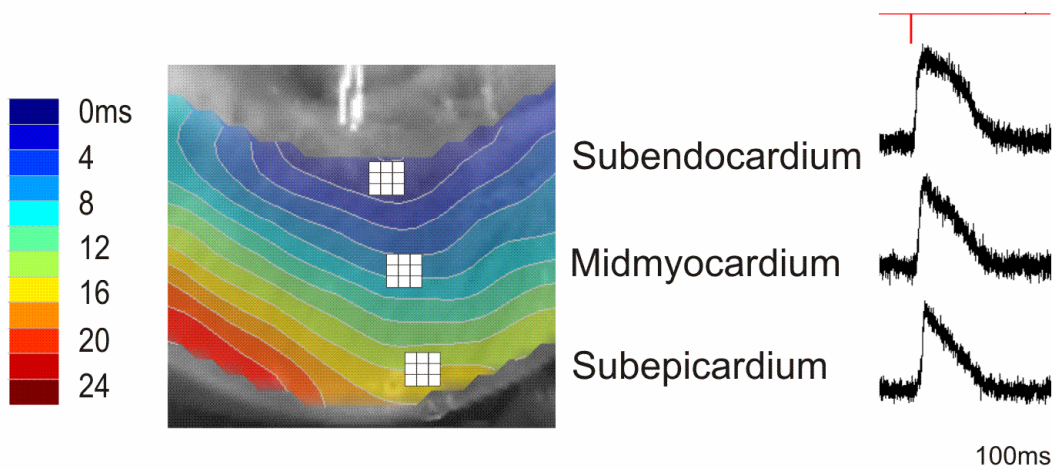


Figure 3.1 Transmural optical action potentials

An isochronal map of transmural activation time during endocardial stimulation, superimposed on a plain image of the transmural surface, with the stimulating electrode visible. The 3×3 pixel sampling sites for subendocardium, midmyocardium and subepicardium are indicated. Examples of AP traces from each region are given, along with the endocardial stimulus artefact in red.

Table 3.1 Baseline transmural electrophysiology

	Mean (SEM)
Transmural conduction velocity (cm/sec)	30.0 ± 0.9
Transmural APD ₉₀ (ms)	
Subendocardial APD ₉₀	164.5 ± 4.5
Midmyocardial APD ₉₀	155.6 ± 4.3 [†]
Subepicardial APD ₉₀	147.1 ± 3.7 ^{‡#}
Transmural dispersion (ms/mm ²)	
Activation time	0.47 ± 0.07
Repolarisation time	1.77 ± 0.36
APD ₉₀	1.10 ± 0.24

cm/sec = centimetres per second, ms = milliseconds, SEM = standard error of the mean.

n = 8, one-way ANOVA, [†] p < 0.01 vs. subendocardium, [‡] p < 0.001 vs. subendocardium, [#] p < 0.01 vs. midmyocardium.

Transmural APD₉₀ in the intact heart: comparison with isolated cell data

A comparison was made between transmural APD₉₀ data recorded from the LV wedge preparation and those recorded previously from single rabbit ventricular cardiomyocytes isolated from different transmural layers. The isolated cell data were provided by Dr Marie MacIntosh, and the comparison shown in Figure 3.2. The same transmural pattern of APD₉₀ (subendocardium > midmyocardium > subepicardium) was evident in the mean data from isolated cells and in the intact myocardium of the LV wedge. The magnitude of the difference in the intact myocardium was around 60% of that seen in isolated cells (17 vs. 28ms) at comparable CLs (350 vs. 333ms). Also, the absolute value of APD₉₀ was significantly shorter in the LV wedge preparation than in isolated cells, across all regions of the myocardium. A subpopulation of the cells isolated from the midmyocardial layer displayed typical M cell behaviour, with APD prolongation evident at slow stimulation rates, but M cell behaviour was not seen in the intact myocardium.

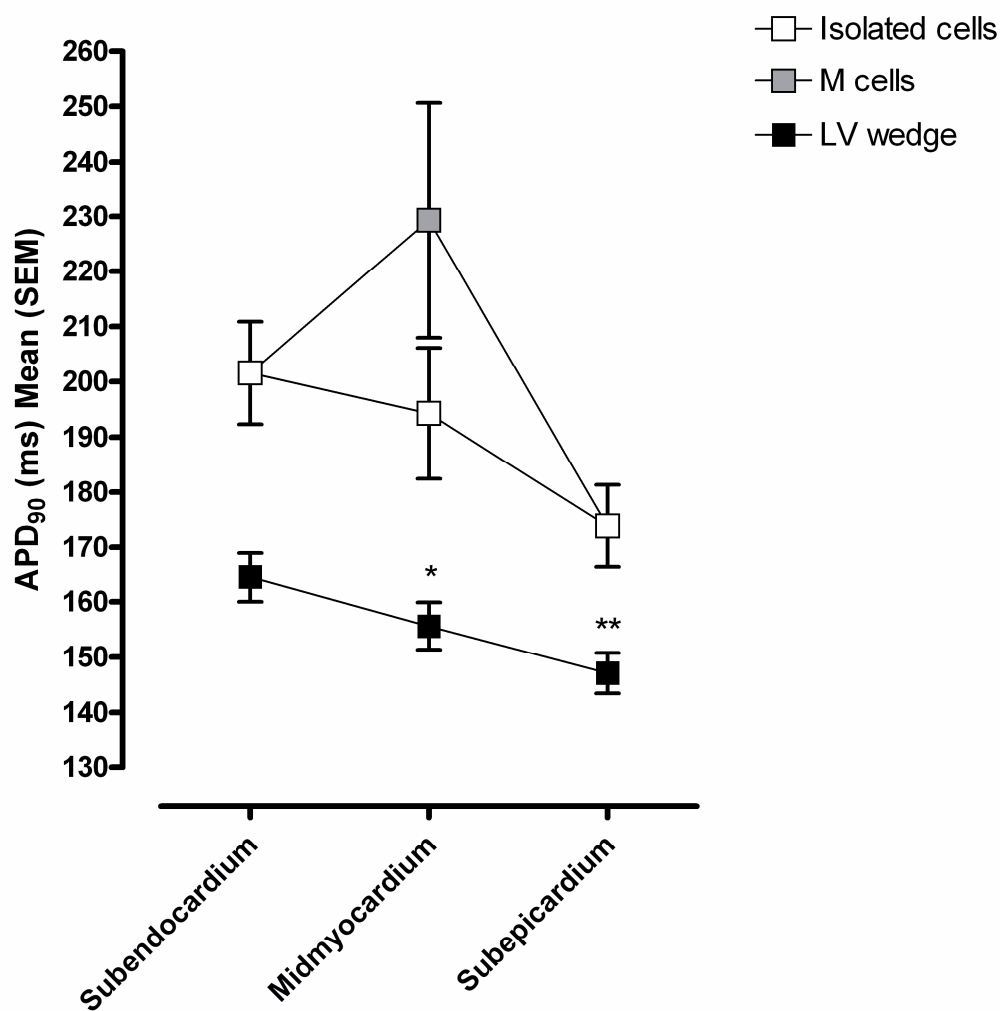
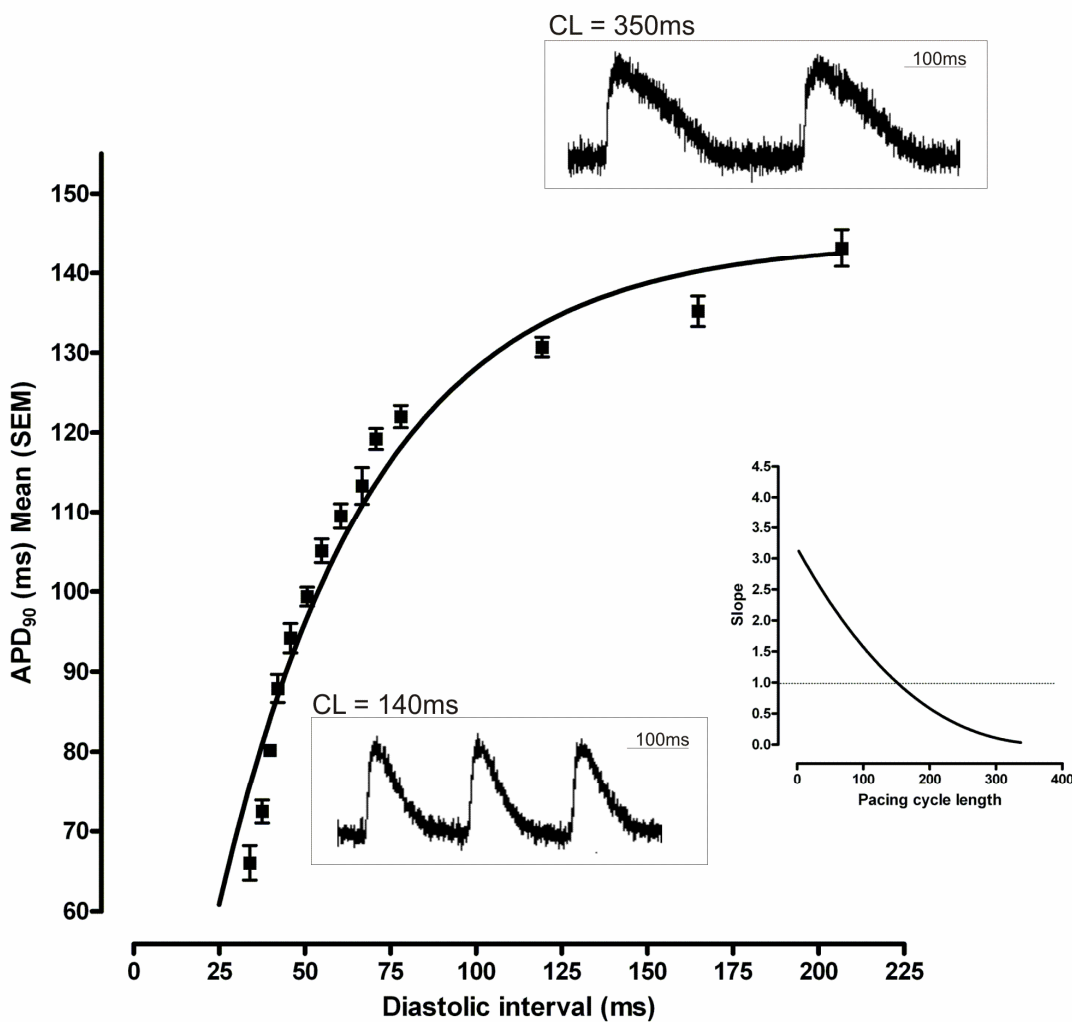


Figure 3.2 Transmural APD₉₀ in isolated cells and intact myocardium

Mean transmural APD₉₀ from subendocardium, midmyocardium and subepicardium in isolated cells (open squares, n = 12 hearts) and the intact LV wedge preparation (closed squares, n = 8). The grey square indicates the APD₉₀ recorded in the subpopulation of isolated midmyocardial cells displaying typical M cell behaviour. The isolated cell data were recorded at 37°C during field stimulation at a CL of 333ms. The intact LV wedge data were recorded at 37°C during endocardial stimulation at a CL of 350ms. Isolated cell data are courtesy of Dr Marie McIntosh. One-way ANOVA, * p < 0.01 vs. subendocardium, ** p < 0.001 vs. subendocardium and < 0.01 vs. midmyocardium. Differences between the isolated cell data were not significant.

APD₉₀ restitution

The data for APD₉₀ restitution during endocardial stimulation at 37°C is shown in Figure 3.3, the inset shows the slope of the APD₉₀ restitution curve as a function of pacing CL. The best fit Y_{max} value for the exponential curve fitted to the APD₉₀ data was $144.1 \pm 3.6\text{ms}$, and the rate constant was 0.02197 ± 0.00134 . The maximal APD restitution slope was $1.17 \pm 0.08\text{ms/ms}$.

**Figure 3.3 Mean APD restitution**

Mean data for restitution behaviour, with an exponential curve fit ($n = 8$). The insets show raw traces at CLs of 350ms and 140ms and the slope of the APD restitution curve as a function of pacing CL, and the dotted line indicates the point at which the APD restitution slope becomes >1 .

Transmural gradients of APD₉₀ during rapid stimulation

Transmural gradients of APD₉₀ during rapid pacing are shown in Figure 3.4. At baseline, subendocardial APD₉₀ was longer than midmyocardial or subepicardial APD₉₀. This gradient was maintained to a CL of 200ms, but became less evident as CL shortened further. There was no significant difference in APD₉₀ across the transmural surface at the shortest CL with 1:1 capture (130ms). There was a trend towards a reduction in the magnitude of the transmural APD₉₀ gradient as CL was progressively shortened, although this was not statistically significant ($22.6 \pm 4.8\text{ms}$ [$n = 8$] at 350ms vs. $6.3 \pm 1.8\text{ms}$ [$n = 3$] at 130ms, $p = 0.0771$). When expressed as a percentage of subendocardial APD₉₀, the magnitude of the transmural gradient remained relatively more stable through changes in CL (Figure 3.5). Again, there was a statistically insignificant trend towards a reduction in the magnitude of the transmural APD₉₀ gradient at shorter CLs ($14.1 \pm 2.6\text{ms}$ [$n = 8$] at 350ms vs. $6.9 \pm 1.8\text{ms}$ [$n = 3$] at 130ms, $p = 0.1442$).

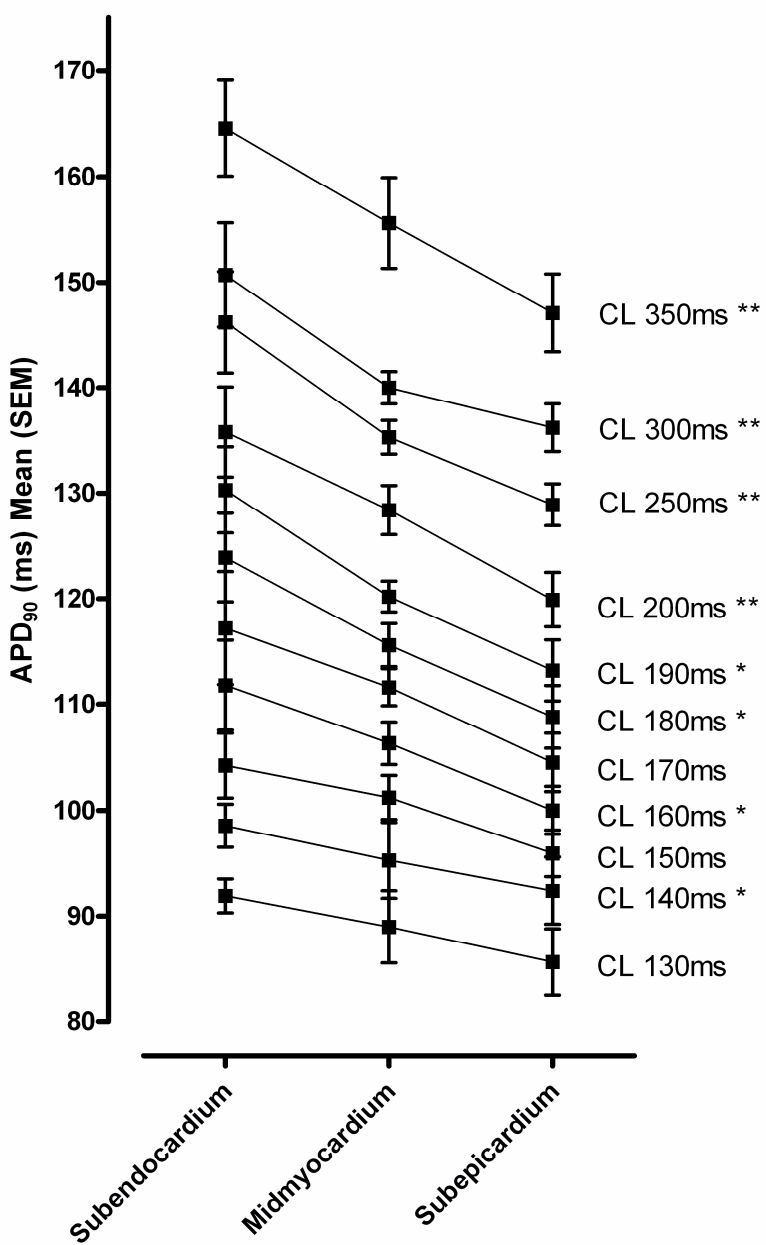


Figure 3.4 Regional APD₉₀ at rapid stimulation rates

Transmural gradients of APD₉₀ at each pacing CL. n = 8, one-way ANOVA, * p < 0.05 for subendocardium vs. subepicardium, ** p < 0.05 for subendocardium vs. midmyocardium and subepicardium.

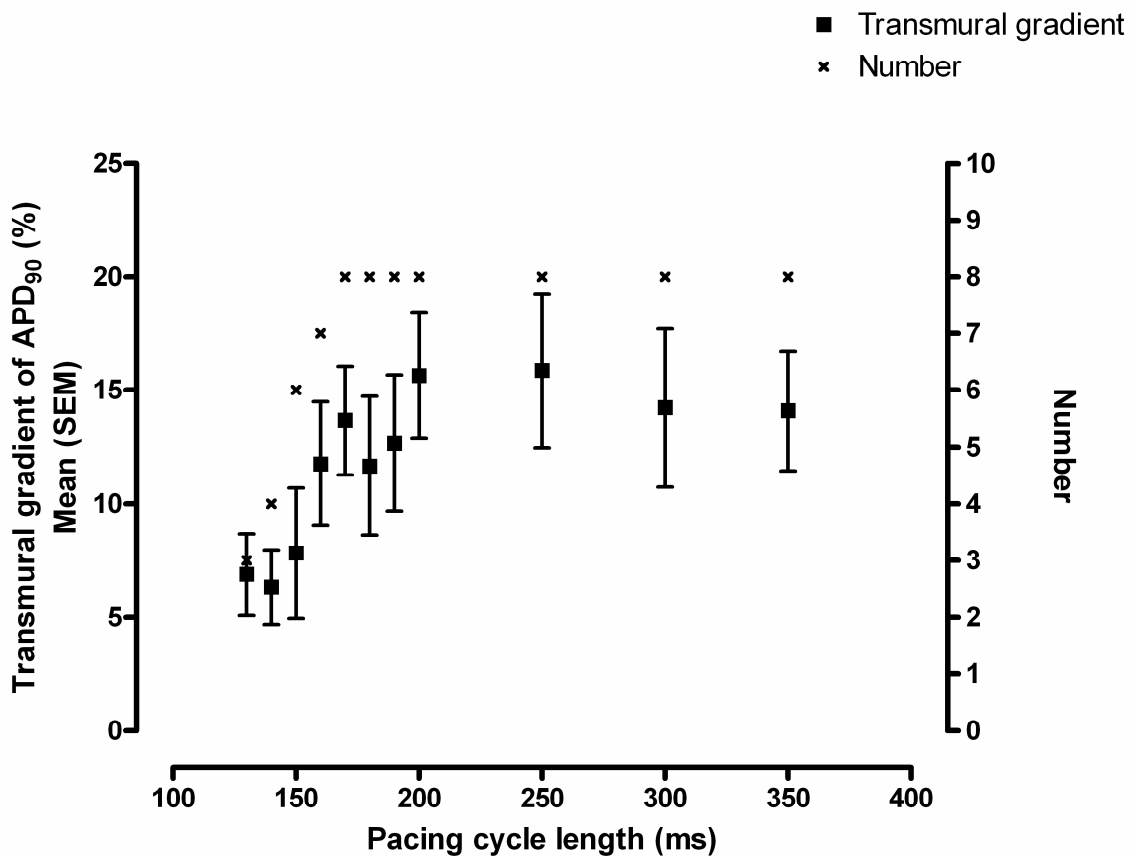
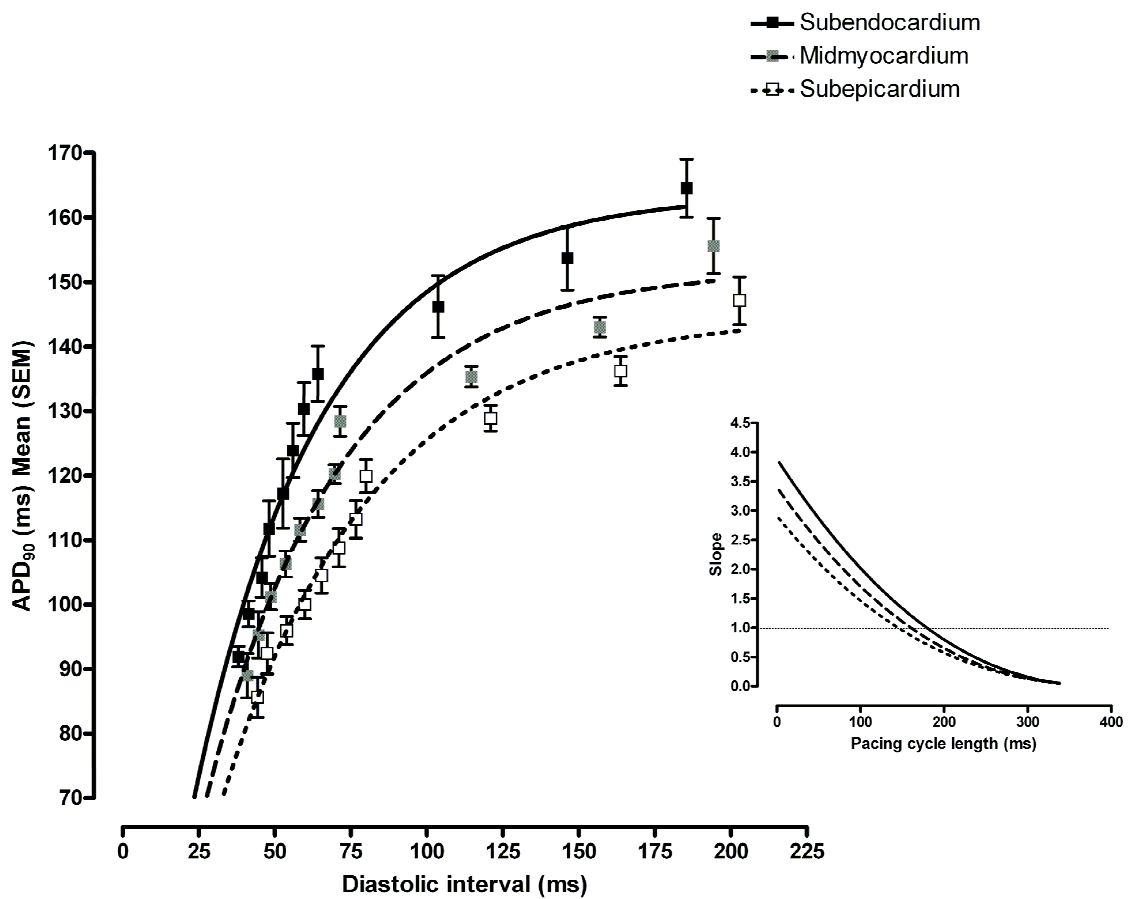


Figure 3.5 Magnitude of the transmural APD₉₀ gradient during rapid stimulation
Transmural gradients of APD₉₀, expressed as a percentage of subendocardial APD₉₀ according to pacing CL. The crosses indicate the number of measurements (experiments) included in each point, plotted on the right Y axis. One-way ANOVA, p > 0.05.

Transmural APD₉₀ restitution

Transmural restitution curves for subendocardium, midmyocardium and subepicardium, are shown in Figure 3.6 along with the slope of each curve, shown in the inset. As shown in Table 3.2, the previously demonstrated transmural gradients of APD₉₀ are reflected in the Y_{max} values of the restitution curves. Y_{max} was greater in the subendocardial region than in the midmyocardium or subepicardium. There were no transmural differences in the rate constants of the curves fitted to the APD₉₀ restitution data. The maximal transmural APD₉₀ restitution slopes are shown in Figure 3.7. There were significant transmural differences in the maximal APD₉₀ restitution slope, with the steepest slope in the subendocardial region, with progressively shallower slopes in the midmyocardium and subepicardium.

**Figure 3.6 Transmural APD_{90} restitution**

Mean data for transmural restitution behaviour, with corresponding exponential curve fits ($n = 8$). The inset shows the slope of each APD restitution curve as a function of pacing CL, and the dotted line indicates the point at which the APD restitution slope becomes >1 .

Table 3.2 Transmural APD_{90} restitution curve characteristics

Mean (SEM)	Subendocardium	Midmyocardium	Subepicardium	P value
Y_{max} (ms)	163.7 ± 3.9	$152.1 \pm 3.0^*$	$144.9 \pm 2.4^{**}$	< 0.01
Rate constant	0.02373 ± 0.00140	0.02236 ± 0.00113	0.02007 ± 0.00084	> 0.05
Maximal slope (ms/ms)	1.75 ± 0.13	$1.28 \pm 0.08^{**}$	$0.81 \pm 0.01^{***,\#}$	< 0.0001

ms = milliseconds, SEM = standard error of the mean. P value refers to a one-way ANOVA, * $p < 0.05$ vs. subendocardium, ** $p < 0.01$ vs. subendocardium, *** $p < 0.001$ vs. subendocardium and # $p < 0.01$ vs. midmyocardium.

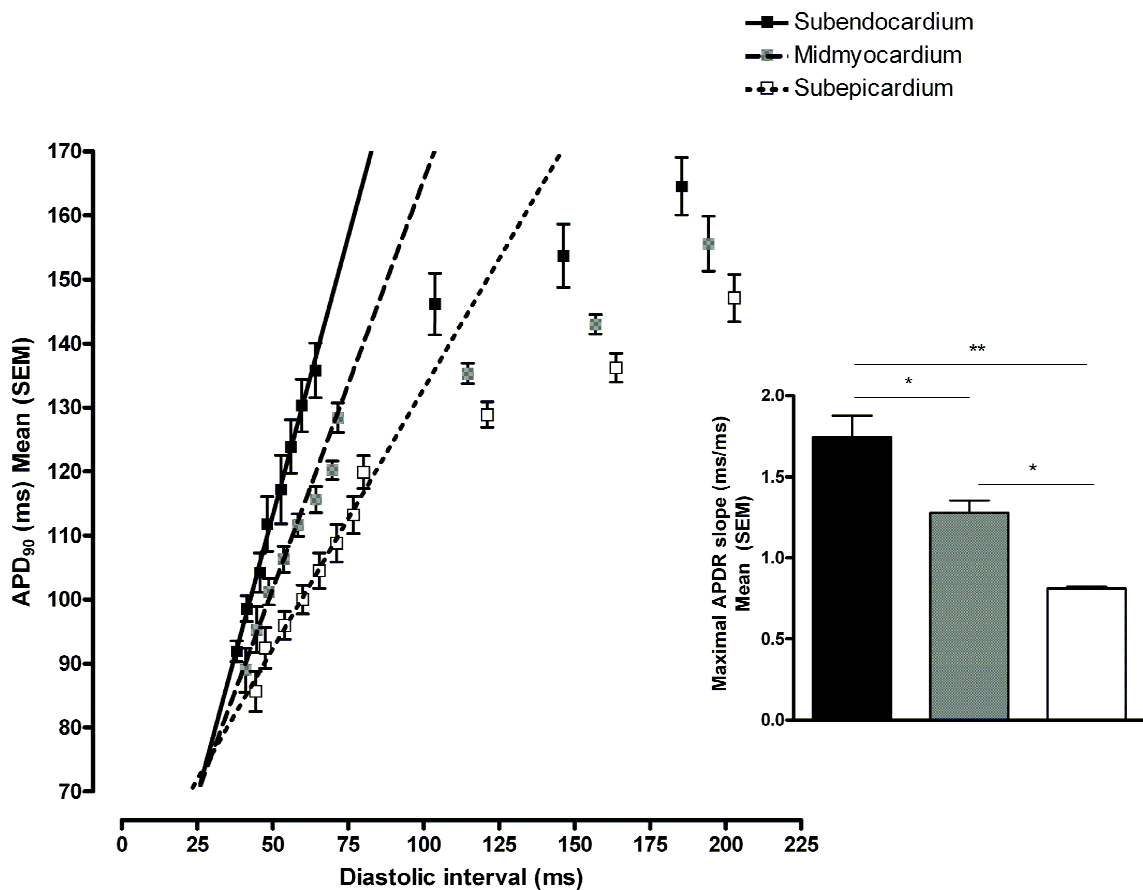


Figure 3.7 Transmural APD_{90} restitution

Mean data for transmural restitution behaviour, with corresponding linear fits to the data points recorded at the five shortest CLs ($n = 8$). The inset shows the maximal slope of each APD restitution curve generated from the fitted linear segments shown in the main graph. One-way ANOVA * $p < 0.01$, ** $p < 0.001$

The effect of low temperature on transmural electrophysiology

The effects of low temperature (30°C) on transmural electrophysiology during endocardial stimulation at a CL of 350ms are summarised in Table 3.3. Transmural conduction velocity was reduced by 27% at 30°C . Low temperature was associated with an increase in APD_{90} across the entire transmural surface, the magnitude of which was $\sim 13\text{-}15\%$. This resulted in a similar transmural gradient of APD_{90} as had been observed at 37°C (subendocardial $APD_{90} >$ midmyocardial $APD_{90} >$ subepicardial APD_{90}). At 37°C the magnitude of the transmural gradient of APD_{90} during endocardial pacing at a CL of 350ms was $22.6 \pm 4.8\text{ms}$, or $14.1 \pm 2.6\%$ of the subendocardial value. At 30°C the magnitude of the transmural gradient was $19.2 \pm 5.5\text{ms}$, or $10.1 \pm 2.4\%$ of the subendocardial value ($p = 0.2754$ vs. 37°C). There were no statistically significant changes observed in the transmural dispersion of activation time, repolarisation time or APD_{90} at low temperature when compared with values recorded at 37°C .

Table 3.3 Transmural electrophysiology at low temperature

Mean (SEM)	37°C (n = 8)	30°C (n = 9)	Relative change	P value
Transmural conduction velocity (cm/sec)	30.0 ± 0.9	22.6 ± 1.1	- 27%	0.0001
Transmural APD ₉₀ (ms)				
Subendocardial APD ₉₀	164.5 ± 4.5	186.2 ± 3.6	+ 13%	< 0.01
Midmyocardial APD ₉₀	155.6 ± 4.3	176.1 ± 3.8	+ 13%	< 0.05
Subepicardial APD ₉₀	147.1 ± 3.7	169.4 ± 5.0	+ 15%	< 0.01
Transmural dispersion (ms/mm ²)				
Activation time	0.47 ± 0.07	0.54 ± 0.08	-	> 0.05
Repolarisation time	1.77 ± 0.36	0.86 ± 0.23	-	> 0.05
APD ₉₀	1.10 ± 0.24	0.80 ± 0.27	-	> 0.05

cm/sec = centimetres per second, ms = milliseconds, ms/mm² = milliseconds per square millimetre, SEM = standard error of the mean. P value refers to an unpaired t-test for CV and to a one-way ANOVA for transmural APD₉₀ and dispersion.

Transmural gradients of APD₉₀ during rapid stimulation at low temperature

At low temperature, the transmural gradient of APD₉₀ observed at baseline was maintained across all cycle lengths tested (350ms-140ms), as shown in Figure 3.8. Subendocardial APD₉₀ was always greater than subepicardial APD₉₀ during rapid stimulation, and was also significantly greater than midmyocardial APD₉₀ at baseline pacing CL (350ms) and during rapid pacing (200-150ms). The transmural APD₉₀ gradient did not change significantly as CL was progressively shortened (19.2 ± 5.5 ms [n = 9] at 350ms vs. 14.2 ± 4.7 ms [n = 3] at 140ms, p = 0.6324). As shown in Figure 3.9, when expressed as a percentage of subendocardial APD₉₀, the magnitude of the transmural gradient remained stable through changes in CL (10.1 ± 2.4 ms [n = 9] at 350ms vs. 13.0 ± 3.9 ms [n = 3] at 140ms, p = 0.5545), and was not significantly different in magnitude to that seen at 37°C.

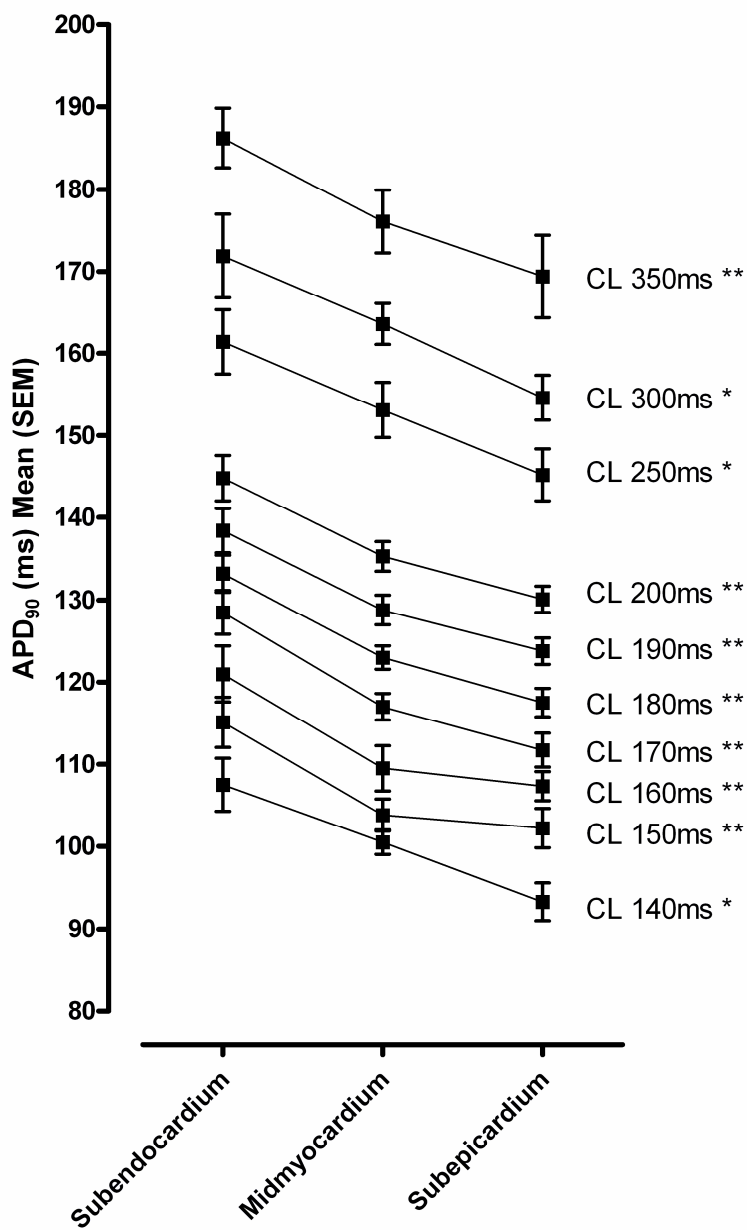


Figure 3.8 Regional APD₉₀ at rapid stimulation rates at low temperature
 Transmural gradients of APD₉₀ at each pacing CL. n = 9, one-way ANOVA, * p < 0.05 for subendocardium vs subepicardium, ** p < 0.05 for subendocardium vs. midmyocardium and subendocardium vs. subepicardium.

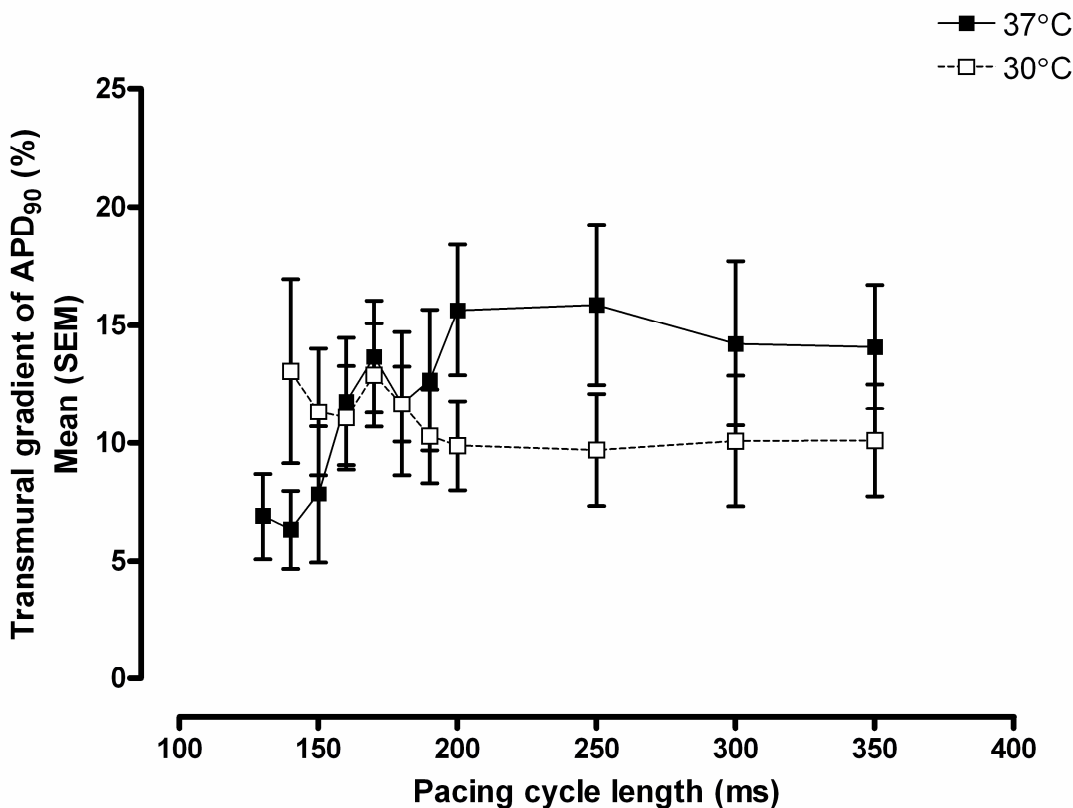


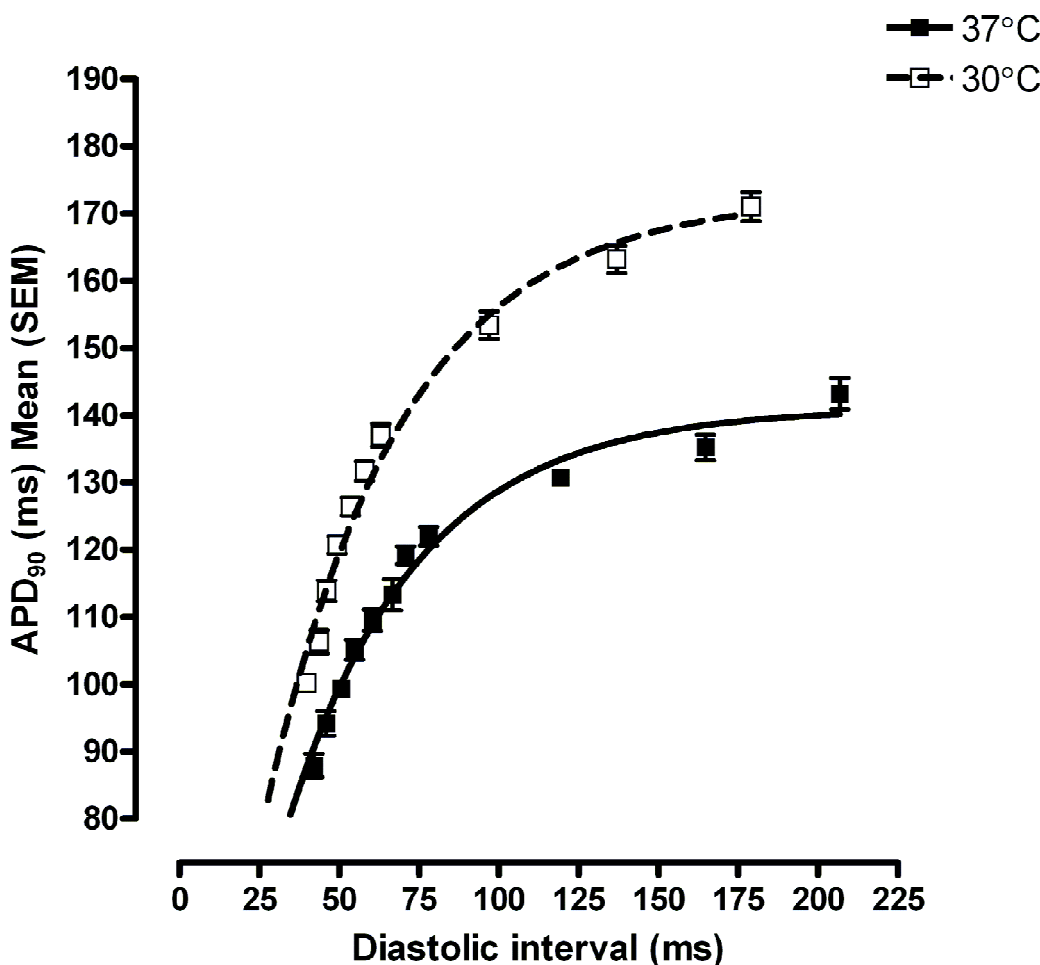
Figure 3.9 Magnitude of the transmural APD₉₀ gradient during rapid stimulation at low temperature

Transmural gradients of APD₉₀, expressed as a percentage of subendocardial APD₉₀ according to pacing CL in normal hearts at 37°C (closed squares and solid line, n = 8) and 30°C (open squares and dashed line, n = 9).

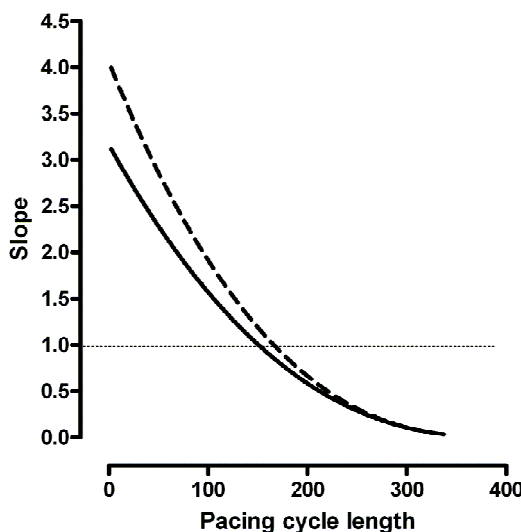
APD₉₀ restitution at low temperature

A comparison of APD₉₀ restitution curves at 30°C and 37°C, along with the corresponding plots of restitution slope against CL is given in Figure 3.10. As noted previously, APD₉₀ at baseline was significantly longer at 30°C than 37°C, and the transmural gradient persisted across all CLs tested. This is reflected in the higher Y_{max} of the curve fitted to the 30°C APD₉₀ restitution data compared to the corresponding value for the 37°C data (177.7 ± 3.8 vs. 144.1 ± 3.7 ms respectively, $p < 0.0001$). However, the rate constant of the exponential fitted to the APD₉₀ restitution data at 30°C was not different to that at 37°C (0.02197 ± 0.00134 vs. 0.02219 ± 0.00113 respectively, $p = 0.9032$). The maximal APD₉₀ restitution slope was greater at 30°C (1.99 ± 0.16 ms/ms) than at 37°C (1.17 ± 0.08 ms/ms, $p = 0.005$).

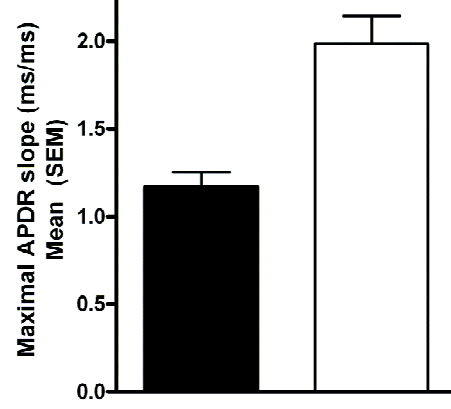
A.



B.



C.

**Figure 3.10 The temperature dependence of APD_{90} restitution**

A. Mean data for restitution behaviour, with corresponding exponential curve fits for data at 37°C (closed squares and solid line, $n = 8$) and at 30°C (open squares and dashed line, $n = 9$). B. The slope of each restitution curve as a function of pacing CL. The dotted line indicates the point at which the restitution slope becomes >1 . C. The maximal slope of each APD_{90} restitution curve generated from linear segments fitted to the five data points at the shortest DIs in the main graph. Unpaired t-test * $p < 0.01$.

Transmural APD₉₀ restitution curves for subendocardium, midmyocardium and subepicardium at 30°C, and the corresponding plots of restitution slope against pacing CL and maximal APDR slope are shown in Figure 3.11. APD₉₀ at baseline was previously noted to be significantly longer in the subendocardium, with progressively shorter values in the midmyocardium and subepicardium across all of the CLs tested. This is reflected in the Y_{max} values of the curves fitted to the APD₉₀ restitution data, shown in Table 3.4. There were no transmural differences in the rate constants of the exponentials fitted to the APD₉₀ restitution data. There was a trend towards the maximal restitution slope being steepest at the subendocardium, but this was not statistically significant.

Table 3.4 Transmural APD₉₀ restitution curve characteristics at 30°C

Mean (SEM)	Subendocardium	Midmyocardium	Subepicardium	P value
Y _{max} (ms)	185.2 ± 1.7	179.2 ± 3.4	171.7 ± 4.0*	< 0.05
Rate constant, K	0.02726 ± 0.00064	0.02002 ± 0.00089	0.01846 ± 0.00098	> 0.05
Maximal slope (ms/ms)	1.79 ± 0.22	1.32 ± 0.23	1.30 ± 0.25	> 0.05

ms = milliseconds, SEM = standard error of the mean. P value refers to a one-way ANOVA, * post test p < 0.05 vs. subendocardium.

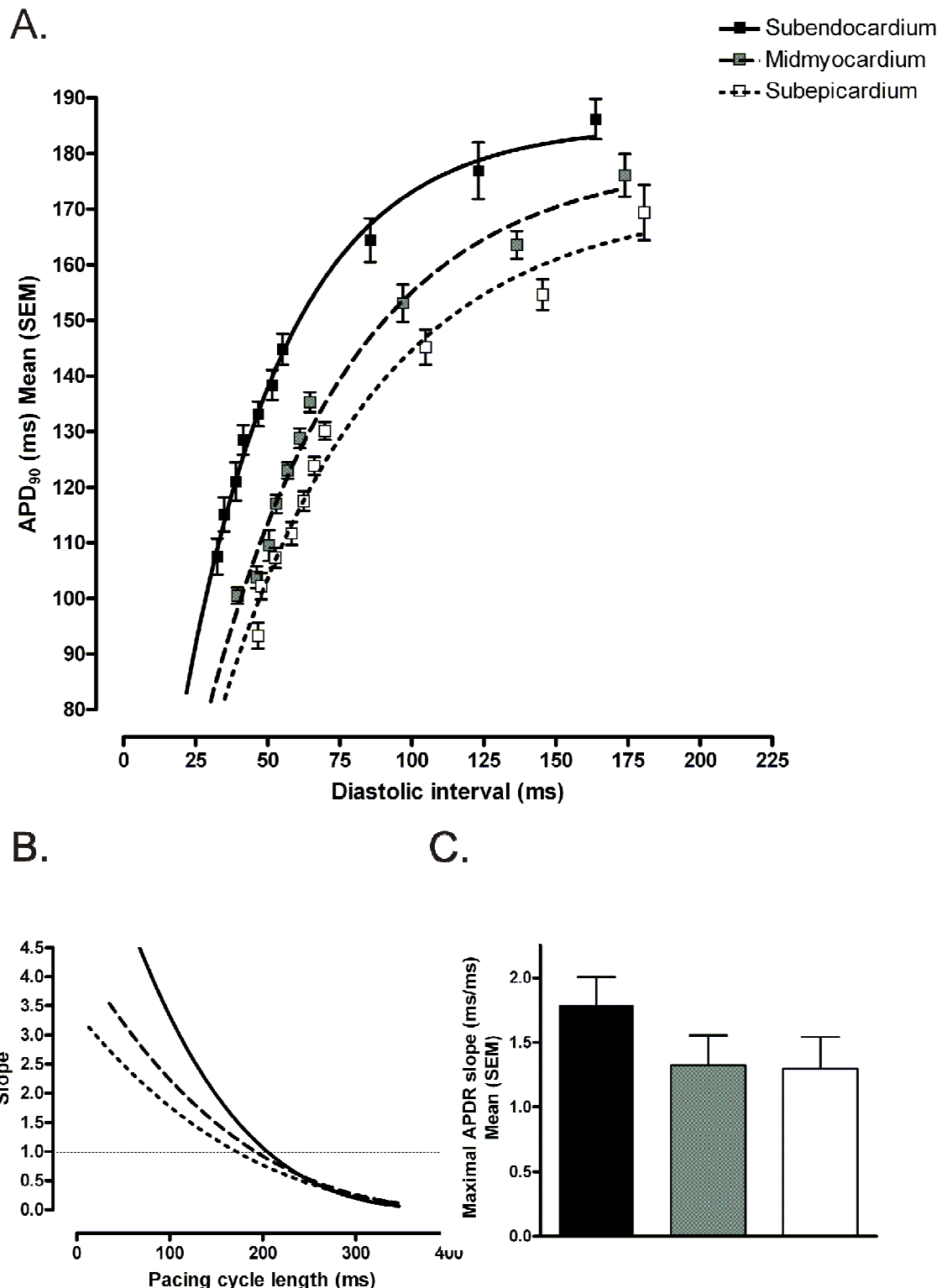


Figure 3.11 Transmural APD₉₀ restitution at low temperature

A. Mean data for transmural restitution behaviour, with corresponding exponential curve fits ($n = 9$). B. The slope of each restitution curve as a function of pacing CL, and the dotted line indicates the point at which the restitution slope becomes >1 . C. The maximal slope of each APD₉₀ restitution curve generated from linear segments fitted to the five data points at the shortest DIs in the main graph. One-way ANOVA, $p > 0.05$.

A comparison of transmural and epicardial electrophysiology

Recordings from the epicardial surface were made during endocardial pacing at 37°C and epicardial AP parameters were compared with those recorded from the transmural surface. Mean epicardial APD₉₀ ($152.7 \pm 6.1\text{ms}$, n = 4) was not significantly different from that recorded from the subepicardial region of the transmural surface ($147.1 \pm 3.7\text{ms}$, n = 8, p = 0.4258). During endocardial stimulation, near synchronous breakthrough activation of the epicardial surface was seen, which resulted in a significantly lower dispersion of activation time than was seen across the transmural surface (Table 3.5). Dispersion of repolarisation time was also lower across the epicardial surface, and there was a trend towards reduced epicardial dispersion of APD₉₀ compared with the transmural surface, but this was not statistically significant.

Table 3.5 A comparison of transmural and epicardial dispersion

Mean (SEM)	Transmural (n = 8)	Epicardial (n = 4)	P value
Dispersion of activation time (ms/mm ²)	0.47 ± 0.07	0.11 ± 0.01	< 0.05
Dispersion of repolarisation time (ms/mm ²)	1.77 ± 0.36	0.39 ± 0.13	< 0.05
Dispersion of APD ₉₀ (ms/mm ²)	1.10 ± 0.24	0.35 ± 0.12	> 0.05

ms = milliseconds, ms/mm² = milliseconds per square millimetre, SEM = standard error of the mean. P value refers to a one-way ANOVA.

Epicardial and transmural restitution

Mean transmural and epicardial APD₉₀ restitution curves, and their slopes, were similar, as shown in Figure 3.12. There were no significant differences in the best fit values for Y_{max} or K between the fitted curves for transmural and epicardial restitution.

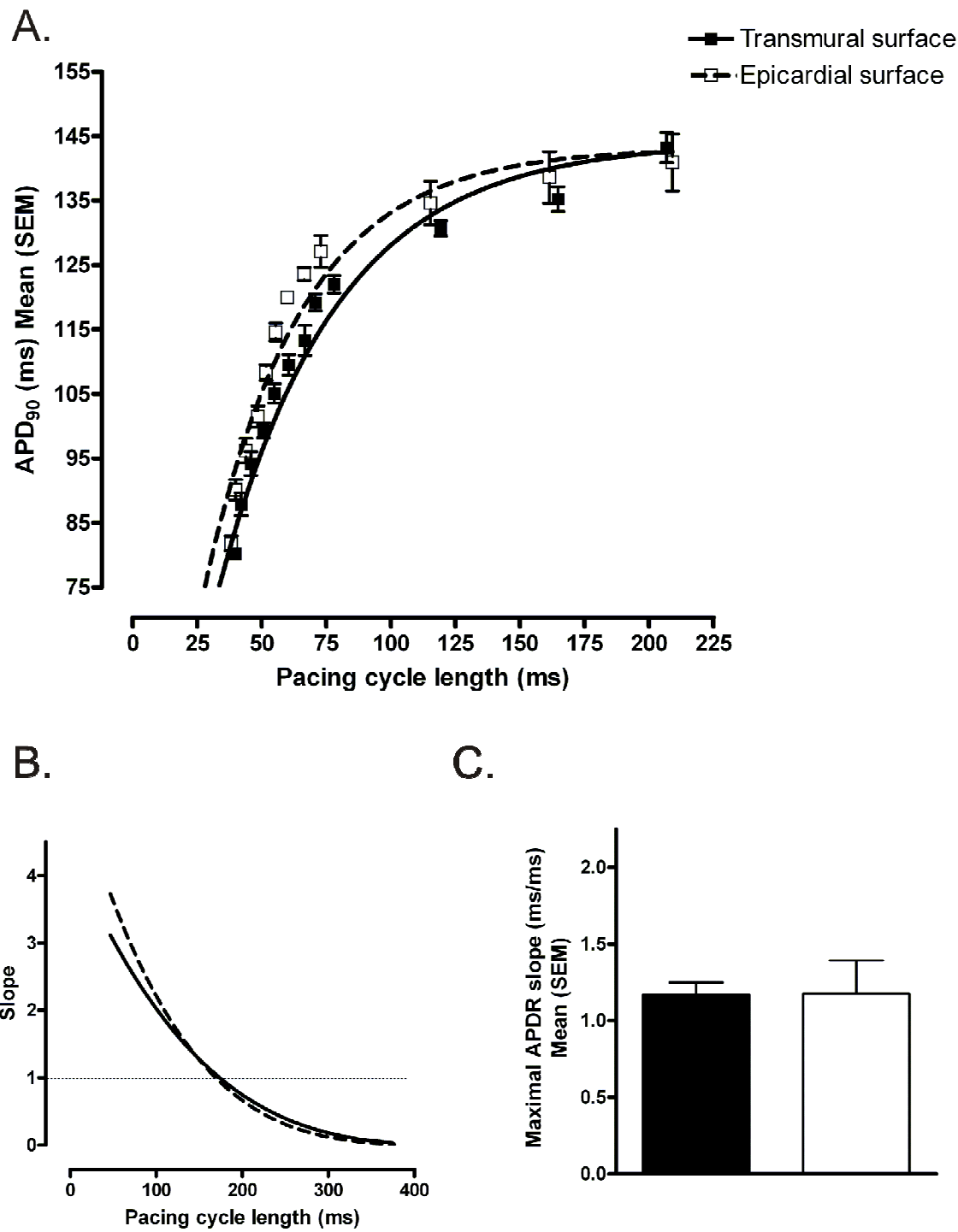


Figure 3.12 A comparison of transmural and epicardial APD₉₀ restitution

A. Mean data for regional restitution behaviour, with exponential curves fitted showing values from the transmural surface (closed squares and solid line, $n = 8$) and the epicardial surface (open squares and dashed line, $n = 4$). B. The slope of each restitution curve as a function of pacing CL. The dotted line indicates the point at which the restitution slope becomes >1 . C. The maximal slope of each APD₉₀ restitution curve generated from linear segments fitted to the five data points at the shortest DIs in the main graph. Unpaired t-test, $p > 0.05$.

Transmural and epicardial electrophysiology at low temperature

At 30°C, mean epicardial APD₉₀ (160.4 ± 2.9 , n = 5) was not significantly different from that recorded from the subepicardial region of the transmural surface (162.7 ± 2.5 , n = 9, p = 0.5762). During endocardial stimulation, as had been observed at 37°C, near synchronous breakthrough activation of the epicardial surface was seen, which resulted in a significantly lower dispersion of activation time than was seen across the transmural surface (Table 3.6). There was a trend towards reduced epicardial dispersion of repolarisation time and APD₉₀ compared with the transmural surface, but these were not statistically significant.

Table 3.6 A comparison of transmural and epicardial dispersion at low temperature

Mean (SEM)	Transmural (n = 9)	Epicardial (n = 5)	P value
Dispersion of activation time (ms/mm ²)	0.54 ± 0.08	0.15 ± 0.04	< 0.01
Dispersion of repolarisation time (ms/mm ²)	0.86 ± 0.23	0.29 ± 0.06	> 0.05
Dispersion of APD ₉₀ (ms/mm ²)	0.80 ± 0.27	0.28 ± 0.07	> 0.05

ms = milliseconds, ms/mm² = milliseconds per square millimetre, SEM = standard error of the mean. P value refers to a one-way ANOVA.

Epicardial and transmural restitution at low temperature

Mean transmural and epicardial APD₉₀ restitution curves at 30°C, and their slopes, are shown in Figure 3.13. There were no significant differences in the best fit values for Y_{max} or K between the fitted curves for transmural and epicardial restitution. The maximal APD₉₀ restitution slope was not significantly different between the epicardial and transmural surfaces.

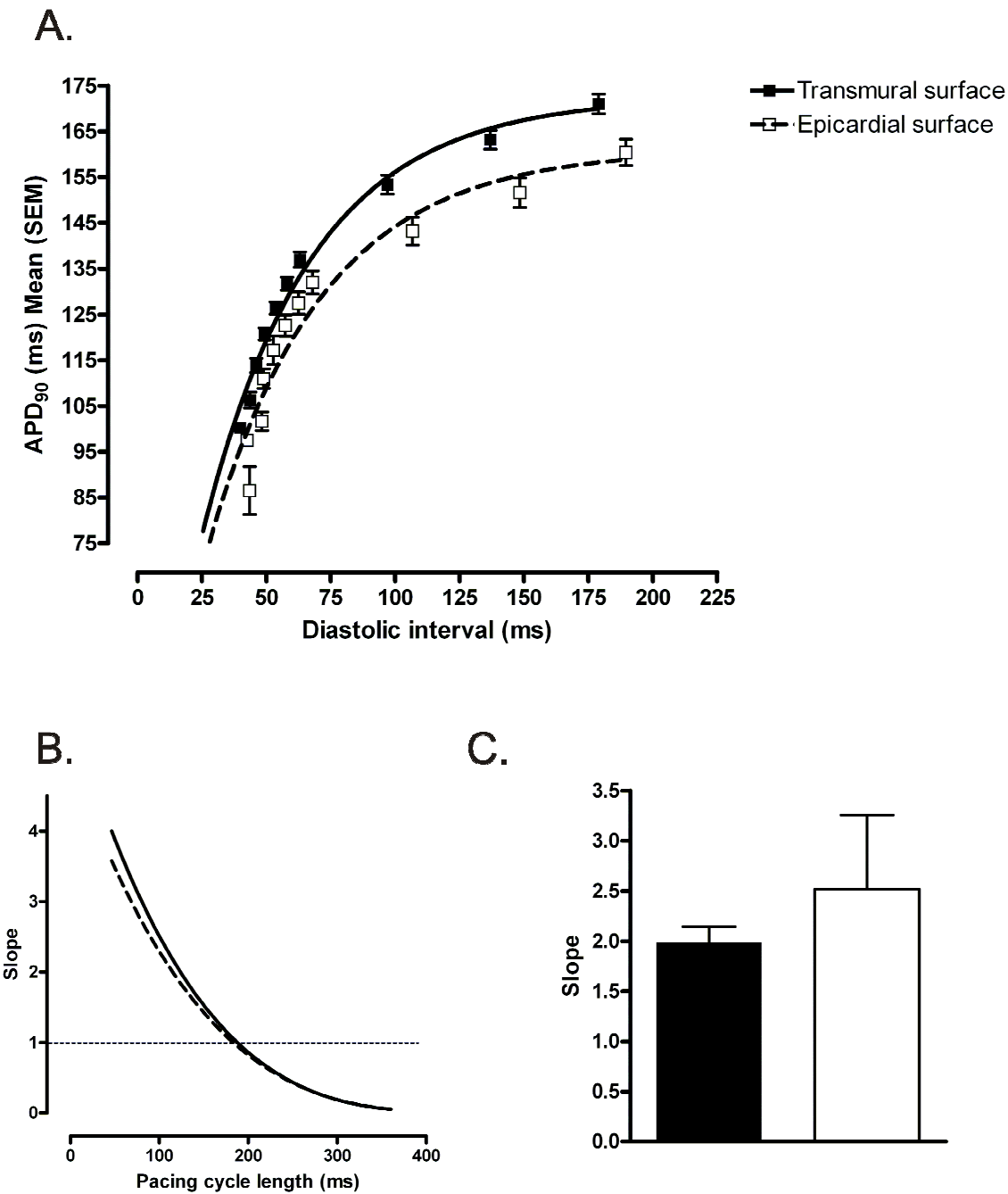


Figure 3.13 A comparison of transmural and epicardial APD₉₀ restitution at low temperature

A. Mean data for regional restitution behaviour, with exponential curves fitted showing values from the transmural surface (closed squares and solid line, n = 9) and the epicardial surface (open squares and dashed line, n = 5). B. The slope of each restitution curve as a function of pacing CL. The dotted line indicates the point at which the restitution slope becomes >1. C. The maximal slope of each APD₉₀ restitution curve generated from linear segments fitted to the five data points at the shortest DIs in the main graph. Unpaired t-test, p > 0.05.

Discussion

Transmural heterogeneity of repolarisation is now a well-established concept in mammalian ventricular electrophysiology, and this study, the first to record optical APs from across the entire transmural surface of rabbit ventricular myocardium, has a number of important findings.

Comparison of optical action potentials with microelectrode recordings

One group has published recordings of transmural APs using single cell microelectrode impalement in a rabbit ventricular wedge preparation¹³¹. The optical APD₉₀ values reported here are in broad agreement with those recorded in that study, in which the range of transmural APD₉₀ was 165-180ms at 37°C and a pacing CL of 500ms. The transmural optical AP values reported in this Chapter are around 10% shorter, ranging from 165-145ms, at the shorter CL of 350ms. In the studies reporting microelectrode recordings, shorter CLs than 500ms were not used, and so direct comparisons of optical and microelectrode APD₉₀ at 350ms are not possible. However, restitution curves plotted from the microelectrode APD₉₀ at longer CLs did display shortening of APD₉₀ between CLs of 1000ms and 500ms (~10%), indicating that further shortening would be expected between CLs of 500ms and 350ms. Moreover, the restitution curves fitted to the experimental data presented in this Chapter display suggest that the system is not in steady state at 350ms, and indicate that a lengthening of APD₉₀ at a CL of 500ms (compared with 350ms) would have been expected. The microelectrode measurements were taken using shank microelectrodes which are passed deep to the transmural surface, and in the absence of pharmacological motion uncouplers. The similarity between these microelectrode recordings and the values measured from transmural optical APs in the rabbit wedge argues against any significant APD shortening due to damaged cells on the cut surface, or indeed any major effect of uncouplers on AP characteristics.

APD differences between isolated cells and intact myocardium

This study demonstrates the marked differences in APD₉₀ recorded from isolated cells and those recorded from cells within the intact ventricular myocardium. Not only are transmural gradients attenuated but baseline APD₉₀, regardless of cell layer, is shorter. There is evidence to suggest that the APD shortening in intact myocardium compared with isolated cells observed here is due to the effect of electrotonic coupling between cells. In isolated rabbit ventricular myocytes, coupling resistance between two cells can

be varied experimentally using a passive resistance and capacitance circuit. Levels of coupling resistance which allowed conduction between the cells produced more than 50% shortening of APD (200ms at infinite coupling resistance to 70ms at 500MΩ)¹⁴². These investigators also demonstrated that the same reduction in coupling resistance enabled the cell to capture at fast stimulation rates (CL 150ms). This is in agreement with the experimental observation that isolated cells cannot be driven at the same fast CLs as intact tissue. The fact that APD₉₀ at a given CL is shorter in the intact myocardium is an extremely important finding for the interpretation of data recorded from isolated cardiomyocytes, as ionic currents and excitation-contraction (EC) coupling will both be modulated by the cellular APD.

Patterns of activation and conduction velocity

In these experiments, transmural conduction velocity during endocardial stimulation was ~ 30cm/sec. The transmural arrangement of fibre orientation in rabbit ventricle means that the majority of transmural conduction will be transverse, rather than longitudinal¹⁶⁶. The values for conduction velocity recorded here are in keeping with published values for epicardial transverse CV in rabbit¹⁰⁹.

Transmural gradients of APD₉₀ in intact rabbit myocardium

These data demonstrate a transmural gradient of APD under physiologically relevant experimental conditions (i.e. 37°C and endocardial pacing at 350ms). Subendocardial APD₉₀ was found to be significantly longer than midmyocardial and subepicardial APD₉₀, with a gradient of the order of 10% of the subendocardial value, which appeared to be evenly distributed across the ventricular wall. In particular, prolongation of midmyocardial APD₉₀ was not observed under these experimental conditions. Typical M cell behaviour has been described in midmyocardial cells isolated from rabbit ventricular myocardium¹³⁴, but these M cells accounted for only a small proportion of midmyocardial cells (~10%). M cells show particularly marked APD prolongation at slow stimulation rates, and it is possible that the CLs used in the experiments described here (≤ 350 ms) were too fast to allow M cell behaviour to be recorded. The isolated cell data demonstrating M cell characteristics used a comparable stimulation rate (CL 333ms). On the other hand, it is possible that M cell behaviour may have been demonstrated in the LV wedge had longer CLs been used. Taken together these data suggest that M cells, although present in rabbit ventricular myocardium, may not be

functionally distinct from other cell types at physiological stimulation rates in intact, electrotonically coupled myocardium.

Rate dependence of APD₉₀ and APD₉₀ restitution

In the current study, APD₉₀ restitution was described using a consistent exponential curve fitted to the experimental data. This is the standard approach, and facilitates comparison between restitution curve characteristics. However, in some instances the fit is not optimal, and it is possible that this may have influenced some of the comparisons of APD restitution slope. For this reason, the maximal slope was also calculated using a linear fit to the steepest segment of the curve. In the current study, similar rate dependence of APD₉₀ and APD₉₀ restitution was recorded from all transmural layers. At short CLs, the steepest restitution was found in the subendocardium. Similar APD restitution in different transmural regions has been reported in normal canine¹⁶⁷ and rabbit myocardium¹³¹ down to CLs of 500ms, although there are few reports of restitution behaviour at shorter CLs.

The effect of low temperature

These data demonstrate the effects of low temperature (30°C) on ventricular electrophysiology in intact rabbit myocardium. Transmural conduction velocity was slowed at low temperature, despite this, dispersion of AT was not significantly increased at low temperature. This may reflect differences in the measurement methods, as transmural CV was measured between two points, whereas dispersion of AT reflects the spatial distribution of AT across the whole imaged surface. Dispersion may therefore be more sensitive to spatial variations in AT, but also more susceptible to errors. Transmural gradients of APD₉₀, which became less distinct during rapid pacing at 37°C, appeared to be relatively more preserved during rapid stimulation at low temperature. Interpretation of this finding is complicated by the fact that the shortest CL captured was longer at low temperature. As the associated APDs at any given CL were also longer at low temperature, small transmural differences are therefore more likely to be resolved by the imaging and analysis programme. For example, at the shortest CL captured at 37°C, APD₉₀ was of the order of 90ms, compared with 105ms at 30°C. Transmural gradients were of the order of 10-15%, which would mean resolving APD₉₀ gradients of the order of 9ms. In addition to this, total numbers became smaller at shorter CL, reducing power to show statistically significant differences. Dispersion of repolarisation and APD₉₀ were unchanged at low temperature. This means that any

temperature dependence of arrhythmogenic spatially discordant alternans could not be accounted for by differences in baseline dispersion of repolarisation or APD₉₀.

The maximal APD₉₀ restitution slope was steeper at 30°C than at 37°C. This suggests that the temperature dependence of repolarisation alternans may be at least partly explained by differences in APD restitution. However, changes in calcium handling, not measured in the current study may also play an important part in the temperature dependence of repolarisation alternans.

Limitations

The data presented here go some way to bridging the gap between the electrophysiological behaviour of isolated cells, which is relatively well characterised, and the situation in intact LV myocardium. However, this remains an *in vitro* preparation, and so does not accurately represent the situation in the living heart.

Microelectrode recordings would have provided a comparison for the optical AP recordings, but were not made, principally because of the practical difficulty inherent in making microelectrode recordings from multiple sites, or during rapid stimulation. However, the values for APD₉₀ derived from the optical recordings described here are similar to microelectrode values published by other investigators, including those from this laboratory¹⁶⁸.

Pharmacological electromechanical uncoupling agents were used to minimise motion artefact during optical recordings, and it is possible that these may have affected AP parameters. The similarity of baseline data to those collected by others using methodologies which obviate EC uncoupling argues against any major effect. However, as high concentrations of BDM have been demonstrated to flatten AP restitution, the lowest possible concentration was used in these experiments¹⁵¹ and the same concentrations were used across all experiments.

Conclusions

In this study, optical action potentials were recorded from across the transmural surface of rabbit ventricle during endocardial pacing at physiologically relevant stimulation rates. The results reveal a transmural gradient of APD₉₀, with the longest APD₉₀ consistently found in the subendocardium. This gradient is similar in pattern although of significantly smaller magnitude than that found in isolated cells. These findings underline the importance of electrotonic coupling between cells in determining the electrophysiological characteristics of intact ventricular myocardium. In particular, these data suggest that there are no functionally distinct M cells in intact rabbit ventricular myocardium at physiological stimulation rates.

Transmural gradients of APD₉₀ were maintained during rapid stimulation and at low temperature, experimental conditions which are used to elicit repolarisation alternans. Low temperature was also associated with a global prolongation of APD₉₀, a reduction in transmural conduction velocity and a steeper maximal restitution slope. The results from the current study may therefore provide an explanation for the commonly observed temperature dependence of repolarisation alternans.

Chapter 4: The effect of transmural activation sequence on action potential duration

Introduction

Transmural gradients of APD in intact myocardium

As described in Chapter 3, transmural gradients of APD exist in intact ventricular myocardium. The nature of the transmural differences seen in intact myocardium is similar to that seen in isolated cells, in that subendocardial APD is longer than subepicardial APD, although the presence of midmyocardial APD prolongation is variable, depending on species and experimental conditions. However, the overall magnitude of the transmural APD difference in intact myocardium is smaller than that seen in isolated cells. This is because intercellular coupling in intact myocardium acts to homogenise electrical behaviour, by allowing passive electronic current flow between cells. The transmural differences in APD seen in intact tissue may simply reflect the transmural differences seen in the repolarisation characteristics of isolated cells, albeit attenuated by electrotonic coupling. However, it is possible that electrotonic influences may be responsible for dynamic modulation of APD in intact myocardium. Theoretically, if the electrotonic load experienced by a cell during repolarisation were to be altered, then differential electrotonic modulation of APD might be seen.

Electrotonic modulation of APD

In early electrophysiological experiments on multicellular preparations, an inverse relationship between activation time and monophasic APD was noted during physiological activation sequences¹⁶⁹. It was hypothesised that electrotonic modulation of APD works to synchronise repolarisation time across a range of activation times and therefore to reduce dispersion of repolarisation^{169;170}. However, in recent experiments using intracellular microelectrodes to record from the endocardium and epicardium of rabbit ventricular wedge preparations, no difference in APD was detected between epicardial and endocardial stimulation at a CL of 2000ms¹⁷¹, suggesting that the transmural differences observed were independent of electrotonic load and likely to be due to intrinsic differences in the repolarisation characteristics of the cells.

The effect of activation sequence on APD

Progressive modulation of APD after a prolonged period (> 30mins) of altered activation sequence is thought to be the basis of the ventricular electrical remodelling (VER) which underlies cardiac memory. VER describes persistent changes in electrophysiological behaviour in response to a change in activation sequence¹⁷². Studies using pharmacological

agents to block specific ion channels have implicated changes in the density and kinetics of epicardial I_{to} ¹⁷³ and the kinetics of I_{Cal} ¹⁷⁴ in the production of VER. The mechanisms by which altered activation sequence triggers these changes in ionic currents remain largely unknown. Changes in circumferential strain produced by altered activation have been implicated in the triggering of ventricular electrical remodelling¹⁷⁵, as have changes in electrotonic load¹⁷⁶.

Gap junctions

Electrotonic current flow between cardiac cells occurs through gap junctions. Gap junction channels are positioned primarily at the intercalated discs and allow the passage of ions (electrical coupling) and small molecules (metabolic coupling) between adjacent cells¹⁷⁷. Each gap junction comprises two hemichannels, called connexons, each of which is formed by six connexin (Cx) subunits, of which a number of isoforms have been identified. In gap junctions found in ventricular myocardium, the commonest isoform is Cx 43, with some expression of Cx 40 and Cx 45 in the ventricular conducting system. Cardiac gap junctional behaviour is modulated by phosphorylation status, intracellular pH and $[Ca^{2+}]_i$.

Carbenoxolone

Carbenoxolone is a mineralocorticoid which reversibly inhibits gap junction communication in cardiac and other cell types. In rabbit ventricular myocardium, 50 μ mol/L carbenoxolone has been demonstrated to reduce both transverse and longitudinal conduction velocity, without any effect on AP morphology or ionic currents¹⁷⁸. The specific molecular mechanism of the uncoupling effect of carbenoxolone on cardiac tissue is unknown. Work carried out in our laboratory has suggested some less specific effects of carbenoxolone, in that it shortened monophasic APD₉₀ and had small but significant effects on the Ca^{2+} transient¹⁵¹.

Rotigaptide

Rotigaptide is a synthetic peptide which acts to increase the conductance of Cx 43 gap junctions¹⁷⁹. It has been shown to have antiarrhythmic properties in animal models, increasing atrial CV and reducing AF duration in canine¹⁸⁰, reversing the reduction in CV and increase in DOR seen with acidosis in Langendorff perfused guinea pig hearts¹⁸¹, and preserving Cx 43 phosphorylation during ischaemia in isolated perfused rat hearts¹⁸².

Aims

This set of experiments was designed to test the hypothesis that transmural gradients of APD₉₀ are determined by intrinsic differences in cellular repolarisation properties and therefore should be independent of activation sequence.

Specific aims were:

To examine the effect of activation sequence on transmural patterns of APD₉₀.

To examine the influence of intercellular coupling on transmural patterns of APD₉₀.

To determine if similar behaviour was found on the epicardial surface.

Methods

In order to investigate transmural electrophysiology in intact rabbit left ventricular myocardium, the CCD-based optical mapping system described in Chapter 2 was used to record optical action potentials from the transmural surface of perfused left ventricular wedge preparations. Hearts from 24 male New Zealand White rabbits were used in these experiments (those described in Chapter 3 plus an additional 8), which conform to standards set out in the UK Animals (Scientific Procedures) Act, 1986.

Experimental protocols

The left ventricular wedge preparations ($n = 24$) used in this set of experiments were prepared as described in Chapter 2. Perfusion was at 37°C ($n = 16$) except where low temperature was specifically investigated ($n = 7$). In a subset of experiments ($n = 3$) pacing protocols were repeated with the LV wedge preparation orientated for epicardial, rather than transmural imaging.

Paired stimulation

In a subset of experiments ($n = 2$), paired endocardial and epicardial stimulation was used. Initially the two stimuli were delivered simultaneously, then the delay between endocardial and epicardial point stimulation was systematically varied such that the fusion point of the two wavefronts occurred at the midmyocardium.

Gap junction modifiers

The endocardial and epicardial stimulation protocol was repeated during infusion of gap junction modifiers. Control recordings were taken at 0 and 15 minutes and then repeated at five minute intervals during drug infusion and washout.

Carbenoxolone

Carbenoxolone (3β -hydroxy-11-oxoolean-12-en-30-oic acid 3-hemisuccinate, Sigma-Aldrich, Steinheim, Germany) was added to the physiological solution prior to the filtering stage. A final concentration of $50\mu\text{mol/L}$ was used. This concentration has previously been shown to reduce CV in rabbit ventricular myocardium, without the toxic effects seen at higher doses¹⁵¹.

Rotigaptide

Rotigaptide was provided by Dr Ninian Lang and Professor David Newby of the University of Edinburgh. Rotigaptide, at a final concentration of 1 μ mol/L was added to the physiological solution prior to the filtering stage.

Data analysis

Data analysis was performed as described in Chapter 2. As described in Chapter 3, transmural APD₉₀ was measured using three 3 x 3 pixel selections, equally spaced across the transmural surface and orientated between the stimulating electrodes, such that the sampling sites were perpendicular to the activation wavefronts.

Statistical analyses

All data are expressed as mean \pm SEM, and statistical analyses were carried out as described in Chapters 2 and 3, except for the comparison of APD₉₀ at multiple sites across the transmural surface during endocardial and epicardial stimulation. For this, a two-way ANOVA in R software was used, in which stimulation site was considered as a categorical variable and transmural position, or activation time as continuous variables.

Results

The effect of transmural activation sequence

Transmural activation wavefronts and conduction velocity

Patterns of activation and transmural conduction velocity were compared during endocardial and epicardial stimulation at 37°C, and are shown in Figure 4.1. During endocardial stimulation, a relatively planar transmural activation front was typically seen and during epicardial stimulation a more semi-circular waveform was evident. Mean transmural conduction velocity, measured between the two stimulus points, and perpendicular to the activation isochrones, was significantly greater during endocardial stimulation than during epicardial stimulation (30.0 ± 0.9 vs 24.6 ± 1.2 cm/sec, $n = 8$, $p = 0.0029$).

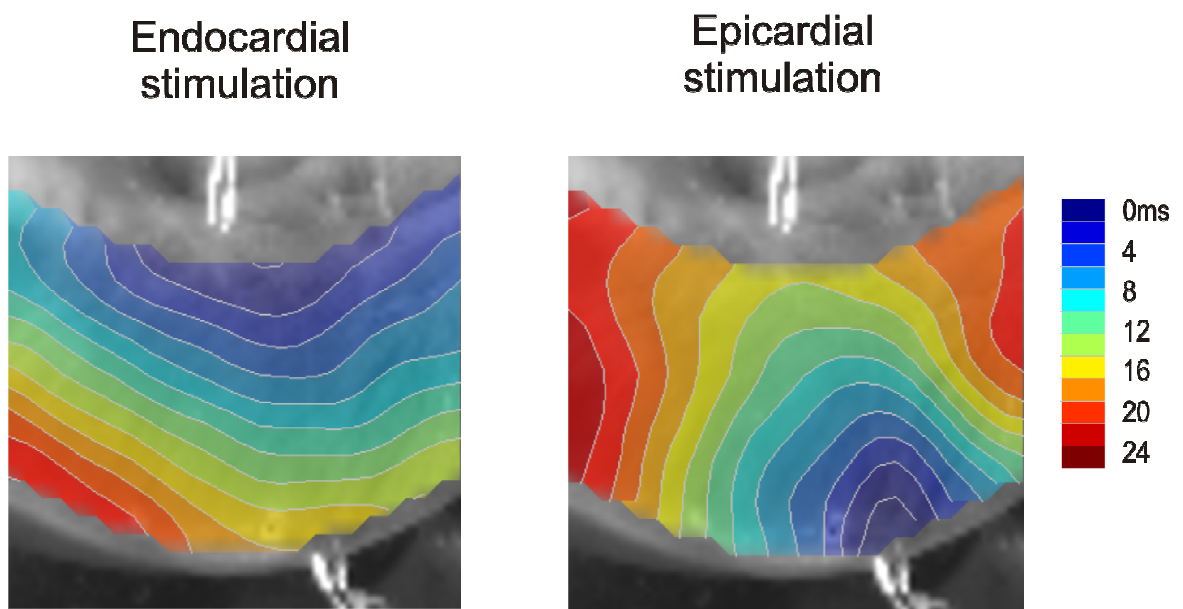


Figure 4.1 Transmural activation wavefronts during endocardial and epicardial stimulation

The left hand panel shows an isochronal map of transmural activation time during endocardial stimulation, superimposed on a plain image of the transmural surface, with the stimulating electrodes visible. The opacity of the overlaid colour is graded according to the magnitude of activation time. The right hand panel shows an isochronal map of transmural activation time during epicardial stimulation in the same experiment.

The effect of transmural activation sequence on transmural dispersion

The effect of transmural activation sequence on transmural dispersion is shown in Table 4.1. Transmural dispersion of activation time was significantly greater during epicardial stimulation when compared with endocardial stimulation. Neither transmural dispersion of repolarisation time nor transmural dispersion of APD₉₀ was significantly different between endocardial and epicardial stimulation.

Table 4.1 Effect of activation sequence on transmural dispersion of activation, repolarisation and APD₉₀

Mean ± SEM	Endocardial stimulation (n = 8)	Epicardial stimulation (n = 8)	P value
Transmural dispersion of activation time (ms/mm ²)	0.47 ± 0.07	0.64 ± 0.05	0.0257
Transmural dispersion of repolarisation time (ms/mm ²)	1.77 ± 0.36	1.10 ± 0.31	0.1185
Transmural dispersion of APD ₉₀ (ms/mm ²)	1.35 ± 0.38	1.54 ± 0.31	0.2305

ms/mm² = milliseconds per square millimetre, SEM = standard error of the mean. P value refers to a paired t-test.

The effect of transmural activation sequence on transmural APD₉₀

Different transmural patterns of APD₉₀ were recorded when the activation sequence was changed from endocardium-to-epicardium to epicardium-to-endocardium. An example is shown in Figure 4.2. During endocardial stimulation (Figure 4.2A), the longest APD₉₀ values were found at the subendocardium, and progressively shorter APDs tended to be recorded towards the subepicardium. During epicardial stimulation (Figure 4.2B), the opposite pattern was apparent, with the longest APD₉₀ values found at the subepicardium, and APD tending to become progressively shorter towards the subendocardium. As shown by the individual AP traces in Figure 4.2 A(iii) and B(iii), this appears to have the effect of minimising transmural differences in repolarisation time.

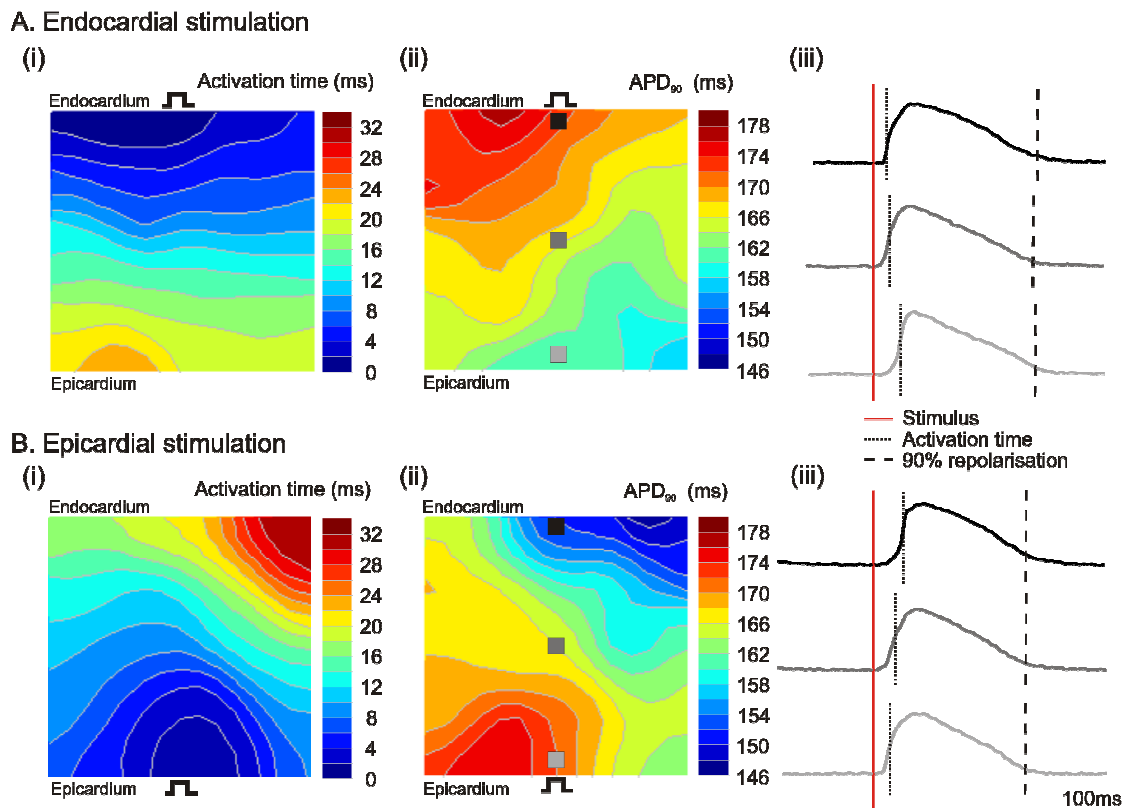


Figure 4.2 Modulation of transmural APD_{90} by activation sequence

A. Endocardial stimulation: (i) isochronal map of activation time from endocardial point stimulation (ii) contour map showing the transmural pattern of APD_{90} (iii) single pixel optical AP traces taken at three points equally spaced across the transmural surface perpendicular to the axis of activation (subendocardium in black, midmyocardium in dark grey and midmyocardium in light grey) with the stimulus (red line), activation time (dotted line) and time at 90% repolarisation (dashed line) marked. B. Epicardial stimulation: (i) isochronal map of activation time from epicardial point stimulation (ii) contour map showing the transmural pattern of APD_{90} (iii) single pixel optical AP traces taken at the same three points across the transmural surface.

The mean data for subendocardial, midmyocardial and subepicardial APD_{90} ($n = 8$) at 37°C are shown in Figure 4.3. During endocardial point stimulation, the longest APD_{90} was found in the subendocardial region ($164.5 \pm 4.5\text{ms}$), with an intermediate value at the midmyocardium ($155.6 \pm 4.3\text{ms}$) and the shortest at the subepicardium ($147.1 \pm 3.7\text{ms}$). During epicardial point stimulation, the opposite pattern was observed, with the longest APD_{90} at the subepicardium ($162.1 \pm 4.3\text{ms}$), an intermediate value at the midmyocardium ($150.9 \pm 4.2\text{ms}$) and the shortest at the subendocardium ($148.2 \pm 5.5\text{ms}$). In a subset of experiments ($n = 5$), a more detailed analysis was carried out, examining five points across the transmural surface, to delineate transmural gradients better (Figure 4.3, inset), and suggested a relatively smooth gradient of APD_{90} across the transmural surface in each case.

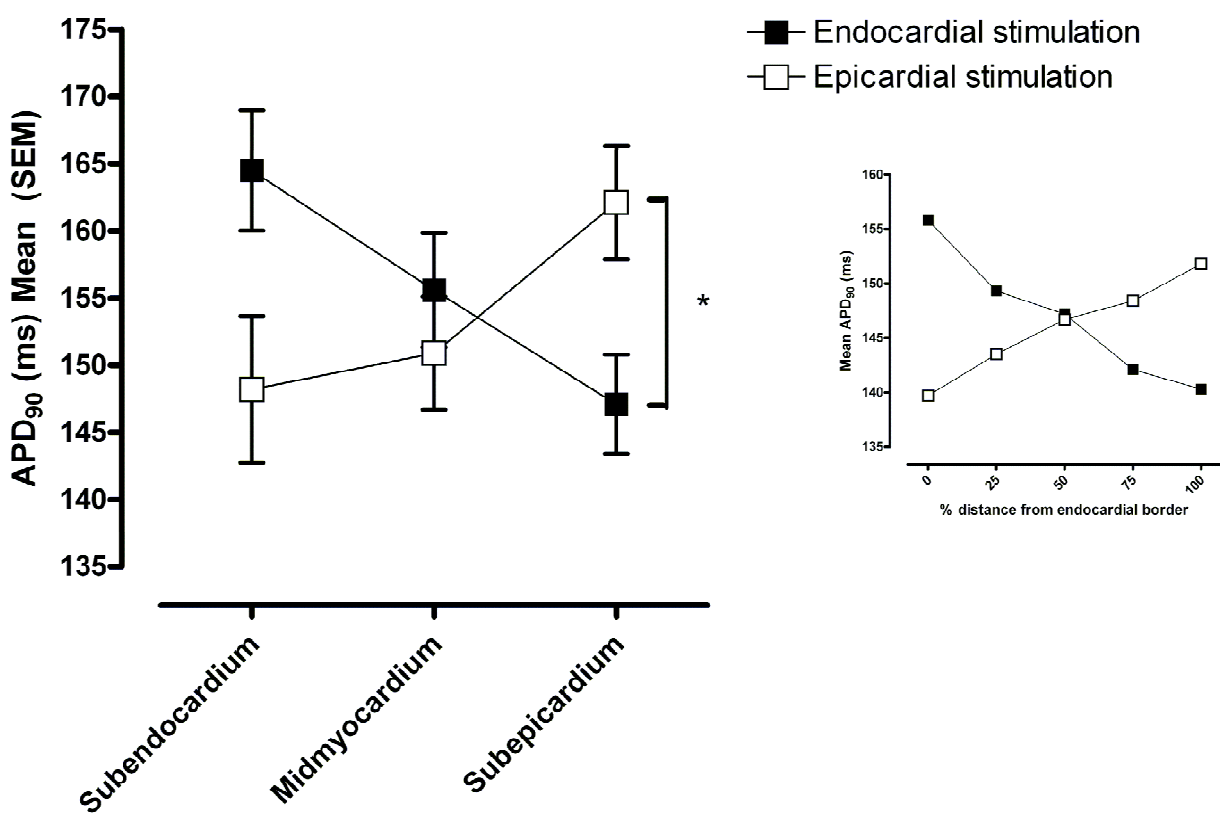


Figure 4.3 The effect of activation sequence on transmural APD_{90}

Mean data ($n = 8$) for APD_{90} in the three transmural regions during endocardial (closed squares) and epicardial (open squares) stimulation. The statistical comparison was performed using a two-way ANOVA, * $p < 0.05$. Inset shows mean data ($n = 5$) for APD_{90} in five equally spaced transmural regions during endocardial (closed squares) and epicardial stimulation (open squares).

This suggested that the longest APD_{90} was found close to the stimulus site. In order to explore this further, the mean activation time relative to the earliest transmural activation was calculated for each transmural region and the effect of proximity to the stimulus was assessed by plotting the same transmural APD_{90} data shown in Figure 4.3 against mean activation time. During endocardial stimulation, the mean activation time was significantly shorter in the subendocardial region ($4.0 \pm 1.4\text{ms}$), when compared with midmyocardium ($9.2 \pm 1.4\text{ms}$, $p < 0.001$) and subepicardium ($17.1 \pm 1.4\text{ms}$, $p < 0.001$ vs. subendocardium and midmyocardium). During epicardial stimulation, activation time was shortest at the subepicardium ($5.6 \pm 1.0\text{ms}$) and longer in the midmyocardium ($10.8 \pm 1.2\text{ms}$, $p < 0.001$) and subendocardium ($17.2 \pm 1.5\text{ms}$, $p < 0.001$ vs. subendocardium and midmyocardium). The plot of mean APD_{90} against mean activation time for each transmural region during endocardial and epicardial stimulation is shown in Figure 4.4. This demonstrates an inverse relationship between activation time and APD_{90} , such that sites activated early displayed a longer APD_{90} , irrespective of their transmural position.

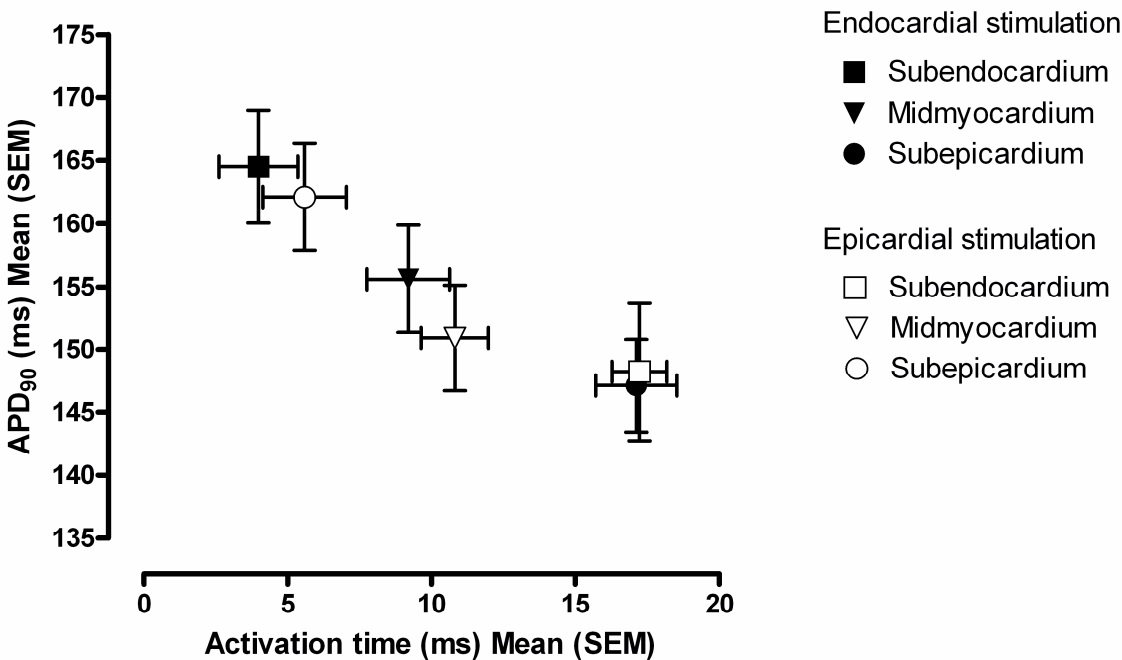


Figure 4.4 Transmural APD₉₀ as a function of mean activation time

Mean data ($n = 8$) for APD₉₀ and activation time (relative to the earliest transmural activation) in the subendocardium (squares), midmyocardium (triangles) and subepicardium (circles) during endocardial (closed symbols) and epicardial stimulation (open symbols).

The relationship between activation time and transmural APD₉₀

The contour maps of APD₉₀ suggest that the relationship between activation time and transmural APD₉₀ across the entire transmural surface is more complex than that indicated by the analysis of discrete transmural regions parallel to the endocardial and epicardial surfaces. To assess the relationship between activation time and transmural APD₉₀ across the whole transmural surface, two approaches were used. Firstly, in a selection of the experimental datasets, the values of APD₉₀ for each individual pixel during endocardial and epicardial stimulation were plotted against the corresponding activation time. A linear regression was then performed to quantify the relationship between activation time and APD₉₀. An example of this is shown in Figure 4.5, which shows an inverse relationship between activation time and APD₉₀. The longest APD₉₀ values were generally associated with the earlier activation times, during both endocardial and epicardial stimulation ($p < 0.0001$ in both cases). This inverse relationship was seen in the majority of the regressions performed, although in some of the experiments analysed, no relationship was seen between APD₉₀ and activation time. A positive relationship between activation time and APD₉₀ was never observed.

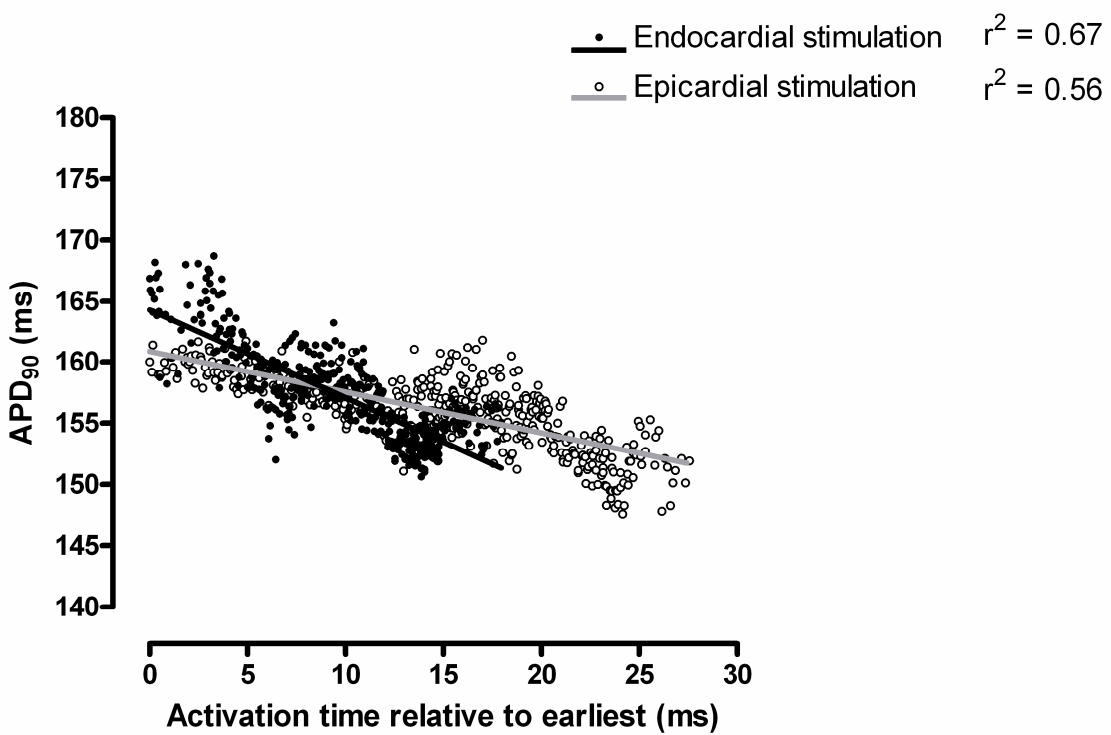


Figure 4.5 Linear regression of the relationship between APD₉₀ and activation time
 APD₉₀ against activation time for each transmural pixel during endocardial (closed circles) and epicardial stimulation (open circles). The corresponding linear regression for each dataset is also plotted. For endocardial stimulation (black line) the relationship was significant ($r^2 0.67$, $p < 0.0001$) and for epicardial stimulation (grey line) the relationship was also significant ($r^2 0.56$, $p < 0.0001$). Data are taken from a single experiment.

In this example, a small but significant difference was seen between subendocardial APD₉₀ during endocardial stimulation and subepicardial APD₉₀ during epicardial stimulation when sites activated within the first 5ms were compared (163.4 ± 0.3 vs. 159.6 ± 0.2 ms respectively, $p < 0.0001$). Each of the saved APD₉₀ matrices were partitioned into 5ms steps of activation time according to the corresponding activation time map, as illustrated in Figure 4.6. The mean data for this comparison are shown in Figure 4.7. During endocardial stimulation, the mean APD₉₀ for pixels activated in the first 5ms was significantly longer than the mean APD₉₀ in pixels activated in the last 5ms (156.1 ± 4.3 vs. 147.3 ± 4.1 , $p = 0.0165$). During epicardial stimulation, the mean APD₉₀ for pixels activated early was again significantly longer than the mean APD₉₀ in pixels activated later (152.4 ± 3.6 vs. 143.4 ± 5.8 , $p = 0.0041$). When APD₉₀ was expressed according to activation time, rather than transmural position, the difference in terms of APD₉₀ between endocardial and epicardial stimulation was no longer apparent.

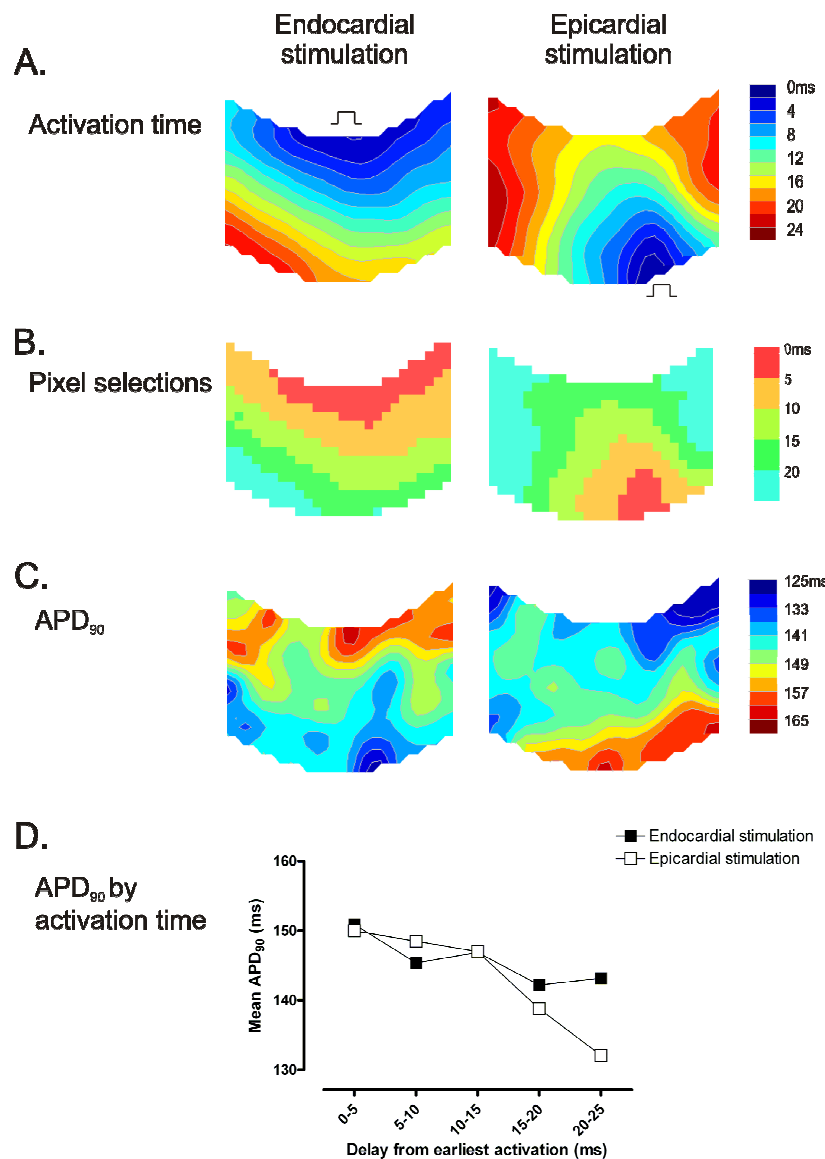


Figure 4.6 Partitioning of APD_{90} data by activation time

A. Isochronal maps of transmural activation time during endocardial and epicardial stimulation. B. The corresponding pixel selections determined by activation time (relative to the earliest transmural activation). C. Isochronal maps of transmural APD_{90} during endocardial and epicardial stimulation. D. The data displayed in (C) are partitioned according to the pixel selections shown in (B), resulting in a plot of mean APD_{90} in steps of activation time, from earliest to latest.

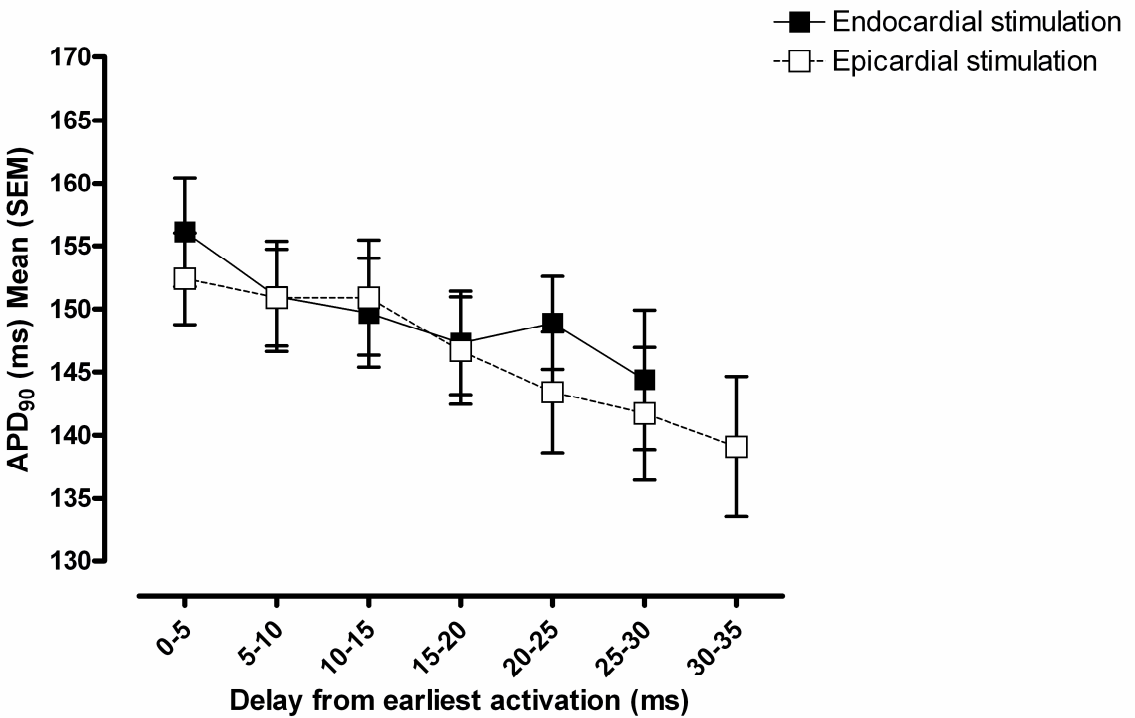


Figure 4.7 Mean transmural APD₉₀ by activation time

Mean transmural APD₉₀ ($n = 8$) for each 5ms increment in activation time from the earliest transmural activation during endocardial (closed squares) and epicardial stimulation (open squares). Two-way ANOVA, $p > 0.05$.

The effect of transmural activation sequence on epicardial APD₉₀

In a subset of experiments ($n = 3$ at 37°C), the effect of activation sequence on epicardial APD₉₀ was examined. An example is shown in Figure 4.8. Endocardial stimulation resulted in a rapid breakthrough activation pattern on the epicardial surface. During epicardial stimulation, relatively slower, anisotropic conduction was observed. Mean dispersion of activation time was significantly greater during epicardial stimulation compared to endocardial stimulation (0.37 ± 0.06 vs. 0.09 ± 0.01 ms/mm², $n = 3$, $p = 0.01$), whereas neither dispersion of repolarisation time (0.27 ± 0.07 vs. 0.40 ± 0.03 ms/mm², $p = 0.1630$) nor dispersion of APD₉₀ (0.18 ± 0.06 vs. 0.24 ± 0.05 ms/mm², $p = 0.4852$) were significantly different during epicardial stimulation. As shown by the contour maps in Figure 4.8, epicardial APD₉₀ was different during endocardial and epicardial stimulation. Figure 4.9 shows a comparison between subepicardial APD₉₀ (recorded from the transmural surface) and epicardial APD₉₀ in sites close to the stimulus.

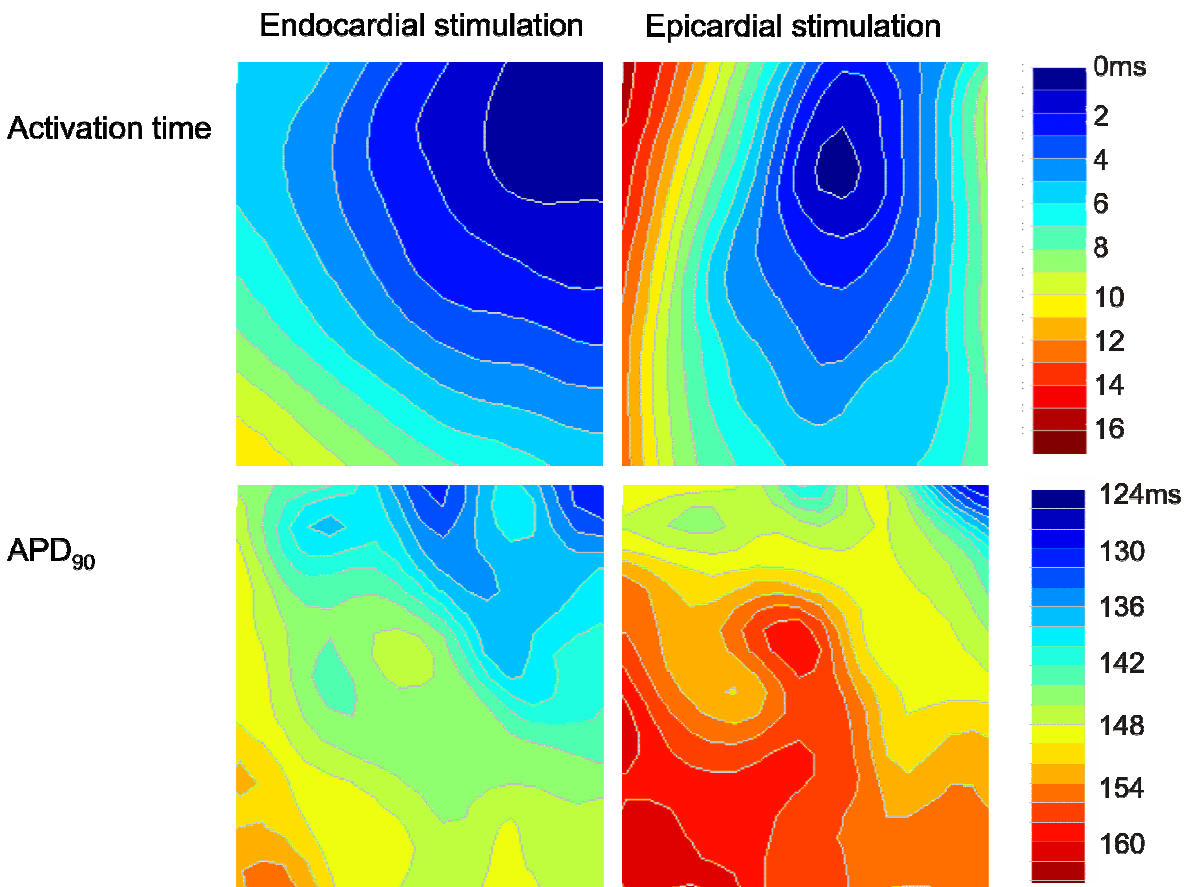


Figure 4.8 Activation sequence and epicardial APD₉₀

Contour maps showing the spread of activation (top panels) and distribution of APD₉₀ (lower panels) across the epicardial surface during endocardial (left panels) and epicardial stimulation (right panels).

In order to quantify the effect of activation sequence on epicardial APD₉₀, a detailed spatial analysis of epicardial APD₉₀ was performed. Pixel selections were assigned depending on their proximity to the epicardial stimulus. In order to achieve this, pixel selections were made using the epicardial activation map during epicardial stimulation and divided up in 1ms steps of activation from the epicardial stimulus, in a way analogous to that described for the transmural surface in Figure 4.6. Mean APD₉₀ for each selection during epicardial stimulation was then compared to mean APD₉₀ during endocardial stimulation. The results are shown in Figure 4.10. Mean epicardial APD₉₀ was significantly greater during epicardial stimulation than during endocardial stimulation when the pixels examined were activated within ~ 5-7ms from the earliest epicardial activation. During endocardial and epicardial stimulation, mean APD₉₀ values recorded from the subepicardial region of the transmural surface were $147.1 \pm 3.7\text{ms}$ and $162.1 \pm 4.2\text{ms}$ respectively. Corresponding values on the epicardial surface from pixels activated within 1ms of the epicardial stimulus were $145.8 \pm 5.0\text{ms}$ ($p = 0.8533$ vs. transmural surface) and $160.1 \pm 7.2\text{ms}$ ($p = 0.8113$ vs. transmural surface) respectively.

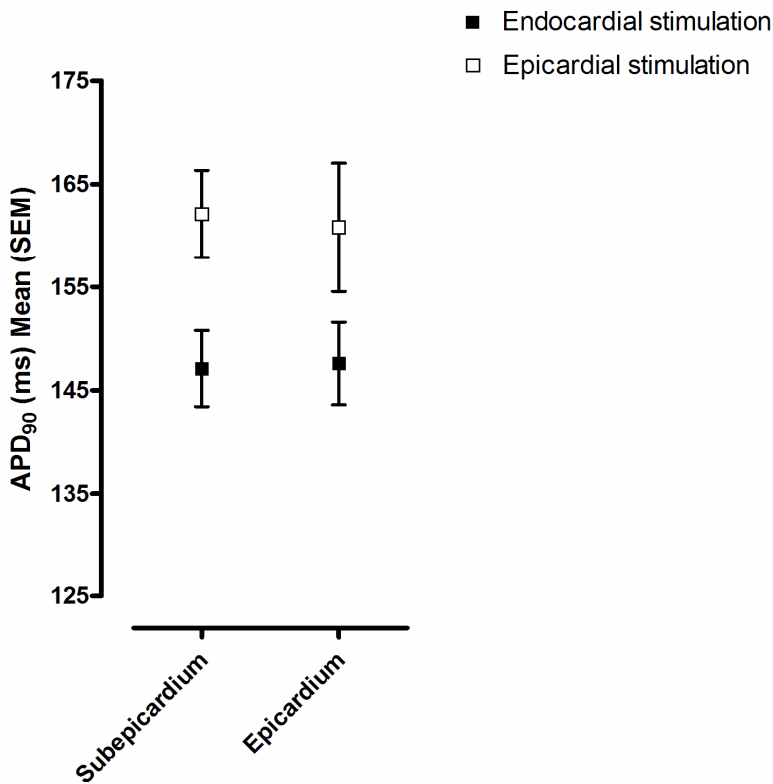


Figure 4.9 The effect of activation sequence on subepicardial and epicardial APD_{90}
A comparison of APD_{90} during endocardial (closed squares) and epicardial (open squares) stimulation. Transmural subepicardial sites ($n = 8$) were compared with sites close to the stimulating electrode on the epicardial surface ($n = 3$, activation delay 0-5ms).

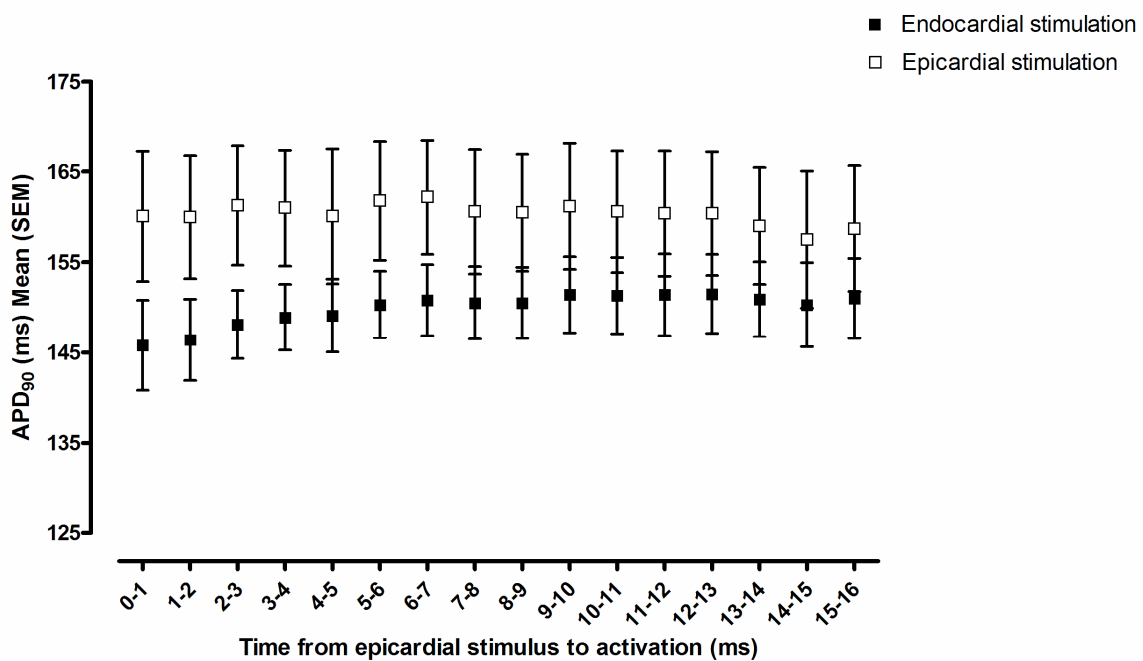
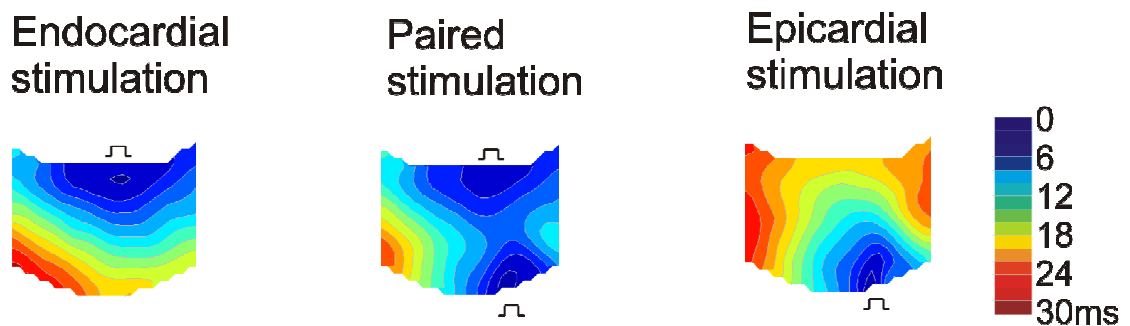


Figure 4.10 The effect of activation sequence on epicardial APD_{90}
A graph to show mean epicardial APD_{90} during endocardial (closed squares) and epicardial stimulation (open squares) across the epicardial surface, depending on the activation delay from the epicardial stimulus during epicardial stimulation ($n = 3$).

The effect of paired stimulation on transmural APD₉₀

In two experiments, the effect of paired endocardial and epicardial stimulation on transmural APD₉₀ was examined. Mean APD₉₀ values for the subendocardium, midmyocardium and subepicardium were compared. An example of the results is shown in Figure 4.11. During endocardial stimulation, the previously described pattern of APD₉₀ was observed (subendocardium > midmyocardium > subepicardium), and this pattern reversed during epicardial stimulation. During paired stimulation, midmyocardial APD₉₀ during paired stimulation (136.5 ± 0.5 ms, n = 38 APs) was significantly shorter than midmyocardial APD₉₀ during endocardial (141.4 ± 0.6 ms, n = 10 APs) or epicardial stimulation (140.5 ± 1.3 ms, n = 10 APs; p < 0.001 for endocardial vs. paired and p < 0.01 for epicardial vs. paired stimulation).

A.



B.

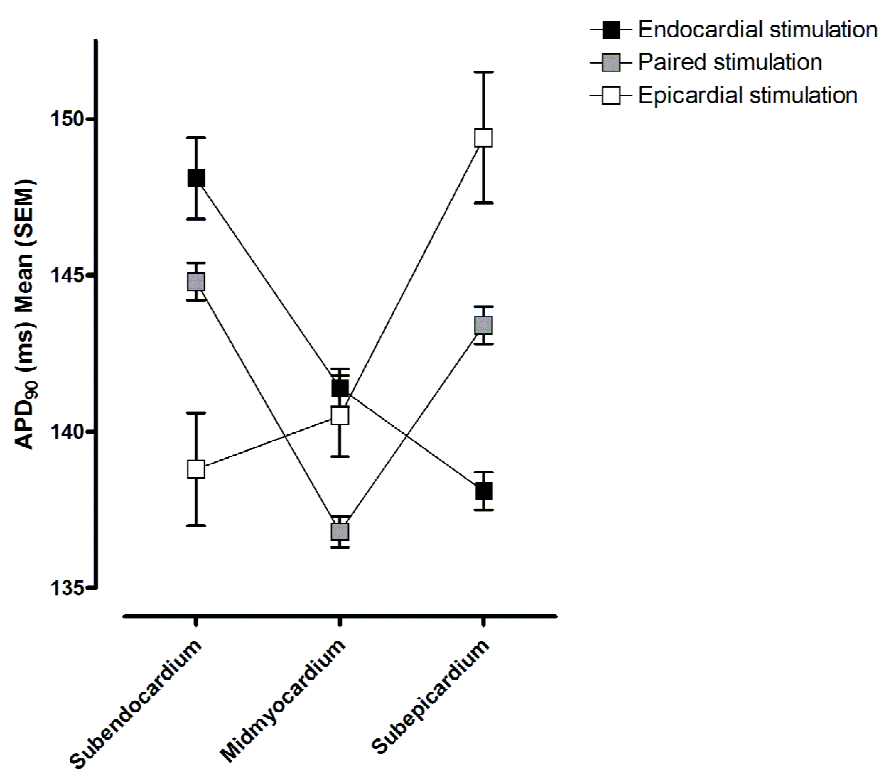


Figure 4.11 The effect of paired stimulation on transmural APD_{90}

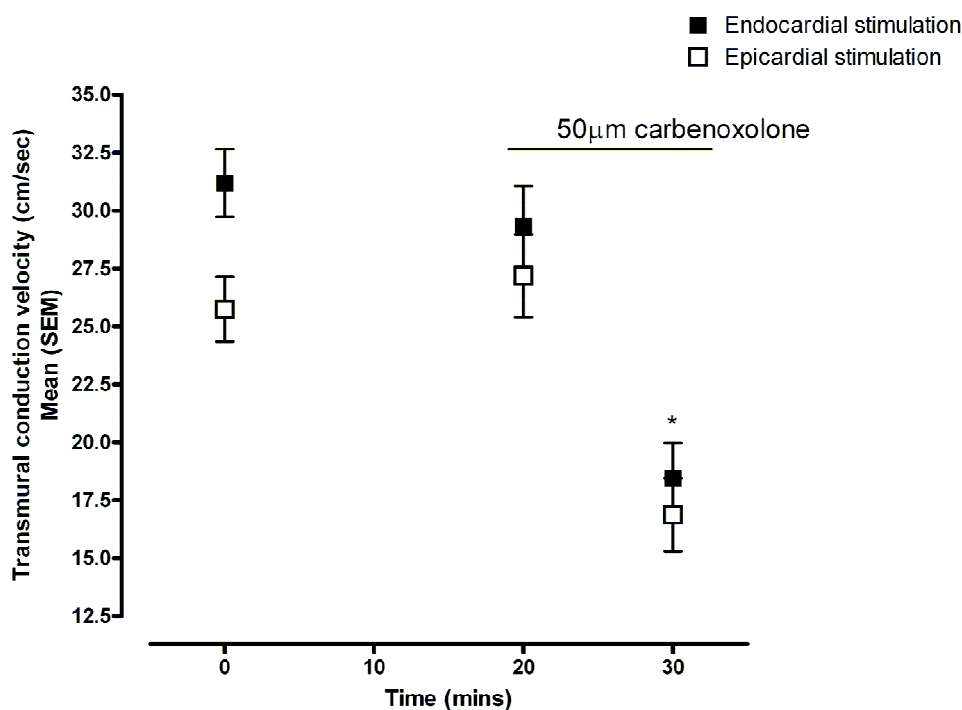
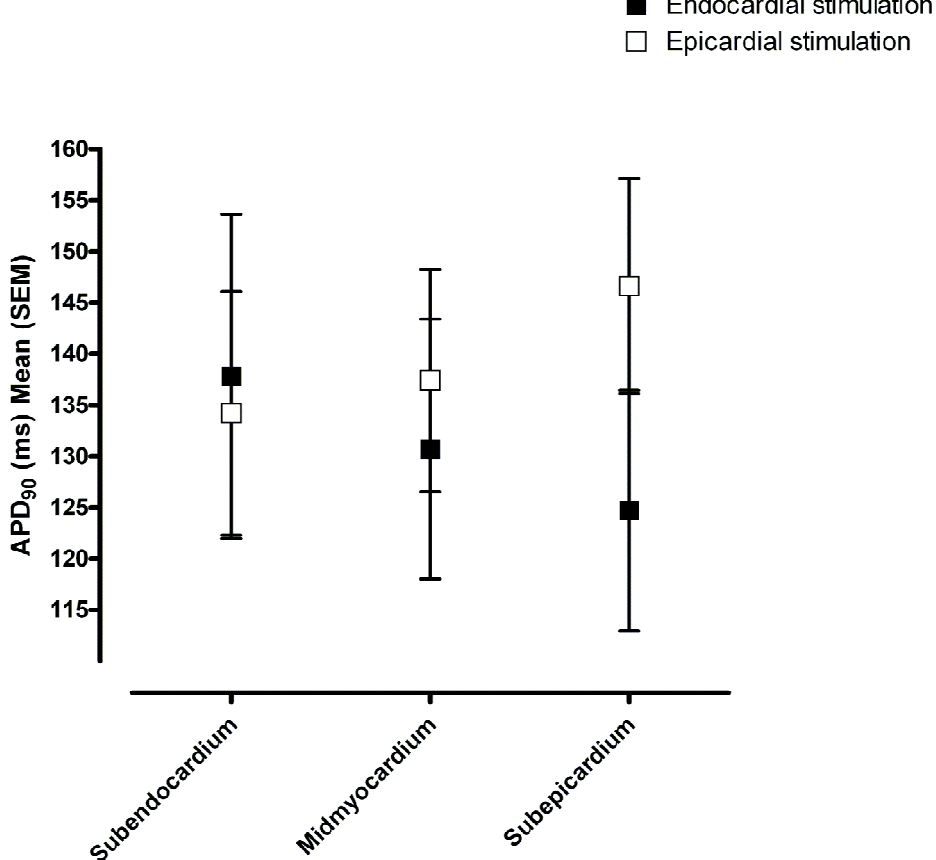
A. Isochronal maps showing the spread of activation across the transmural surface during endocardial stimulation, paired stimulation from both endocardium and epicardium and epicardial stimulation. B. Mean APD_{90} values for each of the transmural sampling sites during endocardial (black), paired (grey) and epicardial (white) stimulation. Data are taken from a single experiment and error bars relate to variability between APs.

The effect pharmacological modification of gap junction conductance on the transmural modulation of APD₉₀***Carbenoxolone***

The effects of the gap junction uncoupler carbenoxolone on transmural conduction velocity and transmural APD₉₀ are shown in Figure 4.12. There was no change in transmural CV over a 20 minute control period without drug (31.2 ± 1.5 vs. 29.3 ± 1.7 cm/sec during endocardial stimulation, $p = 0.4426$ and 25.7 ± 1.4 vs. 27.2 ± 1.8 during epicardial stimulation, $p = 0.5490$). At baseline, the transmural patterns of APD₉₀ during endocardial and epicardial stimulation in this subset were similar to those observed for the whole dataset. $50\mu\text{mol/L}$ carbenoxolone significantly slowed conduction velocity, from 31.2 ± 1.5 cm/sec to 18.5 ± 1.5 during endocardial stimulation ($p = 0.0006$) and from 25.8 ± 1.4 cm/sec to 16.9 ± 1.6 during epicardial stimulation ($p = 0.001$). Carbenoxolone produced a significant shortening of APD₉₀ (mean APD₉₀ 146.9 ± 3.9 vs. 131.1 ± 7.3 ms, $p = 0.0207$) along with a reduction in the signal quality and an increase in perfusion pressure observed during the experiment, indicating a toxic effect on the preparation. These effects of carbenoxolone were not reversible on washout of the drug. The previously noted transmural patterns of APD₉₀ according to stimulus site were not seen following carbenoxolone administration.

Rotigaptide

The effects of rotigaptide on transmural conduction velocity and detailed transmural APD₉₀ are shown in Figure 4.13. There was no change in transmural CV over a 15 minute control period without drug (32.7 ± 3.3 vs. 33.4 ± 2.8 cm/sec during endocardial stimulation, $p = 0.8768$ and 20.8 ± 1.6 vs. 21.4 ± 1.6 during epicardial stimulation, $p = 0.7998$). At baseline, the transmural patterns of APD₉₀ during endocardial and epicardial stimulation in this subset were similar to those observed for the whole dataset. $1\mu\text{mol/L}$ rotigaptide significantly increased transmural conduction velocity during epicardial stimulation (21.4 ± 1.6 cm/sec prior to rotigaptide vs. 29.4 ± 1.7 following rotigaptide, $p = 0.0140$) but had no significant effect on transmural CV during endocardial stimulation (33.4 ± 2.8 cm/sec vs. 37.6 ± 1.3 , $p = 0.2226$). Following rotigaptide infusion, APD₉₀ was significantly shorter (mean APD₉₀ 168.1 ± 3.9 vs. 137.1 ± 4.7 ms, $p = 0.0023$) and neither clear transmural gradients of APD₉₀ during endocardial stimulation, nor modulation of transmural APD₉₀ during epicardial stimulation were seen.

A.**B.****Figure 4.12 The effects of gap junction uncoupling with carbenoxolone**

A. The effects of carbenoxolone on transmural conduction velocity during endocardial (closed squares) and epicardial (open squares) stimulation ($n = 4$). One-way ANOVA, *** indicates $p < 0.001$ vs. 0 and 20mins for both endocardial and epicardial stimulation. B. Transmural APD₉₀ following 10 minutes of perfusion with carbenoxolone.

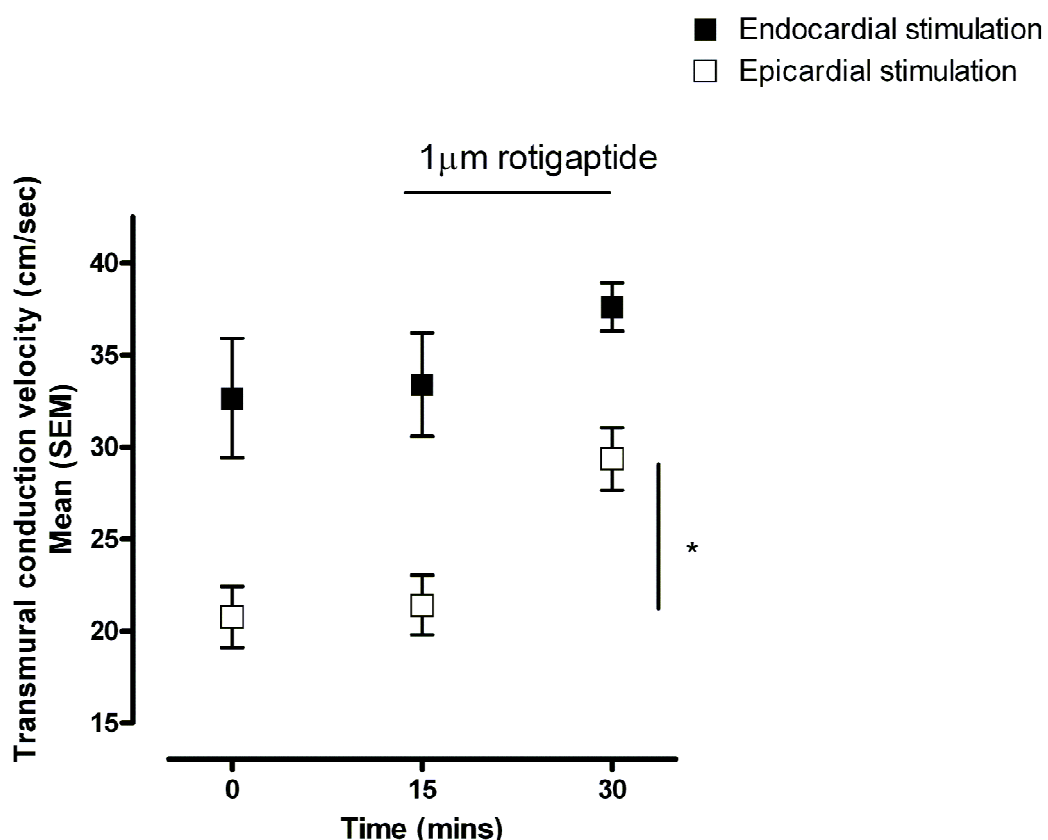
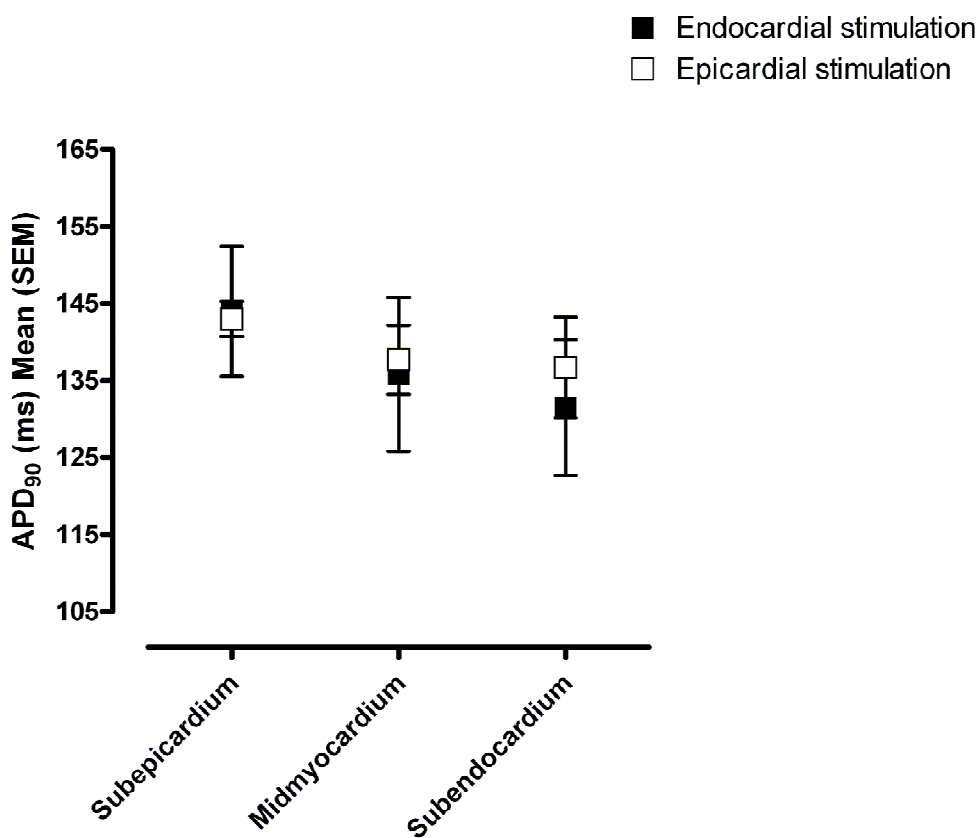
A.**B.**

Figure 4.13 The effect of rotigaptide on transmural conduction velocity and APD₉₀
 A. The effects of rotigaptide on transmural conduction velocity during endocardial (closed squares) and epicardial (open squares) stimulation ($n = 4$). One-way ANOVA, * $p < 0.05$ vs. 0 and 15 mins B. Transmural APD₉₀ following 15 minutes of perfusion with rotigaptide.

The effect of activation sequence on transmural electrophysiology at low temperature

Transmural conduction velocity at low temperature

Transmural conduction velocity was reduced at low temperature (Figure 4.14). During endocardial stimulation, transmural CV was reduced from 30.0 ± 0.9 at 37°C to $22.6 \pm 1.1\text{cm/sec}$ at 30°C ($p < 0.001$) and during epicardial stimulation transmural CV was reduced from 24.6 ± 1.2 at 37°C to $18.4 \pm 1.4\text{cm/sec}$ at 30°C ($p < 0.01$). The difference between endocardial-to-epicardial and epicardial-to-endocardial conduction velocity was not statistically significant at 30°C (22.0 ± 1.5 vs. $18.4 \pm 1.4\text{cm/sec}$, $n = 7$, $p > 0.05$).

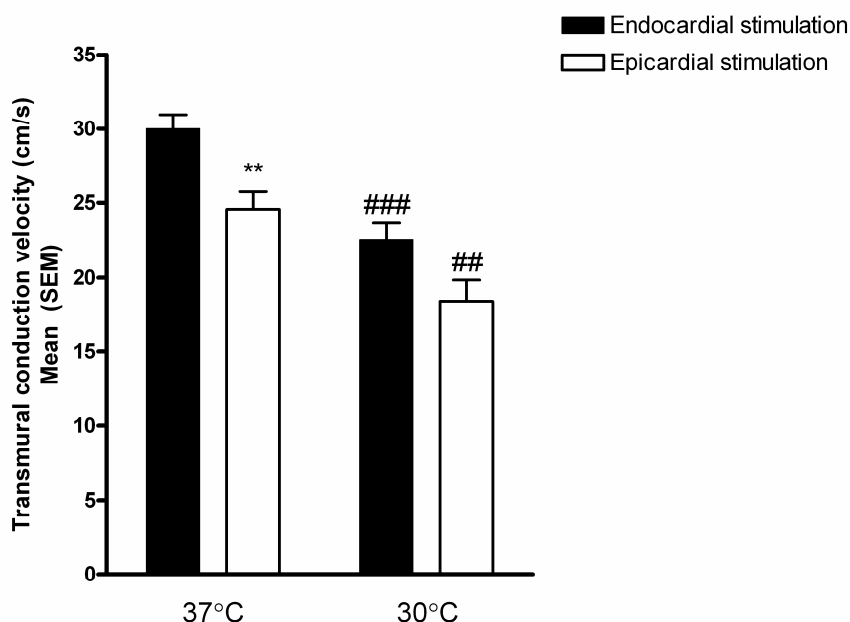


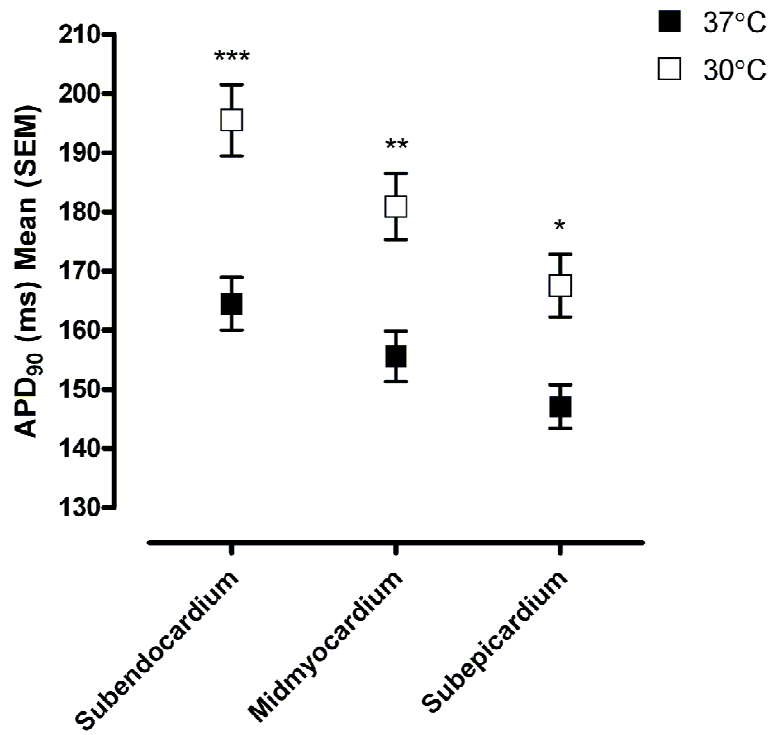
Figure 4.14 The temperature dependence of transmural conduction velocity

Transmural conduction velocity during endocardial and epicardial stimulation at 37°C ($n = 8$) and 30°C ($n = 7$). One-way ANOVA, ** $p < 0.01$ vs. endocardial stimulation, # $p < 0.01$ vs. 37°C , ## $p < 0.001$ vs. 37°C .

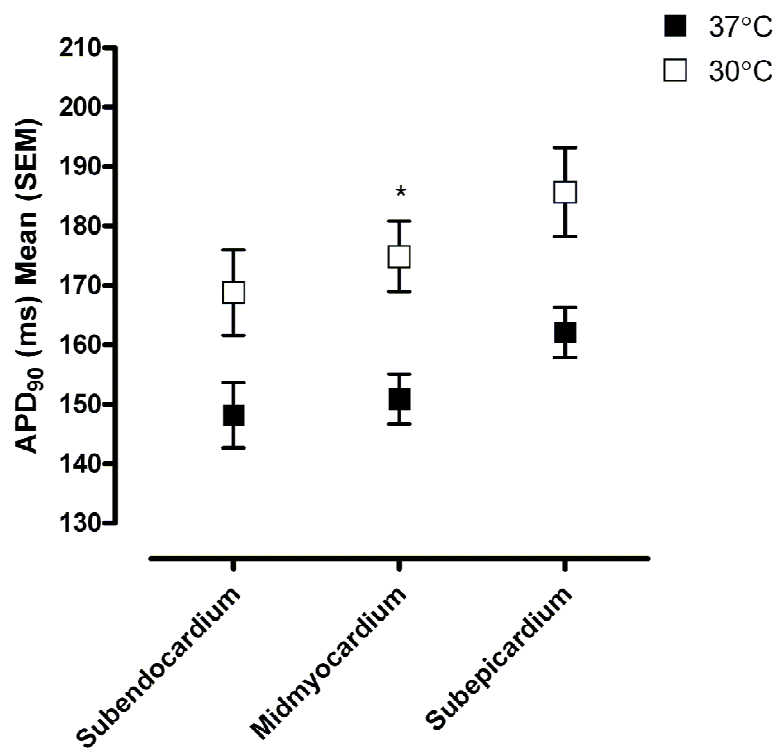
Modulation of transmural APD₉₀ by activation sequence at low temperature

As described in Chapter 3, APD₉₀ was longer at low temperature. As shown in Figure 4.15, the same modulation of APD₉₀ with activation sequence was observed at 30°C as had been observed at physiological temperature (two-way ANOVA, $p < 0.05$).

A.



B.

**Figure 4.15 The temperature dependence of APD_{90}**

A. Transmural patterns of APD_{90} during endocardial stimulation at 37°C (n = 8) and 30°C (n = 9) B. Transmural patterns of APD_{90} during epicardial stimulation. One-way ANOVA, *** p < 0.001, ** p < 0.01, * p < 0.05 vs. 37°C.

Discussion

The effects of transmural activation sequence on activation wavefronts and transmural conduction velocity

These experiments demonstrate the difference in activation wavefront between endocardial and epicardial stimulation. The wavefront during endocardial-to-epicardial propagation was typically relatively planar, whilst the wavefront during epicardial-to-endocardial propagation was more semi-circular. In agreement with these findings, transmural optical measurements in canine ventricular wedge preparations show that the activation front configuration is markedly different between endocardial and epicardial stimulation¹⁸³. The presence of a penetrating Purkinje fibre network on the endocardial surface is likely to contribute to the planar activation wavefront seen during endocardial point stimulation. The observed differences in wavefront curvature may also be attributable in part to transmural differences in gap junction expression, which have been shown to be reduced in the subepicardium¹⁸⁴. In these experiments, transmural CV during epicardial stimulation was found to be significantly slower than during endocardial stimulation, as has previously been reported in canine ventricular myocardium¹⁸³. Slower epicardial-to-endocardial propagation is likely to be due to several factors. The lack of an epicardial Purkinje fibre network may contribute to the relatively faster endocardial-epicardial conduction. It has been suggested that the increased curvature of the epicardial-endocardial wavefront may produce a greater source-sink mismatch during epicardial stimulation¹⁸³.

Transmural dispersion of repolarisation

Transmural dispersion of activation time was greater during epicardial stimulation, due to the slower epicardial-to-endocardial CV; dispersion of APD₉₀ was also greater. However, transmural dispersion of repolarisation did not change during epicardial stimulation in these experiments. This suggests that modulation of APD₉₀ must occur during a change in activation sequence. As repolarisation time is equal to activation time plus APD, if transmural gradients of APD₉₀ are fixed, transmural dispersion of repolarisation time would increase during epicardial stimulation. This is because the epicardium, which has the shortest APD₉₀ also experiences the shortest AT, producing an earlier RT than would be seen during endocardial stimulation, as subendocardial APD₉₀ is longer. Similarly, if subendocardial APD₉₀ remains long during epicardial stimulation, then the combination of this with the late subendocardial AT would result in a later RT than that seen during endocardial stimulation. Fixed transmural gradients of APD₉₀ have been observed in rabbit

myocardium at slow stimulation rates¹⁷¹. In that study, single cell microelectrode impalements were used to record APD₉₀ from subendocardial and subepicardial cells in a wedge preparation at cycle length of 2000ms. These investigators found that there was an increase in transmural dispersion of repolarisation during epicardial stimulation, which was accounted for by an increase in transmural conduction time, with no change in APD₉₀. The differences between the results presented here and those of Medina-Ravell *et al* may be due to differences in the experimental methods and conditions, particularly pacing CL.

Modulation of APD₉₀ by activation sequence

In these experiments, different transmural patterns of APD₉₀ were seen during endocardial and epicardial stimulation. This observation was made at both 37°C and 30°C. A gradient from the longest APD₉₀ at the subendocardium to shortest at the subepicardium was seen during endocardial stimulation, and this pattern reversed on epicardial stimulation. This has the effect of synchronising transmural repolarisation time, which is reflected in the mean dispersion data. The magnitude of the transmural APD₉₀ difference seen in the mean data was around 16-17ms, around 10% of the longest APD₉₀ value, and was similar during endocardial and epicardial stimulation. This difference is of sufficient magnitude to be resolved by the optical mapping system, and also to be of physiological relevance. In open-chest canine experiments, the refractory period of extracellular electrograms was always shorter when stimulation was distant to the measurement site compared with stimulation at the measurement site¹⁶⁹. Over distance of 4-6mm, change in repolarisation time was always less than the observed change in activation time, indicating a shortening of APD, which was estimated to be of the order of 5%. In the experiments described in this Chapter, the transmural distance separating the two stimulation sites was ~ 5mm.

The relationship between activation time and APD₉₀

The mean data for transmural APD₉₀ suggested not only that transmural APD₉₀ changed during a change in activation sequence, but also that APD₉₀ is linked to transmural activation time. When transmural position was replaced with transmural activation time, there was no difference in APD₉₀ seen during endocardial and epicardial stimulation. Sites close to the stimulus, which were activated early, had the longest APD₉₀; sites distant from the stimulation site, which were therefore activated later, had the shortest APD₉₀. However, these mean data were taken from three discrete sampling sites across the transmural surface, which were orientated perpendicular to the activation isochrones. Consequently, this comparison did not take into account either the differences in wavefront configuration

seen between endocardial and epicardial stimulation or apex-base heterogeneities in APD₉₀, both of which may contribute to the observed transmural patterns of APD₉₀. Indeed, it is evident from the contour maps that, in contrast to the transmural spread of activation, complex spatial patterns of transmural APD₉₀ were observed.

Regression

To explore the relationship between AT and APD₉₀ across the whole transmural surface, linear regressions were performed in a subset of experiments. For each of the transmural pixels, APD₉₀ was plotted against activation time during endocardial and epicardial stimulation. In the example given, a similar linear relationship exists between APD₉₀ and activation time during both activation sequences. Also, the plot shows a slightly shorter APD₉₀ at early activated (subepicardial) sites during epicardial stimulation than is seen at early activated (subendocardial) sites during endocardial stimulation. This suggests that some of the intrinsic cellular differences in APD₉₀ differences may be manifest in intact myocardium. The regression also suggests that significant variability in APD₉₀ exists which is not accounted for by differences in AT. This type of analysis is not amenable to averaging over experiments, and there were variable regression results in the individual experiments analysed, requiring that the relationship between AT and APD₉₀ be interrogated across the entire dataset.

Mean APD₉₀ by activation time

In order to examine the relationship between activation time and APD₉₀ across all experiments, transmural APD₉₀ was analysed according to 5ms steps of activation time, from the earliest transmural activation. When APD₉₀ was analysed in this way, such that pixels which were activated early were compared with those pixels which were activated later, the gradient of APD₉₀ observed was the same for both types of stimulation, with the longest APD₉₀ being associated with the areas close to the stimulus.

Paired stimulation

In two experiments, the effect of paired stimulation on transmural APD₉₀ was compared with endocardial and epicardial stimulation. During paired stimulation, midmyocardial APD₉₀ became shorter than either subendocardial or subepicardial APD₉₀, and midmyocardial APD₉₀ during paired stimulation was significantly shorter than midmyocardial APD₉₀ during either endocardial or epicardial stimulation. These results are again compatible with the effects of electrotonic load on APD₉₀. When paired stimulation

is used, the midmyocardial AP will experience a repolarising electrotonic influence from both subendocardium and subepicardium, rather than a repolarising influence from the tissue activated before it but a depolarising influence from the tissue activated after it, as would occur during either endocardial or epicardial stimulation.

Modulation of epicardial APD₉₀ by transmural activation sequence

The possible changes in APD₉₀ and electrotonic load imposed by the presence of a cut surface are difficult to predict. However, the recordings from the epicardial surface show changes in APD₉₀ in the pixels activated within a few milliseconds of the epicardial stimulus which are comparable to those seen in the subepicardial region of the transmural surface. That a similar change in APD₉₀ was observed with a change in activation sequence on the epicardial surface suggests that the modulation of transmural APD₉₀ observed in these experiments is not a cut surface effect. The relationship between APD₉₀ and activation time across the entire epicardial surface was not the same. Electrotonic modulation of APD₉₀ has been shown to be more marked in the transverse axis¹⁶⁹. Fibre orientation in the LV free wall in the rabbit is such that the cells are arranged perpendicular to the cut surface, meaning that transmural propagation is predominantly in the transverse axis. On the epicardial surface, however, cells are aligned parallel to the surface, meaning that much more of the activation wavefront is propagated longitudinal to the fibre axis. This is reflected in the anisotropic spread of activation seen in the epicardial activation map during epicardial stimulation, shown in Figure 4.8.

Pharmacological gap junction modification

Carbenoxolone

Carbenoxolone slowed conduction velocity in these experiments, suggesting that it was effective in producing a degree of gap junction uncoupling. Following the administration of carbenoxolone, the same gradients of APD₉₀ were not evident across the transmural surface. However, the signal quality was markedly lowered by carbenoxolone, there was a shortening of mean APD₉₀, effects which were not reversible following washout of carbenoxolone. This combination tends to suggest a toxic effect of carbenoxolone on the preparation. Indeed, previous work carried out in our laboratory noted toxic effects of carbenoxolone at concentrations higher than 60mmol/L. Langendorff perfused rabbit hearts exhibited a marked increase in perfusion pressure and end-diastolic pressure¹⁵¹. Although the current experiments were carried out using a lower concentration, these data should therefore be interpreted with caution.

Rotigaptide

Rotigaptide is thought to be a relatively specific potentiator of Cx43 mediated gap junction coupling. The data presented here show that rotigaptide increased transmural conduction velocity during epicardial stimulation but not during endocardial stimulation. Rotigaptide has previously been shown to increase epicardial CV during epicardial stimulation, but not during physiological activation sequences¹⁸⁵. The explanation for this observation is not immediately obvious. A broad interpretation of the available evidence on the effect of rotigaptide on ventricular conduction velocity is that it does not increase CV under normal conditions but rather that some compromise in CV is required before the effects of rotigaptide become apparent^{179;181;182}. In an analogous way, it may be speculated that epicardial-to-endocardial conduction is a sufficiently inefficient process that reserve for an increase in CV exists, but that endocardial-to-epicardial conduction is facilitated by the presence of subendocardial Purkinje fibres, and is therefore maximal. It is also possible that differences in the Cx isoform expression between ventricular myocardium (predominantly Cx 43) and the ventricular conducting system (predominantly Cx 40 and 45) may explain the differences in the response to rotigaptide depending on activation sequence. The differential effects of rotigaptide on transmural CV confound the transmural APD₉₀ data and make its interpretation difficult. It is also likely that the number of experiments was not sufficient to resolve the expected magnitude of any change in APD₉₀, based on the small magnitude of the increase in CV observed.

Conclusions

In this study, baseline APD₉₀ was recorded during both endocardial and epicardial stimulation. The hypothesis being tested was that transmural gradients of APD₉₀ reflect intrinsic differences in cellular repolarisation properties, and as such are independent of activation sequence. Instead, the results demonstrate that transmural gradients of APD₉₀ are modified by activation sequence. This conclusion is strengthened by the fact that similar modulation was observed consistently across different temperatures, during paired stimulation and during both transmural and epicardial imaging. These data suggest that as the distance from the site of stimulation increases, APD₉₀ shortens, resulting in a synchronisation of transmural repolarisation time. The results are consistent with an effect of electrotonic current flow between cells modulating the repolarisation phase of the AP. Considering a site close to the stimulus, during the repolarisation phase, downstream sites will be earlier in the AP and thus more depolarised. The effect of electrotonic current flow will therefore be to hold the cell more depolarised, prolonging repolarisation. Conversely, a site distant from the stimulus will be surrounded by cells which were activated earlier and are therefore more repolarised, which will tend to drive faster repolarisation. These experiments suggest that, in intact tissue, electrotonic modulation of APD by activation sequence dominates over the effects of intrinsic transmural differences in cellular repolarisation characteristics.

Chapter 5: Transmural electrophysiology in heart failure

Introduction

Patients with chronic heart failure are at significantly increased risk of arrhythmic sudden cardiac death. As the survival rates following sudden cardiac arrest are low, an effective preventative strategy is necessary. The only currently available effective preventative therapy for arrhythmic sudden cardiac death is the implantable cardioverter defibrillator (ICD). ICDs are expensive and associated with significant complication rates and as such are unsuitable for use as part of a widespread primary prevention strategy. Moreover, the ideal preventative strategy would actually reduce the occurrence of arrhythmias, rather than treating them when they do occur. In order to develop more effective preventative measures for SCD, it is important to understand the mechanisms behind the increased propensity to ventricular arrhythmias in heart failure. The effects of heart failure on the electrophysiology of mammalian ventricle have been widely investigated. A variety of electrophysiological changes have been reported, depending on the species and the type of model used, and a number of mechanisms by which the electrophysiological changes seen translate into an increased propensity to ventricular arrhythmias and sudden cardiac death have been suggested¹⁰.

Electrophysiological changes in heart failure

Action potential characteristics

In ventricular myocytes isolated from patients with end-stage heart failure undergoing cardiac transplantation, APD₉₀ at a stimulation frequency of 0.5Hz has been reported to be significantly longer than in cells isolated from normal donor hearts¹⁸⁶. APD prolongation has also been demonstrated in multicellular human ventricular preparations¹⁸⁷, although the difference between failing and normal ventricle was only significant at slow stimulation rates (0.33Hz) and was not apparent at more physiological rates (1Hz). Similar APD prolongation, again confined to low stimulation rates, has been recorded in myocytes isolated from canine hearts which had been subjected to chronic rapid pacing to induce dilated cardiomyopathy and heart failure^{188;189}. In other experimental models of heart failure, such as combined pressure and volume overload in the rabbit, intrinsic APD is unchanged compared with normal myocytes¹⁹⁰.

APD prolongation and arrhythmogenesis

APD prolongation in heart failure could conceivably be protective against re-entrant arrhythmias, through the maintenance of relatively longer refractory periods. Conversely, APD prolongation may be pro-arrhythmic, through the promotion of after-depolarisations and triggered activity. In midmyocardial cells isolated from canine hearts with pacing-induced heart failure, APD was prolonged and early afterdepolarisations (EADs) were more common¹⁹¹. APD prolongation may be reflected in the QT interval, and QT prolongation has not only been described in patients with heart failure but has also been linked to arrhythmic risk¹⁹².

In rabbit and human ventricular trabeculae from failing hearts, delayed afterdepolarisations (DADs) and triggered activity were more common than in normal rabbit trabeculae, but only when the superfusion solution was modified to contain low potassium, low magnesium and noradrenaline¹²⁹. This underlines the importance of the interplay between cellular electrophysiology and the extracellular milieu in arrhythmogenesis in heart failure.

Heart failure-induced changes in repolarising currents

Prolongation of intrinsic APD in heart failure has been attributed principally to changes in the density of repolarising K⁺ currents. A reduction in the functional density of the transient outward K⁺ current (I_{to}), which sets the plateau potential, has been shown in humans^{130;193} and animals¹⁸⁸ with heart failure. Rapid pacing in canine myocytes produces a reduction in the size of the AP notch, an increase in the plateau potential and a prolongation of APD in midmyocardial cells, consistent with overall APD prolongation being due to a reduction in I_{to} . Moreover, pharmacological I_{to} blockade produces similar effects on the AP in normal cells¹⁸⁸. However, the effects of changes in I_{to} on APD are difficult to predict, as changes in the plateau potential will also influence the magnitude of the L-type Ca²⁺ current. Depending on the relative balance of other ionic currents, a reduction in I_{to} may prolong or abbreviate the ventricular AP. The effect of changes in I_{to} on APD may also exhibit marked species differences¹⁹⁴. A reduction in the inward rectifier current (I_{K1}), which contributes to terminal repolarisation, has also been shown in human heart failure¹³⁰ and following pacing-induced heart failure in canine ventricle¹⁸⁸. I_{K1} blockade produces EADs and spontaneous activity in failing myocytes, suggesting that I_{K1} downregulation might lead to instability in the repolarisation phase of the AP in the failing heart¹⁸⁹. A reduction in the density of the slow component of the delayed rectifier K⁺

current (I_{Ks}) has also been linked to APD prolongation and EADs in canine tachycardia-induced heart failure¹⁹¹.

Calcium cycling in heart failure

A number of abnormalities in Ca^{2+} cycling have been demonstrated consistently in failing hearts. In isolated cells¹⁸⁶ and ventricular muscle¹⁸⁷ from humans with end-stage heart failure, the intracellular Ca^{2+} transient (Ca^{2+}_T) amplitude is lower, its decay is prolonged and diastolic Ca^{2+} levels are elevated. These changes have been linked to functional abnormalities of Ca^{2+} handling proteins and their associated regulatory proteins¹⁹⁵.

Although these changes are clearly central to the development of contractile dysfunction, the role of abnormal Ca^{2+} cycling in ventricular arrhythmogenesis in heart failure is also increasingly recognised. As a result of the intricate coupling which exists between $[\text{Ca}^{2+}]_i$ and membrane potential (V_m) in cardiomyocytes, arrhythmias in heart failure may be Ca^{2+} dependent. For example, in failing rabbit hearts following pressure and volume overload, the characteristic changes in the Ca^{2+}_T were directly linked to the genesis of DADs in the presence of beta-adrenergic stimulation¹⁹⁶.

L-type Ca^{2+} current

The L-type Ca^{2+} current (I_{CaL}) acts as the trigger for SR Ca^{2+} release. Therefore the magnitude of I_{CaL} influences the amount of Ca^{2+} released, and hence the magnitude of the Ca^{2+}_T . A reduction in I_{CaL} , which would tend to shorten APD, is seen in some experimental models of heart failure, although in others I_{CaL} is unchanged¹⁹⁷. Conversely, an increase in single-channel open probability of L-type calcium channels has been demonstrated in human heart failure and may contribute to APD prolongation¹⁹⁸.

Sarcoplasmic reticulum Ca^{2+} release

Heart failure also affects the SR Ca^{2+} release channel, RyR, resulting in an increased propensity to diastolic Ca^{2+} leak and so to the propagation of spontaneous Ca^{2+} waves which have been implicated in the genesis of DADs¹⁹⁹. In experimental models of heart failure following MI, dysynchronous SR Ca^{2+} release has been suggested as a possible mechanism underlying the abnormal Ca^{2+}_T ²⁰⁰.

Ca^{2+} reuptake to the sarcoplasmic reticulum

Most of the available evidence points to a reduction in the activity of the SR Ca^{2+} reuptake ATPase, SERCA 2a, in heart failure^{201;202}. Impaired SERCA function is also thought to

lead to an increased proportion of cytosolic Ca^{2+} being removed by $\text{Na}^+ \text{-Ca}^{2+}$ exchange (NCX). NCX is electrogenic, and carries an inward current in this forward mode. This may lead to APD prolongation and electrical instability during repolarisation.

Intracellular sodium in heart failure

Intracellular sodium concentration ($[\text{Na}^+]_i$) and $[\text{Ca}^{2+}]_i$ are closely linked, principally through the actions of the electrogenic NCX²⁰³. $[\text{Na}^+]_i$ is also linked to intracellular pH through the $\text{Na}^+ - \text{H}^+$ exchanger (NHE). Increased NHE activity has been demonstrated in experimental heart failure induced by pressure and volume overload in the rabbit²⁰⁴. The resulting increase in $[\text{Na}^+]_i$ was implicated in changes in Ca^{2+} cycling and Ca^{2+} mediated after-depolarisations in myocytes isolated from failing hearts, as these were at least partially prevented by NHE inhibition.

Changes in electrical coupling in heart failure

As discussed in Chapters 3 and 4, the degree of electrotonic coupling which exists between myocytes modulates the degree of electrophysiological heterogeneity which is expressed in intact myocardium. Electrotonic coupling between cells leads to a reduction in APD and has the effect of homogenising electrical activity between cells²⁰⁵. Therefore, increased electrophysiological heterogeneity in heart failure may stem from either heterogeneous changes in AP characteristics or Ca^{2+} cycling at the level of the single cell, or from a reduction in electronic coupling between cells. In ventricular myocardium electronic coupling is mediated by connexin 43 (Cx43) gap junctions. A reduction in Cx43 expression has been shown in both human and experimental heart failure¹⁰⁸.

Structural changes in failing hearts

Experimentally, ventricular arrhythmias are more readily induced in hearts that have undergone remodelling following MI than in controls⁹. In Langendorff perfused human hearts explanted at the time of transplantation for end-stage heart failure, the structural arrangement of the scar, and particularly the surviving myocardial strands within the scar and in the border zone, appeared important for the initiation and maintenance of re-entry¹²⁷. The electrophysiological changes manifest in the remote, non-infarcted myocardium are also important¹²⁸. Increased heterogeneity of APD in the remodelled ventricle can result in increased dispersion of refractoriness, a critical substrate for the development of re-entrant tachyarrhythmias. An increase in fibrosis may result in impairment of cellular coupling.

Transmural electrophysiology in heart failure

As discussed in Chapters 1 and 3, transmural electrophysiological heterogeneity has been linked to the genesis of ventricular arrhythmia in experimental studies. Transmural electrophysiological heterogeneity has also been identified as potentially important in arrhythmogenesis in heart failure¹⁴⁶. I_{to} is more prominent in the subepicardium, and the reduction in I_{to} current density in failing human ventricular myocytes has been shown to be marked in subendocardial, not subepicardial myocytes¹⁹³. In isolated myocytes from canine hearts following the induction of heart failure with rapid pacing, transmural differences in APD, evident at low stimulation rates in normal cells, were masked by inhomogenous AP prolongation in heart failure¹⁹¹. This was attributed to a relatively greater reduction in I_{Ks} in subepicardial and subendocardial myocytes, attenuating transmural gradients of I_{Ks} and consequently, APD. However, in intact ventricular myocardium using the same species and model, heart failure was associated with increased transmural heterogeneity of repolarisation¹⁴⁶. In that study, the midmyocardial layer displayed disproportionate prolongation of APD which appeared to be of consistent magnitude with the prolongation of the QT interval. The resultant increase in transmural dispersion of repolarisation was linked to the development of unidirectional conduction block and the initiation of polymorphic ventricular tachycardia.

Heterogeneity of repolarisation in the rabbit coronary ligation model

Our group has developed and extensively characterised an experimental model of heart failure produced by coronary arterial ligation in the rabbit¹³⁴⁻¹³⁷. Following ligation, rabbits develop a heart failure syndrome and have decreased survival compared with sham-operated controls. Ligated hearts have a lower VF threshold than controls, suggesting that re-entry may occur more readily⁹. Furthermore, this model has two major sources of electrophysiological heterogeneity as a consequence of MI. In the non-infarcted hypertrophied myocardium, APD is prolonged, as has been demonstrated in humans with heart failure¹³⁰. However, this APD prolongation is not uniform across the wall¹³⁴ and transmural dispersion of repolarisation, as measured in isolated cells, is increased. Secondly, there is a defined infarct border zone where surviving myocytes interdigitate with scar tissue at the epicardium and form a thin layer in the subendocardium. Local dispersion of refractoriness, estimated by the VF interval technique, is increased in this border zone⁹.

Repolarisation alternans in heart failure

The aim of this set of experiments was to examine the electrophysiological effects of heart failure in intact rabbit ventricle, with a specific focus on elucidating whether increased transmural electrophysiological heterogeneity exists in failing hearts. In particular, these experiments aimed to characterise the changes in electrophysiological parameters which may be relevant to the production of repolarisation alternans and spatially discordant repolarisation alternans.

Aims

To determine the transmural electrophysiological changes which occur in rabbit ventricle as a result of heart failure following myocardial infarction.

To determine whether heart failure is associated with APD prolongation and/or changes in transmural patterns of APD in intact tissue.

To compare the degree of transmural heterogeneity in repolarisation in the remodelled myocardium with that in normal hearts.

To determine whether the electrophysiological changes seen in heart failure are temperature dependent.

To characterise the electrophysiological changes which occur in the transmural border zone and to examine conduction into the infarct.

Methods

In order to investigate transmural electrophysiology in heart failure the CCD-based optical mapping system described in Chapter 2 was used to record optical action potentials from the transmural surface of perfused left ventricular wedge preparations from normal rabbits and rabbits with heart failure. Hearts from 29 male New Zealand White rabbits were used in these experiments (those described in Chapter 3 plus an additional 13), which conform to standards set out in the UK Animals (Scientific Procedures) Act, 1986.

Heart failure model

The heart failure model was produced by Dr Martin Hicks and Mr Michael Dunne and is described in detail in Chapter 2. Briefly, animals ($n = 11$) underwent surgical coronary arterial ligation under general anaesthesia, to produce apical myocardial infarction. Sham-operated animals underwent thoracotomy, during which the heart was manipulated in a similar fashion except that the artery was not tied. Eight weeks following surgery, echocardiography was carried out to document *in vivo* cardiac function prior to sacrifice. Hearts from normal rabbits ($n = 14$) and sham-operated rabbits ($n = 4$) were used as controls.

Experimental protocols

The left ventricular wedge preparations ($n = 29$) used in this set of experiments were prepared as described in Chapter 2. One set of experiments (normal, $n = 8$; heart failure, $n = 7$) was conducted at 37°C , and another at 30°C (normal, $n = 9$; heart failure, $n = 7$). In one normal and three failing hearts, the protocol was performed at 37°C , the temperature was lowered to 30°C and the protocol was then repeated. In a subset of experiments at 37°C ($n = 5$), the infarct border zone was imaged.

Data analysis

Analysis of optical action potentials

Data analysis was performed as described in Chapter 2. Conduction into the infarct was measured as shown in Figure 5.1. Conduction time was measured using 3 by 1 pixel selections parallel to the endocardial or epicardial border, at the point of earliest activation and 3×1 pixel selection at a fixed point in the apical infarct zone, perpendicular to those in the normal myocardium. The central pixels were used for calculating distance.

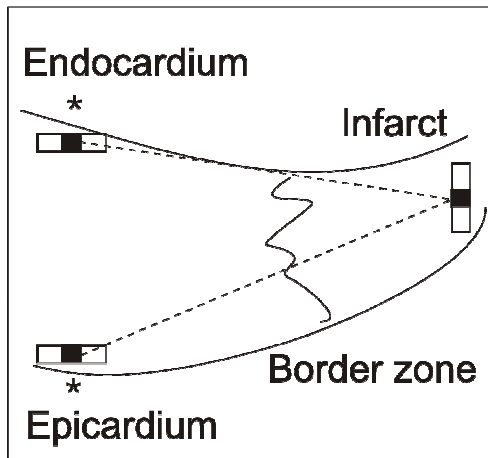


Figure 5.1 Measurement of conduction velocity into the infarct

Illustration of the optical imaging window containing an LV wedge with infarct and border zone visible. Stimulation sites on the endocardium and epicardium are compared using the indicated pixel selections for distance (black) and time (black and white).

Statistical analyses

All data are expressed as mean \pm SEM. Groups of data were compared using a Student's t-test (paired where appropriate), or when more than two groups were compared, using a one-way ANOVA (repeated measures where appropriate) with *post hoc* Tukey-Kramer multiple comparisons tests. All statistical tests were performed using GraphPad software.

Results

Left ventricular remodelling in heart failure

A number of parameters were recorded to assess the degree of left ventricular remodelling which occurred as a consequence of coronary arterial ligation, and these are shown in Tables 5.1 and 5.2. Mean body weight was significantly greater in the ligated animals ($p = 0.0045$). There were no significant differences in the dimensions or weight of the LV wedges between the two groups. Coronary artery ligation was associated with a small but statistically significant reduction in left atrial diameter (LAD), an increase in left ventricular end diastolic diameter (LVEDD) and a reduction in LVEF when compared with sham-operated controls. Age was only available for a subset of animals, but was not significantly different between normal and ligated animals (24.5 ± 2.1 months [$n = 6$] vs. 29.5 ± 1.4 months [$n = 4$], $p = 0.12$).

Table 5.1 Animal weights and LV wedge dimensions

Mean (SEM)	Normal (n = 16)	Heart failure (n = 11)	P value
Body weight (kg)	3.14 ± 0.14	3.53 ± 0.09	0.0045
Transmural distance (mm)	5.0 ± 0.3	5.6 ± 0.5	0.2848
LV wedge weight (g)	4.6 ± 0.3	4.8 ± 0.4	0.6869

g = grams, kg = kilograms, mm = millimetres, SEM = standard error of the mean. P value refers to an unpaired t-test.

Table 5.2 Left ventricular remodelling in heart failure

Mean (SEM)	Sham (n = 4)	Heart failure (n = 11)	P value
LAD (mm)	9.5 ± 0.1	8.3 ± 0.3	0.0358
LVEDD (mm)	17.5 ± 0.4	20.6 ± 0.4	0.0008
LVEF (%)	71.0 ± 0.4	44.0 ± 1.4	< 0.0001

LAD = left atrial diameter, LVEDD = left ventricular end diastolic diameter, LVEF = left ventricular ejection fraction, mm = millimetres, SEM = standard error of the mean. P value refers to an unpaired t-test.

Transmural electrophysiology in remodelled myocardium

Baseline transmural electrophysiological parameters were recorded at transmural sites in the basal section of the LV free wall, distant from the infarct border zone, during endocardial stimulation at 37°C. A comparison of baseline electrophysiological parameters in normal and failing hearts is shown in Table 5.3. There were no significant differences between normal and failing hearts in terms of transmural conduction velocity, dispersion of activation time, dispersion of repolarisation time, dispersion of APD₉₀, mean APD₉₀ (147.5 ± 3.9 vs. 150.9 ± 1.7, p = 0.4612) or transmural APD₉₀. As shown in Figure 5.2 the transmural pattern of APD₉₀ seen in heart failure was identical to that seen in control hearts. The longest APD₉₀ was recorded at the subendocardium, with progressively shorter values being recorded at the midmyocardium and subepicardium respectively. Figure 5.3 shows the transmural gradient of APD₉₀ in normal and failing hearts, which did not change significantly during rapid stimulation.

Table 5.3 Transmural electrophysiology in normal and failing hearts

Mean (SEM)	Normal (n = 8)	Heart failure (n = 7)	P value
Transmural conduction velocity (cm/sec)	30.0 ± 0.9	29.5 ± 1.8	0.9601
Transmural APD ₉₀ (ms)			
Subendocardial APD ₉₀	164.5 ± 4.5	161.2 ± 7.5	> 0.05
Midmyocardial APD ₉₀	155.6 ± 4.3	153.6 ± 6.2	> 0.05
Subepicardial APD ₉₀	147.1 ± 3.7	146.5 ± 7.1	> 0.05
Transmural dispersion (ms/mm ²)			
Activation time	0.47 ± 0.07	0.41 ± 0.06	0.5328
Repolarisation time	1.77 ± 0.36	1.80 ± 0.18	0.9443
APD ₉₀	1.10 ± 0.24	1.26 ± 0.30	0.6805

APD₉₀ = action potential duration at 90% repolarisation, cm/sec = centimetres per second, ms = milliseconds, ms/mm² = milliseconds per square millimetre, SEM = standard error of the mean. P value refers to an unpaired t-test for CV and dispersion and to a one-way ANOVA for APD₉₀.

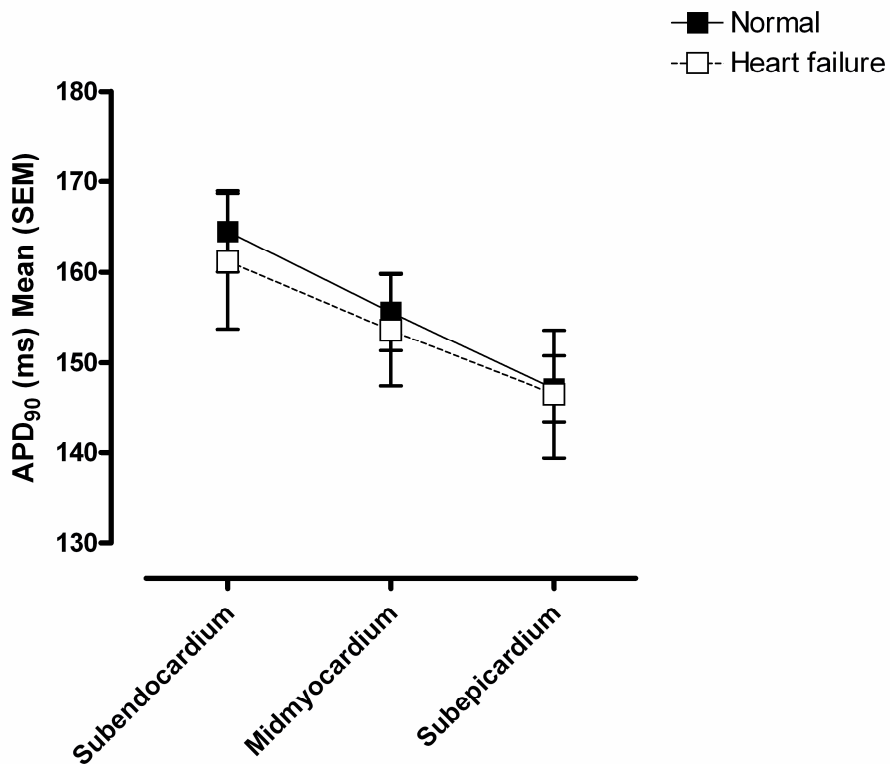


Figure 5.2 The transmural pattern of APD_{90} in normal and failing hearts

Transmural patterns of APD_{90} in failing (open squares, $n = 7$) and normal hearts (closed squares, $n = 8$). One-way ANOVA, $p > 0.05$.

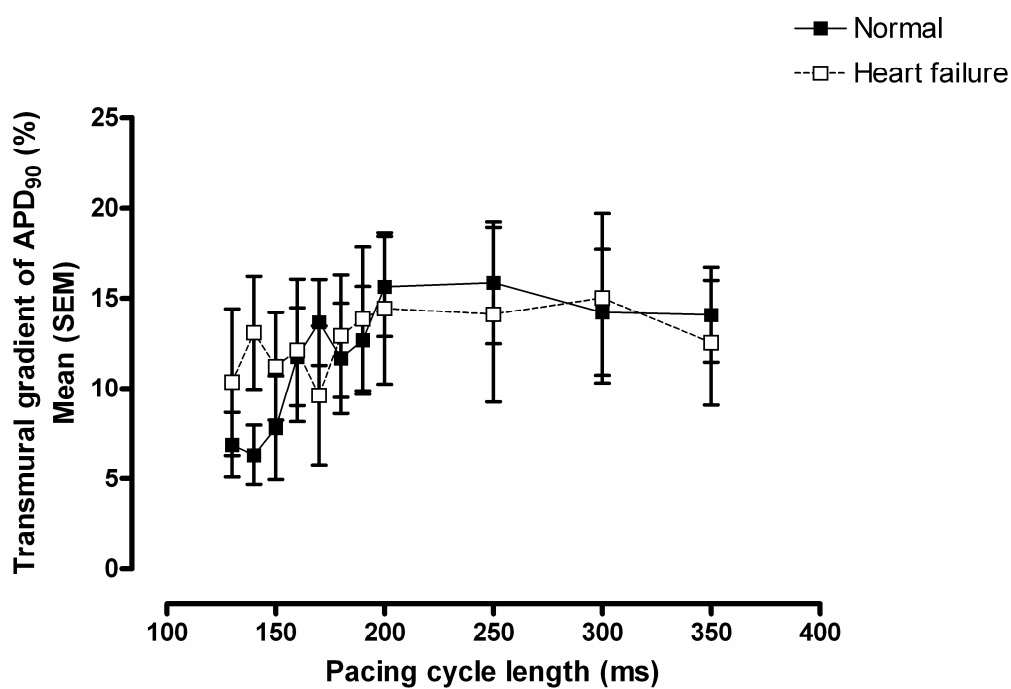


Figure 5.3 Transmural APD_{90} gradient during rapid stimulation in normal and failing hearts

Transmural gradients of APD_{90} , expressed as a percentage of subendocardial APD_{90} as a function of pacing CL. One-way ANOVA, $p > 0.05$.

APD₉₀ restitution in heart failure

The mean data for transmural APD₉₀ restitution during endocardial stimulation at 37°C in normal and failing hearts are shown in Figure 5.4. The insets show the slope of the APD₉₀ restitution curve as a function of pacing CL and the maximal APD₉₀ restitution slope.

There were no differences in APD₉₀ restitution between normal and failing hearts, either in terms of the maximum value (Y_{\max} , $144.1 \pm 3.7\text{ms}$ vs. $145.9 \pm 3.7\text{ms}$ respectively, $p = 0.7376$), the rate constant of the curve (K , 0.02197 ± 0.00134 vs. 0.02057 ± 0.00128 respectively, $p = 0.4669$) or the maximal restitution slope ($1.17 \pm 0.08\text{ms/ms}$ vs. $1.03 \pm 0.04\text{ms/ms}$ respectively, $p = 0.1588$).

Transmural APD₉₀ restitution curves for subendocardium, midmyocardium and subepicardium in failing hearts at 37°C are shown in Figure 5.5. The Y_{\max} value of the curve was greatest in the subendocardium ($162.2 \pm 4.8\text{ms}$) with smaller values at the midmyocardium ($148.9 \pm 2.7\text{ms}$, $p > 0.05$ vs. subendocardium) and subepicardium ($139.6 \pm 5.3\text{ms}$, $p > 0.05$ vs. midmyocardium, $p < 0.01$ vs. subendocardium), reflecting the previously described transmural gradients of APD₉₀. There were no significant differences between the rate constants of the APD₉₀ restitution curves across the transmural surface (subendocardium, 0.0209 ± 0.0014 , midmyocardium 0.0193 ± 0.0008 and subepicardium 0.0183 ± 0.0016 , $p > 0.05$). The maximal APD₉₀ restitution slopes were not significantly different across the different transmural regions. The maximal slope was $1.22 \pm 0.22\text{ms/ms}$ in the subendocardium, $1.13 \pm 0.12\text{ms/ms}$ in the midmyocardium and $0.95 \pm 0.07\text{ms/ms}$ in the subepicardium ($p > 0.05$).

A comparison of APD₉₀ restitution curves for each individual transmural region and the corresponding plots of restitution slope against pacing CL in normal and failing hearts is shown in Figure 5.6. Table 5.4 shows the best fit values and standard errors for the Y_{\max} and rate constant for each of the monoexponential functions fitted to the APD₉₀ restitution data, along with the maximal restitution slope determined from the linear fit of the steepest part of the curve. No differences between normal and failing hearts were apparent from the restitution curves in the subendocardium, midmyocardium or subepicardium. Nor were there any significant differences in Y_{\max} , rate constants or maximal APD₉₀ restitution slope derived from the exponential curve fits in any of the transmural regions.

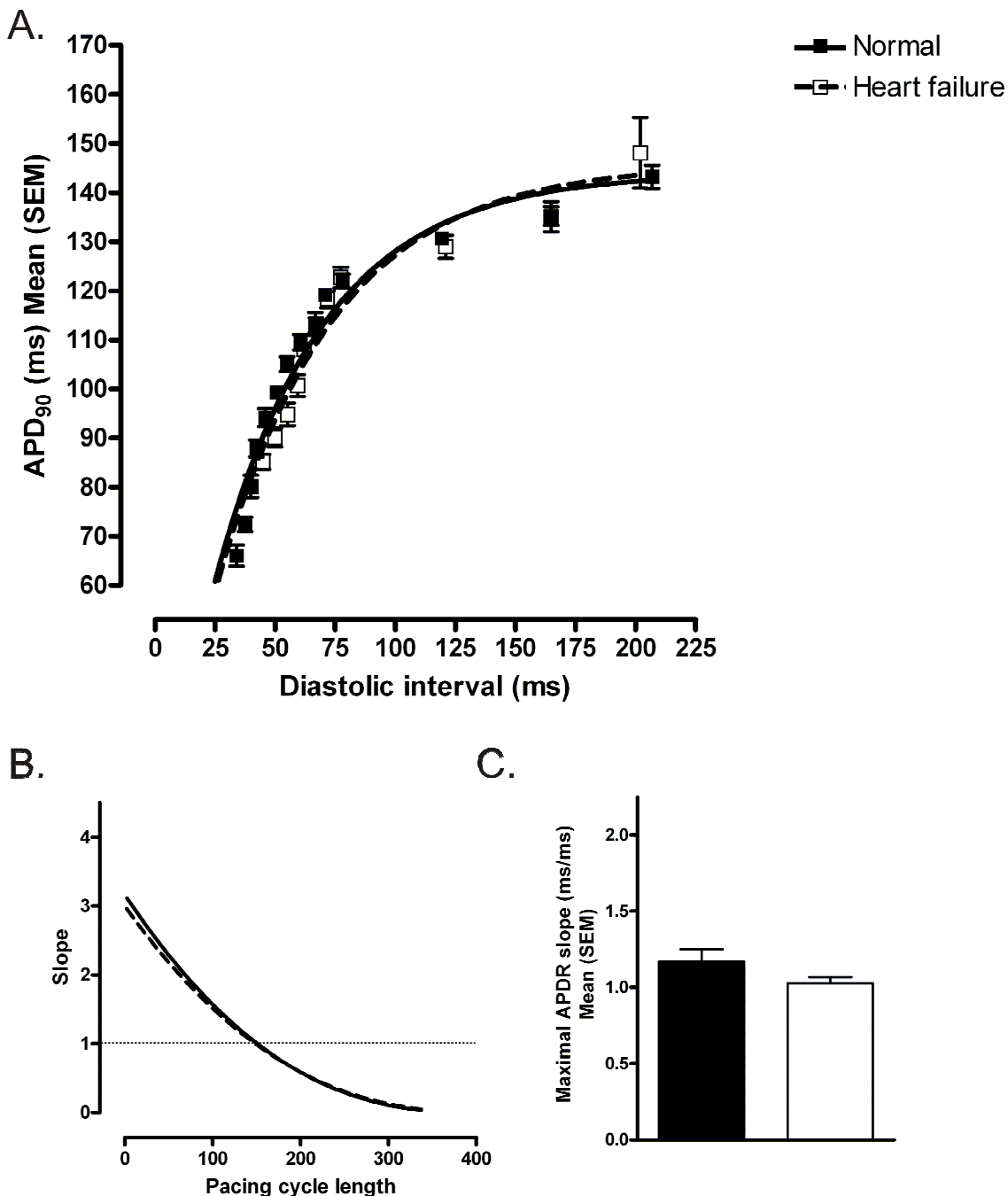


Figure 5.4 Mean APD₉₀ restitution in normal and failing hearts

A. Mean data for restitution behaviour, with corresponding exponential curve fits for normal (closed squares and solid line, $n = 8$) and failing hearts (open squares and dashed line, $n = 7$). B. The slope of each restitution curve as a function of pacing CL. The dotted line indicates the point at which the restitution slope becomes > 1 . C. The maximal slope of each APD₉₀ restitution curve generated from linear segments fitted to the five data points at the shortest DIs in the main graph. Unpaired t-test, $p > 0.05$.

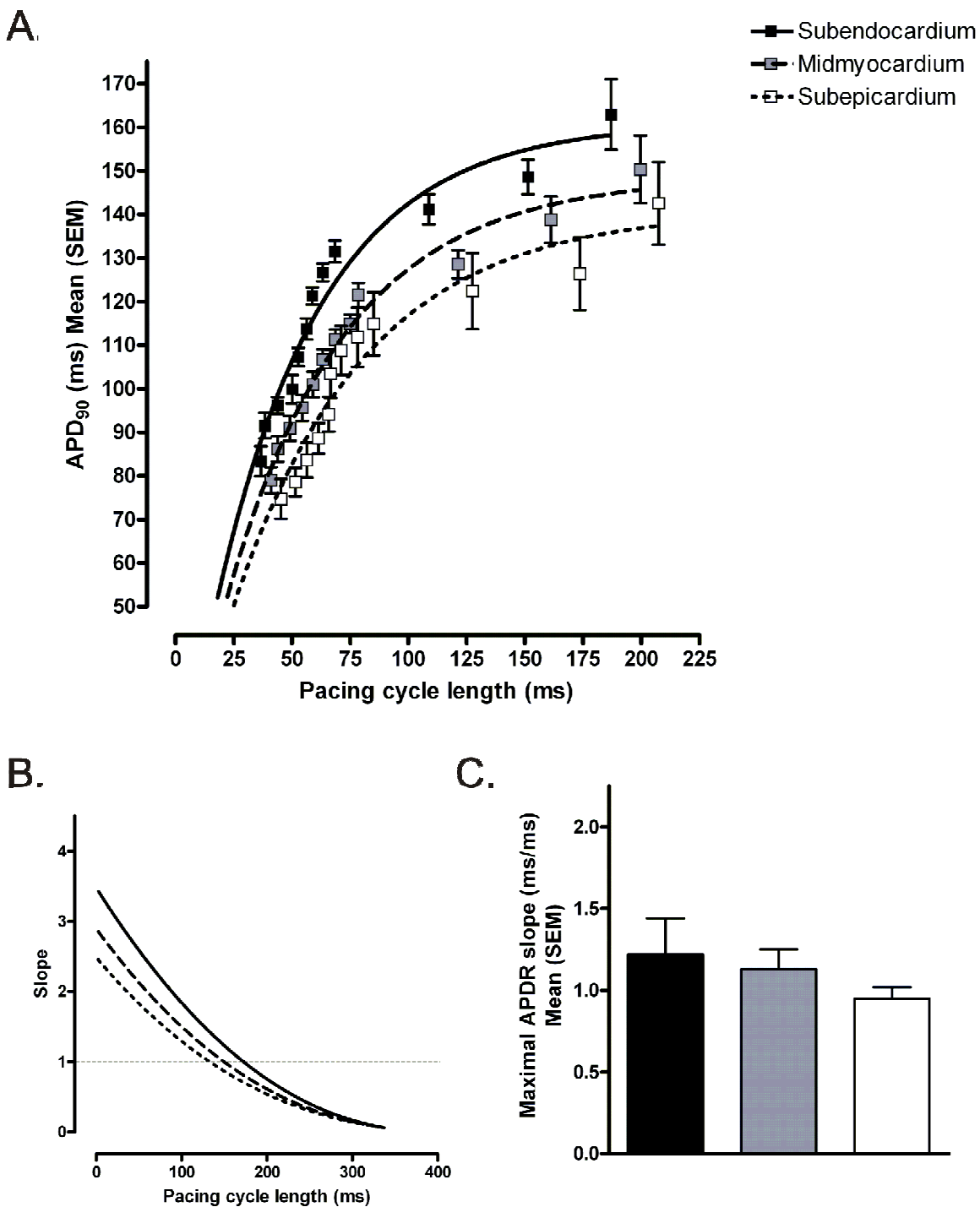


Figure 5.5 Transmural APD₉₀ restitution in failing hearts

A. Mean data for transmural APD₉₀ restitution behaviour, with corresponding exponential curve fits ($n = 7$). B. The slope of each restitution curve as a function of pacing CL. The dotted line indicates the point at which the restitution slope becomes > 1 . C. The maximal slope of each APD₉₀ restitution curve generated from linear segments fitted to the five data points at the shortest DIs in the main graph. One-way ANOVA, $p > 0.05$.

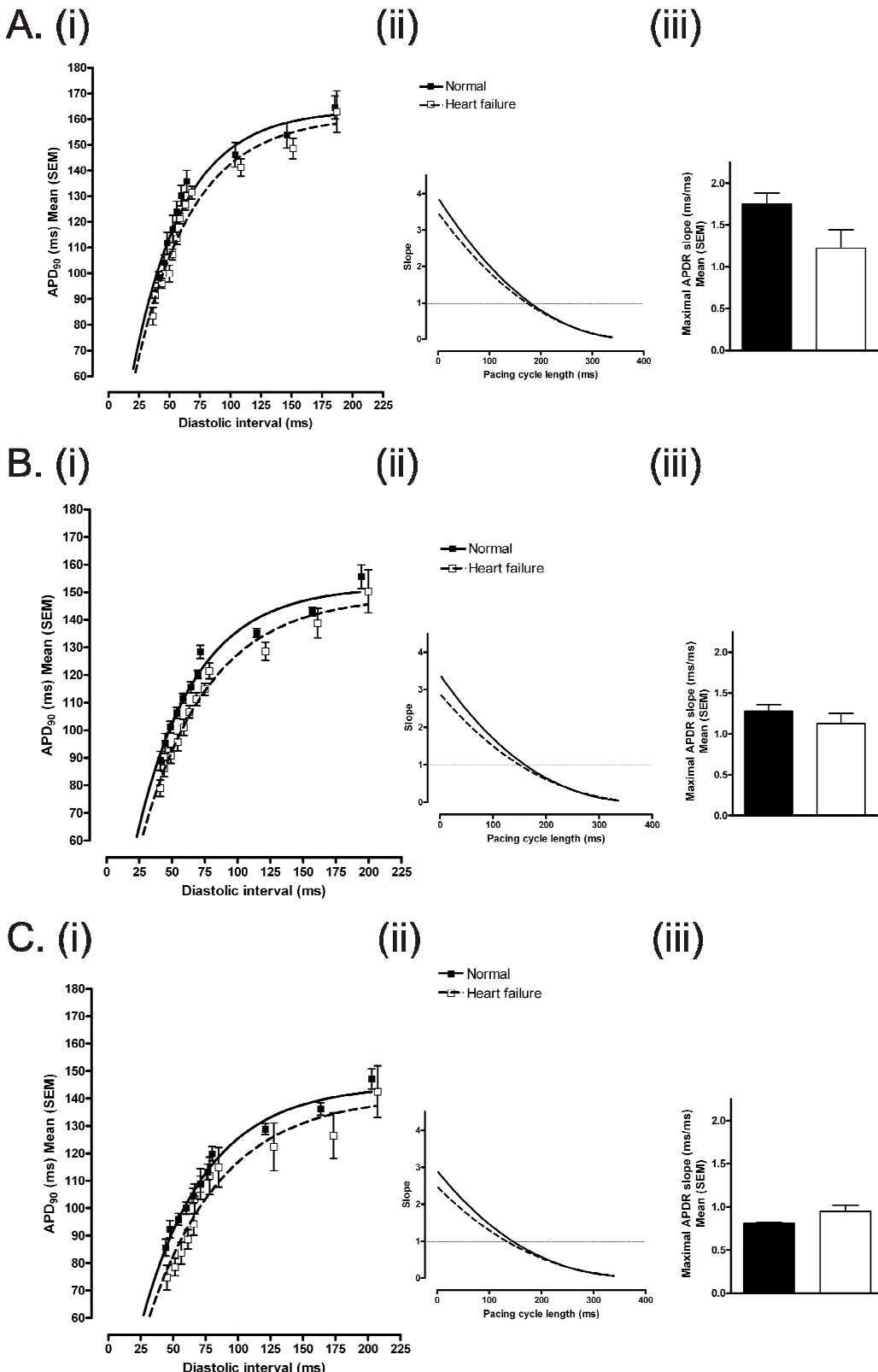


Figure 5.6 Transmural APD₉₀ restitution curves in normal and failing hearts

A. subendocardial, B. midmyocardial and C. subepicardial restitution. (i) Mean data with corresponding exponential curve fits for normal (closed squares and solid line, $n = 8$) and failing hearts (open squares and dashed line, $n = 7$). (ii) The slope of each restitution curve as a function of pacing CL. The dotted line indicates the point at which the restitution slope becomes > 1 . (iii) The maximal slope of each APD₉₀ restitution curve generated from linear segments fitted to the five data points at the shortest DIs in the main graph. Unpaired t-test, $p > 0.05$ in each case.

Table 5.4 Transmural APD₉₀ restitution curve characteristics in normal and heart failure

Mean (SEM)	Normal (n = 8)	Heart failure (n = 7)	P value
Y _{max} (ms)			
Mean	144.1 ± 3.7	145.9 ± 3.7	0.7376
Subendocardium	163.7 ± 3.9	162.2 ± 4.8	0.8103
Midmyocardium	152.1 ± 3.0	148.9 ± 2.7	0.4475
Subepicardium	144.9 ± 2.4	139.6 ± 5.3	0.3582
Rate constant, K			
Mean	0.0220 ± 0.0013	0.0206 ± 0.0013	0.4669
Subendocardium	0.0237 ± 0.0014	0.0209 ± 0.0014	0.1827
Midmyocardium	0.0224 ± 0.0011	0.0193 ± 0.0008	0.1543
Subepicardium	0.0201 ± 0.0008	0.0183 ± 0.0016	0.3140
Maximal slope (ms/ms)			
Mean	1.17 ± 0.08	1.03 ± 0.04	0.1588
Subendocardium	1.75 ± 0.13	1.22 ± 0.22	0.0522
Midmyocardium	1.28 ± 0.08	1.13 ± 0.12	0.3064
Subepicardium	0.81 ± 0.01	0.95 ± 0.07	0.0537

ms = milliseconds, SEM = standard error of the mean. P value refers to an unpaired t-test.

Transmural electrophysiology in heart failure at low temperature

The effect of low temperature on baseline transmural electrophysiology in failing hearts is detailed in Table 5.5. During endocardial stimulation at a pacing CL of 350ms, a reduction in temperature from 37°C to 30°C resulted in a 24% reduction in transmural conduction velocity. At low temperature, APD₉₀ was increased across all transmural regions compared with physiological temperature. Transmural dispersion of activation time, repolarisation time and APD₉₀ in failing hearts were not significantly altered at low temperature. The comparison between heart failure and control at low temperature, shown in Table 5.6 was qualitatively similar to that at physiological temperature (see Table 5.3). Neither transmural conduction velocity, transmural APD₉₀ nor transmural dispersion of activation time, repolarisation time or APD₉₀ was significantly different in failing, as compared to normal hearts, at low temperature.

Table 5.5 The effect of temperature on transmural electrophysiology in heart failure

Mean (SEM)	37°C (n = 7)	30°C (n = 7)	Relative change	P value
Transmural conduction velocity (cm/sec)	29.5 ± 1.8	22.5 ± 2.6	- 24%	0.047
Transmural APD ₉₀ (ms)				
Subendocardial APD ₉₀	158.0 ± 6.2	177.1 ± 6.2	+ 12%	< 0.05
Midmyocardial APD ₉₀	152.3 ± 4.2	166.5 ± 7.4	+ 9%	< 0.05
Subepicardial APD ₉₀	142.5 ± 3.2	163.8 ± 7.0	+ 15%	< 0.05
Transmural dispersion (ms/mm ²)				
Activation time	0.41 ± 0.06	0.51 ± 0.05	-	0.2246
Repolarisation time	1.80 ± 0.18	1.33 ± 0.32	-	0.2247
APD ₉₀	1.26 ± 0.30	1.14 ± 0.27	-	0.7713

APD₉₀ = action potential duration at 90% repolarisation, cm/sec = centimetres per second, ms = milliseconds, ms/mm² = milliseconds per square millimetre, SEM = standard error of the mean. P value refers to an unpaired t-test for CV and dispersion and to a one-way ANOVA for APD₉₀.

Table 5.6 Transmural electrophysiology at low temperature in normal and failing hearts

Mean (SEM)	Normal (n = 9)	Heart failure (n = 7)	P value
Transmural conduction velocity (cm/sec)	22.0 ± 1.5	22.5 ± 2.6	0.8630
Transmural APD ₉₀ (ms)			
Subendocardial APD ₉₀	186.2 ± 3.6	177.1 ± 6.2	> 0.05
Midmyocardial APD ₉₀	176.1 ± 3.8	166.5 ± 7.4	> 0.05
Subepicardial APD ₉₀	169.4 ± 5.0	163.8 ± 7.0	> 0.05
Transmural dispersion (ms/mm ²)			
Activation time	0.54 ± 0.08	0.51 ± 0.05	0.7715
Repolarisation time	0.86 ± 0.23	1.33 ± 0.32	0.2406
APD ₉₀	0.80 ± 0.27	1.14 ± 0.27	0.3960

APD₉₀ = action potential duration at 90% repolarisation, cm/sec = centimetres per second, ms = milliseconds, ms/mm² = milliseconds per square millimetre, SEM = standard error of the mean. P value refers to an unpaired t-test for CV and dispersion and a one-way ANOVA for APD₉₀.

APD₉₀ restitution at low temperature

A comparison of APD₉₀ restitution curves at 30°C and 37°C, along with the corresponding plots of restitution slope against CL and maximal APD₉₀ restitution slope is given in Figure 5.7A. As noted previously, APD₉₀ at baseline was significantly longer at 30°C than 37°C, and this remained true across all CLs tested. This is reflected in the higher Y_{max} of the curve fitted to the 30°C APD₉₀ restitution data compared to the corresponding value for the 37°C data (171.1 ± 3.6 vs. 145.9 ± 3.7ms, p = 0.0004). However, the rate constant of the exponential function fitted to the APD₉₀ restitution data at 30°C was not different to that at 37°C (0.0226 ± 0.0012 vs. 0.0206 ± 0.0013 respectively, p = 0.2804). The maximal APD₉₀ restitution slope was greater in failing hearts at low temperature (1.63 ± 0.21ms/ms) when compared with 37°C (1.03 ± 0.04ms/ms, p = 0.0158). At 30°C there were no significant differences in APD₉₀ restitution characteristics between normal and failing hearts (Figure 5.7B).

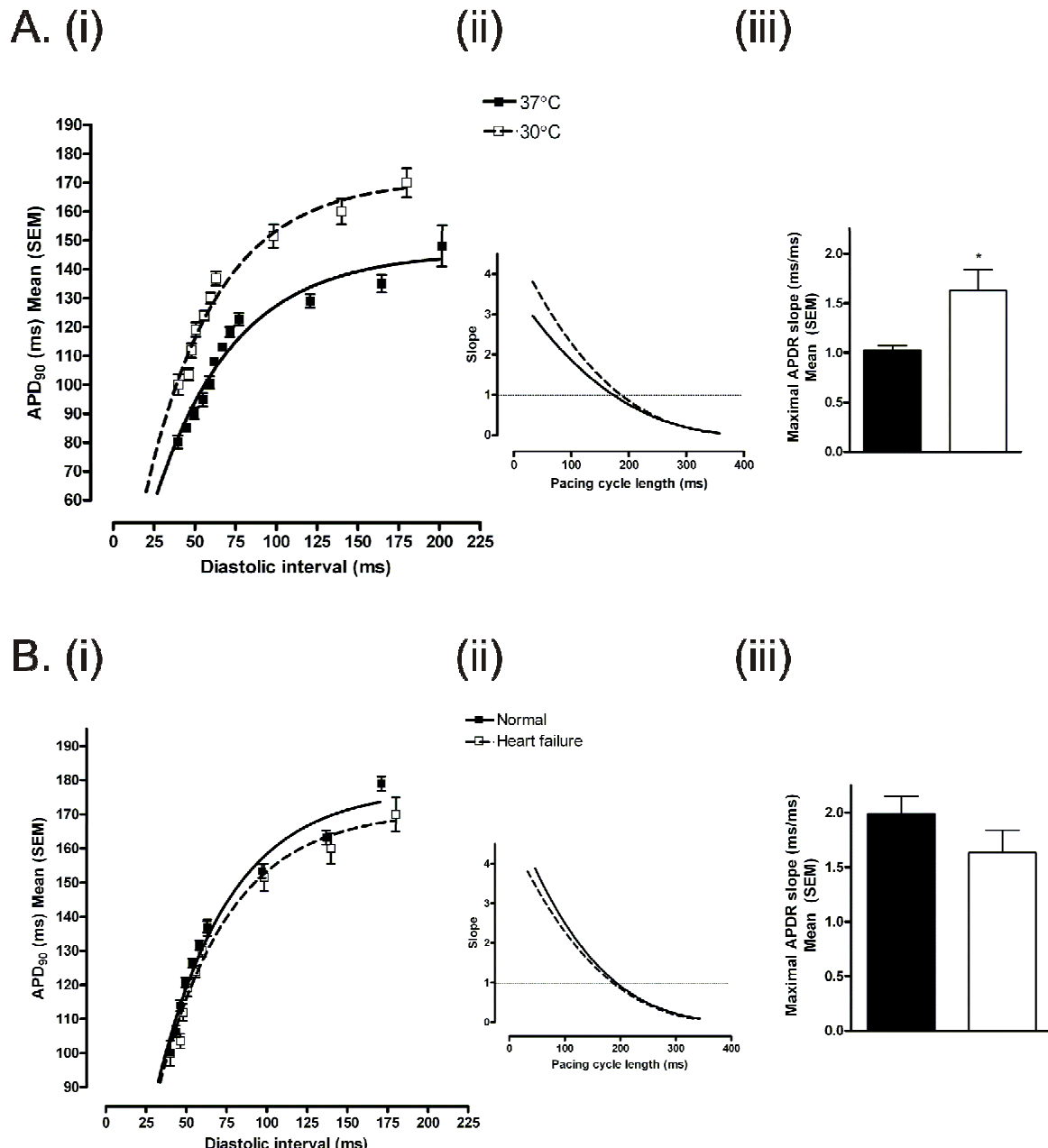


Figure 5.7 The temperature dependence of APD₉₀ restitution in heart failure

A. (i) Mean data for restitution in failing hearts, with exponential curve fits for data at 37°C (closed squares and solid line, $n = 7$) and at 30°C (open squares and dashed line, $n = 7$). (ii) The slope of each restitution curve as a function of CL. The dotted line indicates the point at which the restitution slope becomes > 1 . (iii) The maximal slope of each APD₉₀ restitution curve generated from linear segments fitted to the five data points at the shortest DIs in the main graph. Unpaired t-test, * $p < 0.05$. B. (i) Mean data for restitution behaviour at 30°C, with corresponding exponential curve fits for data in normal (closed squares and solid line, $n = 9$) and failing hearts (open squares and dashed line, $n = 7$). (ii) The slope of each restitution curve as a function of CL. The dotted line indicates the point at which the restitution slope becomes > 1 . (iii) The maximal slope of each APD₉₀ restitution curve generated from linear segments fitted to the five data points at the shortest DIs in the main graph. Unpaired t-test, $p > 0.05$.

Transmural conduction into the infarct

Transmural conduction from non-infarcted myocardium, through the border zone and into the infarct was recorded during baseline pacing in a subgroup of five ligated hearts.

Discernible APs were recorded from the infarcted myocardium in all hearts. Table 5.7 shows a comparison of AP characteristics for the remodelled myocardium remote from the infarct (remote zone), the infarct border zone and the infarct itself. All APs were sampled from the midmyocardium. Signal to noise ratio was significantly lower in both the infarct border zone and in the infarcted myocardium than in the remote zone. AP amplitude was also significantly lower, both in the border zone and in the infarct, when compared with APs recorded in the remote zone. AP rise time was significantly greater in the infarct zone, and there was a trend towards an increased rise time in the border zone, although this did not reach statistical significance. There was no difference in APD₉₀ for signals recorded in the border zone or infarct zone when compared with signals in the remote zone.

Conduction into the infarct during endocardial and epicardial stimulation was compared in all 5 hearts. An example of the results is shown in Figure 5.8. During endocardial stimulation, the presence of the infarct border zone was not apparent from the voltage signals, and the spread of activation progressed smoothly into the infarcted myocardium, without any apparent conduction delay. During epicardial stimulation, conduction into the infarct was significantly slowed compared to endocardial stimulation, and the delay was located at the infarct border zone. During epicardial stimulation, the transmural dispersion of activation time was significantly greater than during endocardial stimulation (1.0 ± 0.3 vs. $1.8 \pm 0.5\text{ms/mm}^2$; $n = 5$, paired t-test, $p = 0.0408$). Conduction velocity into the infarct was significantly slower during epicardial stimulation than during endocardial stimulation (37.3 ± 6.7 vs. $76.6 \pm 17.2\text{cm/sec}$; $n = 5$, paired t-test, $p = 0.0239$).

Table 5.7 Action potential characteristics in the border zone and infarct zone

Mean (SEM)	Remote zone	Border zone	Infarct zone
Signal to noise ratio	22.0 ± 2.3	$10.4 \pm 1.7^{***}$	$5.6 \pm 0.5^{***}$
AP amplitude	605.0 ± 86.9	$243.0 \pm 52.5^{**}$	$104.3 \pm 14.9^{***}$
Rise time (ms)	14.4 ± 1.4	23.9 ± 3.8	$27.9 \pm 2.2^{**}$
APD ₉₀ (ms)	144.9 ± 2.9	139.9 ± 2.6	125.9 ± 11.2

AP = action potential, APD₉₀ = action potential duration at 90% repolarisation, ms = milliseconds, SEM = standard error of the mean. $n = 5$, one-way ANOVA, ** $p < 0.01$ vs. normal zone, *** $p < 0.001$ vs. normal zone.

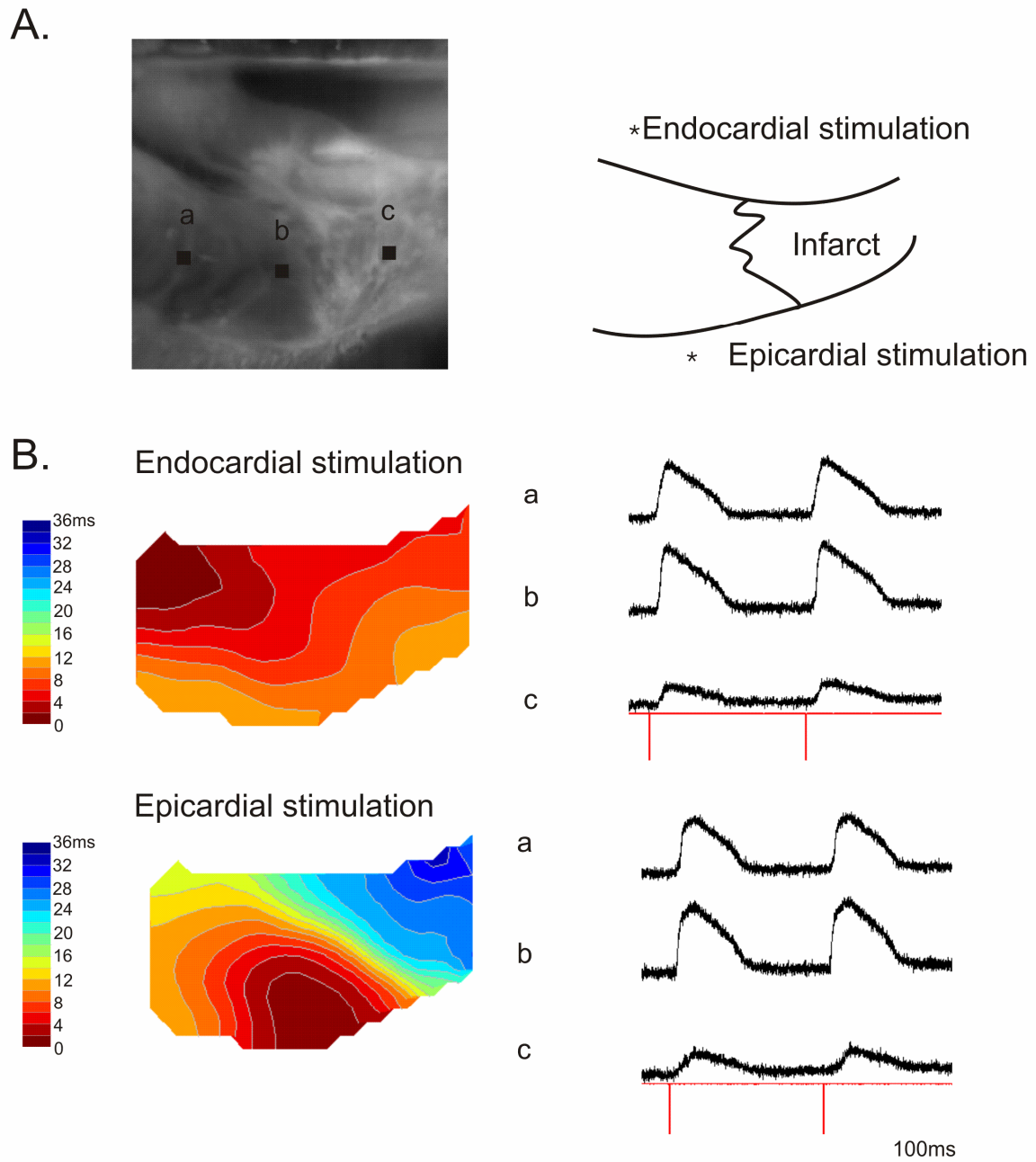


Figure 5.8 Transmural conduction into the infarct

An example of transmural conduction into the infarct during endocardial and epicardial stimulation at a CL of 350ms. A. The upper left panel shows a plain image of the transmural surface of a wedge preparation from a ligated heart, with the endocardium uppermost and the epicardium at the bottom of the picture. The black squares indicate the position from which example APs are shown: a) remote zone b) border zone and c) infarct zone. In the upper right panel is a diagram of the preparation, indicating the position of the infarct border zone and the two pairs of stimulating electrodes (*). B. The upper panel shows isochronal maps of activation during endocardial stimulation along with AP traces from each of the three areas. Corresponding isochrones during epicardial stimulation are shown below. The delay is evident in the action potential traces and can also be seen as a crowding of the isochronal lines.

Discussion

Characterisation of a heart failure syndrome following coronary ligation in the rabbit

Human heart failure is a complex clinical syndrome, and as such may consist of a combination of heterogeneous signs and symptoms. This means that heart failure is difficult to recapitulate accurately using experimental models. The current study has used a rabbit model of heart failure following coronary arterial ligation. As coronary heart disease is the leading cause of heart failure in humans, this model has the benefit of being clinically relevant. Most commonly used animal models of heart failure employ either rapid pacing¹⁴⁶ or combinations of pressure and volume overload¹⁹⁰ to induce heart failure. Pacing-induced heart failure produces thinning of the LV wall¹⁴⁶ rather than LV hypertrophy which is characteristic of most human heart failure. Moreover, the LV remodelling and haemodynamic abnormalities in experimental pacing induced heart failure are quickly reversible on cessation of pacing²⁰⁶. This suggests a different underlying pathophysiological abnormality to human heart failure. The coronary arterial ligation model used in the present study has been extensively characterised elsewhere¹³⁵⁻¹³⁷. The data presented in this Chapter describe a similar degree of LV remodelling associated with heart failure, principally a 38% reduction in LVEF, and a 18% increase in LVEDD. In contrast to prior published work, the ligated animals in the current study displayed a reduction in LA diameter associated with heart failure. Although statistically significant, the magnitude of the observed reduction (~1mm) was such that it is unlikely to be biologically significant. However, the previously observed increase in LA diameter with heart failure following coronary ligation was not reproduced in these animals, suggesting that significant structural atrial remodelling did not occur as a result of heart failure in these animals. The reason for this discrepancy is unclear, but it is unlikely to have a major impact on the results presented, as only ventricular electrophysiology was studied.

The LV wedge preparation in ligated hearts

Viability

Consideration of the viability of the cut surface is central to all experiments performed on ventricular wedge preparations. Although wedge preparations have been successfully studied in pacing-induced heart failure¹⁴⁶, there are no published records of wedge preparations in ventricular myocardium following experimental MI. Arguably, cut surface perfusion may be more likely to be marginal in a ligated heart than in a normal heart. As discussed in previous Chapters, marginal perfusion would be expected to reduce CV,

shorten APD and change AP shape. The transmural conduction times reported here are similar to those recorded by Walker *et al* in Langendorff perfused ligated rabbit hearts ($14.8 \pm 2.5\text{ms}$). This argues against any conduction slowing due to marginal perfusion in the ligated wedge preparations studied here. Transmural conduction velocities were not significantly different between normal and failing hearts, nor were differences in AP shape or APD₉₀ apparent in wedges from failing hearts. Overall, the results suggest that LV wedge perfusion is not compromised by the presence of an 8 week apical infarct.

Tissue dimensions

There is evidence that propensity to ventricular fibrillation is related to tissue bulk²⁰⁷. In this study, there was no significant difference in LV wedge dimensions or weight between normal and failing hearts. This removes a potential confounder from the comparison of the VF inducibility in normal and failing hearts, discussed in Chapter 7.

Transmural electrophysiological heterogeneity in heart failure

Conduction velocity

There was no difference in baseline transmural conduction velocity in the non-infarcted myocardium of failing hearts when compared with normal hearts. This result is in agreement with previously published data from this heart failure model¹⁰⁹ and from experiments on failing rabbit hearts following pressure-volume overload²⁰⁸. However, an increase in the spatial heterogeneity of transmural conduction velocity has been demonstrated in pressure-volume overload heart failure¹⁹⁰. Similarly, localised conduction slowing at a CL of 2000ms has been identified in the subepicardial layers of canine hearts following the induction of heart failure by rapid pacing²⁰⁹. In both studies, localised conduction slowing was attributed to spatial heterogeneities in Cx43 expression, and implicated in the genesis of re-entrant ventricular arrhythmias. However, the nature of the change in Cx43 expression was not concordant between these studies. The failing canine ventricle displayed reduced Cx43 in the subepicardium, while the rabbit myocardium displayed a reduction in midmyocardial Cx43. These differences may be attributable to species differences, the different methods of heart failure induction, or indeed to differences in the measurement techniques employed. The CV measurements were performed on a much smaller scale than those in the current study, which describe only total transmural CV and so would only be expected to detect gross changes in CV. However, there were no differences found in transmural dispersion of activation time, consistent with the fact that transmural conduction velocity was not altered in heart failure

at baseline cycle lengths. It remains possible that localised changes in CV occurred as a consequence of heart failure in this model.

Transmural APD₉₀ in heart failure

In the current study, no difference was found in APD₉₀ between normal and failing hearts. A number of studies have identified prolongation of APD in heart failure; these have either been in isolated myocytes^{130;134} or in intact myocardium at slow stimulation rates^{131;146;184}. The data presented in this Chapter were recorded in intact myocardium at physiologically relevant pacing cycle lengths. This may explain the apparently discrepant results, particularly in light of the data presented in earlier Chapters, which underlines the importance of electrotonic coupling in modulating APD₉₀ in intact myocardium. These data challenge the physiological relevance of the APD prolongation in heart failure seen at very slow stimulation rates. Species differences may also be a factor in the disparity in these results. M cells typically display marked APD prolongation in pathological states, including heart failure, and M cell density varies between species. Therefore, canine ventricle, which has a prominent M cell layer may be expected to show relatively greater APD prolongation in heart failure as compared with species such as human or rabbit, in which M cell density is lower. As discussed in Chapter 3, a proportion of midmyocardial cells isolated from the midmyocardium and subendocardium of rabbit hearts do display M cell behaviour, and have been shown to display marked APD prolongation in the same rabbit model of heart failure as used in the current study, albeit at slow stimulation rates¹³⁴. In isolated failing rabbit myocytes from the pressure-volume overload model, no difference in intrinsic isolated cell APD was found at physiological stimulation rates¹⁹⁰. This, together with the lack of APD prolongation in the intact LV wedge observed in the current study, tends to suggest that preferential M cell remodelling, as has been observed in canine¹⁴⁶ is not apparent to any significant degree in intact failing rabbit ventricular myocardium. In humans, methodological constraints mean that APD is usually estimated from the ARI of unipolar electrograms recorded from discrete sites on the RV endocardium during programmed electrical stimulation. Data from such *in vivo* human studies has shown no difference in APD between patients with heart failure and controls¹²².

Transmural dispersion of repolarisation and APD₉₀ in heart failure

Transmural dispersion of repolarisation and APD₉₀ at a baseline pacing cycle length of 350ms was not altered in heart failure. Transmural dispersion of repolarisation and APD₉₀ were calculated using the 5-95% range of time at 90% repolarisation and APD₉₀

respectively. Each value was then expressed per square millimetre, to ensure that any differences in the transmural area between preparations did not affect the result. Significant interheart variability remained in the dispersion measurements. Consequently, anything other than large differences in dispersion between normal and failing hearts are likely to have been obscured. In order to ensure that the dispersion result was robust, the APD₉₀ heterogeneity index (5-95% range of APD₉₀ / median APD₉₀) was also calculated, and was not different between normal and failing hearts at either 37°C or 30°C (data not shown).

APD₉₀ restitution in failing hearts

APD₉₀ restitution was unchanged in heart failure. This remained the case whether APD₉₀ was calculated from the mean of all transmural pixels, or from discrete selections in the subendocardium, midmyocardium and subepicardium. A detailed analysis of the restitution data was undertaken. Monoexponential curve fits were performed, which were then differentiated to produce a plot of their slope across the range of CLs. This revealed no difference between normal and failing hearts in terms of APD₉₀ restitution. In one study which examined the effect of heart failure on APD restitution in humans, the maximal APD₉₀ restitution slope in patients with heart failure (1.23 ± 0.60) was comparable to that recorded in those with normal hearts (1.27 ± 0.55 , p = NS)¹²². Restitution data recorded from human studies is usually quantified by fitting least squared linear functions in overlapping segments²¹⁰. The linear segments method is considered preferable to fitting monoexponentials as it goes some way to avoiding error generated by over or under-fitting the data. For this reason, the linear least squared method was also used to calculate the maximal restitution slope in each case. No difference was found in the maximal restitution slope between normal and failing hearts.

Other experimental studies which have measured APD restitution behaviour during S1-S2 protocols have found steeper APD restitution in failing canine hearts, using both optical mapping in LV wedge preparations¹⁴⁶ and ARI recordings during open chest experiments²¹¹. In both studies the CLs studies were longer than those used in the current study. The current experiments employed dynamic restitution protocols at relatively short pacing cycle lengths (i.e. close to physiological rates). Dynamic, rather than S1-S2 pacing protocols were chosen because the data would better reflect the dynamic changes produced during the induction of repolarisation alternans.

Transmural electrophysiology in heart failure at low temperature

Low temperature is commonly used to elicit repolarisation alternans in experimental studies. As described in Chapter 3, a number of electrophysiological processes are altered at low temperature, and it was therefore important to establish whether any of these were differentially modulated in heart failure. The electrophysiological measurements made in failing hearts at 37°C were all repeated at 30°C. The nature and magnitude of the changes seen with low temperature in heart failure were similar to those observed in normal hearts, as detailed in Chapter 3. Transmural CV was reduced by around 24%, similar to the 27% reduction in conduction velocity seen in normal hearts. APD₉₀ was prolonged by 12% in the subendocardium, 9% in the midmyocardium and 15% in the subepicardium, as compared with values of 13%, 13% and 15% respectively in normal hearts. There were no changes in dispersion of repolarisation or APD₉₀ with low temperature, again in keeping with the results from normal myocardium. Similarly, the maximal APD₉₀ restitution slope was steeper at low temperature than at physiological temperature in failing hearts. These results suggest that similar electrophysiological changes occur between physiological and low temperature in normal and failing ventricular myocardium. The knowledge that baseline electrophysiology is not differentially modulated by low temperature in normal and failing hearts removes an important potential confounder for the investigation of repolarisation alternans in heart failure.

Conduction into the infarct zone

This study has made direct recordings from the transmural surface of wedge preparations from hearts which had undergone coronary arterial ligation to produce an apical MI. This allowed imaging of voltage signals conducting from the non-infarcted myocardium, through the infarct border zone and into the infarct itself. The voltage signals recorded from the infarct zone were smaller, with an amplitude of ~17% of that found in the remote myocardium, and had a lower signal-to-noise ratio (~25% of remote zone). These differences are likely to reflect the relatively smaller number of cells contributing to the signal in the infarct zone. There is also likely to be less penetration of the voltage-sensitive dye into the infarct zone. The AP rise time was significantly increased in the infarct zone: approximately double that found in the remote zone. The rise time of an optical AP represents the summation of all the cellular AP upstrokes which are included in the pixel area, and as such it represents a spatially averaged voltage signal. Under normal circumstances, an optical AP rise time is of the order of 10ms, compared with that recorded in isolated cells, which are of the order of 1-2ms. Individual surviving myocytes

within the infarct may have relatively normal AP upstrokes, but when these are separated by fibroblasts then intercellular propagation of the impulse is likely to be slower, resulting in an increase in rise time in the spatially averaged optical AP. Although APs were smaller and noisier, the measured APD_{90} in the infarct was not significantly different from those found in the myocardium remote from the infarct.

When endocardial and epicardial pacing were compared, a conduction delay at the infarct border zone was identified during epicardial, but not endocardial pacing. This result is in agreement with published work from our group in which optical APs were recorded from the epicardial surface of Langendorff-perfused ligated rabbit hearts. Walker *et al* were able to record low amplitude voltage signals from the epicardial surface of the infarct zone, and identified that a conduction delay at the infarct border zone only occurred during epicardial stimulation, in contrast to right atrial or endocardial stimulation¹⁰⁹. The pathophysiological basis for this observation is not clear, but a potential explanation is illustrated in Figure 5.9. This hypothesis relies on an interaction between the demonstrated transmural differences in infarct structure discussed earlier and the different transmural activation patterns described in Chapter 3. During endocardial stimulation, a combination of the planar wavefront and the rim of surviving myocytes at the endocardium, allows smooth propagation into the infarcted tissue. However, in the case of epicardial stimulation, the curved activation wavefront first meets the infarct border zone in the subepicardial region, where no surviving rim of myocytes exists and so encounters a delay before being conducted into the infarct. The relative contribution of each of these factors to the border zone delay observed during epicardial stimulation has not been investigated. A number of exploratory experiments were tried to investigate this phenomenon further, but were technically unsuccessful. A number of different mesh and planar stimulating electrodes were made from platinum wire, in an attempt to produce a planar epi-endo activation sequence. However, synchronous activation of the epicardial surface proved technically extremely difficult and, with each wire designed, a curved epi-endo activation sequence persisted. In addition, careful cautery was attempted to ablate the endocardial surface to produce a curved activation front, but due to the convoluted structure of the endocardial surface, this too was unsuccessful. Similar problems were encountered during the attempted ablation of the surviving endocardial rim of the infarct. Given that this surviving rim was not visible to the naked eye, it was not possible to tell whether changes in conduction were accounted for by successful ablation of this region, or by cautery damage to other parts of the myocardium.



Figure 5.9 Rationale for the border zone delay during epicardial stimulation

During endocardial stimulation, a combination of the planar wavefront and the surviving endocardial rim of myocytes, allows smooth propagation into the infarct. In the case of epicardial stimulation, the curved activation wavefront encounters a delay at the infarct border zone, where no surviving rim of myocytes exists.

Limitations

This work has examined a rabbit model of heart failure and although this model has many important similarities to human heart failure, care must be taken in extrapolating these data to human heart failure. Firstly, there are no data regarding the occurrence of spontaneous ventricular arrhythmias in these animals. The conclusion that heart failure predisposes to ventricular arrhythmia in this animal model is based on the increased occurrence of inducible arrhythmias. This is valid in the experimental situation in so far as it is not practical to study the circumstances surrounding spontaneous arrhythmia. In terms of clinical relevance, the occurrence of inducible ventricular arrhythmias in man is associated with the risk of spontaneous ventricular arrhythmia and sudden cardiac death, although the sensitivity and specificity of this technique for predicting spontaneous arrhythmias is not perfect³¹. Secondly, there is much clinical and experimental evidence to suggest that autonomic influences are important in the pathophysiology of arrhythmic sudden cardiac death in heart failure and these experiments were performed in the absence of autonomic stimulation. Finally, as recordings at slow stimulation rates were not made, it remains unclear whether transmural APD differences at slow stimulation rates, as have been reported in other species and preparations may occur in this preparation.

Conclusions

These experiments have examined the transmural electrophysiological changes occurring as a consequence of heart failure secondary to myocardial infarction in intact rabbit ventricular myocardium. The overall conclusion is that this type of experimental heart failure produces few measurable electrophysiological changes at baseline. At physiological temperature and pacing cycle lengths, no significant differences in transmural conduction velocity or APD₉₀ were seen as a result of heart failure. These are extremely important findings as they challenge the relevance of differences detected under less physiological experimental circumstances. Heart failure was not associated with any increases in transmural dispersion of repolarisation at baseline. APD₉₀ restitution was also unchanged in failing hearts. The nature and magnitude of the changes in transmural electrophysiology produced by low temperature did not differ between normal and ligated hearts. This removes an important potential confounder for the investigation of repolarisation alternans, which is commonly performed at low temperature. In isolation, these data provide little explanation for the documented increase in vulnerability to ventricular arrhythmia observed in failing hearts. The lack of fixed, reproducible changes in baseline electrophysiology in heart failure underlines the likely importance of dynamic factors, such as repolarisation alternans, in the induction of ventricular arrhythmias in failing hearts.

Chapter 6: Transmural repolarisation alternans in rabbit ventricular myocardium

Introduction

Alternating T-wave morphology at low heart rates is thought to indicate an increased risk of sudden arrhythmic death in a range of cardiac pathologies²¹². Alternating changes in action potential duration at rapid stimulation rates have previously been shown to be associated with T-wave alternans in experimental studies^{40;66}. At short pacing cycle lengths repolarisation alternans may become spatially discordant. During spatially discordant alternans, two adjacent areas of ventricular myocardium alternate with opposite phase. This situation is thought to be associated with extreme gradients of repolarisation, which may predispose to unidirectional conduction block, thereby facilitating re-entrant excitation⁴⁰. This provides a potential mechanistic link between cardiac alternans and re-entrant ventricular arrhythmia.

The role of gradients of repolarisation in spatially discordant alternans

The theory of discordant alternans identifies spatial heterogeneity of alternans as the link to ventricular arrhythmia. In the guinea pig model, spatial patterns of alternans were consistently orientated in an apex-base direction^{40;77}, independent of pacing site, as are gradients of repolarisation and restitution in this species⁹⁹. This suggests that the development of discordant alternans is related to intrinsic spatial differences in cellular repolarisation. Although in simulations homogenous cardiac tissue is capable of developing discordant alternans when conduction velocity restitution is steep⁸², it occurs more readily in the presence of tissue heterogeneity⁸¹. As discussed in Chapter 3, gradients of repolarisation also exist in the transmural axis¹⁰⁰. Transmural heterogeneity of alternans has been demonstrated in LQTS^{66;101}, and in isolated ventricular myocytes⁸⁷. Transmural heterogeneity of calcium transient alternans has also been demonstrated in a normal canine wedge preparation¹⁰⁴.

The development of spatially discordant alternans may depend upon baseline heterogeneities in repolarisation, including those spanning the ventricular wall, and significant transmural dispersion of repolarisation may be crucial in the genesis of arrhythmias associated with spatially discordant alternans. As discussed in Chapter 1, steep restitution has been implicated in the production of repolarisation alternans. Rate dependence of APD₉₀ has been reported to be steeper in the subendocardium and midmyocardium when compared to the subepicardium in normal canine¹⁶⁷ and rabbit myocardium¹³¹. In these studies rate dependence of APD₉₀ was tested using extrastimulus protocols from a slow stimulation rate down to CLs of 500ms. There are few reports of

restitution behaviour at shorter CLs, like those used to induce repolarisation alternans. In the current study, APD₉₀ restitution was examined using a dynamic protocol over a range of rapid stimulation rates (CL ≤ 350ms). The steepest APD₉₀ restitution slope was found in the subendocardium during endocardial stimulation. The relative contribution of transmural and apex-base heterogeneities to the development of discordant alternans has not been established.

Aims

To record transmural repolarisation alternans during rapid pacing in intact ventricular myocardium.

To record transmural patterns of depolarisation, repolarisation and action potential duration during alternans.

To examine the effect of activation sequence on patterns of repolarisation alternans.

To compare repolarisation alternans on the transmural and epicardial surfaces.

Methods

In order to investigate transmural alternans in intact rabbit left ventricular tissue the CCD-based optical mapping system described in Chapter 2 was used to record optical action potentials from the transmural surface of perfused left ventricular wedge preparations in the rabbit. Hearts from 14 male New Zealand White rabbits were used in these experiments, which conform to standards set out in the UK Animals (Scientific Procedures) Act, 1986.

Experimental protocols

The left ventricular wedge preparations ($n = 14$) used in this set of experiments were prepared as described in Chapter 2. Alternans experiments were initially performed at 30°C. The protocols were repeated at 37°C and during epicardial stimulation.

Data analysis

AP characteristics

Data analysis was performed as described in Chapter 2, and a separate algorithm was used to analyse alternans. This was based on the clinical MTWA algorithm and employed a spectral analysis to identify and quantify repolarisation alternans.

Statistical analysis

All data are expressed as mean \pm SEM. Groups of data were compared using a Student's t-test (paired where appropriate), or when more than two groups were compared, using a repeated measures ANOVA with *post hoc* Tukey-Kramer multiple comparisons testing performed using GraphPad software. To compare the different values at multiple sites across the transmural surface during endocardial and epicardial stimulation a two-way ANOVA in R software (www.r-project.org) was used, in which stimulation site was considered as a categorical variable and position as a continuous variable.

Results

Definition of significant alternans

The results of the spectral analysis program were validated by correlation with the change in APD₉₀ calculated by the standard analysis algorithm. The spectrally derived alternans magnitude matrices were compared with the corresponding data for change in measured APD₉₀ and also with the raw traces, in which alternating behaviour could be visually verified. This determined that a spectrally derived alternans magnitude of 2 correlated best with both a change in APD₉₀ \geq 10ms and the presence of visually apparent AP alternans in the optically recorded traces. An example of the correlation between mean change in APD₉₀ and spectrally derived alternans magnitude is shown in Figure 6.1. In hearts that did not display alternans (by spectral analysis or by visual inspection of AP traces) at a cycle length of 150ms, the measured mean change in APD₉₀ was determined for all pixels, and is shown in Figure 6.2. The measured mean change in APD₉₀ was below 10ms in the majority of the recordings (mean [SD] = 4.1 \pm 2.4ms). The ability of a spectrally derived alternans threshold \geq 2 to predict a difference in APD₉₀ of \geq 10ms was then tested across the entire dataset, as shown in Table 6.1. This shows that the prevalence of a change in APD₉₀ \geq 10ms was around 10%. The positive predictive value of the spectral value for detecting alternans was 30.7% (95% CI: 29.5 – 32.0%), with a negative predictive value of 97.9% (95% CI: 97.6 – 98.1%). The sensitivity was 82.1% (95% CI: 80.3 – 83.7%) and the specificity was 81.6% (95% CI: 81.0 – 82.1%). The definition of significant repolarisation alternans was alternans magnitude \geq 2 in \geq 10 adjacent pixels, along with visual confirmation of an alternating morphology in the AP traces.

Table 6.1 Contingency table for alternans magnitude and mean change in APD₉₀

	Change in APD ₉₀ $>$ 10ms	Change in APD ₉₀ $<$ 10ms	Total
Spectral alternans $>$ 2	1649	3718	5367
Spectral alternans $<$ 2	360	16462	16822
Total	2009	20180	22189

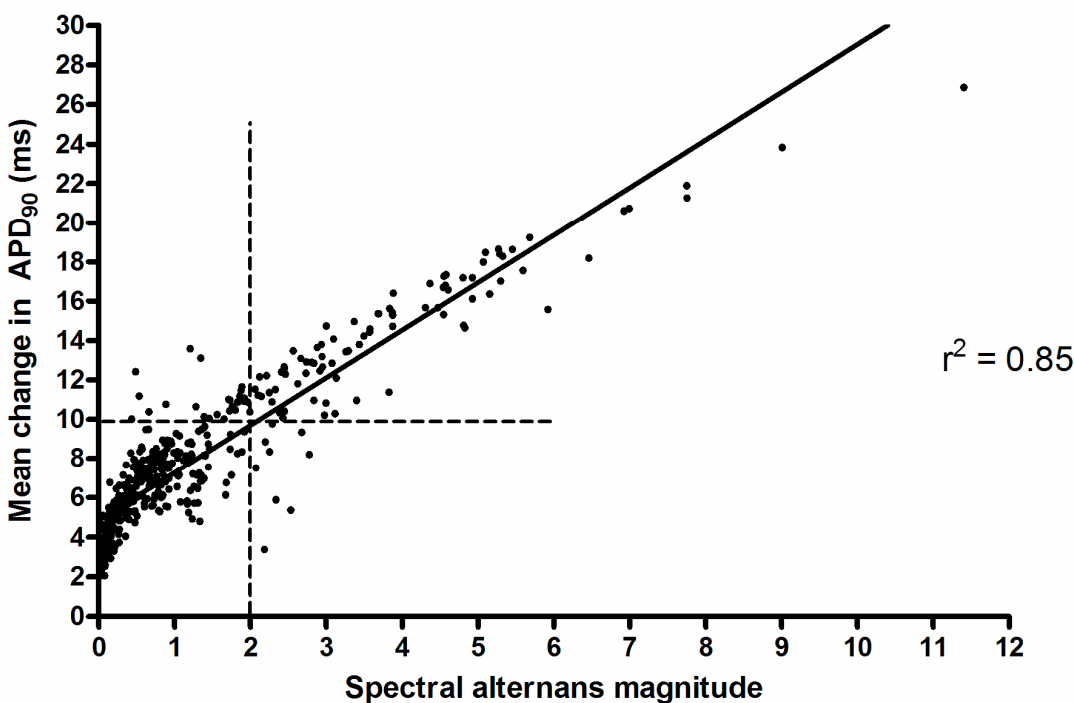


Figure 6.1 Correlation of spectral alternans magnitude with change in APD₉₀ during alternans

A plot to show the relationship between mean difference in measured APD₉₀ and the spectrally defined alternans magnitude in the presence of alternans. Each dot represents a different pixel in a normal heart at a CL of 150ms. For each pixel the mean difference was calculated from a run of 10 APs. The solid line indicates the linear regression ($r^2 = 0.85$). The threshold values for mean difference in APD₉₀ (≥ 10 ms) and spectral alternans magnitude (≥ 2) are indicated by the dashed lines.

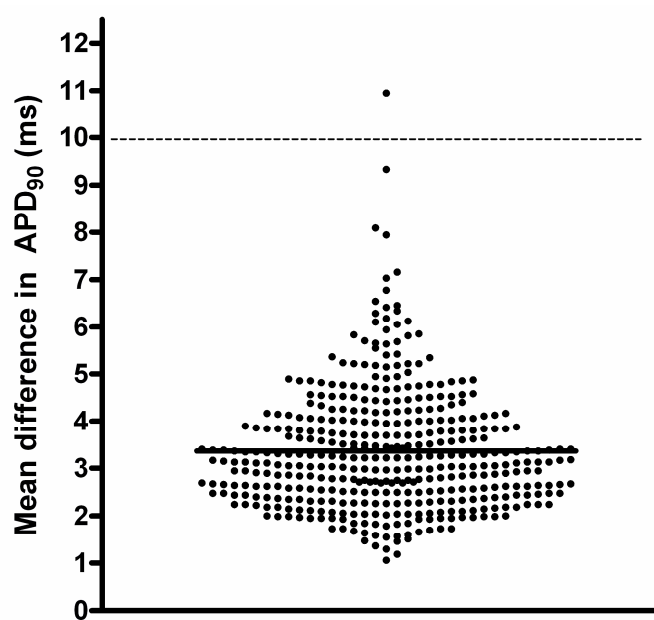


Figure 6.2 Mean change in APD₉₀ in the absence of alternans

Each dot represents a different pixel in a normal heart at a cycle length of 150ms in the absence of alternans. For each pixel the mean difference was calculated from a run of 10 APs. The solid line indicates the mean (3.4 ± 1.3 ms). The chosen threshold value for a significant mean difference in APD₉₀ (≥ 10 ms) is indicated by the dashed line.

Repolarisation alternans

Rapid pacing in normal hearts at 30°C consistently produced alternans in both the pseudoECG and in transmural optical action potentials. An example of transmural repolarisation alternans in one normal heart during endocardial stimulation at a CL of 190ms is shown in Figure 6.3. In this case, alternating behaviour was apparent in both the pseudoECG and in the optical AP traces from the subepicardium. The contour maps detail the transmural patterns of activation, repolarisation, APD₉₀ and AP amplitude, and so illustrate the basis of the alternating behaviour seen. The activation maps show that transmural propagation was relatively slow at this pacing CL. The mean transmural CV at 30°C and a CL of 190ms was 16.6 ± 1.7 cm/sec, compared to a value of 27.2 ± 2.9 cm/sec at 350ms ($p = 0.003$). However, there were no significant differences in mean transmural CV from one beat to the next. The transmural spread of activation showed subtle differences between beat 1 and beat 2. During beat 1 the transmural wavefront was relatively planar. During beat 2 conduction from the subendocardium into subepicardial region 2 was faster than conduction into region 1. Conduction into region 2 during beat 2 was also faster than conduction into the same region during beat 1. The repolarisation maps show that on beat 1, the spread of repolarisation largely follows the spread of activation, and so is relatively planar, but with slightly earlier repolarisation in region 1. On beat 2, region 2 repolarises much earlier. This results in a shorter APD₉₀ in region 2 during beat 2 than was recorded during beat 1, as shown in the APD₉₀ maps. Conversely, region 1 repolarises later during beat 2. This results in a longer APD₉₀ in this area. Repolarisation in this area during beat 2 is also later than had been recorded during beat 1.

Alternans of AP amplitude

Marked alternans of AP amplitude, as well as alternans of repolarisation and APD₉₀, is apparent from the optical AP traces shown in Figure 6.3. In these experiments, alternans of AP amplitude was common, and almost always accompanied alternans of repolarisation and APD₉₀. The magnitude of AP amplitude alternans was spatially heterogeneous and the spatial distribution was similar to that seen for repolarisation alternans, as shown in the AP amplitude maps in Figure 6.3. In areas where alternating behaviour was apparent, late repolarisation was associated with a larger and longer optical AP whereas early repolarisation was associated with a smaller and shorter optical AP.

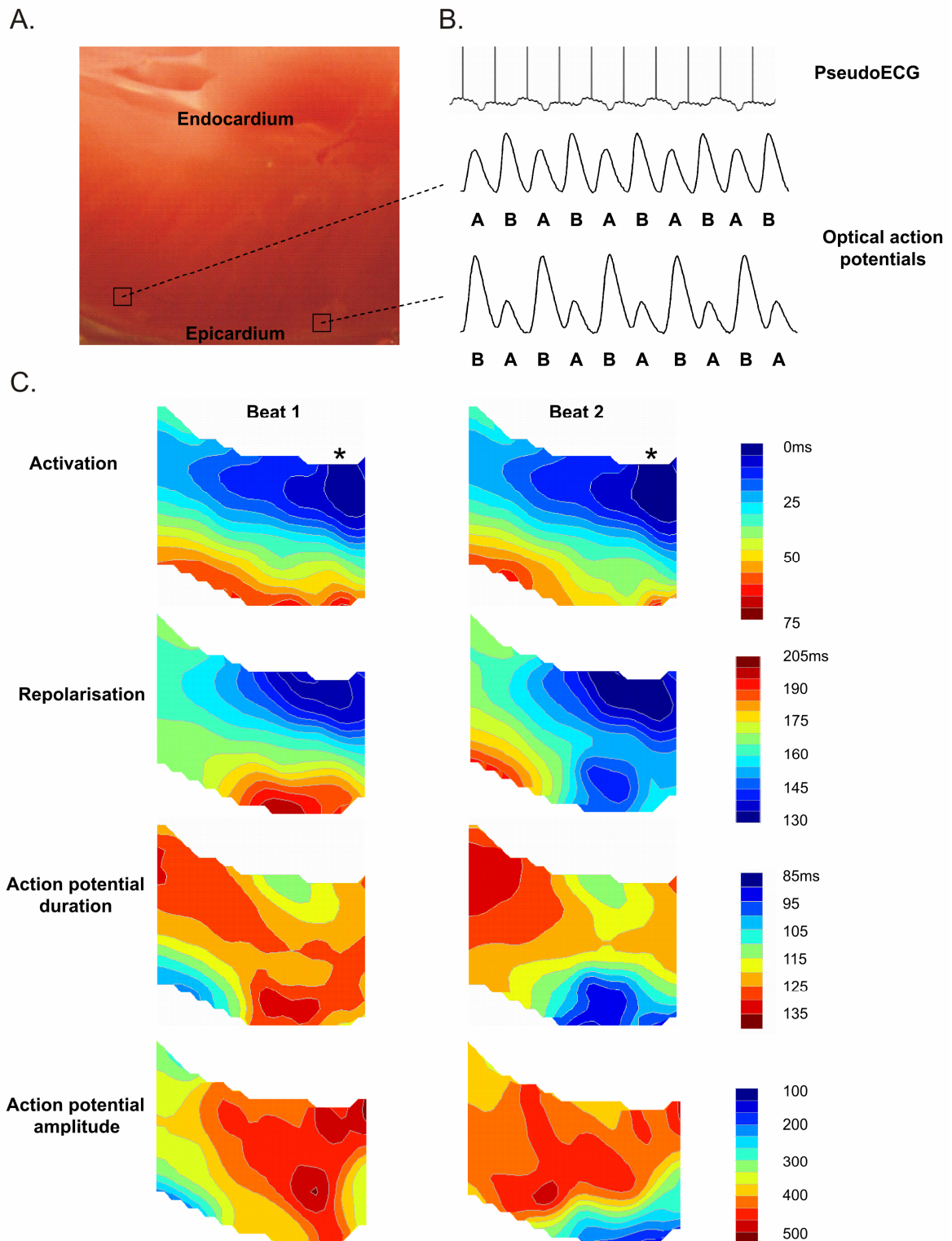


Figure 6.3 Transmural repolarisation alternans

An example of repolarisation alternans recorded from a normal heart at 30°C and a pacing CL of 190ms. A. The transmural imaging surface with the endocardial border uppermost and the epicardial border lowermost. B. The pseudoECG recorded from the chamber and optical AP traces recorded from the pixels indicated. The phase (i.e. large/small) is indicated by A (small APs) or B (large APs). C. Transmural contour maps for activation, repolarisation, APD₉₀ and AP amplitude. The left hand maps correspond to beat 1 and the right hand maps to beat 2 shown in the optical AP traces. The site of endocardial point stimulation is indicated (*).

Spectral analysis of alternans magnitude and phase

Spectral analysis was used to detect alternans in the optical AP traces, and also to quantify spatial patterns in alternans magnitude and phase. The spectral parameters determined for the example sequence used in Figure 6.3 are shown in Figure 6.4. From the maps in Figure 6.3 it is clear that in this example, alternans of repolarisation, APD₉₀ and AP amplitude occurred in subepicardial region 1. In region 2, alternans of activation time also occurred and the alternans of repolarisation, APD₉₀ and AP amplitude had the opposite phase to that seen in region 1. The map of spectral alternans magnitude (Figure 6.4C) shows that significant alternans (alternans magnitude ≥ 2) occurs in the subepicardial region, and is larger in region 2 than in region 1. This is consistent with both the contour maps and the optical AP traces shown in Figure 6.3. The contour map of spectral alternans phase shows that in region 1 alternans phase is negative, in contrast to region 2, where alternans phase is positive. This is again consistent with both the contour maps and the optical AP traces shown in Figure 6.3. In Figure 6.4D contour maps derived from the measured change in APD₉₀ are shown for comparison with the parameters derived from spectral analysis. On the left, the map of mean change in APD₉₀ across the transmural surface shows a similar distribution of alternans in APD₉₀ to that seen in the spectral alternans contour map. There is significant alternans (change in APD₉₀ $\geq 10\text{ms}$) in the subepicardium, with a greater difference in consecutive APD₉₀ values seen in region 2, compared with region 1. When the same data are shown with the corresponding phase of the change in APD₉₀, it is clear that the change in APD₉₀ is negative in region 1 and positive in region 2. This is compatible with the optical AP traces and shows good concordance with the contour map of alternans phase derived from the spectral analysis.

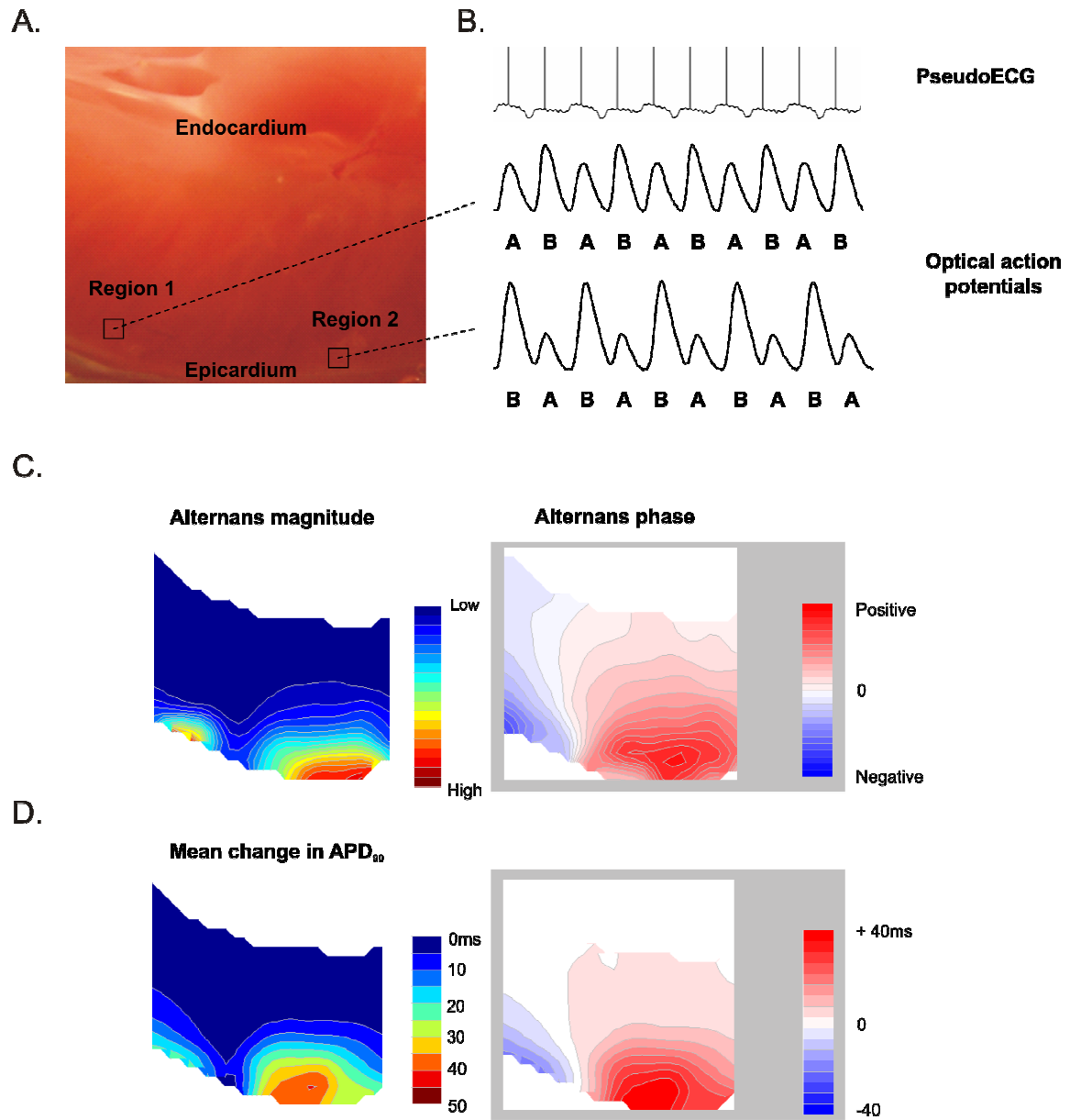
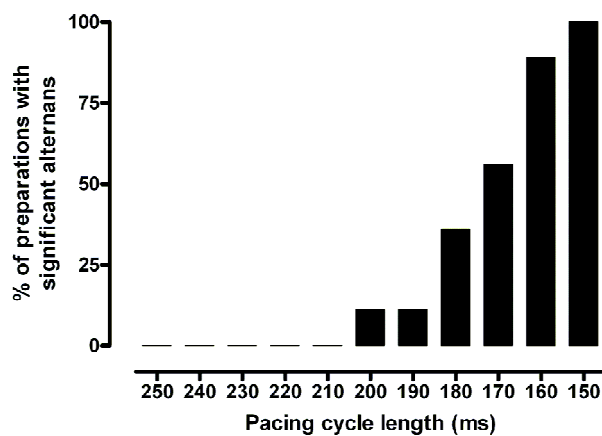
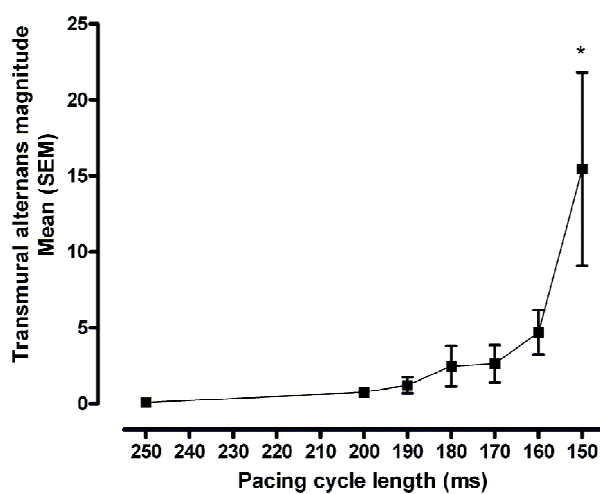
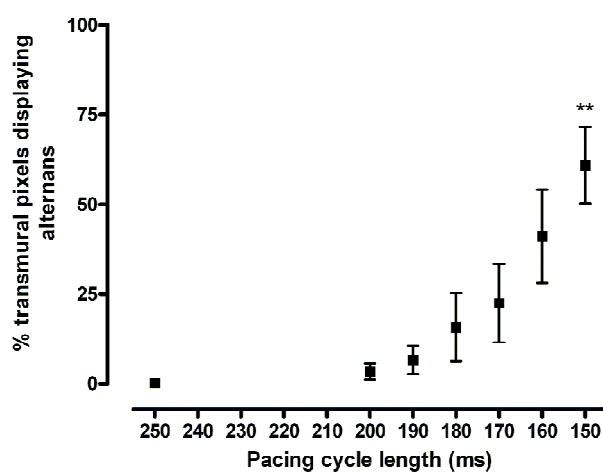


Figure 6.4 Alternans magnitude and phase

The same example of repolarisation alternans shown in Figure 6.3 to illustrate the spectrally derived parameters used to detect and quantify alternans. A. The transmural imaging surface with the endocardial border uppermost and the epicardial border lowermost. B. The pseudoECG recorded from the chamber and the optical AP traces recorded from the pixels indicated. The phase (i.e. large/small) is indicated by A (small APs) or B (large APs). C. Transmural contour maps of spectrally derived alternans magnitude and alternans phase. D. Transmural contour maps of mean change in APD_{90} , as measured by the standard analysis method. The right hand map shows mean change in measured APD_{90} for comparison with the map of spectrally derived alternans magnitude. The left hand map shows the same data, plotted on a scale to demonstrate the phase and magnitude of the mean change in APD_{90} , for comparison with the map of spectrally derived alternans phase.

Heart rate dependence of repolarisation alternans

The occurrence of transmural repolarisation alternans was heart rate dependent, as is shown in Figure 6.5. All preparations captured 1:1 to a CL of 180ms or shorter (heart rate ≥ 333 bpm) and the shortest CL followed 1:1 was 130ms (462bpm). The mean shortest CL was 157 ± 6 ms (heart rate 387 ± 14 bpm), and 6/9 preparations captured 1:1 at a CL of 150ms or shorter (heart rate ≥ 400 bpm). The total number of preparations which displayed significant alternans increased with increasing stimulation rate. One preparation developed transmural repolarisation alternans at a CL of 200ms (300bpm), and all preparations displayed alternans at a CL of 150ms. The mean CL threshold for alternans was 179 ± 4 ms (337 ± 7 bpm). Once established, repolarisation alternans always persisted at faster stimulation rates. Across all experiments, there was an increase in mean alternans magnitude as a function of stimulation rate (15.4 ± 6.4 at 150ms [$n = 6$] vs. 2.5 ± 1.3 at 180ms [$n = 9$], $p = 0.0320$). There was more interheart variability in the alternans magnitude at shorter CLs. The mean proportion of pixels exhibiting significant repolarisation alternans also increased with stimulation rate ($60.9 \pm 10.7\%$ at 150ms [$n = 6$] vs. $15.8 \pm 9.5\%$ at 180ms [$n = 9$], $p = 0.0085$).

A.**B.****C.****Figure 6.5 Heart rate dependence of repolarisation alternans**

A. The percentage of preparations which displayed significant alternans as a function of stimulation rate. B. Transmural alternans magnitude with increasing stimulation rates in normal hearts at 30°C. C. The percentage of transmural pixels which displayed significant repolarisation alternans with increasing stimulation rate. n = 9 normal hearts at 30°C, one-way ANOVA, * p < 0.01 vs. all other points. ** p < 0.001 vs. 250ms.

Spatially discordant alternans

Spatially discordant alternans was defined according to the published description⁴⁰. Spatially discordant alternans required two areas of myocardium displaying significant repolarisation alternans, each having alternans of opposite phase (i.e. long-short vs. short-long) and being separated by an area of no alternans (a nodal line). Transmural spatially discordant alternans was seen in 3/9 normal hearts at 30°C. The heart rate threshold for spatially discordant alternans (369 ± 9 bpm) was significantly faster than that for spatially concordant alternans (337 ± 7 bpm, $p = 0.0376$). There was no significant difference in the fastest stimulation rate followed 1:1 in hearts that did and did not develop spatially discordant alternans during rapid pacing (422 ± 25 bpm vs. 370 ± 14 bpm, $p = 0.0878$). 50% (3/6) of the hearts which did not develop spatially discordant alternans during rapid pacing captured at a rate faster than the threshold heart rate for spatially discordant alternans. As shown in Table 6.2, there was no significant difference in mean alternans magnitude between preparations which did and did not develop spatially discordant alternans. The same was true of peak alternans magnitude, heterogeneity of alternans and the extent of alternans across the transmural surface.

Table 6.2 A comparison of the magnitude and extent of alternans during concordant and discordant alternans

Mean (SEM)	Concordant alternans (n = 6)	Discordant alternans (n = 3)	P value
Mean alternans magnitude	15 ± 6	16 ± 11	0.9323
Peak alternans magnitude	65 ± 19	67 ± 22	0.9509
Heterogeneity of alternans	29 ± 17	31 ± 12	0.9411
% of surface displaying alternans	63 ± 14	59 ± 10	0.8578

SEM = standard error of the mean. P value refers to an unpaired t-test in each case.

Discordant alternans and ventricular arrhythmia

Ventricular arrhythmias were induced in 2/9 normal hearts during rapid stimulation, an example is shown in Figure 6.6. Both of the hearts had displayed discordant alternans. Of the hearts which displayed spatially discordant alternans, 2/3 developed VA during the pacing protocol, compared with 0/6 preparations which did not display spatially discordant alternans ($p > 0.05$). Figure 6.6 illustrates the development of spatially discordant alternans in the three episodes observed. In each case the peak and mean transmural alternans magnitude during rapid stimulation are shown, along with the threshold value for concordant and discordant alternans. In the first example (Figure 6.7A), alternans magnitude increased progressively during rapid stimulation. During discordant alternans, peak alternans magnitude continued to rise but mean alternans magnitude fell, indicating the presence of an area without alternans (a nodal line). VA was induced during a shortening of CL from 150 to 140ms in the presence of discordant alternans. In the second example (Figure 6.7B), alternans magnitude again increased progressively during rapid stimulation. Mean alternans magnitude appeared comparable to that seen in the first example, although peak alternans magnitude at the onset of discordant alternans was much smaller. Transmural discordant alternans persisted only between 150-140ms, with transmural alternans becoming concordant again at 130ms. VA was induced during a shortening of CL from 150 to 140ms in the presence of high mean and peak transmural alternans, but without transmural discordant alternans. In the third example (Figure 6.7C), initial mean and peak alternans are comparable to that in Figure 6.6B, although the onset of significant alternans occurs at a longer CL. However, the increase in alternans magnitude did not appear to increase during discordant alternans and a loss of capture occurred after a shortening of the pacing CL from 150 to 140ms. In these three instances of spatially discordant alternans, there did not appear to be any consistent spatial distribution of alternating areas or of nodal lines.

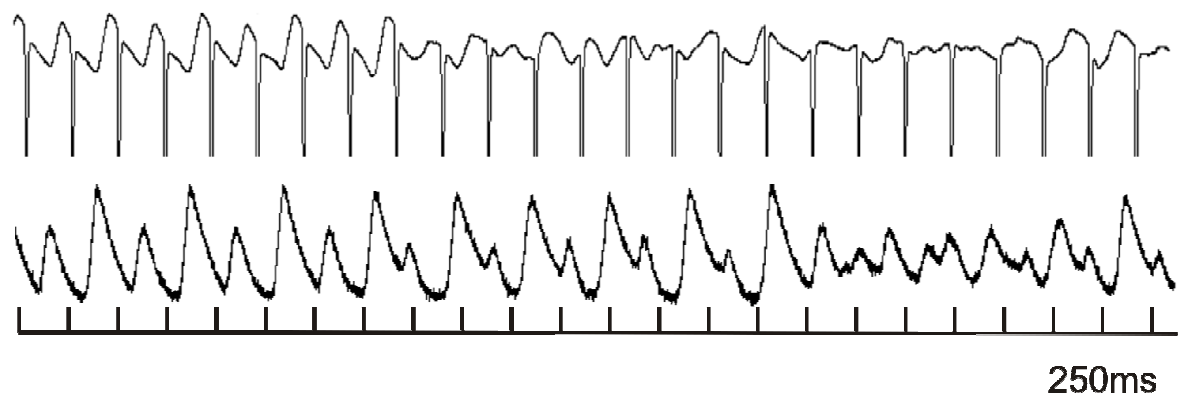


Figure 6.6 An example of ventricular arrhythmia induced during alternans

An example of an arrhythmia induced during alternans at a CL of 120ms in a normal heart at 30°C. The upper trace shows the pseudo ECG and the lower trace shows the optical AP trace.

Alternans magnitude and ventricular arrhythmia

As only 2/9 preparations developed VA it was not possible to make valid statistical comparisons between those preparations which did and did not develop VA in terms of the extent, magnitude and heterogeneity of alternans. However, 2/7 preparations which did not develop VA displayed higher mean and peak alternans magnitude, greater heterogeneity of alternans and greater transmural extent of alternans than the two preparations in which an arrhythmia did occur.

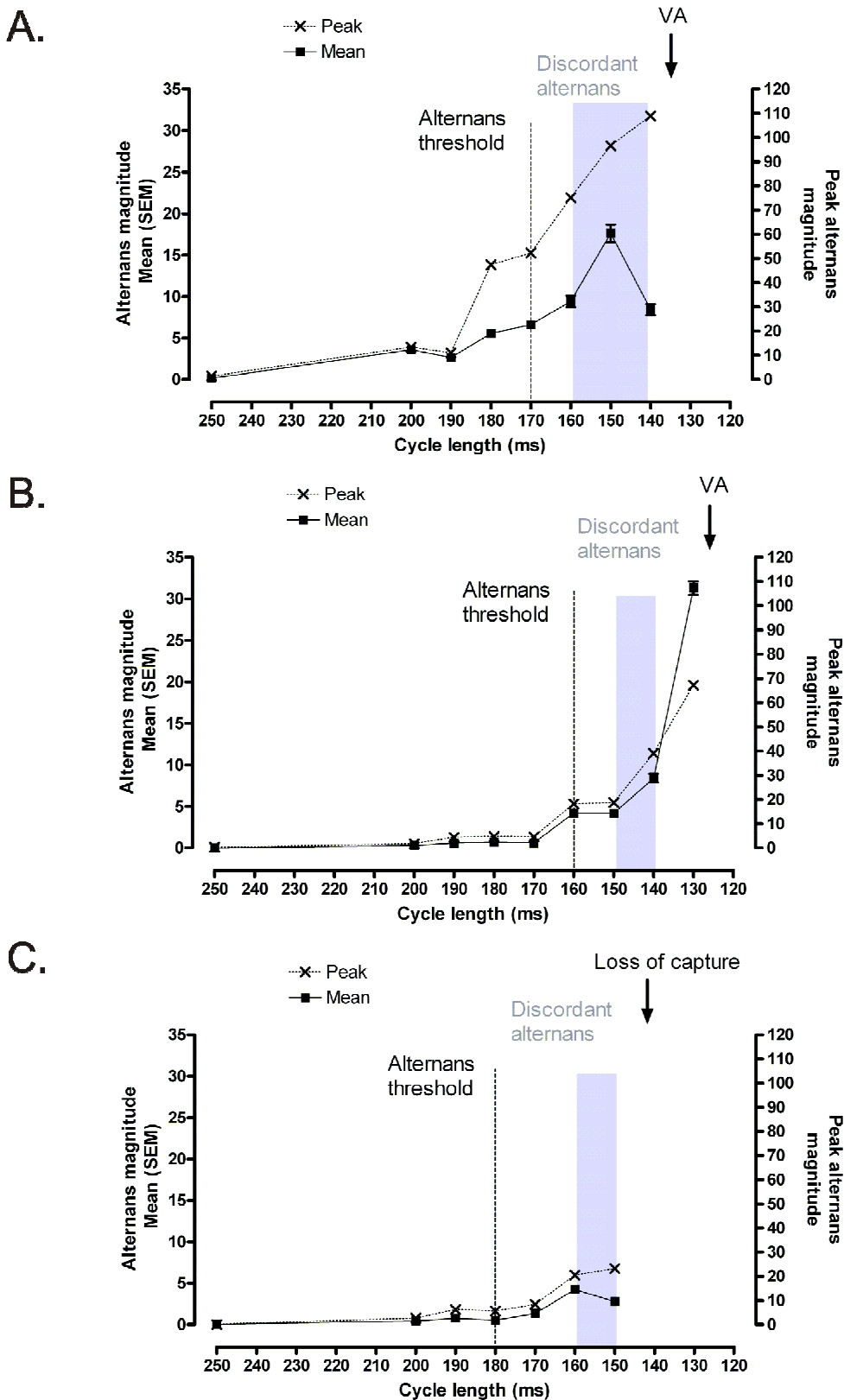


Figure 6.7 Episodes of spatially discordant alternans

A. Mean (squares, left Y-axis) and peak (crosses, right Y-axis) alternans magnitude as a function of pacing CL in a single normal heart at 30°C. In each case the CL threshold for significant alternans is shown (dotted line) as is the period of discordant alternans, which is shaded grey. The endpoint of the pacing protocol, either ventricular arrhythmia (VA) or loss of 1:1 capture is indicated. B. and C. illustrate the two other examples of discordant alternans. Each graph is plotted with the same axes to facilitate comparison.

Transmural patterns of repolarisation alternans

In the majority of experiments, transmural patterns of repolarisation alternans were evident. An example is given in Figure 6.8. During endocardial stimulation, alternans magnitude was greatest at the subepicardium. In order to test whether these transmural gradients were influenced by activation sequence, alternans protocols were repeated during epicardial stimulation in a subset of experiments ($n = 5$). The fastest stimulation rate achieved during epicardial pacing was significantly lower than that achieved during the endocardial stimulation protocols (327 ± 9 vs. 387 ± 14 bpm, $p = 0.0117$).

Transmural APD₉₀ gradients at baseline

As described in Chapter 4, transmural gradients of APD₉₀ were present at baseline and persisted during rapid stimulation. The longest transmural APD₉₀ values were found at the subendocardium (186.1 ± 2.8 ms) compared to the midmyocardium (175.3 ± 4.2) and the subepicardium (165.0 ± 3.6 ms, $p < 0.05$ vs. midmyocardium and subendocardium). As found in Chapter 3, in this subset of experiments, the gradient also reversed when the stimulation site was transferred to the epicardium (two-way ANOVA, $p < 0.05$). During epicardial stimulation, the subendocardial APD₉₀ was shorter (168.7 ± 4.7 ms) compared to values found in the midmyocardium (173.3 ± 5.0 ms) and subepicardium (180.3 ± 5.8 , $p < 0.05$ vs. midmyocardium and subepicardium).

Transmural distribution of alternans

Patterns of alternans were classified according to transmural layer, as shown in Table 6.3. There was no clear pattern in terms of the earliest alternans during endocardial stimulation. Alternans arose in the subendocardium in 5/9 preparations, in the midmyocardium in 1/9, and in the subepicardium in 3/9 ($p > 0.05$). The site of maximal alternans was always in the subepicardium during endocardial stimulation. In contrast, during epicardial stimulation, maximal alternans was found in the subendocardium in 4/5 cases ($p < 0.01$).

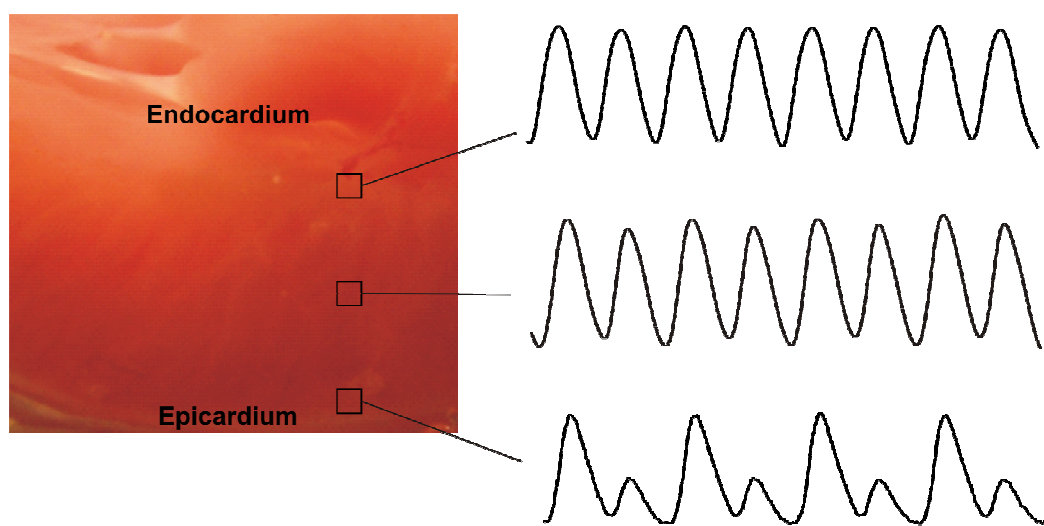
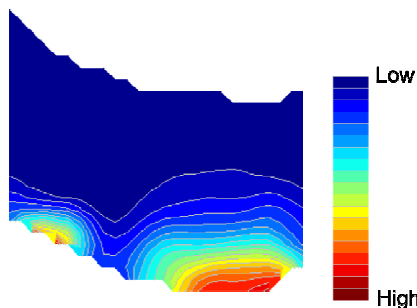
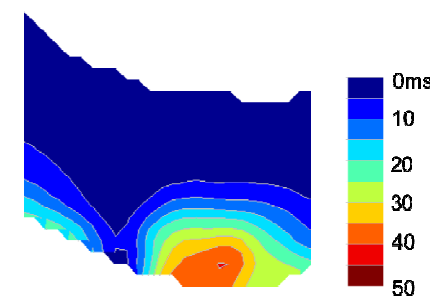
Correspondingly, the mean alternans magnitude was greatest in the subepicardium during endocardial stimulation and in the subendocardium during epicardial stimulation.

Therefore, the spatial patterns of both APD₉₀ and alternans magnitude appeared to be influenced by stimulation site. This relationship is demonstrated in Figure 6.9. During endocardial stimulation, the magnitude of alternans was greatest at the subepicardium, where baseline APD₉₀ was shortest. During epicardial stimulation, when subepicardial APD₉₀ lengthens and the transmural gradient reverses such that the shortest APD₉₀ is found at the subendocardium, the site of maximal alternans also changes to the subendocardium.

Table 6.3 Transmural patterns of alternans

	Subendocardium	Midmyocardium	Subepicardium
Site of earliest alternans n (%)			
Endocardial stimulation	5 (56)	1 (11)	3 (33)
Epicardial stimulation	3 (60)	0 (0)	2 (40)
Site of maximal alternans n (%)			
Endocardial stimulation	0 (0)	0 (0)	9 (100)
Epicardial stimulation	4 (80) **	0 (0) **	1 (20) **
Alternans magnitude Mean \pm SEM			
Endocardial stimulation	7.3 ± 1.6	12.7 ± 5.4	41.8 ± 12.4
Epicardial stimulation	$22.4 \pm 7.5^*$	$6.1 \pm 2.7^*$	$4.4 \pm 1.8^*$

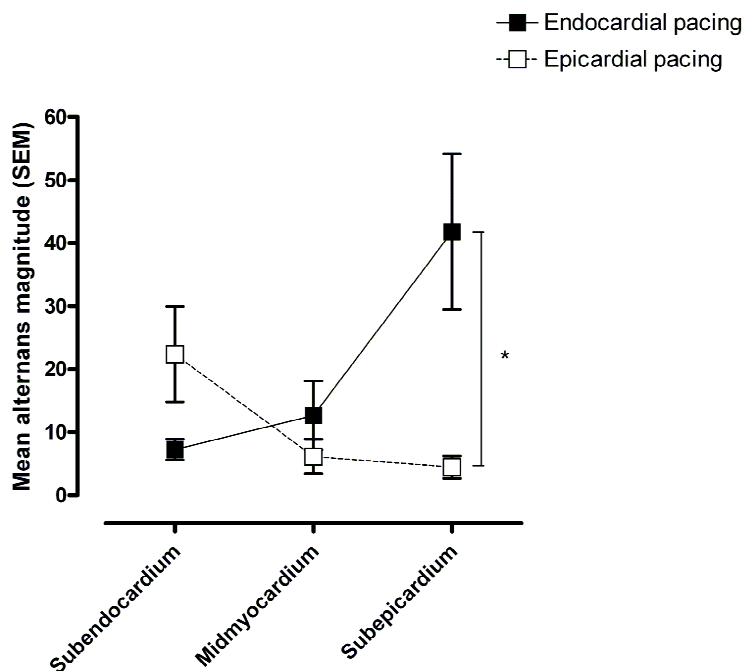
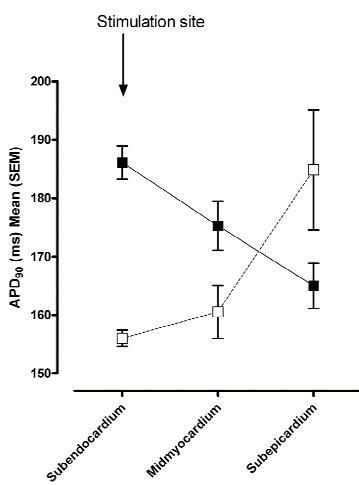
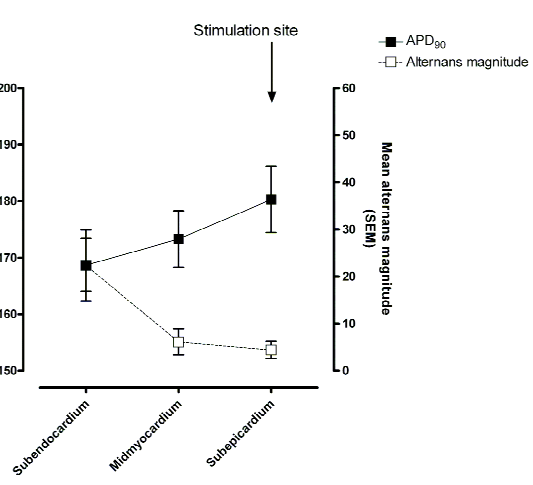
SEM = standard error of the mean. Endocardial stimulation, n = 9 and epicardial stimulation, n = 5. Site of earliest alternans and maximal alternans compared using Fisher's exact test, ** p < 0.01 vs. endocardial stimulation. Alternans magnitude compared by two-way ANOVA, * p < 0.05 vs. endocardial stimulation.

A.**B.****Alternans magnitude****C.****Mean change in APD₉₀****Figure 6.8 Transmural repolarisation alternans**

A. The transmural imaging surface with the endocardial border uppermost and the epicardial border lowermost. On the right are optical AP traces recorded from the pixels indicated in the subendocardium, midmyocardium and subepicardium. B. Transmural contour map of spectral alternans magnitude. C. Transmural contour map showing mean change in APD₉₀, as measured by the standard analysis method.

Temperature dependence of alternans in normal hearts

In contrast to findings at low temperature, at which all 9/9 preparations developed repolarisation alternans, at 37°C, only 1/8 normal hearts developed repolarisation alternans ($p < 0.0001$). Alternans occurred in a single heart at a pacing cycle length of 110ms (545bpm). The fastest stimulation rate supported by normal hearts at 37°C ranged from 400 to 600bpm and was significantly faster than that supported at 30°C (462 ± 26 bpm vs. 387 ± 14 bpm, $p = 0.0192$). The fastest stimulation rate without alternans at 37°C (449 ± 18 bpm) was significantly faster than the equivalent value at 30°C (337 ± 7 bpm, $p < 0.0001$). VA was induced in a single normal heart at 37°C, and this heart had not displayed alternans during rapid pacing.

A.**B. (i)****(ii)****Figure 6.9 The effect of activation sequence on transmural patterns of alternans**

A. Alternans magnitude in each transmural region during endocardial (closed squares and solid line, $n = 9$) and epicardial stimulation (open squares and dashed line, $n = 5$). * $p < 0.05$ following a two-way ANOVA. B. Baseline APD_{90} (closed squares and solid line) and alternans magnitude (open squares and dashed line) in each transmural region during (i) endocardial ($n = 9$) and (ii) epicardial stimulation ($n = 5$).

Repolarisation alternans on the epicardial surface

In a subset of experiments at 30°C (n = 5) the protocols to induce repolarisation alternans were repeated during epicardial imaging. Repolarisation alternans on the epicardial surface was induced in all preparations during rapid endocardial pacing. There was no difference in the threshold stimulation rate for significant alternans on the transmural (337 ± 7 bpm, n = 9) and epicardial surfaces (341 ± 33 bpm, n = 5, p = 0.8785). As shown in Table 6.4, there were no significant differences between the transmural and epicardial surfaces in terms of the mean alternans magnitude, peak alternans magnitude, heterogeneity of alternans or proportion of the imaged surface displaying alternans. Spatially discordant alternans occurred on the epicardial surface in 3/5 preparations, as compared with 3/9 during transmural imaging (p > 0.05). On the epicardial surface, the stimulation threshold for spatially discordant alternans (416 ± 36 bpm) was not significantly higher than that for concordant alternans (341 ± 33 bpm, p = 0.1632). There was no difference in the threshold stimulation rate for spatially discordant alternans on the transmural (369 ± 9 bpm, n = 9) and epicardial surfaces (416 ± 36 bpm, n = 5, p = 0.1273).

Table 6.4 A comparison of the magnitude and extent of alternans across the transmural and epicardial surfaces

Mean (SEM)	Transmural (n = 9)	Epicardial (n = 5)	P value
Mean alternans magnitude	16 ± 5	30 ± 16	0.3165
Peak alternans magnitude	64 ± 14	86 ± 34	0.4924
Heterogeneity of alternans	31 ± 9	67 ± 36	0.2335
% of surface displaying alternans	68 ± 10	60 ± 13	0.6378

SEM, standard error of the mean. P value refers to a one-way ANOVA in each case.

Discussion

Induction and detection of repolarisation alternans

Alternans induction protocols

In these experiments, alternans was induced by a rapid pacing protocol which involved a progressive shortening of CL, rather than step reductions in CL from baseline. Optical imaging was performed after 30s of pacing at each CL, to ensure that steady state was achieved. This pacing protocol was used for two reasons. Firstly, this was the same protocol used in the experimental demonstrations of the potential proarrhythmic effects of alternans in cardiac tissue^{40,67}. Secondly, the protocol for measuring MTWA in patients requires a gradual increase in heart rate, making a progressive increase in stimulation rate the more physiologically relevant protocol. Other investigators have used a step pacing protocol in which CL is abruptly shortened from baseline CL²¹³, which is arguably less clinically relevant.

Alternans analysis

Repolarisation alternans was identified by spectral analysis, in order to distinguish alternans from fluctuations occurring at other frequencies. This method also had the theoretical advantage of being similar to the algorithms used to detect MTWA in clinical practice. The spectral analysis program was specifically written to detect alternans in optical APs recorded at rapid stimulation rates. The main difference from the clinical algorithm was the lack of need for noise correction in the determination of alternans magnitude. In the clinical MTWA analysis, alternans magnitude is corrected against frequency noise, calculated from the standard deviation of the peak occurring in the band 0.45-0.49³⁹. This is because frequency noise near 0.5 cycles/beat may be generated by artefact (usually due to movement or respiration) or by subtle changes in heart rate produced by autonomic influences. In order to avoid contamination of alternans magnitude by such frequency noise, the peak of the spectrum at the alternans frequency is corrected for noise before being reported as alternans magnitude. A high number of sampled beats is required to yield an accurate estimate of the standard deviation of the noise (128 beats in the clinical algorithm). This means that spectral analysis cannot reliably be carried out on shorter data segments, such as electrograms recorded by implantable devices²¹⁴. In the current study, optical data were collected for two seconds, meaning that the number of APs ranged from 5-20, depending on the pacing CL used. In the clinical scenario, these data segments would be too short to allow accurate estimation of noise in the band 0.45-0.49.

However, the experimental situation is quite different, in that the physiological sources of frequency noise present in an exercising human are not present. This removes the need for noise correction of the alternans magnitude data. However, in order to maximise fidelity with the clinical algorithm, the capability for noise correction was written into the program. Correction of alternans magnitude for various noise bands was performed, and none produced more accurate results than the uncorrected power at 0.5 cycles/beat. Alternans magnitude was therefore determined directly from the spectral peak at the alternans frequency.

The spectral analysis program also allowed the repolarisation segment of the AP to be individually identified in each set of traces. Only data within the repolarisation window were included in the spectral analysis. Other methodologies separate depolarisation and repolarisation using a 5ms window centred around the fastest part of the upstroke⁴⁰. This is a potential source of error as optical AP upstrokes are relatively slow and upstroke morphology can be variable, particularly at rapid stimulation rates. It is therefore possible that a fixed window around the fastest upstroke may not always accurately differentiate between depolarisation and repolarisation. In the current study, the use of the repolarisation window along with visual inspection of the alternans window during the analysis session provided better certainty that the repolarisation phase was accurately identified.

Defining alternans parameters

As the spectral analysis algorithm was specifically written for these experiments, validation of the spectral technique and determination of appropriate threshold values were necessary before the algorithm could be used to examine alternans behaviour. A difference in measured $APD_{90} \geq 10\text{ms}$ from one beat to the next was taken to be significant repolarisation alternans. This value was chosen as it was considered physiologically significant and in keeping with values used in the literature⁴⁰. The specificity of this value for alternating behaviour and its integrity at short cycle lengths was then verified by determining the mean change in APD_{90} during rapid pacing where no alternans was apparent. The mean change in APD_{90} plus two standard deviations was 8.9ms. This suggests that a change in $APD_{90} \geq 10\text{ms}$ in the absence of alternans does not occur at short CLs and should be consistently measurable within the error of the system. Careful correlations were made between spectral alternans and the change in APD_{90} measured using conventional analytic methods. The data presented here suggest a good correlation between spectral repolarisation alternans and measured change in APD_{90} . The chosen spectral threshold resulted in a low false negative rate (around 2%) but a high false positive

rate (around 70%). Given the high volume of pixels being screened and the relatively low prevalence of alternans (~10%) the low false negative rate was essential. The high false positive rate was not particularly problematic, as these were easily identified by visual inspection of the pixel traces. In addition, single pixels displaying clear alternans in the AP trace surrounded by non-alternating pixels were not seen. This meant that a spatial constraint could be added, requiring that a certain number of adjacent pixels displayed alternans. This further reduced the likelihood of false positives being considered as significant alternans.

Electrophysiological behaviour during alternans

Although the data analysed were limited to the repolarisation phase of the AP, it is clear that during alternans optical AP traces often show alternans of amplitude and baseline. To suggest that alternans was limited to repolarisation would be an over-simplification. In effect, the spectral analysis identifies an alternating pattern of AP morphology. This study employed both custom written spectral analysis and conventional optical AP analysis algorithms. This allowed better characterisation of the electrophysiological changes which occur during alternans. Figure 6.3 details the transmural patterns of activation time, repolarisation time, APD₉₀ and AP amplitude during alternans. It shows that each of these AP parameters displays alternans, rather than alternans being confined to repolarisation (and so reflected in APD₉₀). Although the spread of activation times appears qualitatively similar in beats 1 and 2, absolute activation times vary as much as 10-15ms in the area where alternans magnitude is greatest. The spread of repolarisation is clearly different from one beat to the next. The area where repolarisation occurs earlier on the second beat correlates to the area which was activated early, and has the largest magnitude of alternans. The APD₉₀ map reflects these observations. As expected, the area which is activated early and repolarises early has a shorter APD₉₀ on that beat. Interestingly, these findings are also manifest in a map of AP amplitude. When the alternating area is activated early and repolarises early, along with having a short APD₉₀, it also has a small AP. When the alternating area is activated later and repolarises later, along with having a longer APD₉₀, it also has a larger AP.

It is clear from the AP traces that the slow upstroke of the optical AP is exaggerated during rapid stimulation. The slowing of the optical AP rise time has been attributed to spatial averaging¹⁵². However, using the transmural conduction velocity reported in Chapter 3 (~30cm/sec), the AP would be expected to cross a pixel dimension of ~300μm in ~ 1ms, meaning that the degree of rise time slowing cannot easily be attributed to spatial

averaging. The reason for rise time slowing is not entirely clear, but is compatible with that seen in other optically recorded traces during alternans⁴⁰.

Alternans of AP amplitude

This study identified that repolarisation alternans measured using conventional optical imaging methods displayed marked alternans of AP amplitude as well as alternans of APD₉₀. This finding is common with those published in other reports employing similar optical imaging methodology^{40;67;77}. Despite this, the basis for AP amplitude alternans has not been clearly explained. In particular, whether such alternans of AP amplitude could occur in single cells remains unclear^{66;87;111}. The resolution of the CCD recordings is such that the optical signal represents the mean voltage within a significant volume of myocardium. A single optical AP therefore represents the summed electrical activity of many hundreds of cardiomyocytes. Alternating amplitude in consecutive action potentials from the same site therefore has two possible explanations. It may indicate an alternating upstroke amplitude in all of the myocytes contributing to the AP in a given pixel area. It could also be produced if some of the myocytes in the pixel area were failing to respond on an every other beat basis. If some cells displayed rate-dependent 2:1 phase-locking while others responded 1:1 then an alternating amplitude would be observed in the summed optical AP. In order to differentiate between these two scenarios experimentally, a higher resolution imaging system would be required. Preliminary work exploring the basis of AP amplitude alternans using such a system is described in the Appendix.

Heart rate dependence of alternans

The occurrence of alternans was heart rate dependent, as is MTWA in patients with heart failure⁵⁶. There was significant interheart variability in terms of alternans magnitude as has been reported by other investigators⁴⁰. However, the observation of an increase in alternans magnitude with increasing stimulation rate was consistent. In each preparation, alternans magnitude increased with stimulation rate, and once established was always present at all higher stimulation rates. Comparisons of mean alternans magnitude were effectively made between cycle lengths of 200ms (the slowest stimulation rate to elicit alternans in normal hearts, n = 9) and 150ms (n = 6). Although 3 of 9 preparations captured at CLs shorter than 150ms, the unbalanced numbers and interheart variability meant that comparisons at shorter CLs were considered to be less valid. Heart rate dependence is an important feature of MTWA in humans^{121;122} and is also documented in other published accounts of repolarisation alternans in ventricular myocardium⁴⁰. The observed heart rate

dependence of alternans magnitude in these experiments therefore suggests that the alternans here is similar to that found under other experimental circumstances, and is relevant to MTWA in humans. However, the stimulation rates described here are extremely fast in comparison to the normal heart rate in a rabbit (130-325bpm). In this context, pro-arrhythmic phenomena occurring at around 600bpm may be more likely to be involved in the progression from VT to VF than in the induction of re-entrant ventricular arrhythmia.

Spatially discordant alternans

Spatially discordant alternans was previously recorded in the isolated epicardium of guinea pig hearts⁴⁰ and was directly linked to the induction of ventricular arrhythmia during a shortening of pacing cycle length. The presence of spatially discordant alternans was associated with an increase in dispersion of repolarisation, which predisposed to unidirectional conduction block and re-entry. In the current study, transmural spatially discordant alternans was recorded in 3/9 normal hearts. Similar to that described by Pastore *et al*⁴⁰, spatially discordant alternans was always preceded by concordant alternans, and had a significantly higher threshold heart rate than that for concordant alternans. There was no apparent relationship between the magnitude or extent of concordant alternans and the development of discordant alternans. Unlike the results presented by Pastore *et al*, the progression from concordant to discordant alternans was not a consistent finding in the current experiments. This may be partly explained by the difference in perfusion temperature, which was 27°C in the experiments carried out by Pastore *et al* compared to 30°C in the current experiments. In addition, only half of the preparations which did not develop spatially discordant alternans captured at a rate faster than the threshold heart rate for spatially discordant alternans. Therefore, capture at faster stimulation rates may have resulted in more episodes of discordant alternans.

The finding in the current study of infrequent transmural discordant alternans is further moderated by the fact that discordant alternans may have been occurring in parts of the preparation not covered by the transmural imaging window. While the development of an alternating pattern in the pseudoECG correlated well with the onset of AP alternans, there were no clear ECG changes during discordant alternans. Consequently, there was no way of determining whether discordant alternans might be present in another part of the preparation. Supporting this, in 2/3 cases spatially discordant alternans persisted at all higher CLs but with differing spatial orientation. In the other case, spatially discordant alternans became concordant at higher stimulation rates. A possible explanation for this observation is suggested by recent work examining spatial patterns of alternans in rabbit

epicardium²¹³. The authors recorded the development and progression of alternans simultaneously across the anterior and posterior surfaces of Langendorff perfused rabbit hearts. By tracking nodal lines between two areas alternating with opposite phase they were able to determine that, under some circumstances patterns of discordant alternans were dynamic. It is therefore likely that areas of discordant alternans existed in these preparations, other than those recorded by transmural optical mapping.

Spatially discordant alternans and ventricular arrhythmia

Ventricular arrhythmias occurred in only 2/9 preparations, and both of these preparations had displayed transmural discordant alternans. In one, transmural discordant alternans directly preceded the onset of ventricular arrhythmia and in the other discordant alternans became concordant within the imaging window prior to the induction of arrhythmia. However, given the above discussion it is likely that the nodal line may have moved away from the transmural imaging window. In neither case was the induction of arrhythmia directly imaged and so it remains unclear whether spatially discordant alternans could have been directly implicated in generating the conditions for re-entry. In both cases, ventricular arrhythmia was induced after a shortening of pacing cycle length. This was also the case in the example published by Pastore *et al*⁴⁰. It is therefore likely that the presence of spatially discordant alternans increases the likelihood of unidirectional conduction block only after a shortening of CL, analogous to an increase in heart rate.

Alternans magnitude and ventricular arrhythmia

As only 2/9 preparations developed an arrhythmia it was not possible to make valid statistical comparisons between those preparations which did and did not develop VA in terms of the extent, magnitude and heterogeneity of alternans. However, 2/7 preparations which did not develop an arrhythmia displayed higher mean and peak alternans magnitude, greater heterogeneity of alternans and greater transmural extent of alternans than the two preparations in which an arrhythmia did occur. Therefore, there does not appear to be a clear relationship between magnitude or extent of alternans and either the development of spatially discordant alternans, or the induction of ventricular arrhythmia.

Transmural electrophysiological heterogeneity

The development of cellular repolarisation alternans has been linked to heterogeneity of cellular action potential restitution and calcium cycling in epicardial mapping studies⁷⁷. More recently, it has been suggested that alternating behaviour in cardiac tissue is dictated

not only by underlying electrophysiological heterogeneity, but also by dynamic factors⁹². Cells with differing repolarisation characteristics span the ventricular wall and these experiments tested the hypothesis that these transmural gradients would influence the production of repolarisation alternans. Studies in isolated guinea pig myocytes⁸⁷ and intact canine wedge preparations¹⁰⁴ have suggested that subendocardial cells are more prone to the development of alternans, and this has been linked to differences in their Ca^{2+} cycling properties. Similar transmural differences in Ca^{2+} cycling have been reported in midmyocardial cells in the rabbit¹³⁴. In these experiments, the site of earliest alternans was inconsistent, suggesting that the initiation of alternans may not entirely depend upon fixed tissue properties. Similarly, in the current study the development and propagation of alternating behaviour appeared to be influenced by dynamic factors. During endocardial pacing at a CL of 350ms, transmural differences in APD_{90} were evident which then changed when the stimulation site was changed to the epicardium. During endocardial pacing, alternans magnitude was greatest at the subepicardium. During epicardial pacing the opposite was observed, and the greatest alternans magnitude was found in the subendocardium. During epicardial pacing, the fastest stimulation rate supported was slower than during endocardial, and this is likely to explain the observation that peak alternans magnitude was smaller during epicardial pacing. Despite differences in the peak alternans magnitude, the transmural distribution of alternans was clearly opposite during endocardial and epicardial stimulation. These results are consistent with the hypothesis set out in Chapter 4 that transmural heterogeneities of repolarisation in rabbit ventricular myocardium are modified by electrotonic influences. They also suggest that this same process influences the transmural distribution of repolarisation alternans. Whether the patterns of alternans result directly from baseline gradients of APD_{90} or whether both are separately modulated by electrotonic influences is not clear. Overall these data suggest that the development of alternans is not solely dictated by cellular repolarisation characteristics, but rather a complex interplay of fixed cellular and dynamic tissue factors.

Spatially discordant alternans in the transmural axis

Spatially discordant alternans has been described in the transmural axis during pharmacological prolongation of the QT interval in canine hearts¹⁰¹. Under long QT conditions, midmyocardial ARI was longer and restitution steeper than in the subendocardium or subepicardium, producing an extreme degree of transmural dispersion of repolarisation not found in normal myocardium. Under these conditions discordant alternans occurred consistently between subepicardial and midmyocardial sites. In the current study there was no consistent transmural orientation of spatially discordant

alternans, despite relatively consistent transmural gradients of APD and transmural patterns of alternans. This suggests that in the absence of extreme dispersion of repolarisation, discordant alternans occurs in variable spatial orientations and may be more dependent upon dynamic factors than on underlying tissue heterogeneity.

Temperature dependence of repolarisation alternans

As expected from the published literature⁴⁰ repolarisation alternans was observed during rapid pacing in all preparations at low temperature. However, repolarisation alternans was only observed in a single heart at 37°C. This is in contrast to other reports, where alternans has been elicited at 37°C at higher stimulation rates than at 30°C⁴⁰. Unfortunately, data regarding the heart rate thresholds for alternans at 37°C were not given to allow comparisons with the rates achieved in the current study. The possibility exists that the stimulation rates achieved in these experiments were not sufficiently fast to induce alternans. In the current study, the fastest stimulation rate supported by normal hearts at 37°C was significantly faster than that supported at 30°C. The difference between the two temperatures in terms of the fastest CL captured was ~ 75bpm (24ms, ~ 15% of the value at 30°C). Assuming a constant relationship between alternans threshold and fastest stimulation rate achieved at the two temperatures and applying the same 15% reduction to the alternans threshold observed at 30°C would predict an alternans threshold of around 152ms (395bpm) at 37°C. In fact all preparations at 37°C captured at least to 400bpm and still alternans was not consistently observed. This tends to suggest that the stimulation rates achieved at 37°C should have been sufficiently fast to induce alternans, assuming that alternans threshold and fastest CL captured are indeed modified to the same extent by low temperature. It seems likely that some specific electrophysiological property present at low temperature is required for the induction of alternans. The data presented in Chapter 3 show that low temperature was associated with a global prolongation of APD₉₀, a reduction in transmural conduction velocity and a steeper maximal restitution slope. It is likely that the steeper restitution slope, along with the reduction in conduction velocity explain the increased occurrence of alternans at low temperature. Spatially discordant alternans did not occur in any normal heart at 37°C. However, using a similar estimate based on results at 30°C, spatially discordant alternans at 37°C would not be predicted to occur at the stimulation rates achieved in these experiments.

The requirement for low temperature to induce both alternans and spatially discordant alternans challenges the relevance of this paradigm to the induction of arrhythmia in normal hearts. However, a recent study has shown both concordant and discordant

alternans on the epicardial surface of rabbit hearts during rapid pacing at 37°C²¹³. A decremental pacing protocol was used and steady state pacing at a CL of 150-170ms (353-400bpm) resulted in APD₉₀ alternans of up to 10ms, with spatially discordant alternans occurring at around 140-150ms (400-429bpm). One possible explanation for the differences between the findings is likely to be the extent of the ventricular myocardium imaged. In the study by Mironov *et al*, the entire anterior and posterior surface of the ventricle was mapped, whereas the current study focussed on a smaller area. In addition, the definition of significant alternans employed was ≥ 3ms and alternans was not confirmed by spectral analysis. The magnitude of APD alternans reported is generally smaller than that seen in the current study. PseudoECGs were not recorded and it is therefore not clear whether the small magnitude of APD alternans seen at 37°C would have been reflected in the ECG. Importantly, Mironov *et al* did not report data regarding the occurrence of re-entrant arrhythmias during the spatially discordant alternans they observed. The importance of discordant alternans as a mechanism for the induction of ventricular arrhythmias at 37°C remains to be demonstrated.

Alternans occurring on the epicardial surface

There were no significant differences between the alternans recorded on the transmural and epicardial surfaces. As discussed in Chapter 3, the only difference between the electrophysiological parameters recorded on the epicardial surface compared with the transmural surface during endocardial stimulation at 30°C was a reduction in the dispersion of activation time. There was no significant difference in dispersion of APD₉₀ or in APD₉₀ restitution.

Limitations

In these experiments, an *in vitro* preparation was used, which was not exposed to the mechanical and autonomic inputs present *in vivo*. These may influence electrophysiology in general and alternans in particular. The use of mechanical uncouplers was required to reduce motion artefact during optical imaging. 2,3-BDM is known to have effects on AP restitution and so may conceivably have influenced alternans behaviour. Calcium is important in the development of cellular alternans and is likely to influence alternans development in tissue. Dual calcium and voltage imaging may therefore have given some supplementary information regarding the exact origins of alternans. In these studies, repolarisation alternans was accompanied by T-wave alternans in the pseudoECG, the best available experimental surrogate for MTWA. Although data from electrophysiological

studies in humans do suggest that monophasic AP alternans does occur during MTWA, it remains possible that different cellular processes to those described here underlie MTWA in human hearts.

Conclusions

This set of experiments has identified and characterised the occurrence of repolarisation alternans in rabbit ventricular myocardium. Like repolarisation alternans described under other experimental conditions, the alternans recorded in this study was heart rate and temperature dependent. Unlike other published accounts, the progression to spatially discordant alternans was not a consistent finding. However, both episodes of ventricular arrhythmia at 30°C did occur following an increase in stimulation rate during spatially discordant alternans.

During repolarisation alternans, changes in the AP were not limited to the repolarisation phase. Alternating changes in activation time and AP amplitude were also found. This suggests that an interplay between conduction and repolarisation occurs during alternans. The transmural magnitude of alternans was modulated by activation sequence, in a similar manner to that described for APD₉₀ in Chapter 4. Sites distant to the stimulus displayed a greater degree of alternans. This points to the importance of dynamic mechanisms in determining alternans in ventricular myocardium. The temperature dependence of alternans could be explained by an interplay of slow conduction and steep APD₉₀ restitution at low temperature, as described in Chapter 3. Considering these findings together suggests that the electrophysiological basis for the alternans seen here involves slowed conduction interacting with changes in repolarisation, perhaps caused by steep restitution, to produce alternans of both APD₉₀ and AP amplitude.

The near absolute requirement for low temperature, along with the very rapid stimulation rates required to induce alternans challenge the relevance of this paradigm to the induction of re-entrant arrhythmia in normal hearts.

Chapter 7: Repolarisation alternans and arrhythmogenesis in heart failure

Introduction

Microvolt T-wave alternans occurs at low heart rates in patients with heart failure and left ventricular systolic dysfunction following myocardial infarction, particularly in those with prior ventricular arrhythmia³⁸. There is some clinical evidence that the presence of MTWA at low heart rates may predict the future occurrence of ventricular arrhythmia⁵⁴, although recent evidence is conflicting^{52;63}. Alternans of cellular repolarisation is thought to underlie MTWA^{40;66}. In isolated guinea-pig epicardium at short pacing cycle lengths, spatially discordant repolarisation alternans is associated with extreme gradients of repolarisation, unidirectional conduction block and re-entrant ventricular arrhythmia⁴⁰. This provides a potential mechanistic link between alternans and arrhythmia. However, as outlined in Chapter 1, repolarisation alternans has not been investigated in clinically relevant models of pathology. This set of experiments was designed to examine the occurrence and consequences of repolarisation alternans in a rabbit model of heart failure.

Alternans in heart failure

Investigation of contractile dysfunction has demonstrated that mechanical alternans occurs more readily in heart failure^{138;139}. Calcium transient alternans was observed with rapid pacing in mice over-expressing cardiac TNF α ¹⁴⁰, but this was not mechanistically linked to arrhythmia. Although the transgenic animals developed a heart failure syndrome, they displayed an overall reduction in heart rate. There were no tachyarrhythmic deaths, indicating important differences from human heart failure. In canine hearts following MI, alternation of the area under the QRST deflection on unipolar electrograms was found to be of greater magnitude in animals with inducible VF²¹⁵. A lowered heart rate threshold for discordant repolarisation alternans has been observed in canine pacing-induced heart failure, a model that has previously been shown to display a two-fold increase in transmural dispersion of repolarisation compared with controls¹⁴⁶. The hypothesis is that heart failure gives rise to increased electrophysiological heterogeneity, which would be expected to increase propensity to discordant repolarisation alternans. However, this has yet to be shown definitively.

Aims

To determine whether repolarisation alternans and spatially discordant alternans occur more readily in failing hearts.

To explore the effect of heart failure on the onset, patterns and consequences of repolarisation alternans across the transmural surface of intact rabbit left ventricle

To investigate whether repolarisation alternans and spatially discordant alternans lead to ventricular arrhythmia in failing hearts.

Methods

In order to investigate transmural alternans in intact rabbit left ventricular tissue the CCD-based optical mapping system described in Chapter 2 was used to record optical action potentials from the transmural surface of perfused left ventricular wedge preparations in the rabbit. Hearts from 32 male New Zealand White rabbits were used in these experiments, which conform to standards set out in the UK Animals (Scientific Procedures) Act, 1986.

Experimental protocols

The left ventricular wedge preparations ($n = 32$) used in this set of experiments were prepared as described in Chapter 2. Perfusion was at 37°C ($n = 16$) except where low temperature was specifically investigated ($n = 16$).

Data analysis

Data analysis was performed as described in Chapter 2.

Statistical analyses

All data are expressed as mean \pm SEM. Groups of data were compared using a Student's t-test (paired where appropriate), or when more than two groups were compared, using a repeated measures ANOVA with post-hoc Tukey-Kramer multiple comparisons testing. All statistical analyses were performed using GraphPad software.

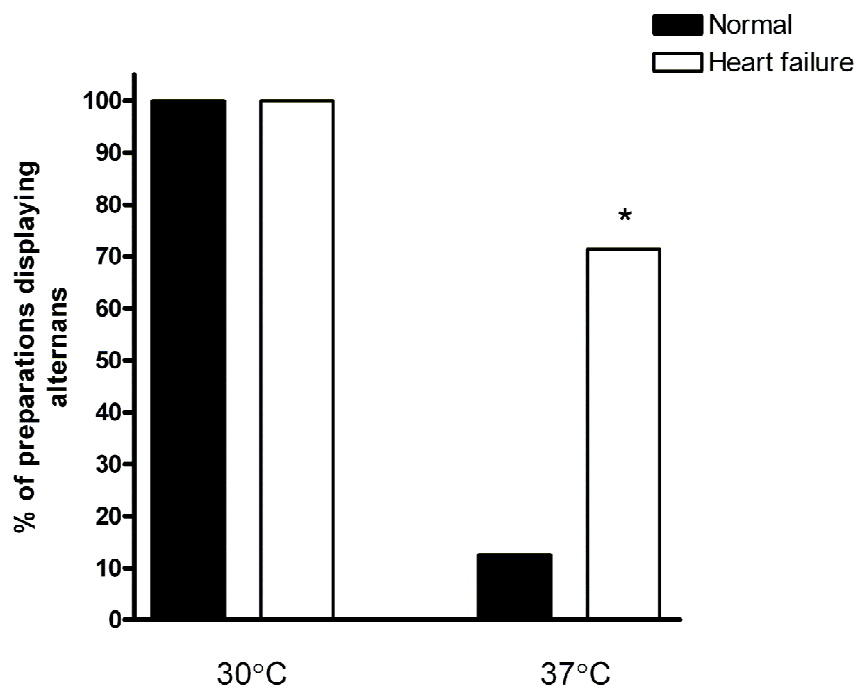
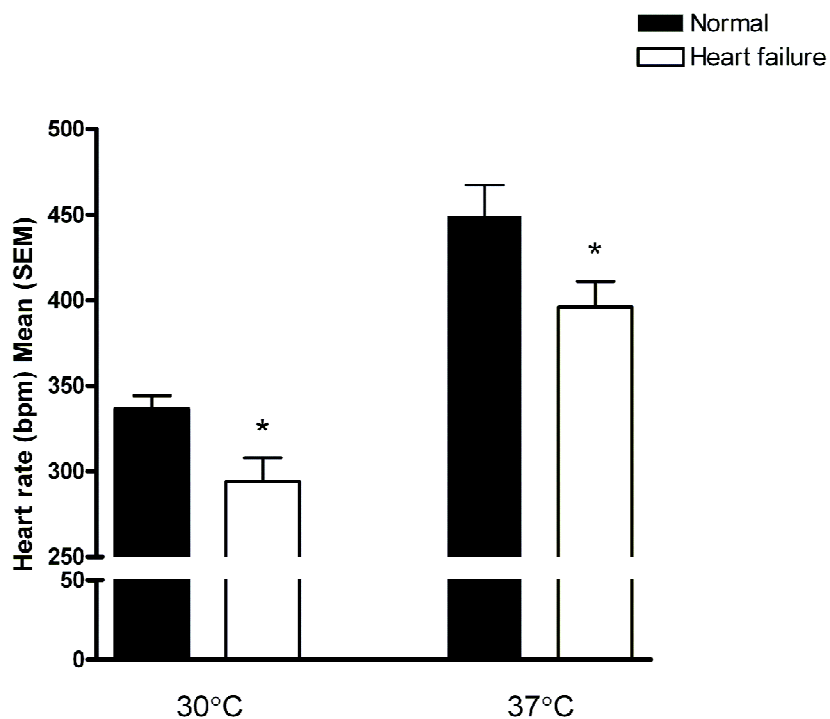
Results

The occurrence of repolarisation alternans in heart failure

Repolarisation alternans occurred in a total of 22/31 rapid pacing protocols (71%). The inducibility of repolarisation alternans during rapid pacing in normal hearts was compared with that in failing hearts. Figure 7.1A compares the inducibility of repolarisation alternans during rapid pacing in normal and failing hearts at low (30°C) and normal (37°C) temperature. Figure 7.1B compares the heart rate thresholds for repolarisation alternans in normal and failing hearts at 30°C and 37°C . The heart rate threshold for alternans is expressed as the fastest stimulation rate without significant alternans. At low temperature repolarisation alternans was elicited in all normal (9/9) and all failing hearts (7/7). The heart rate threshold for alternans was significantly lower in failing hearts than in normal hearts at 30°C ($294 \pm 14\text{bpm}$ vs. $337 \pm 7\text{bpm}$, $p = 0.0107$). At physiological temperature, failing hearts were significantly more likely to develop repolarisation alternans, which occurred in 5/7 failing hearts compared with 1/8 normal hearts ($p = 0.0406$). At 37°C the heart rate threshold for alternans was also significantly lower in failing hearts compared with normal hearts ($396 \pm 18\text{bpm}$ vs. $449 \pm 14\text{bpm}$, $p = 0.0349$). Of the 7 normal hearts which did not develop repolarisation alternans at 37°C , all captured to a CL of at least 400bpm (mean $442 \pm 19\text{bpm}$).

Spatially discordant alternans in heart failure

Spatially discordant alternans was observed in 1/14 failing hearts, compared with 3/17 normal hearts ($p = 0.6067$). Transmural spatially discordant alternans was seen in a single failing heart at 30°C . In this particular heart, discordant alternans was not preceded by concordant alternans, and was induced at a cycle length of 200ms (300bpm). Transmural discordant alternans persisted through rapid stimulation and this heart went on to develop a ventricular arrhythmia during a shortening of CL from 160 to 150ms. Transmural spatially discordant alternans was never observed at 37°C , either in normal or failing hearts.

A.**B.****Figure 7.1 The occurrence of repolarisation alternans in normal and failing hearts**

A. The proportion of preparations displaying alternans at 30°C and 37°C in normal (black bars, n = 9 at 30°C, n = 8 at 37°C) and heart failure (white bars, n = 7 at each temperature). Fishers exact test, * p < 0.05. B. The heart rate threshold for alternans (expressed as the fastest HR without alternans) at 30°C and 37°C in normal (black bars, n = 9 at 30°C, n = 8 at 37°C) and heart failure (white bars, n = 7 at each temperature). Unpaired t-test, * p < 0.05.

Extent and magnitude of repolarisation alternans in normal and failing hearts

A comparison of the extent and magnitude of repolarisation alternans at 30°C is shown in Figure 7.2. The number of preparations displaying significant alternans was higher in failing hearts at low stimulation rates. There were no significant differences between normal and failing hearts in terms of mean alternans magnitude at any pacing cycle length, peak magnitude of alternans (64 ± 14 [n = 9] vs. 73 ± 38 [n = 7], p = 0.8105), maximal heterogeneity of alternans (31 ± 9 [n = 9] vs. 38 ± 24 [n = 7], p = 0.7686) or the peak extent of transmural alternans ($68 \pm 10\%$ [n = 9] vs. $50 \pm 13\%$ [n = 7], p = 0.2825).

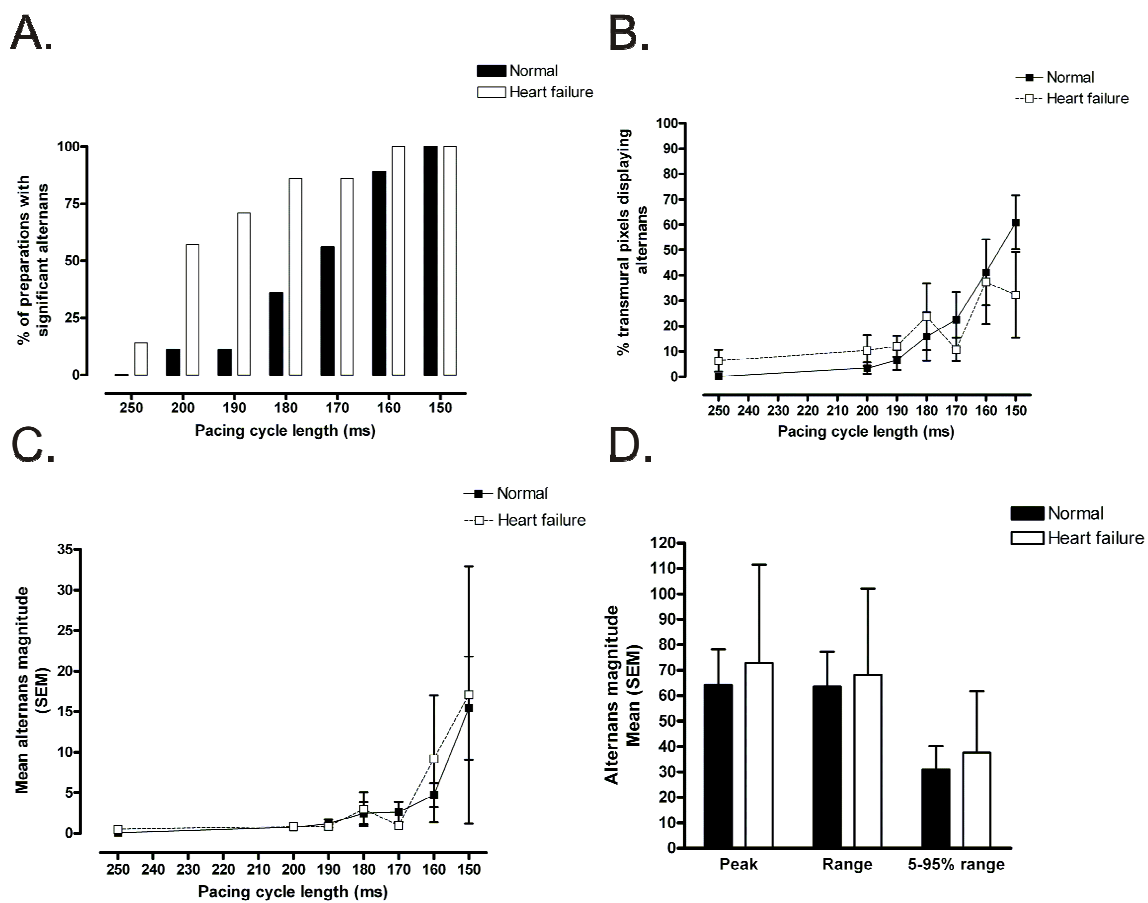


Figure 7.2 The magnitude and extent of transmural repolarisation alternans in normal and failing hearts

A. The percentage of preparations which displayed significant alternans at each pacing CL in normal (black bars) and failing hearts (white bars). B. The proportion of transmural pixels which showed significant alternans at each pacing CL in normal (closed squares) and failing hearts (open squares). C. Mean alternans magnitude at each pacing CL in normal and failing hearts. D. Comparison of peak alternans magnitude, range of alternans magnitude and 5-95% range of alternans magnitude in normal and failing hearts. Normal hearts, n = 9 at 250ms and n = 6 at 150ms. Failing hearts, n = 7 at 250ms and n = 4 at 150ms.

Transmural gradients of repolarisation alternans in heart failure

In failing hearts at 30°C, the site of earliest alternans was in the subepicardium in 5/7 cases and in the subendocardium in 2/7 cases. The site of maximal alternans was in the subepicardium in 5/7 cases. As shown in Figure 7.3, similar transmural patterns of alternans were seen in failing hearts as were described for normal hearts in Chapter 6, with greater alternans magnitude at the subepicardium. However, in the group of failing hearts the interheart variability was greater than that seen in normal hearts. Consequently, the differences in alternans magnitude between different transmural regions were not significant.

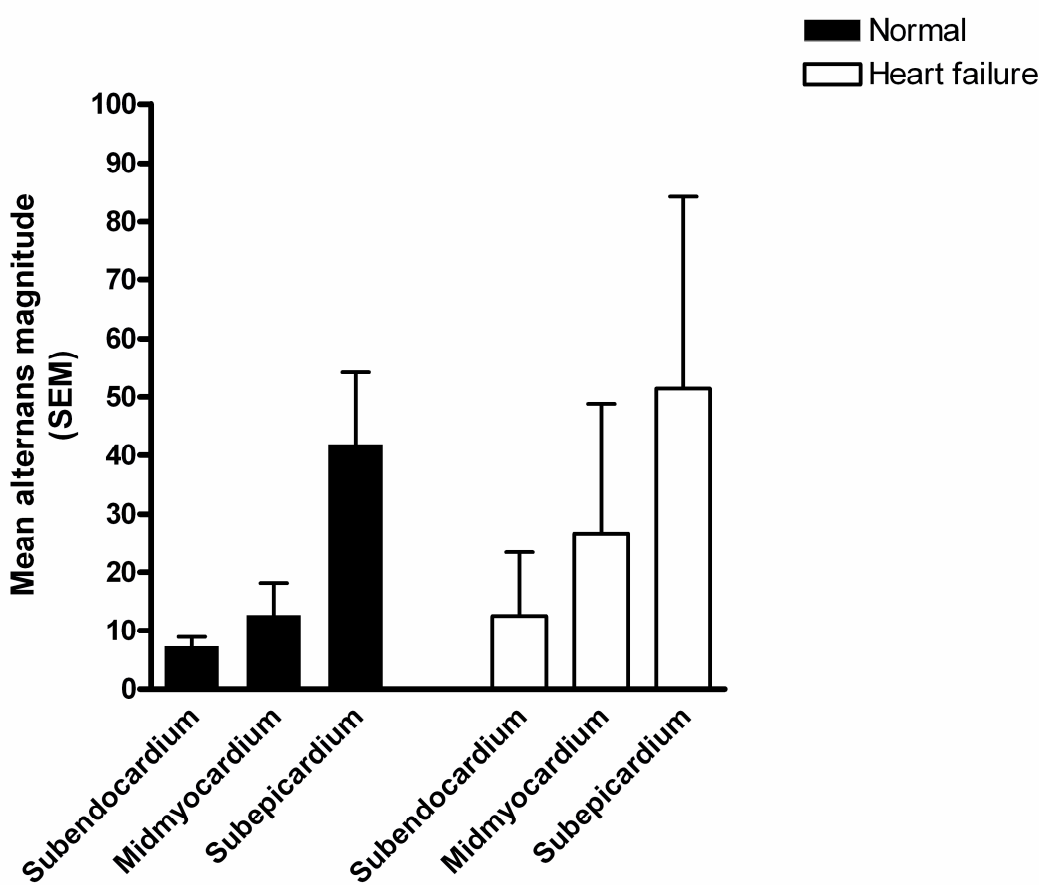


Figure 7.3 Transmural alternans magnitude in normal and failing hearts

A comparison of mean alternans magnitude (at maximal alternans for each preparation) in different transmural regions in normal (black bars, n = 9) and failing hearts (white bars, n = 7). One-way ANOVA, p = 0.2938.

Alternans and APD₉₀ restitution in heart failure

In order to examine the role of APD₉₀ restitution in the increased vulnerability to alternans in failing hearts, separate APD₉₀ restitution curves were constructed for sites which were prone to and resistant to the development of repolarisation alternans. Alternans prone sites were defined as those pixels which displayed significant alternans at the slowest stimulation rate. Other transmural sites were considered alternans resistant. There were no significant differences in the Y_{max} values or rate constants associated with the exponential curve fits, as shown in Table 7.1. In both normal and failing hearts, the maximal APD restitution slope in alternans prone sites was significantly greater than the maximal restitution slope found in alternans resistant sites. The maximal slope of the APD₉₀ restitution curve in alternans prone sites in failing hearts (3.22 ± 0.14) was greater than the maximal slope in alternans prone sites in normal hearts (2.58 ± 0.12), but this difference did not reach statistical significance after multiple comparisons testing.

Table 7.1 APD₉₀ restitution curve characteristics in alternans prone and resistant sites in normal and failing hearts

Mean (SEM)	Normal (n = 9)		Heart failure (n = 7)		<i>P</i> value
	Prone	Resistant	Prone	Resistant	
Y _{max}	171.5 ± 3.7	171.1 ± 2.2	170.4 ± 3.8	164.4 ± 2.7	0.4017
Rate constant	0.0277 ± 0.0016	0.0257 ± 0.0008	0.0230 ± 0.0013	0.0249 ± 0.0011	0.0899
Maximal slope	2.58 ± 0.12	$1.25 \pm 0.17^*$	3.22 ± 0.14	$1.30 \pm 0.29^{**}$	< 0.0001

SEM, standard error of the mean. *P* value refers to a one-way ANOVA in each case. * *p* < 0.001 vs. alternans prone sites in normal hearts, ** *p* < 0.001 vs. alternans prone sites in failing hearts.

Transmural dispersion during alternans

Transmural dispersion of activation time, repolarisation time and APD₉₀ were calculated for each pacing cycle length in normal and failing hearts. These data were then separated into two groups representing alternans prone and resistant areas.

Transmural dispersion of activation time

The results for transmural dispersion of activation time at 30°C are shown in Figure 7.4. There was a non-significant trend towards an increase in dispersion of activation time during rapid stimulation. In normal hearts there was no significant difference in dispersion of activation time between alternans prone and alternans resistant areas at any stimulation rate (Figure 7.4A (i)). In failing hearts, dispersion of activation time was significantly greater in alternans prone areas compared to alternans resistant areas at all stimulation rates (Figure 7.4A (ii)). There were no significant difference between normal and failing hearts in the dispersion of activation time associated with alternans prone (Figure 7.4B (i)) or alternans resistant areas (Figure 7.4B (ii)).

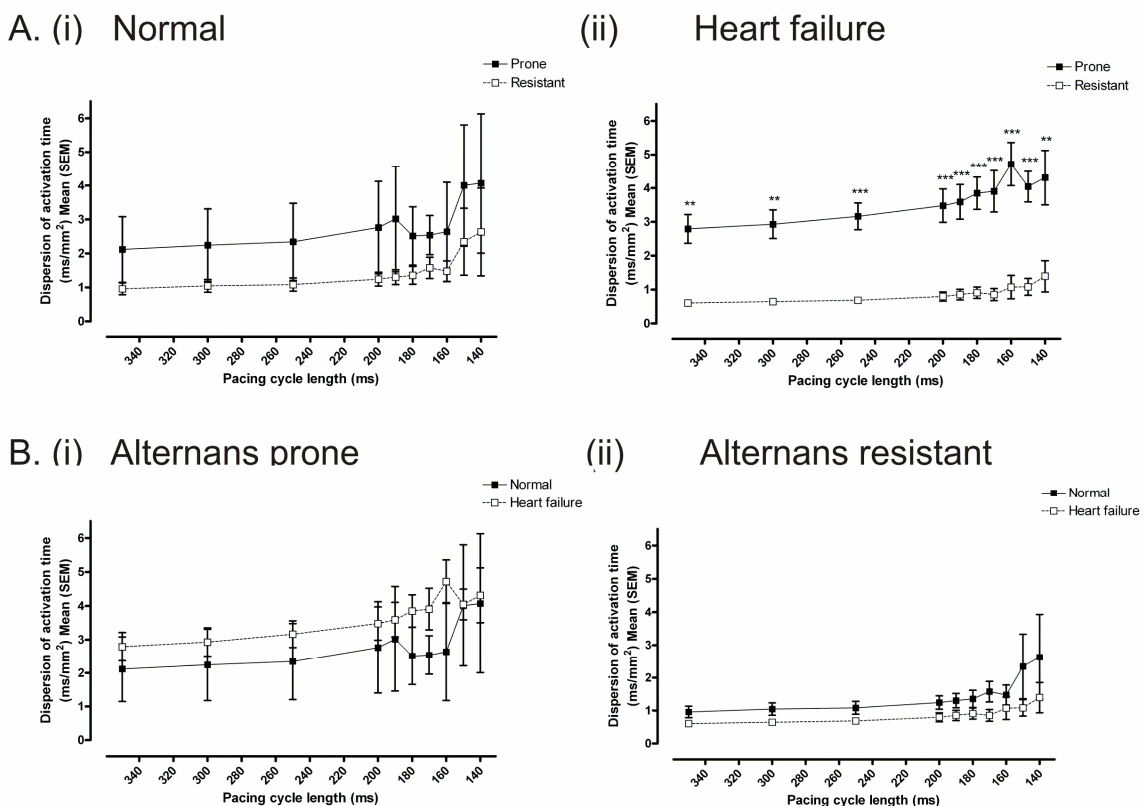


Figure 7.4 The relationship between transmural dispersion of activation time and cycle length

A. (i) Mean dispersion of activation time as a function of cycle length in alternans prone regions (closed squares and solid line) and alternans resistant regions (open squares and dashed line) in normal hearts ($n = 9$). (ii) Mean dispersion of activation time as a function of cycle length in alternans prone regions (closed squares and solid line) and alternans resistant regions (open squares and dashed line) in failing hearts ($n = 7$). B. (i) Mean dispersion of activation time as a function of cycle length in alternans prone regions in normal hearts ($n = 9$, closed squares and solid line) and failing hearts ($n = 7$, open squares and dashed line). (ii) Mean dispersion of activation time as a function of cycle length in alternans resistant regions in normal hearts ($n = 9$, closed squares and solid line) and failing hearts ($n = 7$, open squares and dashed line). One-way ANOVA with Tukey-Kramer post tests, ** $p < 0.01$, *** $p < 0.001$.

Transmural dispersion of repolarisation time

The results for transmural dispersion of repolarisation time at 30°C are shown in Figure 7.5. There was no significant or consistent change in dispersion of repolarisation time during rapid pacing. In normal hearts there was no significant difference in dispersion of activation time between alternans prone and alternans resistant areas at any stimulation rate (Figure 7.5A (i)). In failing hearts dispersion of repolarisation time was significantly greater in alternans prone areas compared to alternans resistant areas at cycle lengths of 350-250ms, but not at shorter CLs (Figure 7.5A (ii)). There were no significant difference between normal and failing hearts in the dispersion of repolarisation time associated with alternans prone (Figure 7.5B (i)) or alternans resistant areas (Figure 7.5B (ii)).

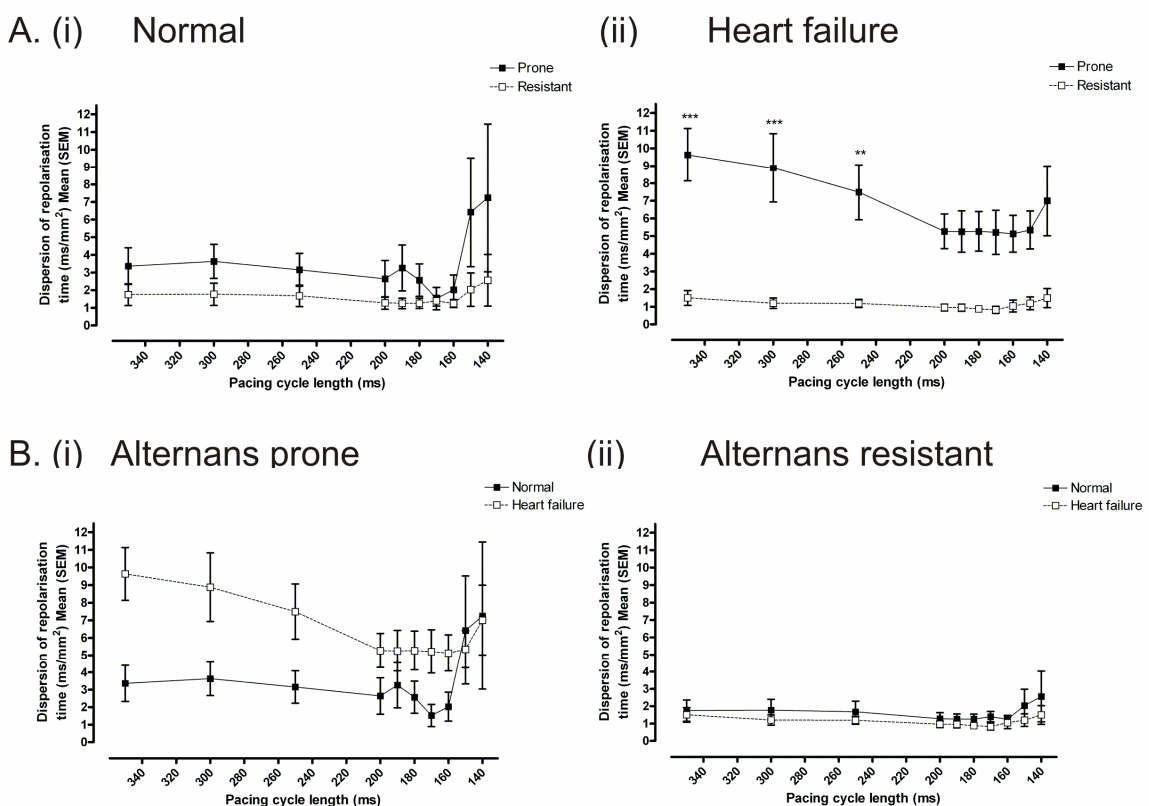


Figure 7.5 The relationship between transmural dispersion of repolarisation time and cycle length

A. (i) Mean dispersion of repolarisation time as a function of cycle length in alternans prone regions (closed squares and solid line) and alternans resistant regions (open squares and dashed line) in normal hearts ($n = 9$). (ii) Mean dispersion of repolarisation time as a function of cycle length in alternans prone regions (closed squares and solid line) and alternans resistant regions (open squares and dashed line) in failing hearts ($n = 7$). B. (i) Mean dispersion of repolarisation time as a function of cycle length in alternans prone regions in normal hearts ($n = 9$, closed squares and solid line) and failing hearts ($n = 7$, open squares and dashed line). (ii) Mean dispersion of repolarisation time as a function of cycle length in alternans resistant regions in normal hearts ($n = 9$, closed squares and solid line) and failing hearts ($n = 7$, open squares and dashed line). One-way ANOVA with Tukey-Kramer post tests, ** $p < 0.01$, *** $p < 0.001$.

Transmural dispersion of APD₉₀

The results for transmural dispersion of APD₉₀ at 30°C are shown in Figure 7.6. There was no significant or consistent change in dispersion of APD₉₀ time during an increase in stimulation rate. In normal hearts there was no significant difference in dispersion of APD₉₀ between alternans prone and alternans resistant areas at any stimulation rate (Figure 7.6A (i)). In failing hearts dispersion of APD₉₀ was significantly greater in alternans prone areas compared to alternans resistant areas at cycle lengths of 350-250ms (Figure 7.6A (ii)). Alternans prone areas in failing hearts were associated with a greater dispersion of APD₉₀ than alternans prone areas in normal hearts at the longest CLs (Figure 7.6B (i)). There were no significant difference between normal and failing hearts in the dispersion of repolarisation time associated with alternans resistant areas (Figure 7.6B (ii)).

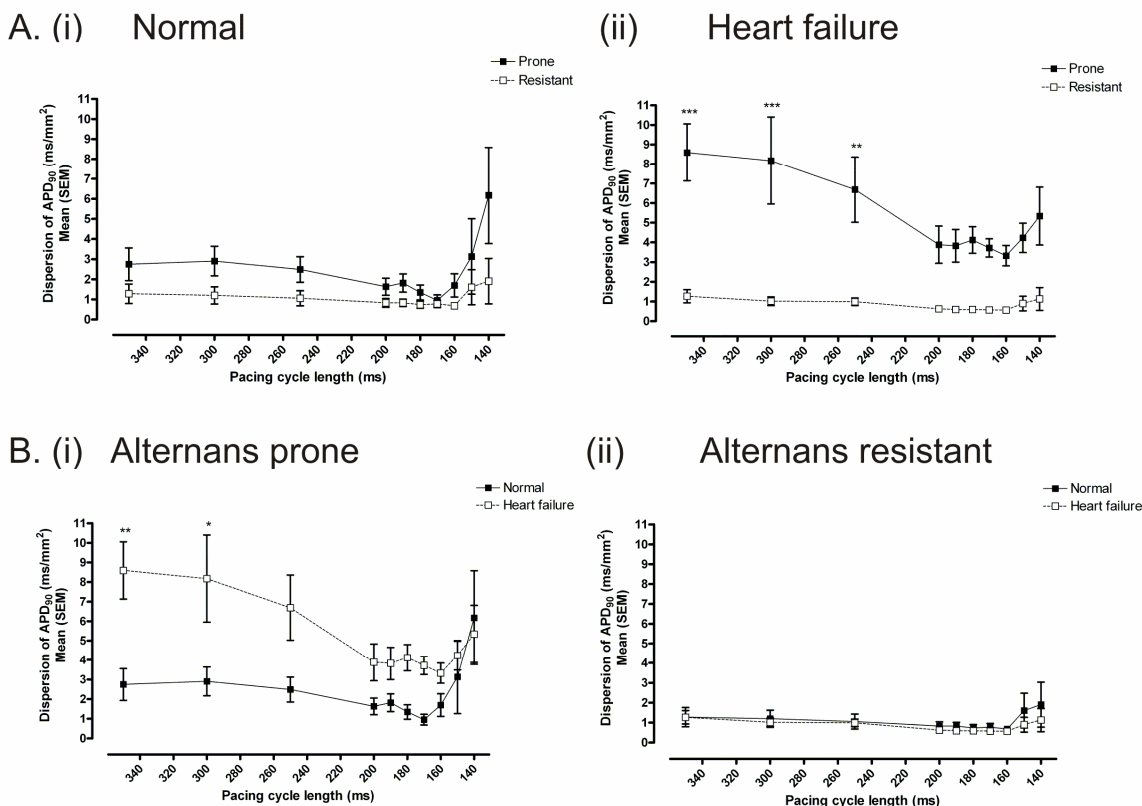


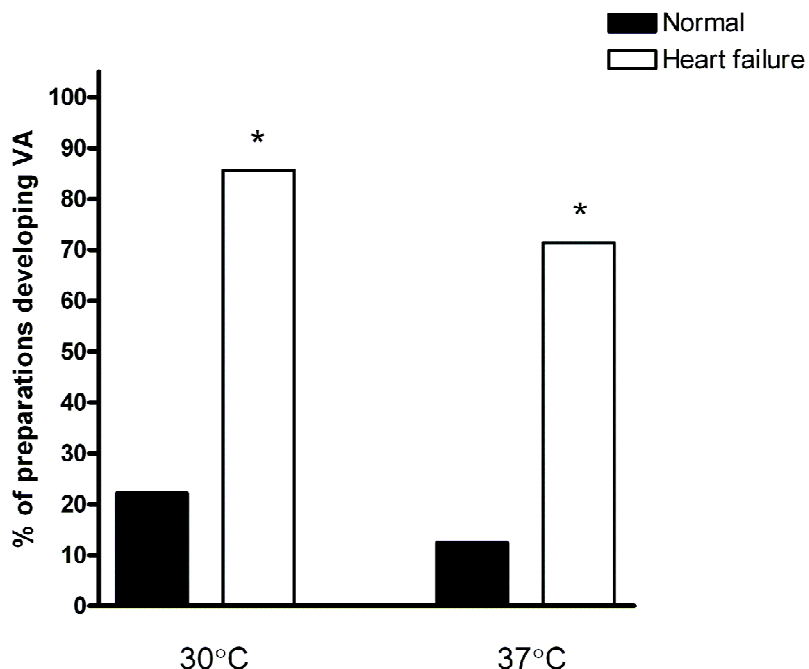
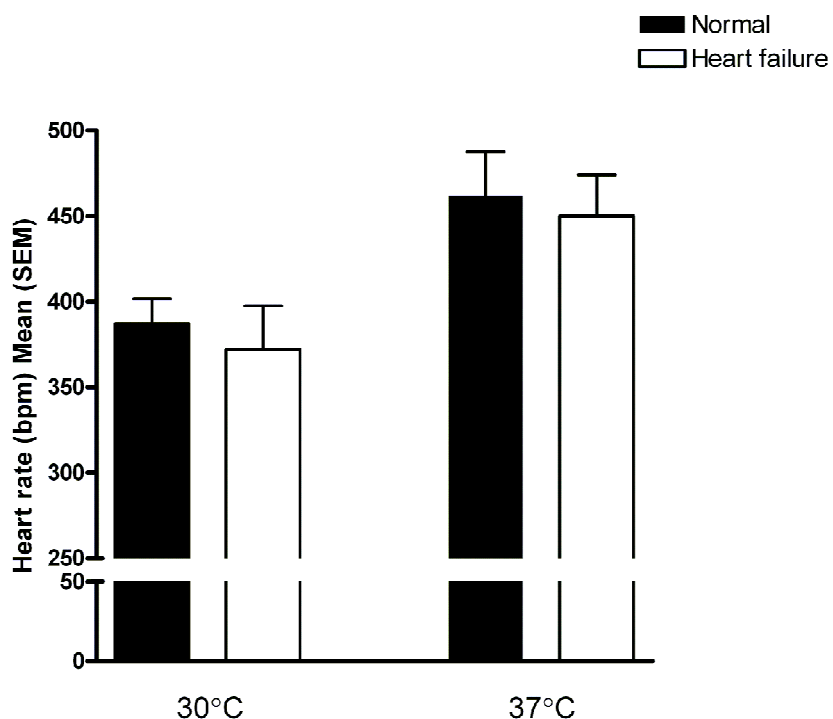
Figure 7.6 The relationship between transmural dispersion of APD₉₀ and cycle length

A. (i) Mean dispersion of APD₉₀ as a function of cycle length in alternans prone regions (closed squares and solid line) and alternans resistant regions (open squares and dashed line) in normal hearts ($n = 9$). (ii) Mean dispersion of APD₉₀ as a function of cycle length in alternans prone regions (closed squares and solid line) and alternans resistant regions (open squares and dashed line) in failing hearts ($n = 7$). B. (i) Mean dispersion of APD₉₀ as a function of cycle length in alternans prone regions in normal hearts ($n = 9$, closed squares and solid line) and failing hearts ($n = 7$, open squares and dashed line). (ii) Mean dispersion of APD₉₀ as a function of cycle length in alternans resistant regions in normal hearts ($n = 9$, closed squares and solid line) and failing hearts ($n = 7$, open squares and dashed line). One-way ANOVA with Tukey-Kramer post tests, ** $p < 0.01$, *** $p < 0.001$.

Ventricular arrhythmias in heart failure

The inducibility of ventricular arrhythmias during rapid pacing protocols was compared in normal and failing hearts. A total of 14 ventricular arrhythmias occurred during 31 rapid pacing protocols (45%). All episodes of ventricular arrhythmia were sustained, in that they lasted > 30 seconds or required intervention to terminate them. 11 arrhythmias occurred in 14 failing hearts (79%) and 3 arrhythmias in 17 normal hearts (18%, $p = 0.0011$). Figure 7.7A compares the inducibility of ventricular arrhythmia during rapid pacing in normal and failing hearts at low (30°C) and normal (37°C) temperature. Figure 7.7B compares the heart rate thresholds for ventricular arrhythmia in normal and failing hearts at 30°C and 37°C . The heart rate threshold is expressed as the fastest stimulation rate without VA, and therefore equates to the fastest stimulation rate supported 1:1 by the preparation.

At low temperature, ventricular arrhythmias were induced by rapid pacing in 2/9 normal and 6/7 failing hearts ($p = 0.0408$). At 30°C the fastest stimulation rate followed 1:1 was not significantly different between normal and failing hearts ($387 \pm 14\text{bpm}$ vs. $372 \pm 25\text{ bpm}$, $p = 0.5881$). Of the 7 normal hearts which did not develop an arrhythmia at 30°C , all captured to a CL of at least 333bpm (mean $371 \pm 12\text{bpm}$). At physiological temperature, failing hearts were significantly more likely to develop ventricular arrhythmias. VA occurred in 5/7 failing hearts compared with 1/8 normal hearts ($p = 0.0408$). At 37°C the fastest stimulation rate followed 1:1 was not significantly different between normal and failing hearts ($462 \pm 26\text{bpm}$ vs. $450 \pm 24\text{ bpm}$, $p = 0.7425$). Of the 7 normal hearts which did not develop an arrhythmia at 37°C , all captured to a CL of at least 400bpm (mean $450 \pm 26\text{bpm}$).

A.**B.****Figure 7.7 Inducibility of ventricular arrhythmias in failing and normal hearts**

A. The proportion of preparations which developed ventricular arrhythmia at 30°C and 37°C in normal (black bars, n = 9 at 30°C, n = 8 at 37°C) and heart failure (white bars, n = 7 at each temperature). Fishers exact test, * p < 0.05. B. The heart rate threshold for ventricular arrhythmia (expressed as the fastest HR without VA) at 30°C and 37°C in normal (black bars, n = 9 at 30°C, n = 8 at 37°C) and heart failure (white bars, n = 7 at each temperature).

The relationship between alternans and ventricular arrhythmia

Concordant alternans and ventricular arrhythmias during rapid pacing

At 30°C, ventricular arrhythmias were elicited during rapid pacing in 8/16 hearts. All hearts at 30°C displayed alternans at the shortest CL captured. Consequently, all episodes of VA at 30°C occurred in the context of pre-existing transmural alternans. 8/16 hearts displayed concordant alternans but did not develop ventricular arrhythmia during rapid pacing. Of these, 1/8 was a failing heart and 7/8 were normal hearts.

At 37°C ventricular arrhythmias were elicited during rapid pacing in 6/15 hearts. 4/6 (66%) episodes of VA occurred in hearts which displayed repolarisation alternans directly prior to the induction of the arrhythmia. 2/6 episodes of ventricular arrhythmia at 37°C occurred in hearts which did not display alternans (one normal heart and one failing heart). 2/15 hearts displayed alternans but did not develop ventricular arrhythmia during rapid pacing (one normal heart and one failing heart).

Discordant alternans and ventricular arrhythmias during rapid pacing

Spatially discordant alternans was observed in 4/31 hearts (1/14 failing hearts and 3/17 normal hearts). Transmural spatially discordant alternans was never observed at 37°C, either in normal or failing hearts. Of the 8 VA episodes at 30°C, 3 were preceded by transmural discordant alternans (1 failing heart and 2 normal hearts). Discordant alternans did not precede any of the 6 episodes of VA at 37°C.

Alternans magnitude and ventricular arrhythmias

The numbers in each group precluded separate comparisons between alternans magnitude in those preparations which did and did not develop VA in normal ($n = 2$ and 7 respectively) and failing hearts ($n = 6$ and 1 respectively). For these comparisons normal and failing hearts were considered together and alternans magnitude was compared between those preparations which did and did not develop VA during rapid pacing ($n = 8$ in each group). There was no significant difference in the shortest cycle length captured ($154 \pm 4\text{ms}$ no VA vs. 168 ± 13 with VA, $p = 0.3208$). The results of the comparison of alternans magnitude are shown in Table 7.2. There was no significant difference in the mean alternans magnitude, peak alternans magnitude or heterogeneity of alternans. Similarly, there was no difference in the extent of transmural alternans in those preparations which did and did not develop ventricular arrhythmia.

Table 7.2 Magnitude and extent of alternans according to the subsequent occurrence of ventricular arrhythmia

Mean (SEM)	No VA (n = 8)	VA (n = 8)	P value
Mean alternans magnitude	12 ± 5	26 ± 15	0.3909
Peak alternans magnitude	49 ± 14	83 ± 33	0.3590
Heterogeneity of alternans	25 ± 10	41 ± 21	0.5028
% of surface displaying alternans	$62 \pm 12\%$	$62 \pm 13\%$	1.0000

SEM, standard error of the mean. VA, ventricular arrhythmia. P value refers to an unpaired t-test in each case.

Discussion

The occurrence of repolarisation alternans in heart failure

These experiments show that experimental heart failure is associated with an increased vulnerability to repolarisation alternans. At low temperature, all normal and failing hearts developed repolarisation alternans during rapid stimulation. The heart rate threshold for alternans was significantly lower in failing hearts. Importantly, at physiological temperature repolarisation alternans was very rarely elicited in normal hearts, but was consistently elicited with rapid pacing in failing hearts. Again, the stimulation rate threshold for the induction of repolarisation alternans was significantly lower in failing hearts. In order to make these comparisons, alternans threshold was expressed as the fastest stimulation rate without alternans. This definition was used as it allowed comparison of alternans thresholds between groups when only small numbers of preparations in one group developed alternans. However, this definition could be influenced by differences in the fastest stimulation rate supported by the preparations in each group. It is therefore important to note that there were no significant differences in the fastest stimulation rates achieved in normal and failing hearts at each temperature. Moreover, all of the normal hearts which did not develop alternans at 37°C captured to rates at least as fast as the mean threshold for alternans in failing hearts at 37°C. Together these data provide convincing evidence that failing hearts are more prone to develop repolarisation alternans than normal hearts, irrespective of temperature and stimulation rate. As discussed in Chapter 1, one of the gaps in our current knowledge of the clinical relevance of repolarisation alternans is that it has not been investigated in experimental models relevant to the pathologies which cause MTWA in man. Therefore, these data considerably strengthen the pathophysiological correlation between MTWA and experimental repolarisation alternans.

Spatially discordant alternans in heart failure

Spatially discordant alternans was not a common occurrence in these experiments. Moreover, spatially discordant alternans did not appear to be more common in failing hearts. It is possible that the stimulation rates achieved were not sufficiently fast to induce discordant alternans. However, given that around half of the preparations which did not develop spatially discordant alternans captured at a faster rate than the threshold for spatially discordant alternans, insufficient stimulation rates are unlikely to account fully for the lack of spatially discordant alternans in these hearts. As discussed in Chapter 6, it is

more likely that spatially discordant alternans was occurring in other parts of the preparation not within the transmural imaging window.

Magnitude and extent of alternans in heart failure

The data from these experiments do not support the idea that alternans magnitude is greater in failing hearts. Comparisons of spectrally-derived alternans magnitude were made at the CL with maximal alternans (which was always the shortest CL captured) in order to maximise numbers for comparison. Despite this, the comparison was complicated by significant inter-heart variability and in this context it is possible that the group sizes were too small to detect a difference in mean alternans magnitude. However, even comparing the peak value, the heterogeneity of alternans (reflected in the range and 5-95% range) and the transmural extent of alternans failed to show a difference between normal and failing hearts in terms of alternans magnitude.

Transmural gradients of alternans in heart failure

The transmural gradients of alternans magnitude observed in failing hearts were qualitatively similar to those described for normal hearts in Chapter 6. This suggests that the same interaction between underlying cellular heterogeneity and electrotonic influences determine alternans magnitude in failing hearts.

APD₉₀ restitution and alternans in heart failure

It appears from the data presented here that areas of the myocardium prone to alternans have steeper maximal APD₉₀ restitution slopes than those without alternans. This was the case in both normal and failing myocardium. Steep restitution may be associated with the induction of alternans and is likely to be one of the factors driving the development and maintenance of alternans in tissue²¹⁶. As described in Chapter 5, APD₉₀ restitution was not found to be significantly steeper in failing hearts. This remains true when alternans prone areas are specifically examined. It therefore appears that although vulnerability to alternans is associated with areas of steeper restitution, this does not explain the increased vulnerability to alternans seen in failing hearts.

Vulnerability to ventricular arrhythmia in heart failure

The ventricular arrhythmias observed in these experiments were generally sustained, in contrast to some experimental models where ventricular arrhythmias are self-terminating within a short timescale¹⁴⁶. At each temperature, VA were more common in failing hearts than in normal hearts. Clearly, ventricular arrhythmias may simply be a function of stimulation rate. It is therefore important to consider differences in the stimulation rates achieved when comparing the inducibility of ventricular arrhythmias during rapid pacing. In these experiments there was no significant difference in the fastest stimulation rate supported in normal and failing hearts at each temperature. This suggests that the differences in VA between normal and failing hearts is not due to stimulation rate. These data therefore confirm that this experimental model of heart failure is associated with an increased vulnerability to ventricular arrhythmias.

Spatially discordant alternans and re-entrant ventricular arrhythmia

Published accounts of discordant repolarisation alternans emphasise the key role of discordant alternans in the induction of re-entrant ventricular arrhythmias. In contrast to this, in the majority of cases in the current study, discordant alternans was not observed prior to the development of ventricular arrhythmia. In particular, discordant alternans did not precede any ventricular arrhythmias in failing hearts at physiological temperature. These are precisely the most clinically relevant experimental circumstances, and those in which discordant alternans has not previously been investigated. In mitigation of these conclusions, as there were no ECG correlates of discordant alternans it was not possible to determine whether it may have been present in another part of the preparation. It therefore remains possible that discordant alternans was associated with the induction of re-entrant VA in these experiments.

Limitations

These experiments used an *in vitro* preparation, which did not have normal mechanical and autonomic inputs which may influence alternans *in vivo*. Moreover, although a clinically relevant model of heart failure was used deliberately in these experiments, animal models are unable to replicate exactly the behaviour of a human heart. Ventricular arrhythmias were more easily inducible in failing hearts during rapid pacing, and this is interpreted as representing a pro-arrhythmic substrate associated with experimental heart failure. However, although inducible arrhythmias are associated with an increased risk of sudden

cardiac death in patients with post-infarction heart failure, inducible arrhythmias are not a surrogate for spontaneous re-entry.

Conclusions

These experiments demonstrate an increased vulnerability to repolarisation alternans in a rabbit model of heart failure following myocardial infarction. This finding is an important step in investigating the possible mechanistic link between alternans and arrhythmia. The increased vulnerability to alternans in failing hearts places the experimental paradigm in a clinically relevant model of pathology. Failing hearts were also more vulnerable to ventricular arrhythmia during rapid pacing. As regards the progression from alternans to re-entry, these experiments fail to demonstrate an association between spatially discordant alternans and the development of ventricular arrhythmia, in particular in failing hearts and at physiological temperature. In summary, although heart failure was associated with both alternans and ventricular arrhythmia, alternans could not be mechanistically linked to ventricular arrhythmias in failing hearts. Equally, these results do not disprove such an association and underline the complexity inherent in investigating the induction of ventricular arrhythmias.

Chapter 8: Summary and conclusions

Rationale for the current study

The aim of this thesis was to investigate experimental repolarisation alternans in heart failure, and to examine if there may be a mechanistic link between alternans and the induction of ventricular arrhythmias in failing hearts. These aims were developed using an established background of both basic and clinical science knowledge regarding alternans. Patients with heart failure are more prone to MTWA and to ventricular arrhythmias³⁸ and MTWA testing may be a potentially useful risk stratification tool for sudden cardiac death²¹². Repolarisation alternans underlies MTWA and spatially discordant alternans has been linked experimentally to the induction of re-entrant ventricular arrhythmias⁴⁰. This work aimed to bridge an important gap in the current state of knowledge regarding repolarisation alternans by examining it in an experimental model of heart failure. The focus was on developing a clinically relevant understanding of the basic science which could not only improve our knowledge of arrhythmia mechanisms in heart failure but may also help to inform clinical use of MTWA testing.

Aims and hypotheses

This study was designed to investigate whether increased regional heterogeneity of repolarisation as a result of heart failure would predispose to the development of arrhythmogenic spatially discordant alternans. The hypotheses were that in the presence of alternans, at a given cycle length, the transmural pattern of alternans would be dependent on intrinsic cellular repolarisation properties, and hence, independent of stimulus site. Heterogeneity of alternans would increase with stimulation rate until discordant alternans developed. Discordant alternans would be a necessary pre-condition for unidirectional conduction block and re-entry. In heart failure, that increased transmural heterogeneity of repolarisation in the surviving hypertrophied myocardium would predisposes to alternans, such that it occurs at slower stimulation rates and with greater magnitude than in normal hearts. Finally, that in failing hearts, the onset of discordant alternans and the induction of re-entry would occur at slower stimulation rates than in normal hearts.

In order to test these hypotheses, transmural electrophysiology was first characterised in both normal and failing ventricular myocardium. Experiments were then conducted to compare alternating behaviour and the relationship to arrhythmia in normal and failing hearts.

Baseline electrophysiology in normal rabbit ventricular myocardium

Electrophysiology in intact ventricular tissue

In this study, optical action potentials were recorded from across the transmural surface of rabbit ventricle during endocardial pacing at physiologically relevant stimulation rates. The first important finding from this study is the demonstration of the marked differences in APD₉₀ recorded from isolated cells and those recorded from cells within the intact ventricular myocardium. Not only are transmural gradients attenuated but baseline APD₉₀ in intact myocardium is significantly shorter than that observed in isolated cells. This is an extremely important finding for the interpretation of data recorded from isolated cardiomyocytes, as ionic currents and excitation-contraction coupling will both be modulated by the cellular APD. This may be particularly important when investigating rate dependent phenomena such as alternans, and underlines the importance of replicating electrophysiological findings from isolated cells in intact tissue.

Transmural heterogeneity of repolarisation

In isolated myocytes, transmural differences in AP morphology, APD, and the rate dependence of APD have been observed in a wide variety of species, including humans, at slow stimulation rates. If this heterogeneity were to exist in intact myocardium it would potentially be extremely important, as dispersion of repolarisation in ventricular myocardium is a powerful substrate for the generation of ventricular arrhythmia⁹. Moreover, the development of spatially discordant alternans may depend upon baseline heterogeneities in repolarisation, including those spanning the ventricular wall, and significant transmural dispersion of repolarisation may be crucial in the genesis of arrhythmias associated with spatially discordant alternans.

This is the first study to record optical action potentials from across the entire transmural surface of rabbit ventricular myocardium and provides a detailed characterisation of transmural ventricular electrophysiology in intact myocardium at physiological stimulation rates. The data presented in Chapter 3 demonstrate that transmural gradients of APD₉₀ do exist under physiologically relevant experimental conditions, but that there does not appear to be any identifiable M cell behaviour. Transmural gradients of APD₉₀ were maintained during rapid stimulation and at low temperature, experimental conditions which are used to elicit repolarisation alternans. Low temperature was also associated with a global prolongation of APD₉₀, a reduction in transmural conduction velocity and a steeper maximal restitution slope. Slow conduction and steep restitution have been implicated in

the induction of alternans and so these results may provide an explanation for the commonly observed temperature dependence of repolarisation alternans.

Modulation of APD₉₀ by activation sequence

In this study, baseline electrophysiological characteristics were recorded during both endocardial and epicardial stimulation. This was to test the hypothesis that if transmural gradients of APD₉₀ were due to differences in intrinsic cellular repolarisation, then they would exist independent of activation sequence. Instead, the data demonstrate that transmural gradients of APD₉₀ are modified by activation sequence, consistent with a modulatory effect of electrotonic current flow on the repolarisation phase of the AP. This suggests that electrotonic influences between cells are important in determining APD *in vivo*.

Electrophysiological changes as a consequence of heart failure

The effects of heart failure on the electrophysiology of mammalian ventricle have been widely investigated. The aim of this set of experiments was to examine the electrophysiological effects of heart failure in intact rabbit ventricle, with a specific focus on elucidating whether transmural heterogeneity exists, and also to characterise the changes in electrophysiological parameters that may be relevant to the production of repolarisation alternans and spatially discordant repolarisation alternans.

These experiments have examined the transmural electrophysiological changes occurring as a consequence of heart failure secondary to myocardial infarction in intact rabbit ventricular myocardium. This work adds to the published literature characterising the electrophysiological consequences of heart failure following coronary arterial ligation in the rabbit^{9;134-137}. The main hypothesis as regards the induction of discordant alternans was that increased heterogeneity of repolarisation is a feature of heart failure. Conversely the data suggest that in heart failure, there is no increase in transmural heterogeneity of repolarisation in the surviving hypertrophied myocardium. Indeed, these experiments were able to identify very few baseline electrophysiological differences between normal and failing hearts, underlining the potential importance of dynamic mechanisms in arrhythmogenesis in this context.

The occurrence of repolarisation alternans

Alternans was induced with a combination of low temperature and rapid pacing. In accordance with the hypotheses, the magnitude and heterogeneity of alternans was heart rate dependent. The data suggest that the electrophysiological basis for alternans involves slowed conduction interacting with changes in repolarisation, perhaps caused by steep restitution, to produce alternans of both APD₉₀ and AP amplitude.

One of the main hypotheses in the current study was that transmural pattern of alternans is dependent on intrinsic cellular repolarisation properties, and hence is independent of stimulus site. This is underpinned by published work suggesting that gradients of alternans in tissue mirror gradients of APD. However, in the current study, the hypothesis that gradients of alternans are dictated by intrinsic cellular gradients of APD is not upheld. Indeed, transmural gradients of both APD₉₀ and alternans were modulated by activation sequence, and this phenomenon appeared to be consistent with electrotonic influences on the repolarisation phase of the action potential. The theory of spatially discordant alternans identifies spatial heterogeneity of alternans as the key in the development of a pro-arrhythmic substrate. Thus the spatial determinants of alternans in tissue are extremely important. In the current study, electrotonic influences appear to be a major determinant of both APD and patterns of alternans in intact myocardium. Consequently, dynamic electrotonic influences may be critical in the development of spatially discordant alternans.

Spatially discordant repolarisation alternans

The development of discordant alternans could not be studied definitively, as only areas of discordant alternans within the transmural imaging window were detected. During the episodes that did occur it did not appear that heterogeneity of alternans was closely related to the development of discordant alternans. Ventricular arrhythmia did occur in the absence of discordant alternans on the imaged part of the transmural surface. However it is perfectly possible that discordant alternans was present in another part of the ventricle. Therefore whether discordant alternans is a necessary pre-condition for unidirectional conduction block and re-entry cannot be determined from these data. Similarly, although heart failure was not associated with a significantly higher incidence of spatially discordant alternans, this may be a reflection of the volume of myocardium imaged.

Spatially discordant alternans has been demonstrated to be directly responsible for the induction of re-entry under extremely non-physiological experimental conditions.

Discordant alternans produces re-entry after pharmacological APD prolongation and where the endocardial surface has been ablated to leave a thin rim of viable epicardial cells. It may be that these extreme changes - in the first case, marked APD prolongation and in the second case significant cellular uncoupling - are necessary for marked gradients of repolarisation, which may not occur under conditions which are more pathophysiological relevant.

Repolarisation alternans as a mechanism of ventricular arrhythmia in heart failure

If repolarisation alternans is to be considered a mechanism of arrhythmogenesis, then this paradigm should be reproducible in experimental models of heart failure. These experiments show that heart failure is associated with an increased vulnerability to repolarisation alternans. This finding was not only at low temperature, where the heart rate threshold for alternans was significantly lower in failing hearts, but importantly also at physiological temperature. In combination with the robust clinical relevance of the experimental model used, these data considerably strengthen the correlation between MTWA in man and experimental repolarisation alternans.

In these experiments, as has been shown previously, the rabbit coronary ligation model of heart failure was associated with an increased vulnerability to ventricular arrhythmia, and these arrhythmias were consistently preceded by alternans. However, although heart failure was associated with an increased vulnerability to both the development of repolarisation alternans and to ventricular arrhythmia, the induction of arrhythmias could not be directly attributed to alternans. Although an association exists between heart failure and inducibility of arrhythmias and also between heart failure and alternans, a direct link has yet to be shown.

The results from this study suggests an association between alternans and arrhythmia, but present a number of complex paradigms. In particular, the development and propagation of alternating behaviour in tissue appears to be much more dependent on dynamic factors dictated by the tissue conditions than on intrinsic cellular properties pertaining to repolarisation. Whether transmural gradients of APD produce transmural gradients of alternans, or whether these phenomena are merely associated is as yet unclear. The observation of amplitude alternans underlines the possibilities that multiple underlying processes may contribute to the development of cardiac alternans. Overall, the results from this study suggest that the development of cardiac alternans is not solely dictated by cellular repolarisation characteristics, but rather a complex interplay of fixed cellular and

dynamic tissue factors, which may include different factors under different experimental or pathophysiological conditions.

Future directions

Two main future directions are suggested by this work. The first is to further explore the clinical relevance of this model of alternans to MTWA in humans. An increased vulnerability to repolarisation alternans *in vitro* has been demonstrated, and the natural extension is to examine whether a similar association exists *in vivo*. Algorithms for detecting MTWA from ambulatory ECG records have been developed for use in humans, and with some minor technical adaptations these same algorithms could be applied to ambulatory monitoring in rabbits. This approach would also provide invaluable data regarding the occurrence of and circumstances surrounding spontaneous ventricular arrhythmias in animals with heart failure.

The second avenue for future research is to improve our scientific understanding of the relationship between alternans and arrhythmia. The finding in this study of amplitude alternans which does not appear to be present in single cells but may rather be due to heterogeneous coupling and 2:1 failure to capture in some groups of cells, is intriguing. Not only does this observation provide a potential framework by which macroscopically similar alternans could be produced by entirely different underlying processes, but also it could be hypothesised that intermittent failure to respond in some cells but not in others could be pro-arrhythmic in some circumstances. To clarify and investigate this possibility requires a rigorous examination of the behaviour of single cells in intact myocardium, which would then allow a detailed comparison of the cellular events underlying alternans produced by different experimental interventions relating to the disparate clinical pathologies which provoke alternans.

Conclusions

The main hypothesis of the current study was that increased baseline heterogeneity of APD in heart failure would result in increased heterogeneity of alternans and ultimately lead to a greater vulnerability to discordant alternans and therefore to re-entrant arrhythmia. The experimental data demonstrate an increased vulnerability to repolarisation alternans and ventricular arrhythmia in heart failure. Although heart failure was associated with both alternans and ventricular arrhythmia, there was no demonstrable mechanistic link between alternans and ventricular arrhythmias in failing hearts. It therefore remains possible that the occurrence of alternans and re-entrant ventricular arrhythmia simply co-exist in failing hearts. Only through understanding the electrophysiological basis of alternans in failing myocardium can we hope to reconcile the now complex clinical data regarding the relationship between alternans and arrhythmia in patients with heart failure. These data establish the occurrence of the experimental paradigm in a clinically relevant pathology, and so constitute an important step forward in our understanding. A definitive mechanistic link between alternans and arrhythmia in heart failure is yet to be shown, and determining whether such a link exists remains a crucial aim in translational cardiac electrophysiology research.

References

1. McMurray JJ, Stewart S. Heart Failure: Epidemiology, aetiology, and prognosis of heart failure. *Heart.* 2000;83:596-602.
2. Packer M. Sudden unexpected death in patients with congestive heart failure: a second frontier. *Circulation.* 1985;72:681-685.
3. Gehi A, Haas D, Fuster V. Primary prophylaxis with the implantable cardioverter-defibrillator: the need for improved risk stratification. *JAMA.* 2005;294:958-960.
4. Myerburg RJ, Castellanos A. Emerging paradigms of the epidemiology and demographics of sudden cardiac arrest. *Heart Rhythm.* 2006;3:235-239.
5. Greenberg H, Case RB, Moss AJ, Brown MW, Carroll ER, Andrews ML. Analysis of mortality events in the Multicenter Automatic Defibrillator Implantation Trial (MADIT-II). *J Am Coll Cardiol.* 2004;43:1459-1465.
6. Effect of metoprolol CR/XL in chronic heart failure: Metoprolol CR/XL Randomised Intervention Trial in Congestive Heart Failure (MERIT-HF). *Lancet.* 1999;353:2001-2007.
7. Cleland JG, Massie BM, Packer M. Sudden death in heart failure: vascular or electrical? *Eur J Heart Fail.* 1999;1:41-45.
8. Engdahl J, Holmberg M, Karlson BW, Luepker R, Herlitz J. The epidemiology of out-of-hospital 'sudden' cardiac arrest. *Resuscitation.* 2002;52:235-245.
9. Burton FL, McPhaden AR, Cobbe SM. Ventricular fibrillation threshold and local dispersion of refractoriness in isolated rabbit hearts with left ventricular dysfunction. *Basic Res Cardiol.* 2000;95:359-367.
10. Janse MJ. Electrophysiological changes in heart failure and their relationship to arrhythmogenesis. *Cardiovascular Research.* 2004;61:208-217.
11. Pfeffer MA, Braunwald E, Moye LA, Basta L, Brown EJ, Cuddy TE, Davis BR, Geltman EM, Goldman S, Flaker GC. Effect of captopril on mortality and morbidity in patients with left ventricular dysfunction after myocardial infarction. Results of the survival and ventricular enlargement trial. The SAVE Investigators. *N Engl J Med.* 1992;327:669-677.

12. McMurray JJ, Pfeffer MA. Heart failure. *Lancet*. 2005;365:1877-1889.
13. Uretsky BF, Thygesen K, Armstrong PW, Cleland JG, Horowitz JD, Massie BM, Packer M, Poole-Wilson PA, Ryden L. Acute coronary findings at autopsy in heart failure patients with sudden death: results from the assessment of treatment with lisinopril and survival (ATLAS) trial. *Circulation*. 2000;102:611-616.
14. McMurray JJ, Ostergren J, Swedberg K, Granger CB, Held P, Michelson EL, Olofsson B, Yusuf S, Pfeffer MA. Effects of candesartan in patients with chronic heart failure and reduced left-ventricular systolic function taking angiotensin-converting-enzyme inhibitors: the CHARM-Added trial. *Lancet*. 2003;362:767-771.
15. Hillege HL, Nitsch D, Pfeffer MA, Swedberg K, McMurray JJ, Yusuf S, Granger CB, Michelson EL, Ostergren J, Cornel JH, de Zeeuw D, Pocock S, van Veldhuisen DJ. Renal function as a predictor of outcome in a broad spectrum of patients with heart failure. *Circulation*. 2006;113:671-678.
16. Kendall MJ, Lynch KP, Hjalmarson A, Kjekshus J. Beta-blockers and sudden cardiac death. *Ann Intern Med*. 1995;123:358-367.
17. Domanski MJ, Krause-Steinrauf H, Massie BM, Deedwania P, Follmann D, Kovar D, Murray D, Oren R, Rosenberg Y, Young J, Zile M, Eichhorn E. A comparative analysis of the results from 4 trials of beta-blocker therapy for heart failure: BEST, CIBIS-II, MERIT-HF, and COPERNICUS. *J Card Fail*. 2003;9:354-363.
18. Pfeffer MA, Swedberg K, Granger CB, Held P, McMurray JJ, Michelson EL, Olofsson B, Ostergren J, Yusuf S, Pocock S. Effects of candesartan on mortality and morbidity in patients with chronic heart failure: the CHARM-Overall programme. *Lancet*. 2003;362:759-766.
19. Pitt B, Zannad F, Remme WJ, Cody R, Castaigne A, Perez A, Palensky J, Wittes J. The effect of spironolactone on morbidity and mortality in patients with severe heart failure. Randomized Aldactone Evaluation Study Investigators. *N Engl J Med*. 1999;341:709-717.
20. Echt DS, Liebson PR, Mitchell LB, Peters RW, Obias-Manno D, Barker AH, Arensberg D, Baker A, Friedman L, Greene HL, . Mortality and morbidity in patients receiving encainide, flecainide, or placebo. The Cardiac Arrhythmia Suppression Trial. *N Engl J Med*. 1991;324:781-788.

21. Waldo AL, Camm AJ, deRuyter H, Friedman PL, MacNeil DJ, Pauls JF, Pitt B, Pratt CM, Schwartz PJ, Veltri EP. Effect of d-sotalol on mortality in patients with left ventricular dysfunction after recent and remote myocardial infarction. The SWORD Investigators. Survival With Oral d-Sotalol. *Lancet*. 1996;348:7-12.
22. Bardy GH, Lee KL, Mark DB, Poole JE, Packer DL, Boineau R, Domanski M, Troutman C, Anderson J, Johnson G, McNulty SE, Clapp-Channing N, Davidson-Ray LD, Fraulo ES, Fishbein DP, Luceri RM, Ip JH. Amiodarone or an implantable cardioverter-defibrillator for congestive heart failure. *N Engl J Med*. 2005;352:225-237.
23. Mirowski M. The automatic implantable cardioverter-defibrillator: an overview. *J Am Coll Cardiol*. 1985;6:461-466.
24. Gold MR, Higgins S, Klein R, Gilliam FR, Kopelman H, Hessen S, Payne J, Strickberger SA, Breiter D, Hahn S. Efficacy and temporal stability of reduced safety margins for ventricular defibrillation: primary results from the Low Energy Safety Study (LESS). *Circulation*. 2002;105:2043-2048.
25. Alter P, Waldhans S, Plachta E, Moosdorf R, Grimm W. Complications of implantable cardioverter defibrillator therapy in 440 consecutive patients. *Pacing Clin Electrophysiol*. 2005;28:926-932.
26. Moss AJ. MADIT-II and its implications. *Eur Heart J*. 2003;24:16-18.
27. Zipes DP, Camm AJ, Borggrefe M, Buxton AE, Chaitman B, Fromer M, Gregoratos G, Klein G, Moss AJ, Myerburg RJ, Priori SG, Quinones MA, Roden DM, Silka MJ, Tracy C, Blanc JJ, Budaj A, Dean V, Deckers JW, Despres C, Dickstein K, Lekakis J, McGregor K, Metra M, Morais J, Osterspey A, Tamargo JL, Zamorano JL, Smith SC, Jr., Jacobs AK, Adams CD, Antman EM, Anderson JL, Hunt SA, Halperin JL, Nishimura R, Ornato JP, Page RL, Riegel B. ACC/AHA/ESC 2006 guidelines for management of patients with ventricular arrhythmias and the prevention of sudden cardiac death--executive summary: A report of the American College of Cardiology/American Heart Association Task Force and the European Society of Cardiology Committee for Practice Guidelines (Writing Committee to Develop Guidelines for Management of Patients with Ventricular Arrhythmias and the Prevention of Sudden Cardiac Death) Developed in collaboration with the European Heart Rhythm Association and the Heart Rhythm Society. *Eur Heart J*. 2006;27:2099-2140.

28. A comparison of antiarrhythmic-drug therapy with implantable defibrillators in patients resuscitated from near-fatal ventricular arrhythmias. The Antiarrhythmics versus Implantable Defibrillators (AVID) Investigators. *N Engl J Med.* 1997;337:1576-1583.
29. Connolly SJ, Gent M, Roberts RS, Dorian P, Roy D, Sheldon RS, Mitchell LB, Green MS, Klein GJ, O'Brien B. Canadian implantable defibrillator study (CIDS) : a randomized trial of the implantable cardioverter defibrillator against amiodarone. *Circulation.* 2000;101:1297-1302.
30. Larsen G, Hallstrom A, McAnulty J, Pinski S, Olarte A, Sullivan S, Brodsky M, Powell J, Marchant C, Jennings C, Akiyama T. Cost-effectiveness of the implantable cardioverter-defibrillator versus antiarrhythmic drugs in survivors of serious ventricular tachyarrhythmias: results of the Antiarrhythmics Versus Implantable Defibrillators (AVID) economic analysis substudy. *Circulation.* 2002;105:2049-2057.
31. Huikuri HV, Castellanos A, Myerburg RJ. Sudden death due to cardiac arrhythmias. *N Engl J Med.* 2001;345:1473-1482.
32. Moss AJ, Hall WJ, Cannom DS, Daubert JP, Higgins SL, Klein H, Levine JH, Saksena S, Waldo AL, Wilber D, Brown MW, Heo M. Improved survival with an implanted defibrillator in patients with coronary disease at high risk for ventricular arrhythmia. Multicenter Automatic Defibrillator Implantation Trial Investigators. *N Engl J Med.* 1996;335:1933-1940.
33. Mark DB, Nelson CL, Anstrom KJ, Al Khatib SM, Tsiantis AA, Cowper PA, Clapp-Channing NE, Davidson-Ray L, Poole JE, Johnson G, Anderson J, Lee KL, Bardy GH. Cost-effectiveness of defibrillator therapy or amiodarone in chronic stable heart failure: results from the Sudden Cardiac Death in Heart Failure Trial (SCD-HeFT). *Circulation.* 2006;114:135-142.
34. Bailey JJ, Berson AS, Handelsman H, Hodges M. Utility of current risk stratification tests for predicting major arrhythmic events after myocardial infarction. *J Am Coll Cardiol.* 2001;38:1902-1911.
35. Armandas AA, Nanke T, Cohen RJ. Images in cardiovascular medicine. T-wave alternans preceding torsade de pointes ventricular tachycardia. *Circulation.* 2000;101:2550.

36. Adam DR, Smith JM, Akselrod S, Nyberg S, Powell AO, Cohen RJ. Fluctuations in T-wave morphology and susceptibility to ventricular fibrillation. *J Electrocardiol.* 1984;17:209-218.
37. Smith JM, Clancy EA, Valeri CR, Ruskin JN, Cohen RJ. Electrical alternans and cardiac electrical instability. *Circulation.* 1988;77:110-121.
38. Rosenbaum DS, Jackson LE, Smith JM, Garan H, Ruskin JN, Cohen RJ. Electrical alternans and vulnerability to ventricular arrhythmias. *N Engl J Med.* 1994;330:235-241.
39. Bloomfield DM, Hohnloser SH, Cohen RJ. Interpretation and classification of microvolt T wave alternans tests. *J Cardiovasc Electrophysiol.* 2002;13:502-512.
40. Pastore JM, Girouard SD, Laurita KR, Akar FG, Rosenbaum DS. Mechanism linking T-wave alternans to the genesis of cardiac fibrillation. *Circulation.* 1999;99:1385-1394.
41. Turitto G, Mirandi AP, Pedalino RP, Uretsky S, El Sherif N. Short-term reproducibility of T wave alternans measurement. *J Cardiovasc Electrophysiol.* 2002;13:641-644.
42. Madias JE. Reproducibility of the T-wave alternans and dependence of T-wave alternans on the T-wave amplitude: 2 issues requiring immediate attention. *J Electrocardiol.* 2007;40:364-3.
43. Nearing BD, Verrier RL. Modified moving average analysis of T-wave alternans to predict ventricular fibrillation with high accuracy. *J Appl Physiol.* 2002;92:541-549.
44. Cox V, Patel M, Kim J, Liu T, Sivaraman G, Narayan SM. Predicting arrhythmia-free survival using spectral and modified-moving average analyses of T-wave alternans. *Pacing Clin Electrophysiol.* 2007;30:352-358.
45. Verrier RL, Nearing BD, La Rovere MT, Pinna GD, Mittleman MA, Bigger JT, Jr., Schwartz PJ. Ambulatory electrocardiogram-based tracking of T wave alternans in postmyocardial infarction patients to assess risk of cardiac arrest or arrhythmic death. *J Cardiovasc Electrophysiol.* 2003;14:705-711.
46. Bloomfield DM, Steinman RC, Namerow PB, Parides M, Davidenko J, Kaufman ES, Shinn T, Curtis A, Fontaine J, Holmes D, Russo A, Tang C, Bigger JT, Jr.

- Microvolt T-wave alternans distinguishes between patients likely and patients not likely to benefit from implanted cardiac defibrillator therapy: a solution to the Multicenter Automatic Defibrillator Implantation Trial (MADIT) II conundrum. *Circulation.* 2004;110:1885-1889.
47. Ikeda T, Saito H, Tanno K, Shimizu H, Watanabe J, Ohnishi Y, Kasamaki Y, Ozawa Y. T-wave alternans as a predictor for sudden cardiac death after myocardial infarction. *Am J Cardiol.* 2002;89:79-82.
 48. Ikeda T, Yoshino H, Sugi K, Tanno K, Shimizu H, Watanabe J, Kasamaki Y, Yoshida A, Kato T. Predictive value of microvolt T-wave alternans for sudden cardiac death in patients with preserved cardiac function after acute myocardial infarction: results of a collaborative cohort study. *J Am Coll Cardiol.* 2006;48:2268-2274.
 49. Schwab JO, Weber S, Schmitt H, Steen-Mueller MK, Coch M, Tillmanns H, Becker M, Lenzen C, Waldecker B. Incidence of T wave alternation after acute myocardial infarction and correlation with other prognostic parameters: results of a prospective study. *Pacing Clin Electrophysiol.* 2001;24:957-961.
 50. Tapanainen JM, Still AM, Airaksinen KE, Huikuri HV. Prognostic significance of risk stratifiers of mortality, including T wave alternans, after acute myocardial infarction: results of a prospective follow-up study. *J Cardiovasc Electrophysiol.* 2001;12:645-652.
 51. Hohnloser SH, Ikeda T, Bloomfield DM, Dabbous OH, Cohen RJ. T-wave alternans negative coronary patients with low ejection and benefit from defibrillator implantation. *Lancet.* 2003;362:125-126.
 52. Chow T, Kereiakes DJ, Onufer J, Woelfel A, Gursoy S, Peterson BJ, Brown ML, Pu W, Benditt DG. Does microvolt T-wave alternans testing predict ventricular tachyarrhythmias in patients with ischemic cardiomyopathy and prophylactic defibrillators? The MASTER (Microvolt T Wave Alternans Testing for Risk Stratification of Post-Myocardial Infarction Patients) trial. *J Am Coll Cardiol.* 2008;52:1607-1615.
 53. Rashba EJ, Osman AF, Macmurdy K, Kirk MM, Sarang SE, Peters RW, Shorofsky SR, Gold MR. Enhanced detection of arrhythmia vulnerability using T wave alternans, left ventricular ejection fraction, and programmed ventricular

- stimulation: a prospective study in subjects with chronic ischemic heart disease. *J Cardiovasc Electrophysiol.* 2004;15:170-176.
54. Chow T, Kereiakes DJ, Bartone C, Booth T, Schloss EJ, Waller T, Chung ES, Menon S, Nallamothu BK, Chan PS. Prognostic utility of microvolt T-wave alternans in risk stratification of patients with ischemic cardiomyopathy. *J Am Coll Cardiol.* 2006;47:1820-1827.
 55. Cleland JG, Coletta AP, Abdellah AT, Nasir M, Hobson N, Freemantle N, Clark AL. Clinical trials update from the American Heart Association 2006: OAT, SALT 1 and 2, MAGIC, ABCD, PABA-CHF, IMPROVE-CHF, and percutaneous mitral annuloplasty. *Eur J Heart Fail.* 2007;9:92-97.
 56. Bloomfield DM, Bigger JT, Steinman RC, Namerow PB, Parides MK, Curtis AB, Kaufman ES, Davidenko JM, Shinn TS, Fontaine JM. Microvolt T-wave alternans and the risk of death or sustained ventricular arrhythmias in patients with left ventricular dysfunction. *J Am Coll Cardiol.* 2006;47:456-463.
 57. Kitamura H, Ohnishi Y, Okajima K, Ishida A, Galeano E, Adachi K, Yokoyama M. Onset heart rate of microvolt-level T-wave alternans provides clinical and prognostic value in nonischemic dilated cardiomyopathy. *J Am Coll Cardiol.* 2002;39:295-300.
 58. Hohnloser SH, Klingenheben T, Bloomfield D, Dabbous O, Cohen RJ. Usefulness of microvolt T-wave alternans for prediction of ventricular tachyarrhythmic events in patients with dilated cardiomyopathy: results from a prospective observational study. *J Am Coll Cardiol.* 2003;41:2220-2224.
 59. Grimm W, Christ M, Bach J, Muller HH, Maisch B. Noninvasive arrhythmia risk stratification in idiopathic dilated cardiomyopathy: results of the Marburg Cardiomyopathy Study. *Circulation.* 2003;108:2883-2891.
 60. Baravelli M, Salerno-Uriarte D, Guzzetti D, Rossi MC, Zoli L, Forzani T, Salerno-Uriarte JA. Predictive significance for sudden death of microvolt-level T wave alternans in New York Heart Association class II congestive heart failure patients A prospective study. *Int J Cardiol.* 2005;105:53-57.
 61. Sarzi BS, Vaninetti R, Laporta A, Picozzi A, Pedretti RF. T wave alternans is a predictor of death in patients with congestive heart failure. *Int J Cardiol.* 2004;93:31-38.

62. Klingenheben T, Zabel M, D'Agostino RB, Cohen RJ, Hohnloser SH. Predictive value of T-wave alternans for arrhythmic events in patients with congestive heart failure. *Lancet.* 2000;356:651-652.
63. Gold MR, Ip JH, Costantini O, Poole JE, McNulty S, Mark DB, Lee KL, Bardy GH. Role of microvolt T-wave alternans in assessment of arrhythmia vulnerability among patients with heart failure and systolic dysfunction: primary results from the T-wave alternans sudden cardiac death in heart failure trial substudy. *Circulation.* 2008;118:2022-2028.
64. Chan PS, Bartone C, Booth T, Kereiakes D, Chow T. Prognostic implication of redefining indeterminate microvolt T-wave alternans studies as abnormal or normal. *Am Heart J.* 2007;153:523-529.
65. Kaufman ES, Bloomfield DM, Steinman RC, Namerow PB, Costantini O, Cohen RJ, Bigger JT, Jr. "Indeterminate" microvolt T-wave alternans tests predict high risk of death or sustained ventricular arrhythmias in patients with left ventricular dysfunction. *J Am Coll Cardiol.* 2006;48:1399-1404.
66. Shimizu W, Antzelevitch C. Cellular and ionic basis for T-wave alternans under long-QT conditions. *Circulation.* 1999;99:1499-1507.
67. Pastore JM, Rosenbaum DS. Role of structural barriers in the mechanism of alternans-induced reentry. *Circ Res.* 2000;87:1157-1163.
68. Pastore JM, Laurita KR, Rosenbaum DS. Importance of spatiotemporal heterogeneity of cellular restitution in mechanism of arrhythmogenic discordant alternans. *Heart Rhythm.* 2006;3:711-719.
69. Chinushi M, Hosaka Y, Washizuka T, Furushima H, Aizawa Y. Arrhythmogenesis of T wave alternans associated with surface QRS complex alternans and the role of ventricular prematurity: observations from a canine model of LQT3 syndrome. *J Cardiovasc Electrophysiol.* 2002;13:599-604.
70. Qian YW, Sung RJ, Lin SF, Province R, Clusin WT. Spatial heterogeneity of action potential alternans during global ischemia in the rabbit heart. *Am J Physiol Heart Circ Physiol.* 2003;285:H2722-H2733.
71. Orchard CH, McCall E, Kirby MS, Boyett MR. Mechanical alternans during acidosis in ferret heart muscle. *Circ Res.* 1991;68:69-76.

72. Shimoni Z, Flatau E, Schiller D, Barzilay E, Kohn D. Electrical alternans of giant U waves with multiple electrolyte deficits. *Am J Cardiol.* 1984;54:920-921.
73. Lewis T. Notes upon alternation of the heart. *Q J Med.* 1910;4:141-144.
74. Schwartz PJ, Malliani A. Electrical alternation of the T-wave: clinical and experimental evidence of its relationship with the sympathetic nervous system and with the long Q-T syndrome. *Am Heart J.* 1975;89:45-50.
75. Cheng TC. Electrical alternans. An association with coronary artery spasm. *Arch Intern Med.* 1983;143:1052-1053.
76. Kon-No Y, Watanabe J, Koseki Y, Koyama J, Yamada A, Toda S, Shinozaki T, Fukuchi M, Miura M, Kagaya Y, Shirato K. Microvolt T wave alternans in human cardiac hypertrophy: electrical instability and abnormal myocardial arrangement. *J Cardiovasc Electrophysiol.* 2001;12:759-763.
77. Pruvot EJ, Katra RP, Rosenbaum DS, Laurita KR. Role of calcium cycling versus restitution in the mechanism of repolarization alternans. *Circ Res.* 2004;94:1083-1090.
78. Nolasco JB, Dahlen RW. A graphic method for the study of alternation in cardiac action potentials. *J Appl Physiol.* 1968;25:191-196.
79. Garfinkel A, Kim YH, Voroshilovsky O, Qu Z, Kil JR, Lee MH, Karagueuzian HS, Weiss JN, Chen PS. Preventing ventricular fibrillation by flattening cardiac restitution. *Proc Natl Acad Sci U S A.* 2000;97:6061-6066.
80. Riccio ML, Koller ML, Gilmour RF, Jr. Electrical restitution and spatiotemporal organization during ventricular fibrillation. *Circ Res.* 1999;84:955-963.
81. Qu Z, Garfinkel A, Chen PS, Weiss JN. Mechanisms of discordant alternans and induction of reentry in simulated cardiac tissue. *Circulation.* 2000;102:1664-1670.
82. Watanabe MA, Fenton FH, Evans SJ, Hastings HM, Karma A. Mechanisms for discordant alternans. *J Cardiovasc Electrophysiol.* 2001;12:196-206.
83. Rubenstein DS, Lipsius SL. Premature beats elicit a phase reversal of mechanoelectrical alternans in cat ventricular myocytes. A possible mechanism for reentrant arrhythmias. *Circulation.* 1995;91:201-214.

84. Choi BR, Salama G. Simultaneous maps of optical action potentials and calcium transients in guinea-pig hearts: mechanisms underlying concordant alternans. *J Physiol.* 2000;529 Pt 1:171-188.
85. Blatter LA, Kockskamper J, Sheehan KA, Zima AV, Huser J, Lipsius SL. Local calcium gradients during excitation-contraction coupling and alternans in atrial myocytes. *J Physiol (Lond).* 2003;546:19-31.
86. Huser J, Wang YG, Sheehan KA, Cifuentes F, Lipsius SL, Blatter LA. Functional coupling between glycolysis and excitation-contraction coupling underlies alternans in cat heart cells. *J Physiol.* 2000;524 Pt 3:795-806.
87. Wan X, Laurita KR, Pruvot EJ, Rosenbaum DS. Molecular correlates of repolarization alternans in cardiac myocytes. *J Mol Cell Cardiol.* 2005;39:419-428.
88. Chudin E, Goldhaber J, Garfinkel A, Weiss J, Kogan B. Intracellular Ca(2+) dynamics and the stability of ventricular tachycardia. *Biophys J.* 1999;77:2930-2941.
89. Shannon TR, Ginsburg KS, Bers DM. Potentiation of Fractional Sarcoplasmic Reticulum Calcium Release by Total and Free Intra-Sarcoplasmic Reticulum Calcium Concentration. *Biophys J.* 2000;78:334-343.
90. Diaz ME, O'neill SC, Eisner DA. Sarcoplasmic reticulum calcium content fluctuation is the key to cardiac alternans. *Circ Res.* 2004;94:650-656.
91. Shiferaw Y, Watanabe MA, Garfinkel A, Weiss JN, Karma A. Model of intracellular calcium cycling in ventricular myocytes. *Biophys J.* 2003;85:3666-3686.
92. Weiss JN, Qu Z, Chen PS, Lin SF, Karagueuzian HS, Hayashi H, Garfinkel A, Karma A. The dynamics of cardiac fibrillation. *Circulation.* 2005;112:1232-1240.
93. Picht E, DeSantiago J, Blatter LA, Bers DM. Cardiac alternans do not rely on diastolic sarcoplasmic reticulum calcium content fluctuations. *Circ Res.* 2006;99:740-748.
94. Saitoh H, Bailey JC, Surawicz B. Action potential duration alternans in dog Purkinje and ventricular muscle fibers. Further evidence in support of two different mechanisms. *Circulation.* 1989;80:1421-1431.

95. Hirayama Y, Saitoh H, Atarashi H, Hayakawa H. Electrical and mechanical alternans in canine myocardium in vivo. Dependence on intracellular calcium cycling. *Circulation*. 1993;88:2894-2902.
96. Goldhaber JI, Xie LH, Duong T, Motter C, Khuu K, Weiss JN. Action potential duration restitution and alternans in rabbit ventricular myocytes: the key role of intracellular calcium cycling. *Circ Res*. 2005;96:459-466.
97. Nearing BD, Hutter JJ, Verrier RL. Potent antifibrillatory effect of combined blockade of calcium channels and 5-HT2 receptors with nexpamil during myocardial ischemia and reperfusion in dogs: comparison to diltiazem. *J Cardiovasc Pharmacol*. 1996;27:777-787.
98. Chinushi M, Kozhevnikov D, Caref EB, Restivo M, El Sherif N. Mechanism of discordant T wave alternans in the in vivo heart. *J Cardiovasc Electrophysiol*. 2003;14:632-638.
99. Laurita KR, Girouard SD, Rosenbaum DS. Modulation of ventricular repolarization by a premature stimulus. Role of epicardial dispersion of repolarization kinetics demonstrated by optical mapping of the intact guinea pig heart. *Circ Res*. 1996;79:493-503.
100. Antzelevitch C, Sicouri S, Litovsky SH, Lukas A, Krishnan SC, Di Diego JM, Gintant GA, Liu DW. Heterogeneity within the ventricular wall. Electrophysiology and pharmacology of epicardial, endocardial, and M cells. *Circ Res*. 1991;69:1427-1449.
101. Chinushi M, Restivo M, Caref EB, El Sherif N. Electrophysiological basis of arrhythmogenicity of QT/T alternans in the long-QT syndrome: tridimensional analysis of the kinetics of cardiac repolarization. *Circ Res*. 1998;83:614-628.
102. Salama G, Kanai AJ, Huang D, Efimov IR, Girouard SD, Rosenbaum DS. Hypoxia and hypothermia enhance spatial heterogeneities of repolarization in guinea pig hearts: analysis of spatial autocorrelation of optically recorded action potential durations. *J Cardiovasc Electrophysiol*. 1998;9:164-183.
103. Katra RP, Laurita KR. Cellular mechanism of calcium-mediated triggered activity in the heart. *Circ Res*. 2005;96:535-542.

104. Laurita KR, Katra R, Wible B, Wan X, Koo MH. Transmural heterogeneity of calcium handling in canine. *Circ Res.* 2003;92:668-675.
105. Lamont C, Luther PW, Balke CW, Wier WG. Intercellular Ca²⁺ waves in rat heart muscle. *J Physiol (Lond).* 1998;512:669-676.
106. Aistrup GL, Kelly JE, Kapur S, Kowalczyk M, Sysman-Wolpin I, Kadish AH, Wasserstrom JA. Pacing-induced heterogeneities in intracellular Ca²⁺ signaling, cardiac alternans, and ventricular arrhythmias in intact rat heart. *Circ Res.* 2006;99:e65-e73.
107. Kockskamper J, Blatter LA. Subcellular Ca²⁺ alternans represents a novel mechanism for the generation of arrhythmogenic Ca²⁺ waves in cat atrial myocytes. *J Physiol (Lond).* 2002;545:65-79.
108. Peters NS, Green CR, Poole-Wilson PA, Severs NJ. Reduced content of connexin43 gap junctions in ventricular myocardium from hypertrophied and ischemic human hearts. *Circulation.* 1993;88:864-875.
109. Walker, N. L., Burton, F. L., Smith, G. L., and Cobbe, S. M. Mapping of epicardial activation in a rabbit model of chronic myocardial infarction:response to atrial, endocardial and epicardial pacing. *J Cardiovasc.Electrophysiol.* 2007; 18:862-868.
110. Sato D, Shiferaw Y, Garfinkel A, Weiss JN, Qu Z, Karma A. Spatially discordant alternans in cardiac tissue: role of calcium cycling. *Circ Res.* 2006;99:520-527.
111. Walker ML, Wan X, Kirsch GE, Rosenbaum DS. Hysteresis effect implicates calcium cycling as a mechanism of repolarization alternans. *Circulation.* 2003;108:2704-2709.
112. Langer GA, Brady AJ. The effects of temperature upon contraction and ionic exchange in rabbit ventricular myocardium. Relation to control of active state. *J Gen Physiol.* 1968;52:682-713.
113. Puglisi JL, Bassani RA, Bassani JW, Amin JN, Bers DM. Temperature and relative contributions of Ca transport systems in cardiac myocyte relaxation. *Am J Physiol Heart Circ Physiol.* 1996;270:H1772-H1778.

114. Shattock MJ, Bers DM. Inotropic response to hypothermia and the temperature-dependence of ryanodine action in isolated rabbit and rat ventricular muscle: implications for excitation-contraction coupling. *Circ Res.* 1987;61:761-771.
115. Eisner DA, Lederer WJ. Characterization of the electrogenic sodium pump in cardiac Purkinje fibres. *J Physiol.* 1980;303:441-474.
116. Puglisi JL, Yuan W, Bassani JW, Bers DM. Ca(2+) influx through Ca(2+) channels in rabbit ventricular myocytes during action potential clamp: influence of temperature. *Circ Res.* 1999;85:e7-e16.
117. Kiyosue T, Arita M, Muramatsu H, Spindler AJ, Noble D. Ionic mechanisms of action potential prolongation at low temperature in guinea-pig ventricular myocytes. *J Physiol (Lond).* 1993;468:85-106.
118. Bjornstad H, Tande PM, Lathrop DA, Refsum H. Effects of temperature on cycle length dependent changes and restitution of action potential duration in guinea pig ventricular muscle. *Cardiovasc Res.* 1993;27:946-950.
119. Efimov IR, Huang DT, Rendt JM, Salama G. Optical mapping of repolarization and refractoriness from intact hearts. *Circulation.* 1994;90:1469-1480.
120. Franz MR, Bargheer K, Rafflenbeul W, Haverich A, Lichtlen PR. Monophasic action potential mapping in human subjects with normal electrocardiograms: direct evidence for the genesis of the T wave. *Circulation.* 1987;75:379-386.
121. Selvaraj RJ, Picton P, Nanthakumar K, Mak S, Chauhan VS. Endocardial and epicardial repolarization alternans in human cardiomyopathy: evidence for spatiotemporal heterogeneity and correlation with body surface T-wave alternans. *J Am Coll Cardiol.* 2007;49:338-346.
122. Narayan SM, Franz MR, Lalani G, Kim J, Sastry A. T-wave alternans, restitution of human action potential duration, and outcome. *J Am Coll Cardiol.* 2007;50:2385-2392.
123. Armandas AA, Albert CM, Cohen RJ, Mela T. Utility of implantable cardioverter defibrillator electrograms to estimate repolarization alternans preceding a tachyarrhythmic event. *J Cardiovasc Electrophysiol.* 2004;15:594-597.

124. Shusterman V, Goldberg A, London B. Upsurge in T-wave alternans and nonalternating repolarization instability precedes spontaneous initiation of ventricular tachyarrhythmias in humans. *Circulation*. 2006;113:2880-2887.
125. Severs NJ. Pathophysiology of gap junctions in heart disease. *J Cardiovasc Electrophysiol*. 1994;5:462-475.
126. Kjolby AL, Dikshteyn M, Eloff BC, Deschenes I, Rosenbaum DS. Maintenance of intercellular coupling by the antiarrhythmic peptide rotigaptide suppresses arrhythmogenic discordant alternans. *Am J Physiol Heart Circ Physiol*. 2008;294:H41-H49.
127. de Bakker JM, Coronel R, Tasseron S, Wilde AA, Ophof T, Janse MJ, van Capelle FJ, Becker AE, Jambroes G. Ventricular tachycardia in the infarcted, Langendorff-perfused human heart: role of the arrangement of surviving cardiac fibers. *J Am Coll Cardiol*. 1990;15:1594-1607.
128. Misier AR, Ophof T, van Hemel NM, Vermeulen JT, de Bakker JM, Defauw JJ, van Capelle FJ, Janse MJ. Dispersion of 'refractoriness' in noninfarcted myocardium of patients with ventricular tachycardia or ventricular fibrillation after myocardial infarction. *Circulation*. 1995;91:2566-2572.
129. Vermeulen JT, McGuire MA, Ophof T, Coronel R, de Bakker JM, Klopping C, Janse MJ. Triggered activity and automaticity in ventricular trabeculae of failing human and rabbit hearts. *Cardiovasc Res*. 1994;28:1547-1554.
130. Beuckelmann DJ, Nabauer M, Erdmann E. Alterations of K⁺ currents in isolated human ventricular myocytes from patients with terminal heart failure. *Circ Res*. 1993;73:379-385.
131. Yan GX, Rials SJ, Wu Y, Liu T, Xu X, Marinchak RA, Kowey PR. Ventricular hypertrophy amplifies transmural repolarization dispersion and induces early afterdepolarization. *Am J Physiol Heart Circ Physiol*. 2001;281:H1968-H1975.
132. Aronson RS. Afterpotentials and triggered activity in hypertrophied myocardium from rats with renal hypertension. *Circ Res*. 1981;48:720-727.
133. Barbieri M, Varani K, Cerbai E, Guerra L, Li Q, Borea PA, Mugelli A. Electrophysiological basis for the enhanced cardiac arrhythmogenic effect of

- isoprenaline in aged spontaneously hypertensive rats. *J Mol Cell Cardiol.* 1994;26:849-860.
134. McIntosh MA, Cobbe SM, Smith GL. Heterogeneous changes in action potential and intracellular Ca²⁺ in left ventricular myocyte sub-types from rabbits with heart failure. *Cardiovasc Res.* 2000;45:397-409.
135. Ng GA, Cobbe SM, Smith GL. Non-uniform prolongation of intracellular Ca²⁺ transients recorded from the epicardial surface of isolated hearts from rabbits with heart failure. *Cardiovasc Res.* 1998;37:489-502.
136. Pye MP, Cobbe SM. Arrhythmogenesis in experimental models of heart failure: the role of increased load. *Cardiovasc Res.* 1996;32:248-257.
137. Pye MP, Black M, Cobbe SM. Comparison of in vivo and in vitro haemodynamic function in experimental heart failure: use of echocardiography. *Cardiovasc Res.* 1996;31:873-881.
138. Dumitrescu C, Narayan P, Efimov IR, Cheng Y, Radin MJ, McCune SA, Altschuld RA. Mechanical alternans and restitution in failing SHHF rat left ventricles. *Am J Physiol Heart Circ Physiol.* 2002;282:H1320-H1326.
139. Narayan P, McCune SA, Robitaille PM, Hohl CM, Altschuld RA. Mechanical alternans and the force-frequency relationship in failing rat hearts. *J Mol Cell Cardiol.* 1995;27:523-530.
140. London B, Baker LC, Lee JS, Shusterman V, Choi BR, Kubota T, McTiernan CF, Feldman AM, Salama G. Calcium-dependent arrhythmias in transgenic mice with heart failure. *Am J Physiol Heart Circ Physiol.* 2003;284:H431-H441.
141. Pye MP, Cobbe SM. Mechanisms of ventricular arrhythmias in cardiac failure and hypertrophy. *Cardiovasc Res.* 1992;26:740-750.
142. Tan RC, Joyner RW. Electrotonic influences on action potentials from isolated ventricular cells. *Circ Res.* 1990;67:1071-1081.
143. Antzelevitch C, Sun ZQ, Zhang ZQ, Yan GX. Cellular and ionic mechanisms underlying erythromycin-induced long QT intervals and torsade de pointes. *J Am Coll Cardiol.* 1996;28:1836-1848.

144. Yan GX, Antzelevitch C. Cellular basis for the electrocardiographic J wave. *Circulation*. 1996;93:372-379.
145. Yan GX, Antzelevitch C. Cellular basis for the normal T wave and the electrocardiographic manifestations of the long-QT syndrome. *Circulation*. 1998;98:1928-1936.
146. Akar FG, Rosenbaum DS. Transmural electrophysiological heterogeneities underlying arrhythmogenesis in heart failure. *Circ Res*. 2003;93:638-645.
147. Taggart P, Sutton P, Ophof T, Coronel R, Kallis P. Electrotonic cancellation of transmural electrical gradients in the left ventricle in man. *Progress in Biophysics and Molecular Biology*. 2003;82:243-254.
148. Ding L, Splinter R, Knisley SB. Quantifying spatial localization of optical mapping using Monte Carlo simulations. *IEEE Trans Biomed Eng*. 2001;48:1098-1107.
149. Blanchard EM, Smith GL, Allen DG, Alpert NR. The effects of 2,3-butanedione monoxime on initial heat, tension, and aequorin light output of ferret papillary muscles. *Pflugers Arch*. 1990;416:219-221.
150. Adams W, Trafford AW, Eisner DA. 2,3-Butanedione monoxime (BDM) decreases sarcoplasmic reticulum Ca content by stimulating Ca release in isolated rat ventricular myocytes. *Pflugers Arch*. 1998;436:776-781.
151. Kettlewell S, Walker NL, Cobbe SM, Burton FL, Smith GL. The electrophysiological and mechanical effects of 2,3-butane-dione monoxime and cytochalasin-D in the Langendorff perfused rabbit heart. *Exp Physiol*. 2004;89:163-172.
152. Efimov IR, Nikolski VP, Salama G. Optical imaging of the heart. *Circ Res*. 2004;95:21-33.
153. Gasser RN, Vaughan-Jones RD. Mechanism of potassium efflux and action potential shortening during ischaemia in isolated mammalian cardiac muscle. *J Physiol*. 1990;431:713-741.
154. Burton FL, Cobbe SM. Dispersion of ventricular repolarization and refractory period. *Cardiovasc Res*. 2001;50:10-23.

155. Antzelevitch C. Heterogeneity and cardiac arrhythmias: an overview. *Heart Rhythm*. 2007;4:964-972.
156. Tseng GN, Hoffman BF. Two components of transient outward current in canine ventricular myocytes. *Circ Res*. 1989;64:633-647.
157. Sicouri S, Antzelevitch C. A subpopulation of cells with unique electrophysiological properties in the deep subepicardium of the canine ventricle. The M cell. *Circ Res*. 1991;68:1729-1741.
158. Sicouri S, Quist M, Antzelevitch C. Evidence for the presence of M cells in the guinea pig ventricle. *J Cardiovasc Electrophysiol*. 1996;7:503-511.
159. Yan GX, Wu Y, Liu T, Wang J, Marinchak RA, Kowey PR. Phase 2 early afterdepolarization as a trigger of polymorphic ventricular tachycardia in acquired long-QT syndrome : direct evidence from intracellular recordings in the intact left ventricular wall. *Circulation*. 2001;103:2851-2856.
160. Li GR, Feng J, Yue L, Carrier M. Transmural heterogeneity of action potentials and Ito1 in myocytes isolated from the human right ventricle. *Am J Physiol*. 1998;275:H369-H377.
161. Drouin E, Charpentier F, Gauthier C, Laurent K, Le Marec H. Electrophysiologic characteristics of cells spanning the left ventricular wall of human heart: evidence for presence of M cells. *J Am Coll Cardiol*. 1995;26:185-192.
162. Conrath CE, Wilders R, Coronel R, de Bakker JMT, Taggart P, de Groot JR, Ophof T. Intercellular coupling through gap junctions masks M cells in the human heart. *Cardiovascular Research*. 2004;62:407-414.
163. Anyukhovsky EP, Sosunov EA, Rosen MR. Regional Differences in Electrophysiological Properties of Epicardium, Midmyocardium, and Endocardium: In Vitro and In Vivo Correlations. *Circulation*. 1996;94:1981-1988.
164. Vos MA, Jungschleger JG. Transmural repolarization gradients in vivo: the flukes and falls of the endocardium. *Cardiovasc Res*. 2001;50:423-425.
165. Antzelevitch C. Transmural dispersion of repolarization and the T wave. *Cardiovasc Res*. 2001;50:426-431.

166. Vetter FJ, McCulloch AD. Three-dimensional analysis of regional cardiac function: a model of rabbit ventricular anatomy. *Prog Biophys Mol Biol.* 1998;69:157-183.
167. Yan GX, Shimizu W, Antzelevitch C. Characteristics and distribution of M cells in arterially perfused canine left ventricular wedge preparations. *Circulation.* 1998;98:1921-1927.
168. Caldwell J, Burton FL, Smith GL, Cobbe SM. Heterogeneity of ventricular fibrillation dominant frequency during global ischemia in isolated rabbit hearts. *J Cardiovasc Electrophysiol.* 2007;18:854-861.
169. Toyoshima H, Burgess MJ. Electrotonic interaction during canine ventricular repolarization. *Circ Res.* 1978;43:348-356.
170. Osaka T, Kodama I, Tsuboi N, Toyama J, Yamada K. Effects of activation sequence and anisotropic cellular geometry on the repolarization phase of action potential of dog ventricular muscles. *Circulation.* 1987;76:226-236.
171. Medina-Ravell VA, Lankipalli RS, Yan GX, Antzelevitch C, Medina-Malpica NA, Medina-Malpica OA, Droogan C, Kowey PR. Effect of epicardial or biventricular pacing to prolong QT interval and increase transmural dispersion of repolarization: does resynchronization therapy pose a risk for patients predisposed to long QT or torsade de pointes? *Circulation.* 2003;107:740-746.
172. Libbus I, Rosenbaum DS. Remodeling of cardiac repolarization: mechanisms and implications of memory. *Card Electrophysiol Rev.* 2002;6:302-310.
173. Geller JC, Rosen MR. Persistent T-wave changes after alteration of the ventricular activation sequence. New insights into cellular mechanisms of 'cardiac memory'. *Circulation.* 1993;88:1811-1819.
174. Plotnikov AN, Yu H, Geller JC, Gainullin RZ, Chandra P, Patberg KW, Friezema S, Danilo P, Jr., Cohen IS, Feinmark SJ, Rosen MR. Role of L-Type Calcium Channels in Pacing-Induced Short-Term and Long-Term Cardiac Memory in Canine Heart. *Circulation.* 2003;107:2844-2849.
175. Jeyaraj D, Wilson LD, Zhong J, Flask C, Saffitz JE, Deschenes I, Yu X, Rosenbaum DS. Mechanoelectrical Feedback as Novel Mechanism of Cardiac Electrical Remodeling. *Circulation.* 2007;115:3145-3155.

176. Libbus I, Rosenbaum DS. Transmural action potential changes underlying ventricular electrical remodeling. *J Cardiovasc Electrophysiol.* 2003;14:394-402.
177. van Veen TAB, van Rijen HVM, Ophof T. Cardiac gap junction channels: modulation of expression and channel properties. *Cardiovascular Research.* 2001;51:217-229.
178. de Groot JR, Veenstra T, Verkerk AO, Wilders R, Smits JP, Wilms-Schopman FJ, Wiegerinck RF, Bourier J, Belterman CN, Coronel R, Verheijck EE. Conduction slowing by the gap junctional uncoupler carbenoxolone. *Cardiovasc Res.* 2003;60:288-297.
179. Xing D, Kjolby AL, Nielsen MS, Petersen JS, Harlow KW, Holstein-Rathlou NH, Martins JB. ZP123 increases gap junctional conductance and prevents reentrant ventricular tachycardia during myocardial ischemia in open chest dogs. *J Cardiovasc Electrophysiol.* 2003;14:510-520.
180. Guerra JM, Everett TH, Lee KW, Wilson E, Olgin JE. Effects of the gap junction modifier rotigaptide (ZP123) on atrial conduction and vulnerability to atrial fibrillation. *Circulation.* 2006;114:110-118.
181. Eloff BC, Gilat E, Wan X, Rosenbaum DS. Pharmacological modulation of cardiac gap junctions to enhance cardiac conduction: evidence supporting a novel target for antiarrhythmic therapy. *Circulation.* 2003;108:3157-3163.
182. Axelsen LN, Stahlhut M, Mohammed S, Larsen BD, Nielsen MS, Holstein-Rathlou NH, Andersen S, Jensen ON, Hennan JK, Kjolby AL. Identification of ischemia-regulated phosphorylation sites in connexin43: A possible target for the antiarrhythmic peptide analogue rotigaptide (ZP123). *J Mol Cell Cardiol.* 2006;40:790-798.
183. Poelzing S, Dikshteyn M, Rosenbaum DS. Transmural Conduction Is Not a Two-Way Street. *Journal of Cardiovascular Electrophysiology.* 2005;16:455.
184. Poelzing S, Akar FG, Baron E, Rosenbaum DS. Heterogeneous connexin43 expression produces electrophysiological heterogeneities across ventricular wall. *Am J Physiol Heart Circ Physiol.* 2004;286:H2001-H2009.

185. Dhein S, Larsen BD, Petersen JS, Mohr FW. Effects of the new antiarrhythmic peptide ZP123 on epicardial activation and repolarization pattern. *Cell Commun Adhes.* 2003;10:371-378.
186. Beuckelmann DJ, Nabauer M, Erdmann E. Intracellular calcium handling in isolated ventricular myocytes from patients with terminal heart failure. *Circulation.* 1992;85:1046-1055.
187. Gwathmey JK, Copelas L, MacKinnon R, Schoen FJ, Feldman MD, Grossman W, Morgan JP. Abnormal intracellular calcium handling in myocardium from patients with end-stage heart failure. *Circ Res.* 1987;61:70-76.
188. Kaab S, Nuss HB, Chiamvimonvat N, O'Rourke B, Pak PH, Kass DA, Marban E, Tomaselli GF. Ionic Mechanism of Action Potential Prolongation in Ventricular Myocytes From Dogs With Pacing-Induced Heart Failure. *Circ Res.* 1996;78:262-273.
189. Nuss HB, Kaab S, Kass DA, Tomaselli GF, Marban E. Cellular basis of ventricular arrhythmias and abnormal automaticity in heart failure. *Am J Physiol Heart Circ Physiol.* 1999;277:H80-H91.
190. Wiegerinck RF, van Veen TA, Belterman CN, Schumacher CA, Noorman M, de Bakker JM, Coronel R. Transmural dispersion of refractoriness and conduction velocity is associated with heterogeneously reduced connexin43 in a rabbit model of heart failure. *Heart Rhythm.* 2008;5:1178-1185.
191. Li GR, Lau CP, Ducharme A, Tardif JC, Nattel S. Transmural action potential and ionic current remodeling in ventricles of failing canine hearts. *Am J Physiol Heart Circ Physiol.* 2002;283:H1031-H1041.
192. Vrtovec B, Delgado R, Zewail A, Thomas CD, Richartz BM, Radovancevic B. Prolonged QTc Interval and High B-Type Natriuretic Peptide Levels Together Predict Mortality in Patients With Advanced Heart Failure. *Circulation.* 2003;107:1764-1769.
193. Wettwer E, Amos GJ, Posival H, Ravens U. Transient outward current in human ventricular myocytes of subepicardial and subendocardial origin. *Circ Res.* 1994;75:473-482.

194. Greenstein JL, Wu R, Po S, Tomaselli GF, Winslow RL. Role of the Calcium-Independent Transient Outward Current I_{to} in Shaping Action Potential Morphology and Duration. *Circ Res.* 2000;87:1026-1033.
195. Houser SR, Piacentino V, III, Weisser J. Abnormalities of calcium cycling in the hypertrophied and failing heart. *J Mol Cell Cardiol.* 2000;32:1595-1607.
196. Baartscheer A, Schumacher CA, Belterman CN, Coronel R, Fiolet JW. SR calcium handling and calcium after-transients in a rabbit model of heart failure. *Cardiovasc Res.* 2003;58:99-108.
197. Richard S, Leclercq F, Lemaire S, Piot C, Nargeot J. Ca²⁺ currents in compensated hypertrophy and heart failure. *Cardiovasc Res.* 1998;37:300-311.
198. Schroder F, Handrock R, Beuckelmann DJ, Hirt S, Hullin R, Priebe L, Schwinger RHG, Weil J, Herzig S. Increased Availability and Open Probability of Single L-Type Calcium Channels From Failing Compared With Nonfailing Human Ventricle. *Circulation.* 1998;98:969-976.
199. Ai X, Curran JW, Shannon TR, Bers DM, Pogwizd SM. Ca²⁺/calmodulin-dependent protein kinase modulates cardiac ryanodine receptor phosphorylation and sarcoplasmic reticulum Ca²⁺ leak in heart failure. *Circ Res.* 2005;97:1314-1322.
200. Litwin SE, Zhang D, Bridge JH. Dyssynchronous Ca(2+) sparks in myocytes from infarcted hearts. *Circ Res.* 2000;87:1040-1047.
201. O'Rourke B, Kass DA, Tomaselli GF, Kaab S, Tunin R, Marban E. Mechanisms of altered excitation-contraction coupling in canine tachycardia-induced heart failure, I: experimental studies. *Circ Res.* 1999;84:562-570.
202. Schmidt U, Hajjar RJ, Helm PA, Kim CS, Doye AA, Gwathmey JK. Contribution of abnormal sarcoplasmic reticulum ATPase activity to systolic and diastolic dysfunction in human heart failure. *J Mol Cell Cardiol.* 1998;30:1929-1937.
203. Pogwizd SM, Sipido KR, Verdonck F, Bers DM. Intracellular Na in animal models of hypertrophy and heart failure: contractile function and arrhythmogenesis. *Cardiovasc Res.* 2003;57:887-896.
204. Baartscheer A, Schumacher CA, van Borren MM, Belterman CN, Coronel R, Fiolet JW. Increased Na⁺/H⁺-exchange activity is the cause of increased [Na⁺]i and

- underlies disturbed calcium handling in the rabbit pressure and volume overload heart failure model. *Cardiovasc Res.* 2003;57:1015-1024.
205. Joyner RW, Ramza BM, Osaka T, Tan RC. Cellular mechanisms of delayed recovery of excitability in ventricular tissue. *Am J Physiol Heart Circ Physiol.* 1991;260:H225-H233.
206. Moe GW, Armstrong P. Pacing-induced heart failure: a model to study the mechanism of disease progression and novel therapy in heart failure. *Cardiovascular Research.* 1999;42:591-599.
207. Panfilov AV. Is heart size a factor in ventricular fibrillation? Or how close are rabbit and human hearts? *Heart Rhythm.* 2006;3:862-864.
208. Wiegerinck RF, Verkerk AO, Belterman CN, van Veen TA, Baartscheer A, Ophof T, Wilders R, de Bakker JM, Coronel R. Larger cell size in rabbits with heart failure increases myocardial conduction velocity and QRS duration. *Circulation.* 2006;113:806-813.
209. Poelzing S, Rosenbaum DS. Altered connexin43 expression produces arrhythmia substrate in heart failure. *Am J Physiol Heart Circ Physiol.* 2004;287:H1762-H1770.
210. Taggart P, Sutton P, Chalabi Z, Boyett MR, Simon R, Elliott D, Gill JS. Effect of Adrenergic Stimulation on Action Potential Duration Restitution in Humans. *Circulation.* 2003;107:285-289.
211. Watanabe T, Yamaki M, Yamauchi S, Minamihaba O, Miyashita T, Kubota I, Tomoike H. Regional prolongation of ARI and altered restitution properties cause ventricular arrhythmia in heart failure. *Am J Physiol Heart Circ Physiol.* 2002;282:H212-H218.
212. Gehi AK, Stein RH, Metz LD, Gomes JA. Microvolt T-wave alternans for the risk stratification of ventricular tachyarrhythmic events: a meta-analysis. *J Am Coll Cardiol.* 2005;46:75-82.
213. Mironov S, Jalife J, Tolkacheva EG. Role of conduction velocity restitution and short-term memory in the development of action potential duration alternans in isolated rabbit hearts. *Circulation.* 2008;118:17-25.

214. Swerdlow CD, Zhou X, Voroshilovsky O, Abeyratne A, Gillberg J. High amplitude T-wave alternans precedes spontaneous ventricular tachycardia or fibrillation in ICD electrograms. *Heart Rhythm*. 2008;5:670-676.
215. Yuuki K, Hosoya Y, Kubota I, Yamaki M. Dynamic and not static change in ventricular repolarization is a substrate of ventricular arrhythmia on chronic ischemic myocardium. *Cardiovasc Res*. 2004;63:645-652.
216. Weiss JN, Karma A, Shiferaw Y, Chen PS, Garfinkel A, Qu Z. From pulsus to pulseless: the saga of cardiac alternans. *Circ Res*. 2006;98:1244-1253.

Appendix

Introduction

In optical recordings of repolarisation alternans, the alternating behavior observed is not restricted to the repolarisation phase of the optical AP. Alternans of action potential amplitude is also seen, the basis for which is not known. Whether alternans of AP amplitude occurs in single cells remains unclear. To investigate this we recorded alternans from single cells in intact rabbit ventricular myocardium and compared these with conventional optical recordings. If the alternation in AP amplitude were primary, then this might be expected to have an effect on the APD (i.e. producing “secondary” repolarisation alternans). If alternans of AP amplitude was seen in single cells, then the mechanisms, which remain uninvestigated, may be quite different to those described for repolarisation alternans. Similarly, if amplitude alternans is an artefact of optical records then the possible explanations for this extend beyond alternans of repolarisation. In either case, it is conceivable that changes in recorded AP amplitude may have implications for the development of unidirectional conduction block, and amplitude alternans therefore requires careful consideration, as it raises the possibility that other aspects of electrical activity, aside from repolarisation, may responsible for both TWA and the accompanying proarrhythmic status.

Methods

Hearts from 17 male New Zealand White rabbits were used for these experiments. Epicardial electrical activity was recorded from perfused left ventricular wedge preparations using voltage sensitive dyes. In one set of experiments a CCD-camera detection system (single pixel dimension $\sim 326\mu\text{m}^2$) was used to record optical action potentials ($n = 8$). In a separate set of experiments ($n = 9$), optical action potentials were recorded from single cells within the wedge preparation using 2-photon excitation (920nm) at a depth of $\sim 50\text{mm}$ from the epicardial surface with an x-y resolution of $\sim 1 \times 1\mu\text{m}$ and a z-axis resolution of $\sim 2\mu\text{m}$.

Two photon fluorescence microscopy

In addition to the CCD-based system, a system for imaging voltage in intact tissue using a two-photon fluorescence microscope was developed. Multiphoton fluorescence microscopy combines the advanced optical techniques of laser scanning microscopy with long wavelength multiphoton excitation to capture high-resolution images of specimens stained with specific fluorophores. Two-photon excitation means that two low energy photons are used to excite a fluorophore, resulting in the emission of a high-energy fluorescence photon. This depends on simultaneous absorption of two photons and therefore requires a high intensity of excitation photons, produced by a femtosecond pulsed infrared laser. The laser beam is focused through an objective lens toward the preparation and the fluorescence from the sample is then split by wavelength and collected by two photomultiplier tubes (PMTs). As two-photon excitation only occurs at the focal point of the laser, optical sectioning is produced by the point spread function formed where the pulsed laser beams coincide. This removes the need for a pinhole (used in conventional confocal microscopy) and so improves light transmission efficiency. The use of infrared light to excite fluorophores in tissue is beneficial because longer wavelengths are scattered to a lesser degree than shorter ones, allowing higher spatial resolution. In addition, longer wavelength light is less likely to cause photodamage to the tissue outside the optical section. These properties also mean that imaging can be achieved deeper into the tissue than with conventional confocal microscopy, meaning that two-photon fluorescence microscopy is better suited to imaging intact preparations.

Two-photon optical imaging system

The laser (LSM 510, Carl Zeiss Inc.) was focused on the preparation using a water-dipping objective. Excitation was set at 920nm, the emitted fluorescence was then split from the excitation path using a 700nm main dichroic, and collected using two non-descanned

detectors (PMTs) by splitting emission at 580nm into 510-560nm and >590nm bands (see Figure A). Linescans were gated to the stimulus pulse and recorded at 50-150 μ m from the epicardial surface. With the 40x objective x-y-z resolution was 1x1x2 μ m, and with the 10x objective 4x4x2 μ m.

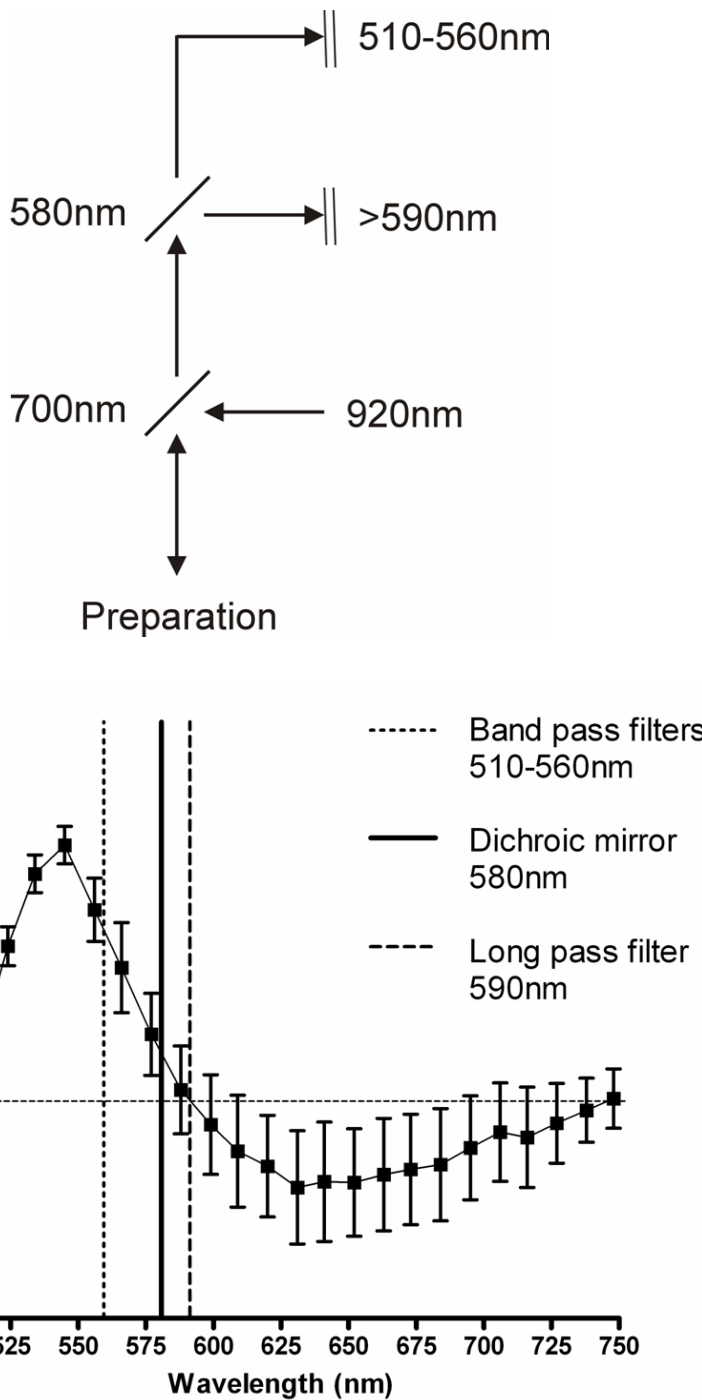


Figure A. Two-photon optical imaging system

The upper panel illustrates the optical settings used for imaging of Di-4-ANEPPS with the two-photon confocal microscope. The lower panel shows fractional change in fluorescence from Di-4-ANEPPS on administration of KCl, measured in isolated rabbit ventricular cardiomyocytes. The optics for the two-photon imaging system are illustrated.

Motion artefact

The two-photon system has a lower tolerance for motion, principally because of its high spatial resolution. This meant that 15mmol/L BDM was insufficient to allow optical recordings by this method. 10 μ mol/L blebbistatin (described in Chapter 2, section 2.7.2) was added to 15mmol/L BDM produced a complete abolition of motion and allowed optical mapping of voltage at this very high spatial resolution. BDM was continued to reduce any potential differences between the protocols used for the two imaging systems. Effects of both compounds (and the combination of the two) were reversible by washout. Blebbistatin (Biomol International) is a recently discovered inhibitor of myosin II isoforms, which has been successfully employed in cardiac optical mapping. In rabbit ventricular myocardium 5-10 μ mol/L blebbistatin abolishes motion without any evident effects on AP parameters, ventricular conduction velocity or effective refractory period (Fedorov, Heart Rhythm, 2006). 10 μ mol/L blebbistatin added to 15mmol/L BDM produced a complete abolition of motion and allowed optical mapping of voltage at high spatial resolution. BDM was continued to reduce any potential differences between the protocols used for the two imaging systems. Effects of both compounds (and the combination of the two) were reversible by washout.

Experimental protocols

In each experiment, baseline pacing from the endocardial surface at a CL of 350ms was initiated after the preparation had been mounted in the imaging section of the chamber. Optical recordings were taken for 2 seconds during steady state pacing, and at least 30s after any change in pacing CL. Baseline recordings were repeated at the end of each protocol, to assess for any changes in the condition of the preparation caused by the protocol. Experiments were performed at 30°C. Optical recordings were taken during baseline endocardial pacing at a CL of 350ms. Pacing CL was then progressively shortened in 50ms decrements to 200ms and then in 10ms decrements, and recordings were taken after 30s of pacing at each CL. Pacing CL was progressively reduced until loss of 1:1 capture or a ventricular arrhythmia (VA) was induced. Where VA was sustained, overdrive pacing was attempted, and where this failed pacing was terminated and a rapid bolus of 25 μ l 1M KCl was administered to induce asystole. At the end of the protocol pacing was returned to a CL of 350ms.

Data analysis

The data files were saved using the Zeiss microscope software and were stored on two hard drives as well as on CD/DVD. Each linescan was 38s worth of APs on two separate channels, which corresponded to the two wavelengths collected. For each wavelength, the

linescan data were exported as a bitmap. These images could then be read into a program which allowed ratio of channel 1 and channel 2, to produce a ratiometric optical signal (see Figure B). Each individual signal in the raw ratio trace was then averaged long the length of the linescan to produce a averaged AP. The program also allowed a number of variations of the averaging algorithm, such that pairs of APs along the trace could be averaged, so that any alternans could be identified and quantified. The averaged APs, regardless of how they were derived, could then be analysed for AT-mid, RT and APD₇₅, using the same definitions as described for the CCD system analysis.

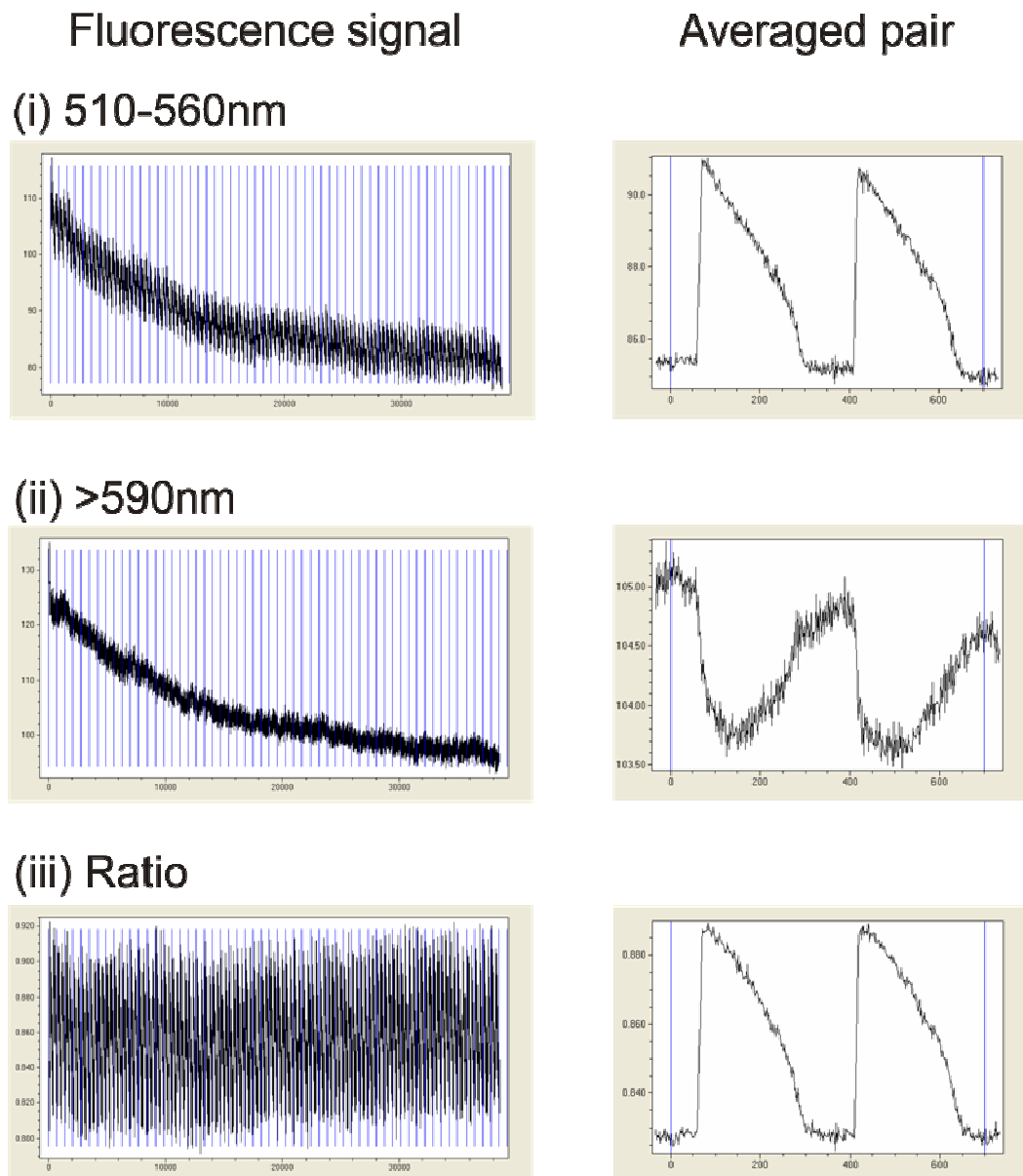


Figure B. Ratiometry and averaging of two-photon linescan data

Raw fluorescence signals taken from a two-photon linescan, along with the corresponding averaged pairs of APs. (i) Fluorescence recorded at 510-560nm (ii) fluorescence recorded at >590nm (iii) ratio fluorescence signal.

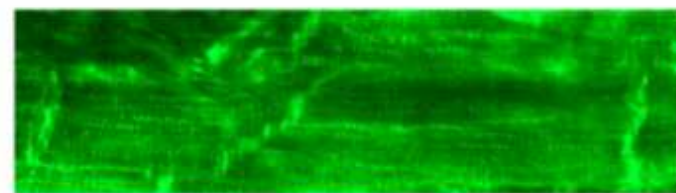
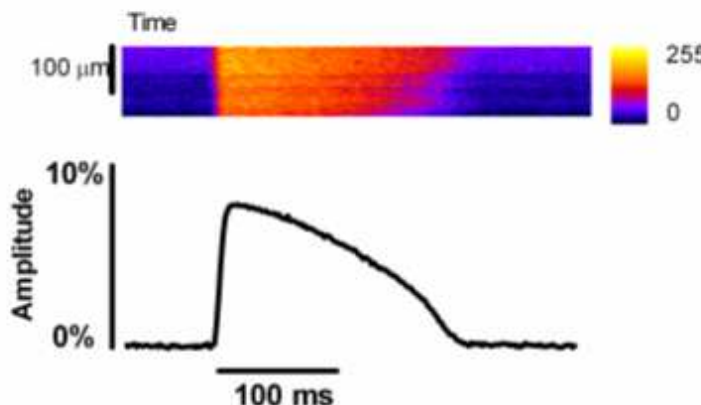
Results

CCD recordings

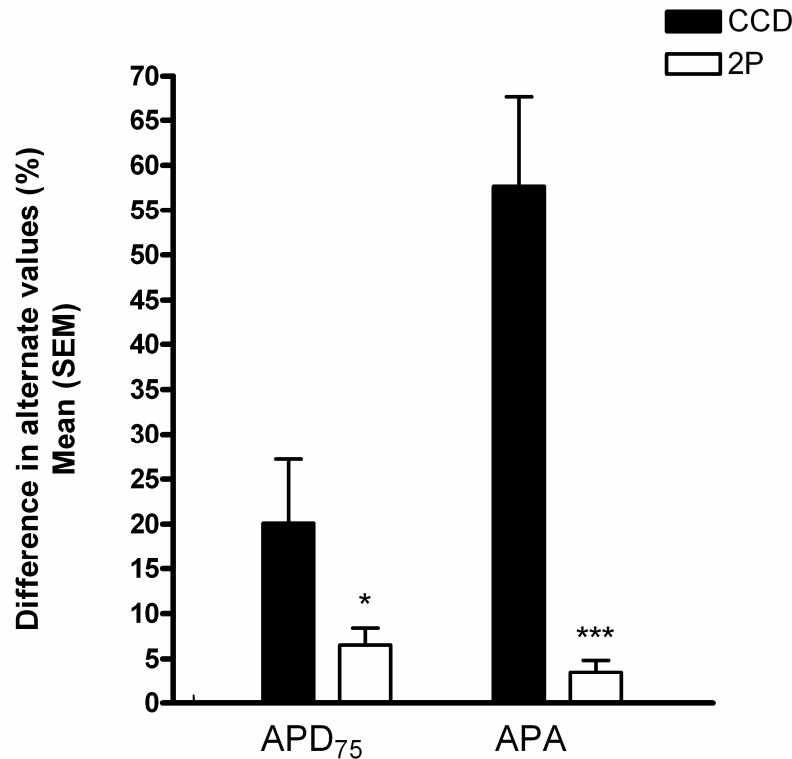
At a cycle length (CL) of 350ms, optical action potentials showed no alternating characteristics. Progressive reduction in CL produced alternans, which was confirmed by spectral analysis. At the shortest cycle length supported, the mean change in alternate APD₇₅ was $20.1 \pm 7.1\%$ and in alternate AP amplitude was $57.7 \pm 9.9\%$ (mean CL $156.7 \pm 5.8\text{ms}$).

Two photon confocal recordings

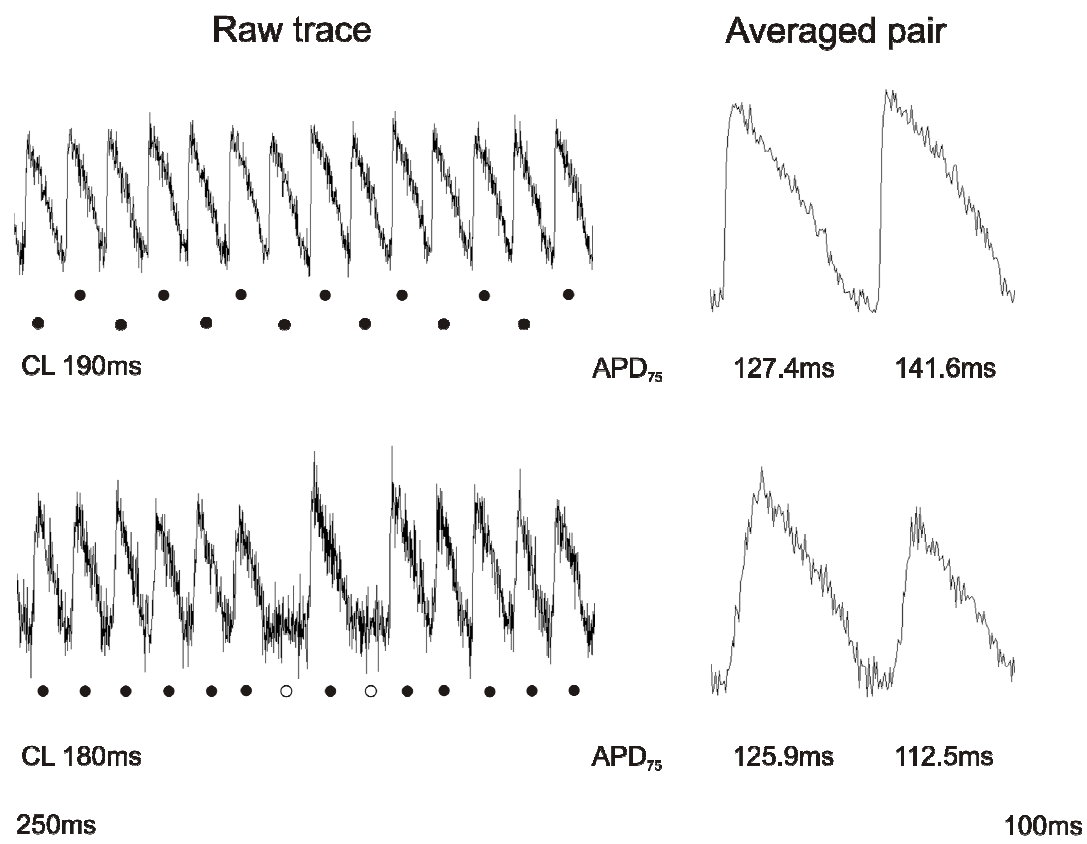
An example of an action potential recorded by two-photon fluorescence microscopy is given in Figure C. As shown in Figure D, at the minimum CL supported (mean $165.0 \pm 7.3\text{ms}$), the changes in alternate APD₇₅ ($6.5 \pm 1.9\%$) and AP amplitude ($3.5 \pm 1.3\%$) were significantly smaller than those seen at the lower spatial resolution. As shown in Figure E, during alternans recorded at high spatial resolution different behaviours were observed in single cells. In some cases, single cells displayed intermittent 2:1 block while in adjacent regions 1:1 coupling was observed, producing alternans of AP amplitude and APD. In others alternans of APD was observed at the single cell level, without clear alternans of AP amplitude.

Example of cardiomyocytes at ~100 μm depthExample of linescan at ~100 μm depth (3Hz)**Figure C. Action potentials in intact myocardium measured by 2P linescan**

Courtesy of Dr Ole Johan Kemi. The upper panel shows a fluorescence image of the subepicardium stained with Di-4-ANEPPS using the 40x objective.

**Figure D. A comparison of results from the CCD and 2P systems**

Percentage difference in APD₇₅ and AP amplitude in each set of experiments, * p < 0.05, *** p < 0.001.

**Figure E. Examples of single cell behavior underlying alternans**

In the upper panel, the raw trace shows alternans of APD, which is reflected in the averaged signal. In the lower trace, intermittent dropout is seen, which results in alternans of both APD and AP amplitude in the averaged signal.

Discussion

These data demonstrate the differences in action potential characteristics recorded during alternans at different spatial resolutions. The resolution of the CCD recordings is such that the signal represents the mean voltage within a significant volume of myocardium. In contrast, the two-photon confocal system allows voltage recordings from a single cell within the intact myocardium. While significant alternans of AP amplitude and APD are recorded at lower spatial resolution, the magnitude of the proportional change is much smaller when recordings are taken from single cells. This raises the possibility that heterogeneous single cell responses may underlie the alternating morphology of the optical action potential measured at a low spatial resolution. Indeed, we did observe different single cell behaviours during alternans, from alternating APD to intermittent action potential failure. These data suggest that in rabbit ventricular myocardium rapid pacing and low temperature induce heterogeneous responses from single cells and consequently, that different cellular behaviours may underlie the alternating changes in AP amplitude and APD recorded from larger areas of myocardium.